JAAVSO

Volume 44
Number 1
2016

The Journal of the American Association of Variable Star Observers

Appearance of Special UGSU-Type Phenomenon in the Light Curve of UGZ White Dwarf Nova RX Andromedae

RX And superoutburst at JD 2456987. The superoutburst of about 10.7 magnitude is superpositioned on the precursor normal outburst of about 11.0 magnitude.

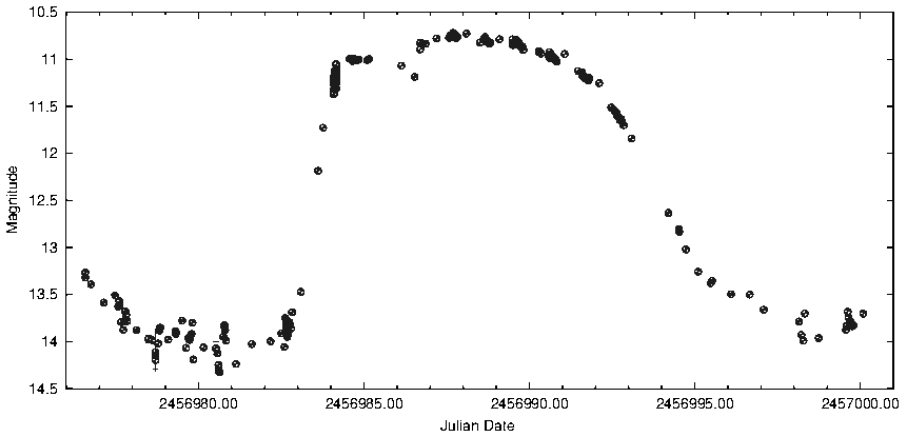

Also in this issue...

The American Association of Variable Star Observers
49 Bay State Road, Cambridge, MA 02138, USA

ISSN 0271-9053 (print)
ISSN 2380-3606 (online)

JAAVSO

The Journal of
The American Association
of Variable Star Observers

Volume 44
Number 1
2016

ISSN 0271-9053 (print)
ISSN 2380-3606 (online)

AAVSO
49 Bay State Road
Cambridge, MA 02138
USA

Publication Schedule

The Journal of the American Association of Variable Star Observers is published twice a year, June 15 (Number 1 of the volume) and December 15 (Number 2 of the volume). The submission window for inclusion in the next issue of JAAVSO closes six weeks before the publication date. A manuscript will be added to the table of contents for an issue when it has been fully accepted for publication upon successful completion of the referee process; these articles will be available online prior to the publication date. An author may not specify in which issue of JAAVSO a manuscript is to be published; accepted manuscripts will be published in the next available issue, except under extraordinary circumstances.

Page Charges

Page charges are waived for Members of the AAVSO. Publication of unsolicited manuscripts in JAAVSO requires a page charge of US $100/page for the final printed manuscript. Page charge waivers may be provided under certain circumstances.

Publication in *JAAVSO*

With the exception of abstracts of papers presented at AAVSO meetings, papers submitted to JAAVSO are peer-reviewed by individuals knowledgable about the topic being discussed. We cannot guarantee that all submissions to JAAVSO will be published, but we encourage authors of all experience levels and in all fields related to variable star astronomy and the AAVSO to submit manuscripts. We especially encourage students and other mentees of researchers affiliated with the AAVSO to submit results of their completed research.

Subscriptions

Institutions and Libraries may subscribe to JAAVSO as part of the Complete Publications Package or as an individual subscription. Individuals may purchase printed copies of recent JAAVSO issues via Createspace. Paper copies of JAAVSO issues prior to volume 36 are available in limited quantities directly from AAVSO Headquarters; please contact the AAVSO for available issues.

Instructions for Submissions

The *Journal of the AAVSO* welcomes papers from all persons concerned with the study of variable stars and topics specifically related to variability. All manuscripts should be written in a style designed to provide clear expositions of the topic. Contributors are encouraged to submit digitized text in MS WORD, LATEX+POSTSCRIPT, or plain-text format. Manuscripts may be mailed electronically to journal@aavso.org or submitted by postal mail to JAAVSO, 49 Bay State Road, Cambridge, MA 02138, USA.

Manuscripts must be submitted according to the following guidelines, or they will be returned to the author for correction:

Manuscripts must be:
1) original, unpublished material;
2) written in English;
3) accompanied by an abstract of no more than 100 words.
4) not more than 2,500–3,000 words in length (10–12 pages double-spaced).

Figures for publication must:
1) be camera-ready or in a high-contrast, high-resolution, standard digitized image format;
2) have all coordinates labeled with division marks on all four sides;
3) be accompanied by a caption that clearly explains all symbols and significance, so that the reader can understand the figure without reference to the text.

Maximum published figure space is 4.5″ by 7″. When submitting original figures, be sure to allow for reduction in size by making all symbols, letters, and division marks sufficiently large.

Photographs and halftone images will be considered for publication if they directly illustrate the text.

Tables should be:
1) provided separate from the main body of the text;
2) numbered sequentially and referred to by Arabic number in the text, e.g., Table 1.

References:
1) References should relate directly to the text.
2) References should be keyed into the text with the author's last name and the year of publication, e.g., (Smith 1974; Jones 1974) or Smith (1974) and Jones (1974).
3) In the case of three or more joint authors, the text reference should be written as follows: (Smith et al. 1976).
4) All references must be listed at the end of the text in alphabetical order by the author's last name and the year of publication, according to the following format: Brown, J., and Green, E. B. 1974, *Astrophys. J.*, **200**, 765.
Thomas, K. 1982, *Phys. Rep.*, **33**, 96.
5) Abbreviations used in references should be based on recent issues of the *Journal* or the listing provided at the beginning of *Astronomy and Astrophysics Abstracts* (Springer-Verlag).

Miscellaneous:
1) Equations should be written on a separate line and given a sequential Arabic number in parentheses near the right-hand margin. Equations should be referred to in the text as, e.g., equation (1).
2) Magnitude will be assumed to be visual unless otherwise specified.
3) Manuscripts may be submitted to referees for review without obligation of publication.

Online Access

Articles published in JAAVSO, and information for authors and referees may be found online at: https://www.aavso.org/apps/jaavso/

The Journal of the American Association of Variable Star Observers
Volume 44, Number 1, 2016

Editorial

Variable Star Research

Instruments, Methods, and Techniques

Table of Contents continued on following pages

Variable Star Data

Education and Outreach

Book Review

Abstracts of Papers and Posters Presented at the 104th Annual Meeting of the AAVSO, Held in Woburn, Massachusetts, November 13–14, 2015

General Paper Session Part I

Table of Contents continued on next page

The (Variable) Stars Belong to Everyone

John R. Percy
Editor-in-Chief, *Journal of the AAVSO*

Department of Astronomy and Astrophysics, and Dunlap Institute for Astronomy and Astrophysics, University of Toronto, 50 St. George Street, Toronto, ON M5S 3H4, Canada; john.percy@utoronto.ca

Received May 31, 2016

The authorship of this issue reminds us that, although the AAVSO is "American," its reach and impact are international. Our members and observers come from around the world.

International Science: There are thousands of VSOers around the world. We need variable star observations made with various instruments, from both north and south, and from all longitudes so there is coverage even when America is in daylight. Friedrich Argelander (1799–1875), the "father of variable star astronomy," admonished observers to publish their observations, and not to just file them in a drawer. But if they were published in a thousand places, with a thousand different methodologies and comparison stars, that would not be very useful. There are great advantages for researchers like me to be able to go to a single source—the AAVSO *International* Database—for systematic, sustained data.

The results of variable star research are published in few dozen journals around the world. *JAAVSO* occupies a special niche. We are a refereed journal which invites papers in English from any country, to serve our readership of professional astronomers, amateurs, students, and other readers who are not necessarily at the level of *The Astrophysical Journal*.

International Organization: Professional astronomy is organized internationally by the International Astronomical Union (IAU: iau.org), whose mission is to promote and safeguard astronomy through international cooperation. IAU Division G, Stars and Stellar Physics, includes several "commissions" or interest groups which are relevant to AAVSO, including Binary and Multiple Star Systems, Massive Stars, Stellar Evolution, and Pulsating Stars. I know, from my time as a commission president, that the AAVSO is highly respected internationally. It can provide a strong voice for all the skilled amateurs who continue to play a significant role in variable star astronomy. AAVSO Council member Joyce Guzik is currently a member of the executive committee of Commission G4: Pulsating Stars.

In addition, there are several dozen VSOing organizations, with objectives similar to those of AAVSO, in countries around the world; 36 of them are listed at https://www.aavso.org/observer-affliations-table. AAVSO has consistently endeavored to maintain effective, respectful partnerships with these groups. The AAVSO's first international meeting was held in Brussels in 1990. Its proceedings (Percy *et al.* 1992) reflects our world-wide reach. An "international union of amateur astronomers" has existed at times, but not currently.

International Astronomy Education: At the graduate level, astronomy education is quite international; at Toronto, our grad students and postdocs and faculty come from all over the world. At the undergraduate level, astronomy education may seem much more national or local, but there are still reasons to have an international perspective. At my university, about half of undergraduate students were born elsewhere. We are also interested in the nature and strengths and weaknesses of other education systems. This is especially true at the school level. Why do countries such as Finland outperform us in international standardized science and math tests? Often, the answers can help us to deal with weaknesses in our own system—the education of immigrant students, Aboriginal students, and other marginalized groups. Can it also help us with a fundamental problem: astronomy is a compulsory part of the elementary and secondary curriculum, but few teachers have any background in astronomy, or astronomy teaching. Jay Pasachoff and I chaired the first international conference on the teaching of astronomy (Pasachoff and Percy 1990). It was inspiring to meet and learn from our "kindred spirits" from around the world.

International Astronomy Outreach: International Year of Astronomy 2009 was a roaring success. To my mind, it was more effective than the international years of physics (2005) and chemistry (2011). It was celebrated in 148 countries around the world. Since this is twice the number of countries which carry out astronomical research, and adhere to the IAU, it follows that, in at least half of countries, IYA was driven, at the grass-roots level, by amateurs and educators. IYA included international, national, and local projects, and certainly benefitted from being a world-wide event. AAVSO also supported and participated in International Year of Light (2015) as an "encore."

The AAVSO has just joined *Astronomers Without Borders* (astronomerswithoutborders.org) to support projects such as Global Astronomy Month. AWB is a non-profit organization dedicated to "bringing the world together to share our passion for astronomy and the wonders of the Universe." In their words: "In the process of looking outward together, we learn about each other and create lasting bonds, regardless of country or culture." It's one world, one sky; the stars belong to everyone.

International Astronomy Development: The stars may belong to everyone, but there are few countries as well-equipped for studying them as ours. But why develop astronomy, or use astronomy as a tool for development in third-world countries which have more pressing needs? One reason is because astronomy is engaging and deeply rooted in culture, and can attract young people to science and technology. They can then pursue more "practical" careers, such as engineering and health care, while retaining astronomy as an interest or hobby.

One of the IAU's highest priorities is astronomical development, which is coordinated through its Office of Astronomy for Development (www.astro4dev.org). But

individual professional or amateur astronomers can contribute, as Canadian amateur Dave Chapman (2016) has done during five trips to Cuba.

So please take a few minutes to reflect on your place in the international astronomical community, and how you can contribute, and how you can benefit.

References

Chapman, D. M. F. 2016, *J. Roy. Astron. Soc. Canada*, **110**, 74.

Pasachoff, J. M., and Percy, J. R. 1990, *The Teaching of Astronomy*, Cambridge University Press, Cambridge.

Percy, J. R., Mattei, J. A., and Sterken, C. 1992, *Variable Star Research: An International Perspective*, Cambridge University Press: Cambridge (a few copies are available on Amazon).

Appearance of Special UGSU-type Phenomenon in the Light Curve of UGZ White Dwarf Nova RX Andromedae

András Timár
1173 Budapest, Parlagfu u. 10., Hungary; andras.timar@t-online.hu

Received November 12, 2015; revised December 11, 2015; accepted December 16, 2015

Abstract The dwarf nova RX Andromedae was examined using data from the AAVSO International Database. It is classified as a Z Cam (UGZ)-type dwarf nova. The cycle of outbursts is short due to the high accretion rate, approximately 13 days. The object has been in standstill several times over the last two decades, as well observed by the AAVSO. According to previous studies, RX And exhibited VY Scl-type light changes. During the analysis of the AAVSO light curve I established that specific UGSU-type characteristics have also developed in RX And since 5 August 2014. Every fourth outburst is a superoutburst, the period of the supercycle being about 55.5 days. The superoutbursts are brighter and longer than other normal outbursts. The superoutburst itself (~10.7 magnitude) is superpositioned on the precursor normal outburst (~11.0 magnitude). It can be established that the precursor triggers the superoutburst. However, we can find uncertainties in the recently-appearing UGSU-type feature of RX And; the star differs from the behavior of a typical UGSU dwarf nova in a number of aspects. Unlike UGSU stars the orbital period of RX And is above the period gap, and in the light curve of RX And there is not any indication of the presence of superhumps. The amplitude of the superoutburst exceeds that of a normal outburst by about 0.4 to 0.5 magnitude. This value is less than the 2 to 4 magnitudes characteristic of UGSU stars. Also, one should be careful in making conclusions, because the investigated period (from 5 August 2014 to 1 February 2015) is not long enough to judge whether the phenomena appearing in the light curve are really supermaxima. The long orbital period and the lack of superhumps in any case need further explanation. As for whether the supercycle remains stabilized in the star, and whether the UGSU characteristics are a normal stage of development for all UGZ dwarf novae or only typical of RX And, remain to be established by further investigations.

1. Introduction

The RX And system has been classified as a Z Cam-type dwarf nova, showing alternating standstills and dwarf nova outbursts (Simonsen *et al.* 2014). Outbursts around 11.0 magnitude were observed from the minimum approximately every 13 days. The pattern of the outbursts was identical to the single peak profile typical of dwarf novae. The brightness varies between the minimum of ~14.5 magnitude and the maximum of ~11.0 magnitude. The continuous cycle was sometimes interrupted by standstills lasting 60 to 90 days. The orbital period of the system is 5.04 hours. The white dwarf of 1.14 $M_{\odot}$ accretes material over from the secondary component with a high accretion rate (Godon and Sion 2003), due to which the average period of outbursts is only about 13 days. Over the past 20 years, the system indicated standstills typical of UGZ stars around 11.5 magnitude.

A significant fraction of cataclysmic variables show phases of low luminosity in their long term light curves. These low states appear to be a general phenomenon among the VY Scl stars, a subclass of the novalike variables. Earlier studies have shown that RX And also has characteristics of a VY Scl star (Schreiber *et al.* 2002). At JD 2450350–2450455 RX And was found in a deep low state, V ~15.4, fainter than the typical quiescent level of V ~14.5. According to Schreiber *et al.* this deep minimum state, having a length of 100 days, is an indication of the VY Scl properties of the system. It should be noted that light decreasing in VY Scl stars are 2 to 4 magnitudes while RX And is only 1 magnitude, but the amplitude and duration of the low states strongly vary between the members of the VY Scl class. Also, Schreiber *et al.* indicated that in morphological terms the low states appearing in the light curve of RX And are similar to the light change observed in diskless AM Her stars having extensive magnetic fields. There is an important difference, however: RX And is a dwarf nova having an accretion disk and it is a non-magnetic system.

RX And has undergone nearly every type of behavior seen in dwarf novae, creating one of the more interesting light curves among dwarf novae (Templeton 2007).

2. Data analysis

The behavior of RX And was analyzed based on the AAVSO light curve. RX And has a long and well observed light curve in the AAVSO International Database (Kafka 2015), with near continuous coverage throughout the recent decades. The continuous curve of several decades is particularly accurate and the high amplitudes of light changes allow visual estimates to be accurate enough for substantial conclusions on the properties of the changing star.

3. Discussion

In the course of analyzing the light curve of RX And, I could establish that the system had been exhibiting UGSU-type superoutbursts since 20 October 2011. The supercycle developed continuously over several years. The uncertain supercycle started to appear on the light curve from JD 2455469. The first definitely identifiable superoutburst took place at JD 2455856 (Figure 1). A cycle that is typical to UGSU stars started to appear on the light curve of RX And from JD 2456876, in which every fourth outburst is a superoutburst (Figure 2).

While RX And was visible in the autumn of 2015 the

superoutburst appeared again at JD 2457277. However, the existence of a supercycle is uncertain, because the fourth superoutburst after JD 2457277 cannot be identified unambiguously (Figure 3).

4. Results

I established that the normal outbursts are about 11.0 magnitude at maximum, and the superoutbursts generally reach an average value of 10.7 magnitude. The length of the normal outburst is about 9.33 days and the superoutbursts are about 17 days long, based on the superoutburst, appearing from time to time since 2010, and on the four superoutbursts occurring in the period from 5 August 2014 to 1 February 2015. The period of the supercycle created by the superoutbursts based on the above period is about 55.5 days. Additionally, the system has a special pattern of superoutbursts. I found that every superoutburst is associated with a precursor. The superoutburst is superpositioned on the precursor normal outburst of about 11.0 magnitude; the precursor thereby triggering the superoutburst (Figures 1 and 4).

4.1. UGSU-type phenomenon in the light curve of RX And

From 5 August 2014 a supercycle developed in the light curve in which the superoutbursts are brighter and longer than other normal outbursts. The precursor-triggered superoutburst, however, is not an exclusive feature of RX And. The precursors were first well-studied in the Kepler sources V344 Lyr and V1504 Cyg (Cannizzo *et al.* 2012). Furthermore, a precursor-triggered superoutburst can be observed in the light curve of the dwarf nova V516 Lyr in the Kepler field (Kato and Osaki 2013).

4.2. Uncertainties in UGSU-type properties

We can find uncertainties in the recently-appearing UGSU-type feature in RX And, and the star differs from the behavior of a typical UGSU dwarf nova in a number of aspects.

The known SU UMa stars lie below the period gap (that is, a 2- to 3-hour orbital period gap for dwarf novae) but the orbital period of RX And is 5.04 hours.

A typical UGSU superoutburst generally exceeds normal outbursts by 2 to 3 magnitudes. In the case of RX And the amplitude of the superoutburst exceeds that of a normal outburst by about 0.4 to 0.5 magnitude, but there are several SU UMa stars that only show increases by this amount.

During superoutbursts the light curves of UGSU stars show superposed periodic oscillations (superhumps), their periods being close to the orbital ones and with amplitudes that are 0.2 to 0.3 magnitude.

In the accurate AAVSO light curve of RX And, however, there is not any indication of the presence of superhumps.

A further source of uncertainty is that the investigated period (from 5 August 2014 to 1 February 2015) is not long enough to judge unambiguously that the new outburst behavior is really a superoutburst, and whether the supercycle really has occurred. The long orbital period and the lack of superhumps, in any case, need further explanation.

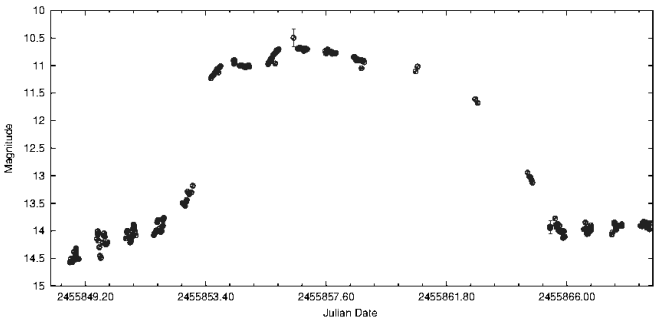

Figure 1. The first definitely identifiable superoutburst of RX And at JD 2455856.

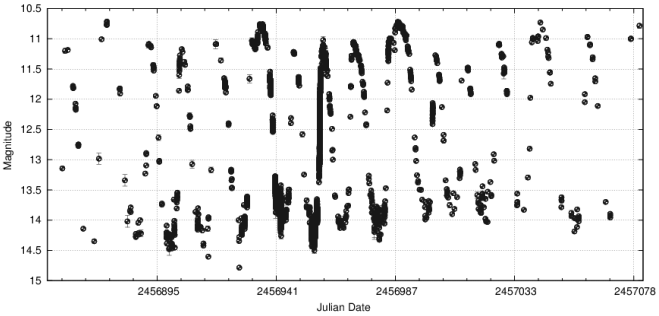

Figure 2. The RX And supercycle identifiable from JD 2456876 to JD 2457042 in which every fourth outburst is a precursor superoutburst.

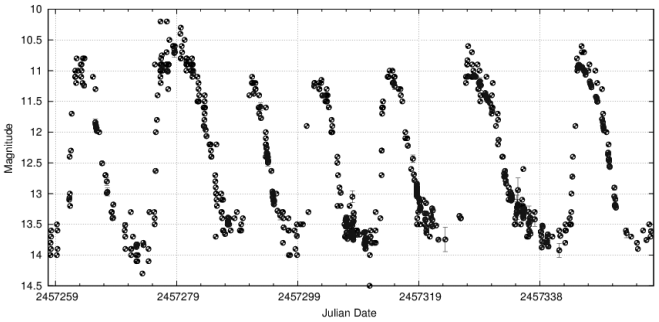

Figure 3. Light curve of RX And from 24 August 2015 to 1 December 2015.

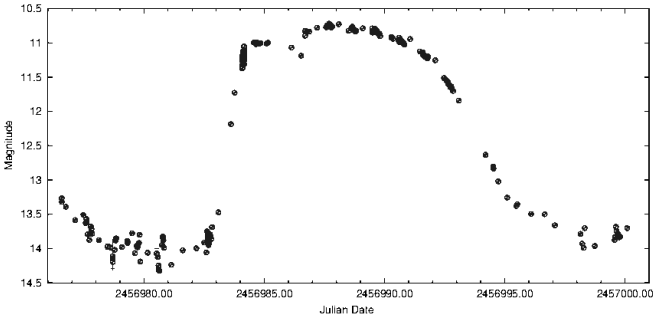

Figure 4. RX And superoutburst at JD 2456987. The superoutburst of about 10.7 magnitude is superpositioned on the precursor normal outburst of about 11.0 magnitude.

5. Conclusion

RX And has essentially exhibited features of all types of dwarf novae over the last two decades. The basic question is whether the different types of dwarf novae represent the phases of the development of objects, through which phases every dwarf nova or UGZ dwarf nova passes, or whether it is a special characteristic of RX And. Further examinations have to be carried out to establish whether or not the supercycle in the star remains stable and unchanged, and whether or not it simultaneously preserves standstills that are typical to UGZ types.

6. Acknowledgements

Without the valuable help and support of László L. Kiss this paper could not have been prepared.

References

Cannizzo, J. K., Smale, A. P., Wood, M. A., Still, M. D., and Howell, S. B. 2012, *Astrophys. J.*, **747**, 117.

Godon, P., and Sion, E. M. 2003, *Astrophys. J.*, **586**, 427.

Kafka, S. 2015, observations from the AAVSO International Database (https://www.aavso.org/aavso-international-database).

Kato, T., and Osaki, Y. 2013, *Publ. Astron. Soc. Japan*, **65**, 97.

Schreiber, M. R., Gänsicke, B. T., and Mattei, J. A. 2002, *Astron. Astrophys.*, **384**, L6.

Simonsen, M., *et al.* 2014, *J. Amer. Assoc. Var. Star Obs.*, **42**, 177.

Templeton, M. 2007, AAVSO variable star of the season (VSOTS; https://www.aavso.org/vsots_rxand).

Analysis of the Petersen Diagram of Double-Mode High-Amplitude δ Scuti Stars

Riccardo Furgoni
Keyhole Observatory MPC K48, Via Fossamana 86, S. Giorgio di Mantova (MN), Italy, and AAMN Gorgo Astronomical Observatory MPC 434, S. Benedetto Po (MN), Italy; riccardo.furgoni@gmail.com

Received December 31, 2015; revised February 9, 2016; accepted February 22, 2016

Abstract I created the Petersen diagram relative to all the Double Mode High Amplitude δ Scuti stars listed in the AAVSO's International Variable Star Index up to date December 29, 2015. For the first time I noticed that the ratio between the two periods P1/P0 seems in evident linear relation with the duration of the period P0, a finding never explicitly described in literature regarding this topic.

1. Introduction

Within the wide range of pulsating variables there is a group with a very large population: the δ Scuti stars. It is a very heterogeneous group composed of stars with radial and non-radial pulsations and normally small amplitudes variations. Nevertheless a small group of stars represents a special subtype: the Double-Mode High-Amplitude δ Scuti stars (from now HADS(B)), characterized by pulsations of higher intensity and a ratio between the period of the fundamental mode (P0) and first overtone (P1) around the value 0.77. The ratio between the two periods has been for a long time the main parameter to identify a HADS(B) compared to a simple HADS. But is there a more complex relation between P0 and P1/P0? In recent years the two major contributions that have attempted to find an extensive model capable to explain the link between the period of the fundamental mode (usually between 0.05 and 0.25 day) and the period ratio P1/P0 were those by Petersen and Christensen-Dalsgaard (1996) and by Poretti *et al.* (2005).

It should be noted, however, that only 7 HADS(B) were used for the model validation in the paper published by Petersen and Christensen-Dalsgaard, instead of 25 stars used in the paper by Poretti *et al.*

With regard to the relationship between the duration of the fundamental mode (P0) and the ratio between this and the first overtone (P1/P0), the first cited paper presents a model (their Figure 5) that predicts a peak value of the ratio around 0.774, which corresponds to log P0 = –0.9. For both increasing and decreasing duration of P0, the model predicts a lower ratio that becomes equal to 0.764 for values of log P0 = –0.55 and equal to 0.770 for log P0 = –1.1. In extreme simplification the model is similar to a downward parabola shape with the vertex (high ratio) for HADS with log P0 = –0.9.

In the paper published by Poretti *et al.* (their Figure 4) the model predicts a ratio characterized by a long standstill between log P0 = –1.30 and log P0 = –0.90. For the shortest period the ratio is increasing (0.778 for SX Phe itself) while for longer periods the ratio is decreasing (0.765 for GSC 04257-00471). In extreme synthesis the result of this model is to identify a direct relationship between the duration of the period and ratio (short periods have higher ratios while long periods have lower ratios) but considering the ratio stable for values between log P0 = –1.30 and log P0 = –0.90. The ratio's variability is mainly explained by lower metallicity for the higher values and in lower masses for the lower values.

On the other side I think it is important to mention the work of Pigulski *et al.* (2006) concerning the analysis of the data obtained from the OGLE-II (Udalski *et al.* 1997) and MACHO (Allsman and Axelrod 2001) projects. In this paper, the authors identify several other HADS(B) and publish a much more detailed Petersen diagram of the work here previously mentioned. However, while deciding to put in direct relation the duration of P0 and the ratio P1 / P0 (not a common choice as the diagram is normally realized with the logarithm of the fundamental period), they do not give any observations concerning a possible linear relation between the data nor, of course, its computed equation.

2. The Petersen diagram of HADS(B) stars

I decided to create a new Petersen's diagram using data from the AAVSO International Variable Star Index (Watson *et al.* 2014*)* related to 85 HADS(B), many of them completely unknown only five years ago. The period ratio was calculated by the author when not present in literature or simply reported when present. From these HADS(B) 8 stars were excluded for the following reasons:

- V798 Cyg: first and second overtone pulsator (Musazzi *et al.* 1998)
- V1719 Cyg: first and second overtone pulsator (Musazzi *et al.* 1998)
- VZ Cnc: first and second overtone pulsator (Fu and Jiang 1999)
- 1SWASP J211253.68+331734.3: probable second and third overtone pulsator (Khruslov 2014)
- ASAS J205850+0854.1: probable second and third overtone pulsator (Khruslov 2011)
- V1553 Sco: probable second and third overtone pulsator (Khruslov 2009)
- V526 Vel: probable second and third overtone pulsator (Khruslov 2011)

- V823 Cas: anomalous HADS because "the periods of the stars are in a transient, resonance affected state, thus do not reflect the true parameters of the object that is in effect a triple-mode pulsating variable." (Jurcsik *et al.* 2006)

The full list of stars used (as well as those not included) to create the Petersen's diagram is presented in Table 1, ordered by increasing P0.

The resulting diagram is shown in Figure 1, where the x-axis represents the log of P0 and the y-axis the ratio between P1 and P0.

Although the purpose of creating a new model capable of predicting the variation of the period and the ratio on the basis of the physical parameters of the star is outside the scope of this work, in observing the Petersen's diagram relative to all the HADS considered we may notice that the relationship between P0 and the period ratio does not appear as predicted by Petersen and Christensen-Dalsgaard (1996) and does not present even the long standstill described by Poretti *et al.* (2005).

Passing from an x-axis expressed as log P0 to an axis simply expressed in days, we notice that in fact the data seem well fitted by a straight line (red line), suggesting a possible linear relationship between the two factors as presented in Figure 2.

A greater scattering is certainly evident for the shortest periods and some stars are markedly outside the line of fit. However, considering the number of stars used for this plot

Table 1. List of stars used (as well as those not included) to create the Petersen's diagram, ordered by increasing P0.

Name	*R. A. (J2000)*			*Dec. (J2000)*			*P0 duration (d)*	*P1 duration (d)*	*P1/P0 ratio*
	h	*m*	*w*	°	′	″			
2MASS J06451725+4122158	06	45	17.25	+41	22	15.9	0.0500071	0.0386898	0.77369
LINEAR 9328902	13	35	49.76	+26	55	16.7	0.05174768	0.04046822	0.78203
[SIG2010] 3269918	20	59	27.28	–01	13	49.0	0.052376	0.040885	0.78061
NSVS 10590484	15	13	22.01	+18	15	58.3	0.0541911	0.0419105	0.77338
USNO–B1.0 0961-0254829	15	52	51.38	+06	06	06.1	0.05492	0.042667	0.77689
SSS_J095657.2-231722	09	56	57.19	–23	17	22.9	0.0566708	0.0442543	0.78090
V879 Her	17	31	12.72	+28	03	16.8	0.0568926	0.044128	0.77564
[MHF2014] J336.0969-15.6349	22	24	23.25	–15	38	05.5	0.057182	0.044534	0.77881
TSVSC1 TN-N231330220-6-67-2	08	58	54.72	+15	22	09.7	0.0576289	0.044596	0.77385
ASAS J061518+0604.2	06	15	17.73	+06	04	12.6	0.0580806	0.044828	0.77182
GSC 02008-00003	14	22	31.21	+24	34	57.0	0.059596	0.046136	0.77415
SDSS J151253.97+231748.4	15	12	53.99	+23	17	48.3	0.06001381	0.0467412	0.77884
GSC 07243-00871	12	08	49.77	–36	33	11.1	0.060031	0.04648	0.77427
BPS BS 16084-151	16	29	40.31	+57	20	33.3	0.06114265	0.0475034	0.77693
LINEAR 1683151	11	32	05.40	–03	48	27.5	0.0618462	0.04820869	0.77949
CSS_J213533.0+124341	21	35	32.99	+12	43	41.3	0.0630537	0.0487775	0.77359
NSVS 2577931	10	55	02.50	+61	42	17.2	0.06404409	0.0496142	0.77469
NSV 7805	16	32	20.12	–02	12	08.3	0.064604	0.050699	0.78477
OGLE BW2 V142	18	02	18.04	–30	08	11.4	0.066041	0.051404	0.77836
NSVS 2684702	13	45	21.66	+54	11	51.2	0.06794351	0.0526002	0.77418
SSS_J095011.1-244057	09	50	11.12	–24	40	58.0	0.0683901	0.0530193	0.77525
SEKBO 112944.737	20	10	22.51	–23	10	59.7	0.0688009	0.0532926	0.77459
LINEAR 16586778	16	13	57.55	+28	28	57.2	0.070751	0.055701	0.78728
V803 Aur	06	12	13.90	+31	48	24.4	0.0710556	0.0550312	0.77448
FASTT 8	00	39	09.42	+00	40	12.1	0.0730198	0.0571184	0.78223
V1392 Tau	04	26	05.90	+01	26	26.2	0.07443025	0.05790307	0.77795
KID 2857323	19	29	49.16	+38	01	21.7	0.07618	0.05897	0.77409
CSS_J214745.8+122726	21	47	45.78	+12	27	26.6	0.07820144	0.06062011	0.77518
[SIG2010] 2345453	21	29	52.69	–01	10	18.9	0.080586	0.0624379	0.77480
OGLE BW1 V207	18	02	14.98	–29	54	08.8	0.085601	0.066234	0.77375
MACHO 116.24384.481	18	13	16.45	–29	49	27.0	0.086914	0.06716	0.77272
GSC 07460-01520	20	33	38.54	–32	55	03.6	0.087011	0.068152	0.78326
NSVS 7293918	07	44	38.60	+29	12	22.8	0.088535	0.068501	0.77372
GSC 03693-01705	02	12	19.83	+57	00	16.4	0.09108389	0.0704693	0.77367
MACHO 115.22573.263	18	09	00.48	–29	14	30.9	0.091754	0.070871	0.77240
RV Ari	02	15	07.46	+18	04	28.0	0.0931281	0.0719466	0.77256
QS Dra	15	21	34.64	+61	29	22.7	0.09442318	0.07304432	0.77358
LINEAR 2653935	11	59	42.51	+06	08	22.0	0.09520999	0.07460334	0.78357
GSC 03949-00386	20	19	44.95	+58	29	20.0	0.095783796	0.073937974	0.77193
ASAS J094303-1707.3	09	43	02.81	–17	07	15.9	0.0991782	0.07651564	0.77150
USNO–A2.0 1425-12623576	21	59	23.24	+59	24	56.9	0.1027306	0.079165	0.77061
MACHO 114.19969.980	18	02	52.20	–29	30	24.5	0.103272	0.079811	0.77282
MACHO 119.19574.1169	18	02	00.37	–29	48	43.2	0.1068464	0.082722	0.77421
GSC 03887-00087	17	08	14.77	+52	53	53.4	0.107183	0.082932	0.77374
ASAS J182536-4213.6	18	25	36.26	–42	13	35.8	0.1071934	0.0821611	0.76648
[SIG2010] 2196466	21	36	30.17	–00	21	27.6	0.107404	0.083675	0.77907
BP Peg	21	33	13.53	+22	44	24.3	0.109543375	0.08451	0.77148
V899 Car	11	09	52.24	–60	57	56.7	0.1108014	0.0858512	0.77482

(Table 1 continued on next page)

Table 1. List of stars used (as well as those not included) to create the Petersen's diagram, ordered by increasing P0, cont.

Name	R. A. (J2000) h m w	Dec. (J2000) ° ′ ″	P0 duration (d)	P1 duration (d)	P1/P0 ratio
MACHO 162.25343.874	18 15 16.33	–26 35 40.2	0.111281	0.085905	0.77196
AI Vel	08 14 05.15	–44 34 32.9	0.11157411	0.08620868	0.77266
ASAS J231801-4520.0	23 18 01.14	–45 19 55.0	0.1150105	0.0889176	0.77313
2MASS J18294745+3745005	18 29 47.55	+37 45 01.5	0.116576	0.090297	0.77458
V1393 Cen	13 57 15.60	–52 55 22.6	0.1177831	0.0908322	0.77118
NSV 9856	17 56 00.20	–30 42 46.6	0.118488	0.0912733	0.77032
MACHO 128.21542.753	18 06 35.93	–28 39 31.3	0.120052	0.09254	0.77083
BPS BS 16553-0026	10 52 48.49	+41 54 35.3	0.125508	0.096953	0.77248
MACHO 114.19840.890	18 02 31.85	–29 27 03.9	0.125566	0.096789	0.77082
ASAS J152315-5603.7	15 23 15.43	–56 03 43.2	0.1267467	0.0976718	0.77061
GSC 04757-00461	05 23 54.48	–03 07 32.3	0.1325305	0.1019376	0.76916
GSC 02860-01552	03 16 02.70	+43 20 34.3	0.13831414	0.10675322	0.77182
V1384 Tau	03 54 07.27	+07 59 15.4	0.1397914	0.1073918	0.76823
V575 Lyr	18 29 43.24	+28 09 54.6	0.1455591	0.1115016	0.76602
ASAS J192227-5622.5	19 22 27.39	–56 22 28.1	0.1490898	0.1127701	0.75639
V703 Sco	17 42 16.81	–32 31 23.6	0.1499615	0.11521772	0.76832
ASAS J062542+2206.4	06 25 41.61	+22 06 19.5	0.1526484	0.117307	0.76848
V403 Gem	06 44 01.06	+22 44 31.7	0.15338	0.117698	0.76736
NSV 14800	00 01 16.22	–60 36 57.1	0.1578385	0.122071	0.77339
USNO–B1.0 1329-0132547	04 44 37.78	+42 54 34.4	0.16189	0.12413	0.76676
GSC 03949-00811	20 26 01.74	+59 30 53.5	0.169751	0.1300791	0.76629
GSC 04257-00471	21 26 01.11	+64 30 57.5	0.173799	0.133084	0.76574
V542 Cam	04 53 46.52	+68 28 26.5	0.174773	0.133986	0.76663
DO CMi	07 12 19.41	+09 21 02.7	0.194506	0.14862	0.76409
ASAS J194803+4146.9	19 48 02.92	+41 46 55.8	0.203636	0.155488	0.76356
VX Hya	09 45 46.85	–12 00 14.3	0.2233889	0.17272	0.77318
V733 Pup	08 18 06.98	–22 14 07.7	0.2287147	0.1742342	0.76180
AG Aqr	22 05 31.82	–22 30 00.7	0.291736	0.2222	0.76165
V829 Aql	19 46 57.29	+03 30 28.5	0.292444	0.220972	0.75560
Stars excluded					
V798 Cyg	19 38 06.90	+30 54 33.5			
V1719 Cyg	21 04 32.92	+50 47 03.3			
VZ Cnc	08 40 52.12	+09 49 27.2			
V823 Cas	00 05 42.38	+63 24 14.2			
1SWASP J211253.68+331734.3	21 12 53.69	+33 17 34.3			
ASAS J205850+0854.1	20 58 49.64	+08 54 05.3			
V1553 Sco	16 20 21.77	–35 41 16.0			
V526 Vel	09 03 13.34	–52 02 28.7			

(almost 3 times compared to the works of Poretti *et al.*) we can actually note that the greatest number of stars lie along the path of the fit line. This evidence is also highlighted by looking at the ratio residuals compared to the best-fit linear regression (the computed equation is Y = –0.084809X +0.782048) as presented in Figure 3.

In this case even a second and third polynomial fit of the residuals (red and blue lines) shows a substantial absence of trend, suggesting that a linear interpretation of the relation is possible, a fact that argues for a more accurate revision of HADS stellar models than so far proposed in the literature.

From a purely theoretical point of view I suggest this interpretion: in short period stars the metallicity could vary greatly simply because double mode pulsators with such short periods are, for example, characteristic of double-mode SX Phe stars, characterized precisely by low metallicity as explained in McNamara (2000). In other words the area with period shorter than 0.1 day is probably a transition area with stars of population I and II mixed together, and thus the stellar parameters are less homogeneous than in typical double-mode HADS. This could result in a stronger scattering that does not, however, affect the linear relation suggested.

Finally, the two stars with the highest residuals in the diagram relative to period > 0.1 day (ASAS J192227-5622.5 and VX Hya) could be stars for which the pure nature of double-mode HADS should be evaluated more carefully, as was the case for the previously cited V798 Cyg. For example, VX Hya was involved in a careful analysis by an AAVSO campaign in 2006 and 2007 and the data obtained (Templeton *et al.* 2009) showed that it is certainly an HADS(B) but characterized by unusual and not fully explained long-term amplitude variations.

The linear relationship proposed in this paper could then more easily show which stars belong to a pure type HADS(B): the presence of unusual peculiarity immediately puts the star clearly outside the best-fit line.

Of course the presence of a greater number of stars identifiable as Double-Mode HADS could significantly improve the results of this work in determining the correct parameters of this possible linear relation. I believe that much work can be done from the large amount of data collected from large

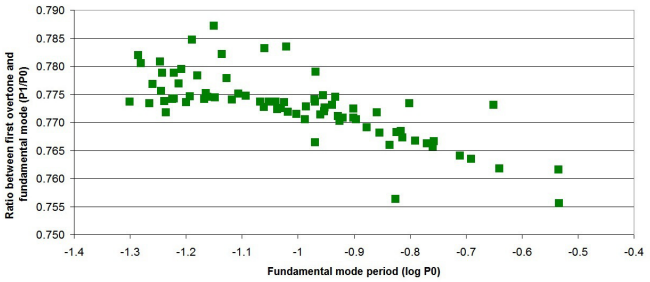

Figure 1. Double Mode HADS Petersen diagram with fundamental mode period expressed as log P0.

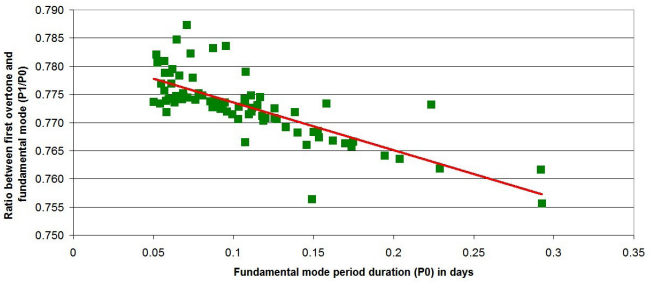

Figure 2. Double Mode HADS Petersen diagram with fundamental mode period expressed in days. The red line represent the best-fit linear regression.

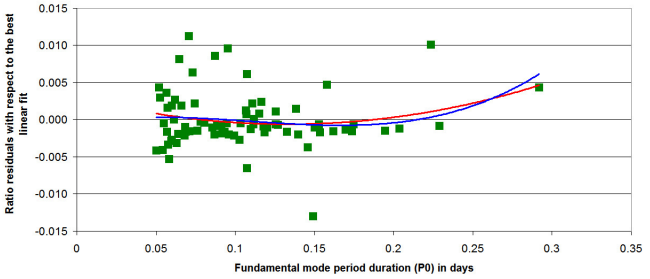

Figure 3. P1/P0 ratio residuals for the best-fit linear regression vs period duration. The red and blue lines represent, respectively, a second and third degree polynomial fit showing no relevant residual trends of the data.

photometric surveys of recent years (OGLE, SuperWASP, ASAS, and so on) and from the data of exceptional quality obtained from the Kepler satellite. This can certainly be a stimulus for new and extensive works.

3. Fit line parameters and statistical correlation evidence

The calculated equation for the best-fit line presented in Figure 2 is:

$$Y = -0.084809\ (\pm 0.008298)X + 0.782048\ (\pm 0.000995) \quad (1)$$

with an RMS error = 0.003765 and a correlation coefficient = 0.762926.

4. Acknowledgements

This work has made use of the International Variable Star Index (VSX; Watson *et al.* 2014) operated by the AAVSO, Cambridge, Massachusetts, USA. The best fit line and relative errors were calculated with the Nonlinear Least Squares Regression (Curve Fitter) courteously provided by Prof. John C. Pezzullo at http://statpages.org/nonlin.html.

References

Allsman, R., and Axelrod, T. S. 2001, arXiv, astro-ph/0108444.
Fu, J.-N., and Jiang, S.-Y. 1999, *Astron. Astrophys. Suppl. Ser.*, **136**, 285.
Jurcsik, J., Szeidl, B., Váradi, M., Henden, A., Hurta, Zs., Lakatos, B., Posztobányi, K., Klagyivik, P., and Sódor, Á. 2006, *Astron. Astrophys.*, **445**, 617.
Khruslov, A. V., 2009, *Perem. Zvezdy, Prilozh.*, **9**, 26.
Khruslov, A. V., 2011, *Perem. Zvezdy, Prilozh.*, **11**, 30.
Khruslov, A. V., 2014, *Perem. Zvezdy, Prilozh.*, **14**, 1.
McNamara, D. H. 2000, in *Delta Scuti and Related Stars*, eds. M. Breger and M. H. Montgomery, ASP Conf. Ser. 210, Astronomical Society of the Pacific, San Francisco, 373.
Musazzi, F., Poretti, E., Covino, S., and Arellano Ferro, A. 1998, *Publ. Astron. Soc. Pacific*, **110**, 1156.
Petersen, J. O., and Christensen-Dalsgaard, J. 1996, *Astron. Astrophys.*, **312**, 463.
Pigulski, A., Kołaczkowski, Z., Ramza, T., and Narwid, A. 2006, *Mem. Soc. Astron. Ital.*, **77**, 223.
Poretti, E., *et al.* 2005, *Astron. Astrophys.*, **440**, 1097.
Templeton, M. R., Samolyk, G., Dvorak, S., Poklar, R., Butterworth, N., and Gerner, H. 2009, *Publ. Astron. Soc. Pacific*, **121**, 1076.
Udalski, A., Kubiak, M., and Szymanski, M. 1997, *Acta Astron.*, **47**, 319.
Watson, C., Henden, A. A., and Price, C. A. 2014, AAVSO International Variable Star Index VSX (Watson+, 2006–2016; http://www.aavso.org/vsx).

Period Analysis, Photometry, and Astrophysical Modelling of the Contact Eclipsing Binary BC Gruis

David J. W. Moriarty
School of Mathematics and Physics, The University of Queensland, QLD 4072, Australia; djwmoriarty@bigpond.com

Received January 20, 2016; revised March 10, 2016 and April 19, 2016; accepted April 20, 2016

Abstract BC Gruis is a W UMa-type contact binary system of the W-subtype with the primary minimum 0.1 magnitude fainter than the secondary minimum. The period is currently 0.3073060 ± 0.0000001 day; it was 4 seconds longer between 1986 and 1991. There were small modulations of 0.001–0.002 day in the Observed–Calculated diagram due to asymmetry in the light curves, most likely caused by star spots. An astrophysical model of the system was developed with a mass ratio of 1.2 determined from light curve analysis. The best fit to light curves in B, V, and I pass bands in 2014 was given by including two large cool star spots on the more massive, cooler component and 1 cool spot on the hotter star. In 2015, the asymmetry in the light curves was different and was modelled best with a hot spot on the more massive component at the neck joining the stars and 1 cool spot on the other component.

1. Introduction

The W Ursae Majoris contact eclipsing binaries have been divided into two classes: A-subtype, in which the more massive and brighter component is the hotter star, and the W-subtype, in which the more massive and brighter component is the cooler star (Binnendijk 1970). The formation and evolution of short period contact binary stars is not well understood. They are old stars whose secondary components are at an advanced stage of evolution, burning hydrogen in the shell around a small helium core, according to an evolutionary model proposed by Stępień (2006). Pribulla and Rucinski (2006) comment that those with periods of less than 1 day should not exist, and suggest they may have formed in triple or larger multiple systems, where angular momentum could be transferred to the distant component, especially if it were in an eccentric orbit that brought it close to the binary.

BC Gruis is a short period W UMa-type contact system of the W-subtype with the components displaying uneven eclipse depths (Plewa and Kałużny 1992). Dall *et al.* (2007) found that it is a triple system with spectral types of approximately K0, K0, and K components. They reported rotational velocities ($v \sin i$) = 165 ± 50 km s^{-1} and 142 ± 50 km s^{-1} for the binary, and ($v \sin i$) = 6 ± 3 km s^{-1} for the third member of the system. An astrophysical model based on a mass ratio of 1.77 was developed by Plewa and Kałużny (1992) before the spectral types were determined and the third component was discovered.

In the *General Catalogue of Variable Stars* (GCVS) the period of BC Gru is listed as 0.26617 day (Kholopov *et al.* 1985). Plewa and Kałużny determined the period to be 0.307356 ± 0.000019 day from their 1986 data. Samec and Becker (1993) determined four times of minimum in 1991 and calculated the period to be 0.30735687 ± 0.00000004 day. They cited a 1988 report by Gomez and colleagues in Argentina of 15 unpublished epochs of minima and an ephemeris with a period of 0.30731 ± 0.00001 day.

The aims of the present study were to determine an accurate, current period from the times of minimum of both primary and secondary eclipses and update the ephemeris of BC Gru. An additional aim was to develop an astrophysical model based on detailed photometric light curves obtained in 2014 and 2015.

2. Methods, observations, and analysis

The instruments used for photometry were a 356-mm Schmidt-Cassegrain telescope with a Moravian G3-6303 charge-coupled device (CCD) camera with exposures of 40 seconds in the B, and 20 seconds in the V and I filters, respectively. The number of observations was usually about 240 each night in each filter. On some nights, only the V and I filters were used in order to obtain faster cadences for more accurate determinations of the times of minima. See Moriarty (2015) for full details of the imaging procedures and photometric analyses. Details of the comparison and check star positions and magnitudes are given

Table 1. Magnitudes and color indices of BC Gru, comparison, and check stars used in this work.

Star	*R.A. (2000)* *h m s*	*Dec. (2000)* ° ‘ “	*B*	*V*	*Ic*	*B–V*	*V–Ic*
TYC 8449 00652-1	22 44 48.725	–48 07 47.22	11.663	10.818	9.893	0.845	0.925
error			0.01	0.051	0.011	0.061	0.062
TYC 8449 00771-1	22 44 37.322	–47 59 38.22	11.879	11.355	10.757	0.524	0.598
error			0.009	0.041	0.02	0.029	0.061
BC Gru	22 44 49.11	–48 10 13.0	11.473	10.662	9.744	0.811	0.918
error			0.145	0.092	0.358	0.503	0.45

Source: APASS DR9 (Henden et al. 2015). The Ic magnitudes were calculated from the Sloan g and i values with the formula $Ic = i - 0.3645 - 0.0743 \times (g-i) + 0.0037 \times (g-i)^2$ *(Munari et al. 2014).*

in Table 1. The epochs and times of minima were determined from a 7-order polynomial fit to the light curves spanning about 1 hour each side of the minima in PERANSO (Vanmunster 2013). These values were analyzed by least squares linear regression in Microsoft EXCEL. Phase-magnitude light curves were produced in PERANSO and exported for modelling.

Values for the period of BC Gru were also determined by two methods using data collected during the All Sky Automated Survey (ASAS) (Pojmański 2002). Firstly, one epoch of minimum was determined from the ASAS data for each season between 2001 and 2008. All the ASAS A and B quality data were imported into PERANSO as a single set. Blocks of 1 season with > 50 observations each were activated and analyzed with the ANOVA period analysis routine. An epoch for a primary minimum within each season was calculated with the ephemeris determined in section 3.1 (Equation 2) and inserted into the Epoch value in the Info form shown in Figure 1. An actual value for the observed epoch of a primary minimum for that season was then obtained by altering the calculated value by small amounts (0.01–0.001 day) until the primary minimum was centered on phase 1.0 (Figure 1, top right). Secondly, a value for the period of BC Gru between 2001 and 2009 was determined in PERANSO by applying the ANOVA period analysis procedure to the full set of A and B quality ASAS data, that is, with all data points activated.

The epochs of minima determined in 2014 and 2015 together with the six times of minima from the ASAS data and the values for 1986–1991 published previously (section 1) were combined in an EXCEL spreadsheet for analysis (Table 2).

Astrophysical models of the BC Gru system for two complete light curves obtained on 2014-09-10 and 2015-09-08 were developed with BINARY MAKER 3.0 (Bradstreet and Steelman 2004). For the modelling process, the procedures described in the BINARY MAKER 3 manual, which is supplied with the software, and by Bradstreet (2005) were used. As the spectral types were reported by Dall *et al.* (2007) to be approximately K0 for both components, the effective temperature of the cooler component was set at 5040 K, as given for a K2V star by Pecaut and Mamajek (2013). The "q method" was used to find a probable mass ratio by trying a range of values for the mass ratio, inclination, fillout factor, and temperature of the hotter component.

3. Results

3.1. Period analysis

In 2014, 12 times of minima and in 2015, 18 times of minima were recorded (Table 2). The orbital period of BC Gru, determined from the times of minima in 2015 by a least squares linear regression, was 0.307305 (± 0.000002) day (Table 3). The following ephemeris was determined from the 2015 data set.

$$\text{HJD (Min I)} = 2457274.0791\ (0.0001) + 0.307305\ (0.000002) \times E \qquad (1)$$

Observed minus calculated (O–C) values for all epochs from 1959 to 2015 do not display a simple pattern, based on an ephemeris using the epoch and period in the GCVS (Figure 2a).

Table 2. BC Gru times of minima, observed minus calculated (O–C) differences in epochs, and photometric data, based on the ephemeris in Equation 2. The epoch from the GCVS was converted to heliocentric Julian days (HJD).

Year	*Cycle*	*Epoch HJD*	*Error*	*O–C*	*Error*	*Band*
1959[a]	–66578.0	2436814.29642	—	0.0313	—	—
1986[b]	–34452.5	2446686.65316	0.00007	0.0336	0.0068	V
1986[b]	–34452.0	2446686.80628	0.00027	0.0330	0.0068	V
1986[b]	–34449.0	2446687.72825	0.00019	0.0331	0.0068	V
1986[b]	–34445.5	2446688.80488	0.00019	0.0341	0.0068	V
1986[b]	–34439.5	2446690.64873	0.00032	0.0341	0.0068	V
1988[c]	–32210.0	2447375.78280	0.0001	0.0295	0.0064	V
1991[c]	–28637.0	2448473.77990	0.0004	0.0223	0.0057	V
1991[c]	–28634.0	2448474.70210	0.0003	0.0225	0.0057	V
1991[c]	–28621.0	2448478.69640	0.0003	0.0219	0.0057	V
1991[c]	–28617.5	2448479.77260	0.0003	0.0225	0.0057	V
2001[d]	–16725.0	2452134.69500	0.00211	0.0010	0.0039	V
2002[d]	–15516.0	2452505.92000	0.00211	0.0003	0.0037	V
2003[d]	–14462.0	2452829.82100	0.00211	0.0008	0.0036	V
2004[e]	–12713.0	2453367.29600	0.00211	–0.0024	0.0033	V
2005[d]	–12288.0	2453597.46700	0.00211	–0.0036	0.0032	V
2007[d]	–9631.0	2454314.41500	0.00211	–0.0005	0.0028	V
2008[d]	–8595.0	2454632.78100	0.00211	–0.0035	0.0027	V
2010[f]	–6103.0	2455398.58800	0.003	–0.0031	0.0032	V
2014	–1116.5	2456930.97436	0.00114	0.0019	0.0012	V
2014	–1116.5	2456930.97363	0.00106	0.0012	0.0011	B
2014	–1116.5	2456930.97445	0.00133	0.0020	0.0014	I
2014	–1116.0	2456931.12715	0.00115	0.0011	0.0012	V
2014	–1116.0	2456931.12722	0.00111	0.0011	0.0011	B
2014	–1116.0	2456931.12745	0.00121	0.0014	0.0012	I
2014	–1064.5	2456946.95300	0.00116	0.0007	0.0012	V
2014	–1064.5	2456946.95342	0.00128	0.0011	0.0013	B
2014	–1064.5	2456946.95355	0.00147	0.0012	0.0015	I
2014	–1064.0	2456947.10552	0.00097	–0.0005	0.0010	B
2014	–1064.0	2456947.10617	0.00112	0.0002	0.0012	V
2014	–1064.0	2456947.10676	0.00112	0.0008	0.0012	I
2015	–97.5	2457244.11610	0.00151	–0.0011	0.0015	I
2015	–97.5	2457244.11729	0.00126	0.0001	0.0013	V
2015	–97.5	2457244.11804	0.00171	0.0008	0.0017	B
2015	–97.0	2457244.27030	0.00133	–0.0006	0.0013	I
2015	–97.0	2457244.27043	0.00107	–0.0005	0.0011	V
2015	–97.0	2457244.27060	0.00143	–0.0003	0.0014	B
2015	–71.0	2457252.26003	0.00092	–0.0008	0.0009	V
2015	–71.0	2457252.26021	0.00107	–0.0006	0.0011	I
2015	–0.5	2457273.92547	0.00133	–0.0004	0.0013	I
2015	–0.5	2457273.92569	0.00136	–0.0002	0.0014	V
2015	–0.5	2457273.92648	0.00144	0.0006	0.0014	B
2015	0.0	2457274.07837	0.00090	–0.0012	0.0009	V
2015	0.0	2457274.07883	0.00104	–0.0007	0.0011	B
2015	0.0	2457274.07904	0.00107	–0.0005	0.0011	I
2015	0.5	2457274.23204	0.00136	–0.0012	0.0014	V
2015	0.5	2457274.23275	0.00133	–0.0005	0.0013	B
2015	0.5	2457274.23282	0.00134	–0.0004	0.0014	I
2015	91.0	2457302.04394	0.00113	–0.0005	0.0011	I
2015	91.0	2457302.04398	0.00118	–0.0004	0.0012	V

Source: (a) Kholopov et al. *1985; (b) Plewa and Kaluzny 1992; (c) Samec and Becker 1983; (d) ASAS, this work; (e) ASAS, Paschke and* Luboš Brat *2004; (f) Paschke 2010.*

Table 3. Orbital periods of BC Gru. The periods in rows 1 and 2 were determined by a least squares linear regression of the epochs and cycles given in Table 2, with the ephemeris in Equation 2. The period in row 3 was determined from the full set of ASAS A and B quality data for the years 2001–2009 (see section 2, Methods).

Years	*Period day/cycle*	*Standard error*	*Number of observations*
2015	0.307305	0.000002	18
2001–2015	0.3073060	0.0000001	36
2001–2009	0.307306	0.000001	510

With the updated ephemeris in Equation 1, a pattern is apparent that suggests there have been period changes (Figure 2b). (If there were no changes in the period, then all values would lie on a single straight line.) The O–C values for the 1986–1991 era have a negative slope, whereas the slope of the O–C values from 2001–2015 is positive (Figure 2b). When all the epochs of minima from 2001 to 2015 were analyzed with a linear regression the period was determined as 0.307306 day (Table 3).

The period calculated from the full set of ASAS A and B quality data was also 0.307306 day (Table 3). Thus the period of the binary system since 2001 is 0.307306 day. A revised ephemeris is shown in Equation 2. The O–C values for the 2001–2015 era differed from zero mostly by less than 0.0015 day, although the ASAS values had larger errors (Figure 2c and Table 2). In contrast, the O–C values from 1986 to 1991 differ from zero by more than 0.02 day (Table 2). The equations for linear regression lines fitted to the two sets of data are shown in Figure 2c.

$$\text{HJD (Min I)} = 2457274.0796\ (0.0002) + 0.3073060\ (0.0000001) \times E \quad (2)$$

A second order polynomial equation (Equation 3) was fitted to the O–C values for the 1986–2015 data as shown in Figure 2d.

$$y = 5 \times 10^{-11}\, x^2 + 7 \times 10^{-7}\, x + 0.0003 \quad (3)$$

The positive value for the quadratic coefficient indicates an apparent period increase of 1 second per 100 years.

3.2. Light curve analysis and modelling

Examples of the light curves in the B, V, and I pass bands are shown in Figure 3. The difference in magnitudes of the primary minima, which were 0.11 to 0.12 fainter than those of the secondary minima in the B and V bands, and 0.07 magnitude fainter in the I band, indicate that the primary star is the cooler star by several hundred degrees (Table 4). The magnitudes at phase 0.25 were brighter than those at phase 0.75 by 0.01 magnitude in B and I and 0.02 magnitude in the V band pass in 2014, but did not differ in 2015 (Table 4). The color index varied during the cycle with a noticeable asymmetry in reddening during and after the primary eclipse in 2015 compared to that in 2014; the asymmetry is enhanced in the B–I index (compare Figures 4a and 4b). The shape of the light curve and the differences in the B–V, B–I, and V–I indices between the primary eclipse (phase 0) and phase 0.25 suggest that the contact zone on the primary component was hotter in 2015 than in 2014. At phase 0 in 2015, BC Gru was 0.03 magnitude brighter in the B band than in 2014 (Table 4). The precision of the aperture photometry was generally ± 1–2 millimagnitudes in the V and I pass bands and 3–4 millimagnitudes in the B pass band.

An astrophysical model with a mass ratio of 1.2 and inclination of 69° gave the best fit to the light curves in the V pass band, with the lowest sums of squared residuals of 0.013 for the light curves in 2014 and 0.007 in 2015 (Figure 5). The residual values were larger with inclinations of 67°, 68°, or 70°. Details of the parameters for the models, including third light, are shown in Table 5. Star spots had to be included before good fits to the observed light curves were obtained. In 2014, the best fit was obtained with two cool spots on the secondary component and one cool spot on the primary component (Figure 6 and Table 6). In contrast, the best fit to the light curves in 2015 was given by a hot spot at the contact zone on the primary star and one cool spot on the secondary star (Figure 7 and Table 6). The model parameters in Table 5 also provided good fits to the light curves in the B and I bandpasses in 2014 and 2015, with one exception: a temperature factor of 0.84 for the B pass band in 2014 gave a better fit for the spot at 250° longitude. The noise in the 2014 light curves around phase 0.15–0.2 is due to the higher airmass of 1.5 at the end of the observing run, compared to 1.08 at the start.

Table 4. Magnitudes of BC Gru at different phases in the orbital cycle. The standard errors at each phase are shown below each magnitude.

Date y-m-d	*Phase*	*B*	*V*	*I*	*B–V*	*V–I*	*B–I*
2014-09-30	0.00	11.804	10.944	9.972	0.860	0.972	1.832
		0.002	0.04	0.003	0.042	0.043	0.005
	0.25	11.284	10.483	9.588	0.801	0.895	1.696
		0.003	0.002	0.001	0.005	0.003	0.004
	0.50	11.676	10.841	9.901	0.835	0.940	1.775
		0.004	0.003	0.004	0.007	0.007	0.008
	0.75	11.288	10.498	9.595	0.790	0.902	1.692
		0.003	0.002	0.002	0.005	0.004	0.005
2015-09-08	0.00	11.773	10.937	9.954	0.836	0.983	1.819
		0.003	0.002	0.002	0.005	0.004	0.005
	0.25	11.271	10.488	9.576	0.783	0.912	1.695
		0.003	0.001	0.003	0.004	0.004	0.006
	0.50	11.649	10.821	9.882	0.828	0.940	1.758
		0.003	0.002	0.003	0.005	0.005	0.006
	0.75	11.275	10.488	9.583	0.787	0.904	1.691
		0.004	0.001	0.002	0.005	0.003	0.006

Table 5. Light curve model data for the models shown in Figures 6 and 7. The convention used in Binary Maker 3 for W-subtype W UMa systems, where the more massive star is the cooler component, is to invert the mass ratio.

Parameter	*Star 1*	*Star 2*
Mass ratio	1.2	1.2
Fillout	0.08	0.08
Inclination	69°	69°
Third light (B)	0.09	0.09
Third light (V)	0.12	0.12
Third light (I)	0.19	0.19
Temperature (K)	5040	5480
Gravity coefficient	0.32	0.32
Limb darkening (B)	0.87	0.81
Limb darkening (V)	0.70	0.63
Limb darkening (I)	0.46	0.41

Table 6. Star spot parameters for the light curve solutions in Figures 6 and 7. In each case, star 1 is the cooler component.

Date and Pass Band	*Star*	*Co-Latitude*	*Longitude*	*Radius*	*Temperature Factor*
2014-09-30	1	90	140	28	0.82
2014-09-30	1	90	250	28	0.82
2014-09-30	2	110	198	28	0.80
2015-09-08	1	90	2	20	1.15
2015-09-08	2	90	170	10	0.94

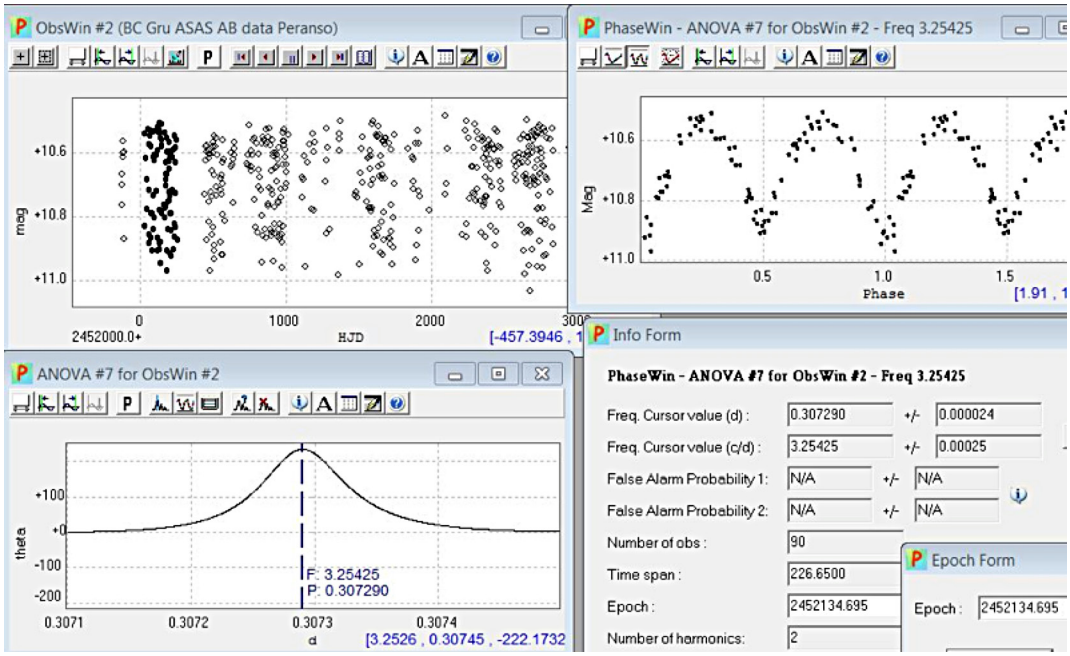

Figure 1. A composite view of 4 windows in PERANSO showing how epochs of primary eclipse minima were determined from the ASAS data (Pojmański 2002). Top right: Phase diagram for the activated 2001 dataset shown highlighted in the top left panel. The primary minimum was usually not centred on phase 1.0 by the frequency cursor in the ANOVA window (bottom left); therefore, an epoch was calculated and inserted into the Epoch tab in the Info form window (bottom right panel) and adjusted as described in section 2.

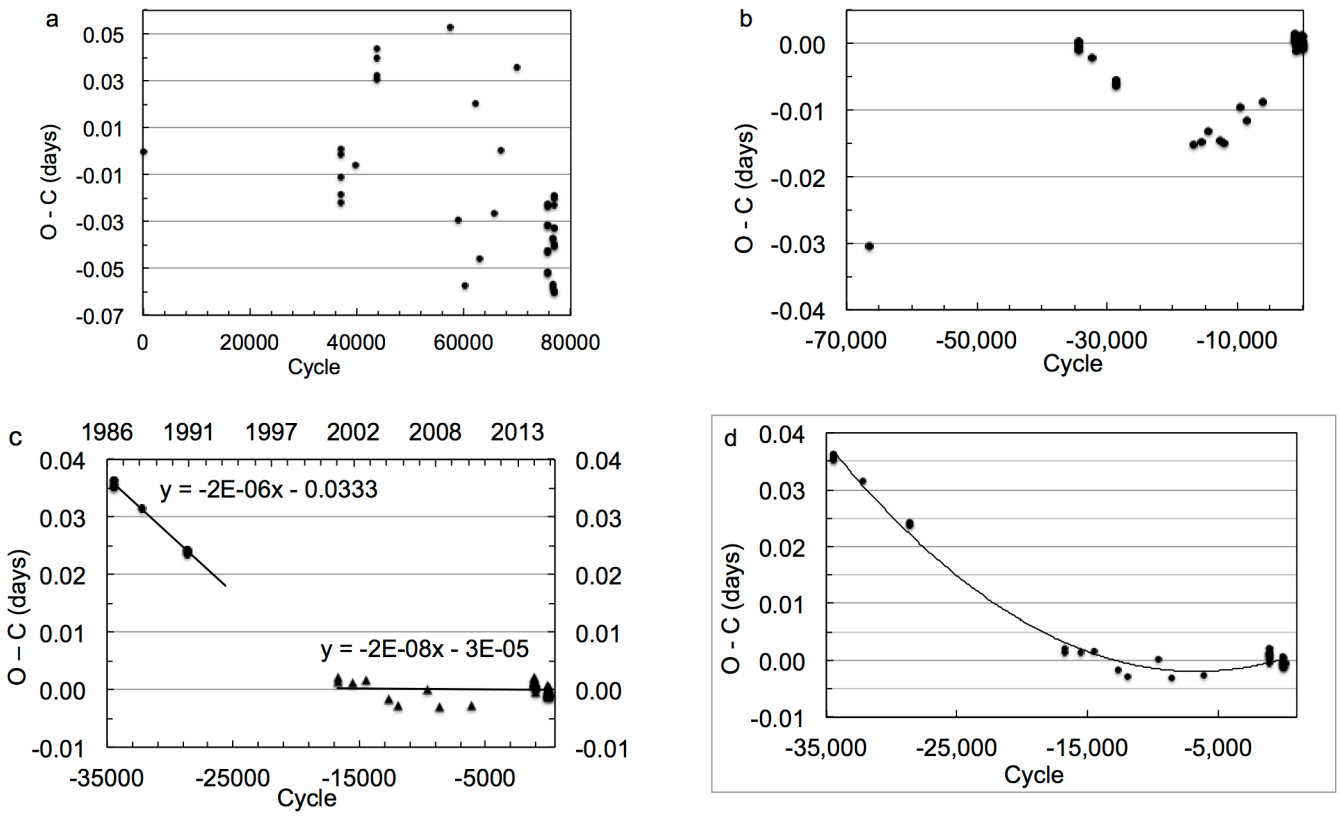

Figure 2. (a) The O–C diagram for BC Gru for the period 1959 to 2015, based on the GCVS ephemeris. (b) The O–C diagram for BC Gru for the period 1959 to 2015, based on the ephemeris in Equation 1. (c) The O–C diagram of the values given in Table 2 for the period 1986 to 2015 based on the ephemeris in Equation 2, with linear regression lines fitted for the periods of 1986–1991 and 2001–2015. (d) The O–C diagram shown in (c) with a second order polynomial fitted. See Table 2 for details of epochs and error values.

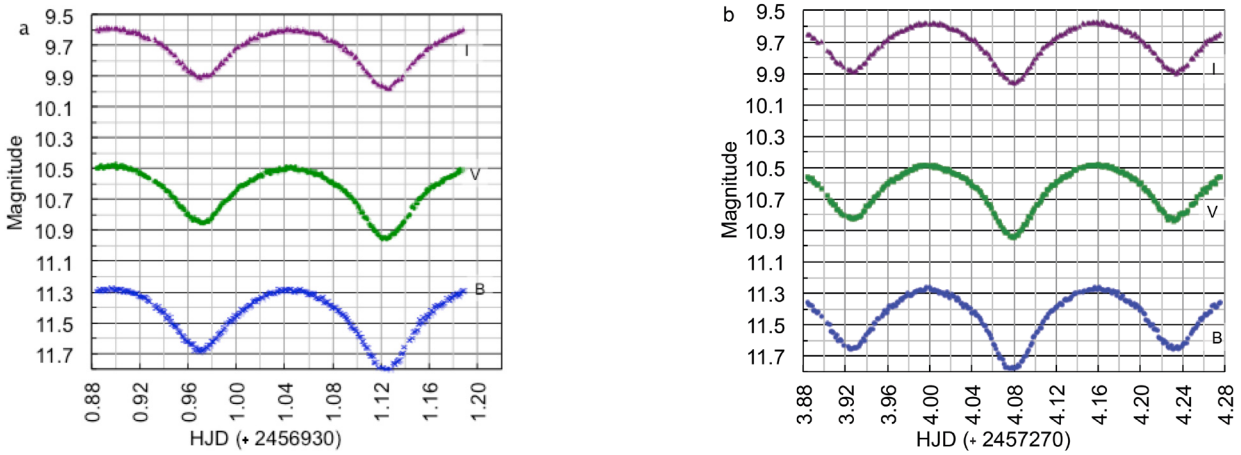

Figure 3. Light curves of BC Gru in B (x), V (●) and I (▲) pass bands on 2014-09-30 (a) and 2015-09-08 (b). Note the larger amplitude of the secondary eclipse in 2014 compared to 2015, particularly in the B pass band.

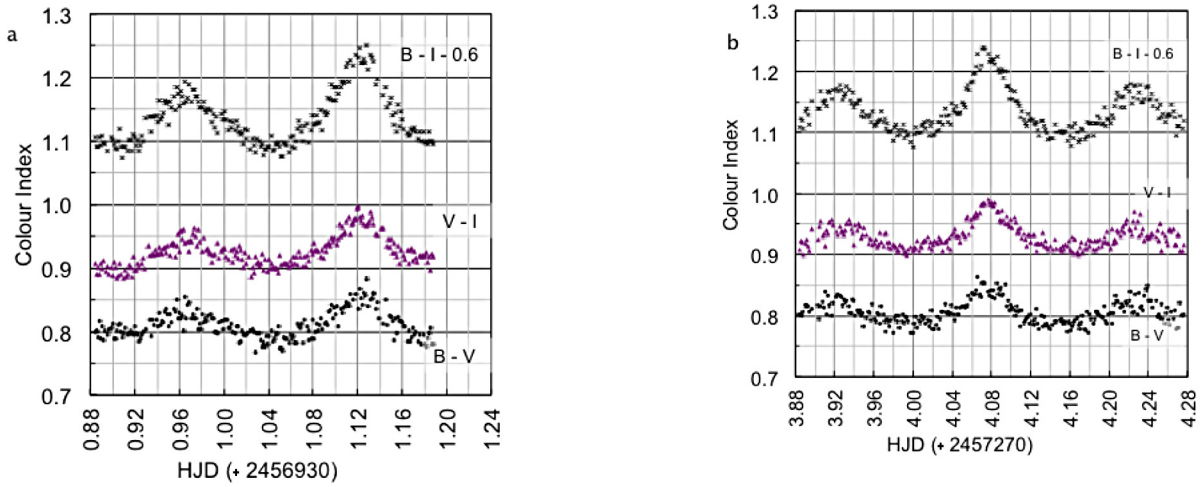

Figure 4. Color indices of the light curves observed on 2014-09-30 (a) and 2015-08-09 (b). The B–I index is offset by –0.6 magnitude.

4. Discussion

4.1. Period analysis

The period of BC Gruis is now 0.307306 day, but as described in the Introduction, the period was reported to be 0.26617 day in 1959 and then between 1986 and 1991, it was found to be 1 hour longer, at 0.307356 day. The period of BC Gru, determined by linear regression analysis of the epochs of minima that included both primary and secondary eclipses for the interval from 2001 to 2015, differs by more than two standard errors from the period reported by Plewa and Kałużny (1992) and Samec and Becker (1993) (see Table 3).

Orbital period changes are studied with the aid of O–C diagrams in which the differences between observed epochs of minima and calculated epochs of minima determined from linear ephemerides are plotted against eclipse cycles. The O–C diagrams based on the updated ephemerides (Equations 1 and 2) of BC Gruis also indicate that there was a change in the period in the interval between 1991 and 2001. The small variations in O–C values between 2001 and 2015 were not due to changes in period, but to the effect of star spots and to variability in the ASAS data sets. In contrast to the decrease in period from 0.0307356 day in 1991 to its present value, the positive value of the quadratic term in the second order polynomial fit implies that there was a smooth increase (Equation 3). However, as there are not sufficient data points in the interval between 1991 and 2001, and with the large variability inherent in the ASAS data, I conclude that it is not appropriate to analyze these O–C values with a quadratic function. Furthermore, residual values from calculations of linear or polynomial functions are not meaningful when the variability in O–C values is 0.01 day or less, due to asymmetry in the light curves caused by stellar spots (as discussed below), and in the case of ASAS data, the low precision of the photometry. The observational data for the photometry in 1986, 1991, 2014, and 2015 that were used to determine times of minimum are quite different from the ASAS data. The former data sets were a series of observations over individual light curve cycles from which times of minimum can be determined accurately (provided that the computer clocks were set accurately), whereas the ASAS light curves were a composite of observations over a whole season; for example, the 2001 light curves in Figure 1 comprised 90 data points taken

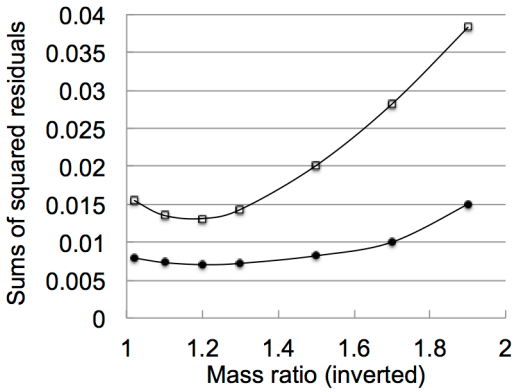

Figure 5. Graph showing the variations in best fit at an inclination of 69° to the light curves in 2014 and 2015: the sum of squared residuals for different mass ratios on 2015-09-08 (●) and 2014-09-30 (□).

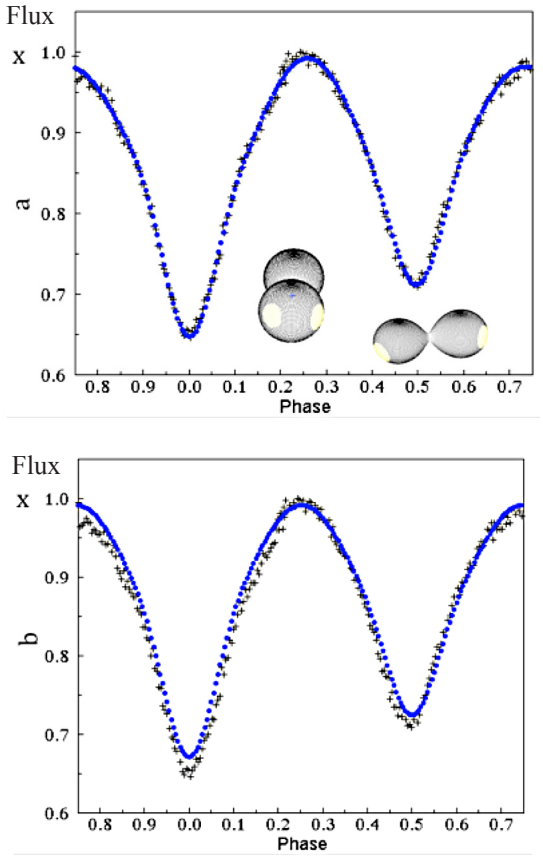

Figure 6. (a) Light curve (crosses) and model fit (blue line) of the V pass band for 2014-09-30. Insets: the binary model at phase 0 (left) showing 2 cool spots on star 1 and phase 0.3 (right) showing a cool spot on star 2. Star 1 is the larger star, on the right at phase 0.3. (b) Light curve (crosses) and model (blue line) with the same parameters as in (a), but without spots.

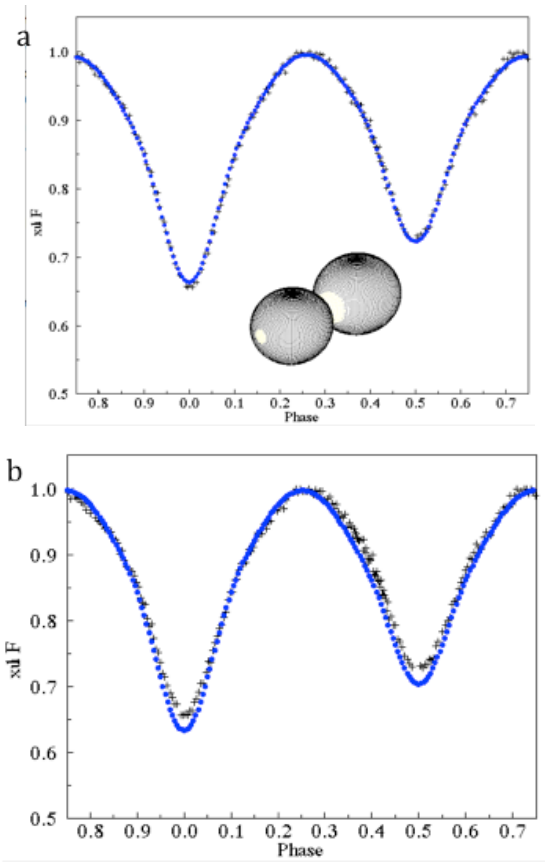

Figure 7. (a) Light curve (crosses) and best fit (blue line) of the V pass band for 2015-9-8 with 12% third light and a hot spot on star 1 around the contact zone and a cool spot on star 2. Inset: the binary model at phase 0.4. (b) Light curve (crosses) and best fit (blue line) of the V pass band for 2015-9-8 without the hot zone and zero third light.

from 735 cycles. In other words, from a statistical viewpoint, the populations of the 1986, 1991, 2014, and 2015 data are different from the populations of ASAS data.

Kalimeris *et al.* (2002) calculated the effect of star spots on O–C values and showed that they caused high frequency, low amplitude variability in the O–C diagram, generally less than 0.01 day. Thus the variability the O–C values of 0.001 to 0.002 day in 2014 and 2015 is a typical effect of star spots and similar to that found for TW Crucis (Moriarty 2015). The presence of star spots causes asymmetry in the light curves. The variability in the epochs of minima determined from some of the ASAS data was larger due to the small number of observations around the selected time of minimum (see section 2). Note that the minima shown in the top right panel in Figure 1 are a composite of minima over a time span of 226 days (Figure 1, bottom right panel). It was not possible for ASAS to provide detailed coverage of individual orbital cycles. For example, in 2001 the selected epoch was based on about 20 out of a total of 90 data points spanning about 780 cycles.

Plewa and Kałużny (1992) commented that the period of 0.26617 day, determined by Meinunger from 1959 photographic data, cannot be reconciled with the period they calculated in 1986, which is an hour longer. If the third star in the system is in a wide eccentric orbit (and not necessarily co-planar with the binary) it could affect the period during a close approach. As discussed below, the binary is a very active system in which

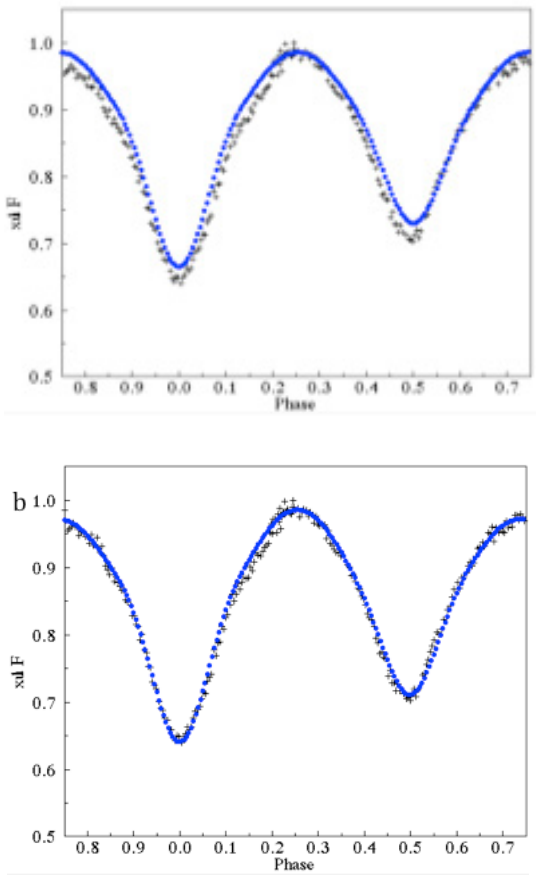

Figure 8. (a) Light curve (crosses) and model fit (blue line) of the V pass band for 2014-9-30 with mass ratio 1.77, fillout 0.011, inclination 66.9° and zero 3rd light (data from Plewa and Kałużny 1982). Teff and other factors are the same as those in Table 5. (b) Light curve (crosses) and model fit (blue line) of the V pass band for 2014-9-30 with mass ratio 1.77, fillout 0.07, inclination 69° and 8% third light and 3 spots (Table 6).

other processes could affect the period. Many more years of observations of this system are needed before more definitive conclusions can be drawn concerning period changes.

4.2. Light curve analysis and modelling

The differences in the light curves between 2014 and 2015, and in particular the probable higher temperature at the contact zone in 2015, suggest that mass or energy transfer is episodic, which would affect the period. Kałużny (1986) found that the asymmetry in the light curve of AU Ser could be explained by the presence of a hot zone at the neck between its components. If the epoch and period listed in the GCVS were correct, they provide further evidence of episodic or sudden changes in the period of BC Gru. Unfortunately, the original data and publication reference given in the GCVS are not available for study.

The analysis of O–C values over longer time scales can reveal period changes or modulations caused by other factors, including a light travel time effect due to a third component, mass transfers or loss, magnetic braking and angular momentum loss, and to gravitational quadrupole moment changes (Lanza and Rodonò 1999). Many more years of observation are required to determine the effects of these and of the third component on the orbital period of the BC Gru binary system. The differences between the light curves in 2014 and 2015 indicate that BC Gru is a chromospherically active system with stellar spots varying on short time scales. Angular momentum and mass loss through the effects of magnetic braking would be expected to occur in this late-type contact binary (see Hilditch (2001) for a discussion of this process). The model solutions derived here are not unique; they are preliminary analyses of the 2014 and 2015 light curves and await better data for the spectral types and spectroscopic mass ratio. The models are in agreement with the conclusion of Plewa and Kałużny (1992) that BC Gru is a W-subtype W-UMa binary. They developed a model with effective temperatures of 5430 K and 5072 K based on B–V values of 0.748 at quadrature phases and an inclination of 66.9 ± 2.8°. However, they determined that a mass ratio of 1.77 gave the best fit to their light curves. They commented that their modelling of BC Gru implied that the surface brightness of the components was not symmetrical, which would be expected when star spots are present.

Although Dall *et al.* (2007) reported the spectral types to be about the same for both components, the difference in V magnitudes of 0.11 between primary and secondary minima indicates a difference in their effective temperatures of several hundred degrees. Therefore, with the effective temperature set for the cooler component at 5040 K, typical of a K2 star on the main sequence, the model indicates that the temperature of the hotter component would be 5480 K, i.e. about type G8. As the best fits for third light to the model required a contribution of 10% greater flux in the infrared band than in the blue, the third component must be a later spectral type than the binary components (Table 5).

As the stars would be tidally locked, their rotational velocities are equal to their orbital velocities. The rotational velocities determined by Dall *et al.* (2007) have a large range of 165 ± 50 and 142 ± 50 km s^{-1}, thus giving a mass ratio of 1.16 with very wide limits. In fact, it is similar to the value of 1.2 determined photometrically for the modelling reported here. As Dall *et al.* (2007) pointed out, spectra at several different orbital phases are required to improve the spectral fitting and velocity determinations and thence improve the astrophysical model and determine absolute masses and radii.

5. Conclusions

BC Gru is a W-subtype W UMa-type contact binary system that is probably very active magnetically, as the best fits of the astrophysical models include star spots that changed in size, temperature, and number between 2014 and 2015. Its period is 0.307306 day now, but was 4 seconds longer between 1986 and 1991. Further time series observations are required to determine the effect of the third component in the system on the period of BC Gru. A longer time series of observations over several years is required to determine the influence of other causes of period change, including angular momentum and mass loss due to magnetic braking and stellar winds. High resolution spectra are needed to determine accurate and precise orbital

radial velocities and thence the mass ratio in order to check and improve the models.

6. Acknowledgements

I thank the referee, whose comments were most helpful and improved the presentation of this work. Some of the equipment was purchased with the aid of grants from the Edward Corbould Research Fund of the Astronomical Association of Queensland. This research made use of the VizieR catalogue access tool and the SIMBAD database, operated at CDS, Strasbourg, France, and the AAVSO Photometric All-Sky Survey (APASS), funded by the Robert Martin Ayers Sciences Fund. Software developed by Tom Richards and other resources from Variable Stars South (http://www.variablestarssouth.org/) were used in this research.

References

Binnendijk, L. 1970, *Vistas Astron.*, **12**, 217.

Bradstreet, D. H. 2005, in The Society for Astronomical Sciences 24th Annual Symposium on Telescope Science (May 24–26, 2005), Society for Astronomical Sciences, Rancho Cucamonga, CA, 23.

Bradstreet, D. H., and Steelman, D. P. 2004, BINARY MAKER 3, Contact Software (http://www.binarymaker.com).

Dall, T. H., *et al.* 2007, *Astron. Astrophys.*, **470**, 1201.

Henden, A. A., *et al.* 2015, AAVSO Photometric All-Sky Survey, data release 9 (http://www.aavso.org/apass).

Hilditch, R. W. 2001, *An Introduction to Close Binary Stars*, Cambridge Univ. Press, Cambridge.

Kalimeris, A., Rovithis-Livaniou, H., and Rovithis, P. 2002, *Astron. Astrophys.*, **387**, 969.

Kałużny, J. 1986, *Acta Astron.*, **36**, 113.

Kholopov, P. N., *et al.* 1985, *General Catalogue of Variable Stars*, 4th ed., Moscow.

Lanza, A. F., and Rodonò, M. 1999, *Astron. Astrophys.*, **349**, 887.

Moriarty, D. J. W. 2015, *J. Amer. Assoc. Var. Star Obs.*, **43**, 151.

Munari, U., Henden, A., Frigo, A., and Dallaporta, S. 2014, *J. Astron. Data*, **20**, 4.

Paschke, A. 2010, *Open Eur. J. Var. Stars*, **130**, 1.

Paschke, A., and Luboš Brat, B. 2004, O–C Gateway (http://var2.astro.cz/ocgate/*)*.

Pecaut, M. J., and Mamajek, E. E. 2013, *Astrophys. J., Suppl. Ser.*, **208**, 9.

Plewa, T., and Kałużny, J. 1992, *Acta Astron.*, **42**, 103.

Pojmański, G. 2002, *Acta Astron.*, **52**, 397.

Pribulla, T., and Rucinski, S. M. 2006, *Astron. J.*, **131**, 2986.

Samec, R. G., and Becker, K. 1993, *Inf. Bull. Var. Stars*, No. 3891, 1.

Stępień, K. 2006, *Acta Astron.*, **56**, 199.

Vanmunster, T. 2013, Light Curve and Period Analysis Software, PERANSO v.2.50 (http://www.peranso.com/).

TU Comae Berenices: Blazhko RR Lyrae Star in a Potential Binary System

Pierre de Ponthière
15 Rue Pré Mathy, Lesve, Profondeville 5170, Belgium; pierredeponthiere@gmail.com

Franz-Josef (Josch) Hambsch
12 Oude Bleken, Mol, 2400, Belgium

Kenneth Menzies
318A Potter Road, Framingham, MA 01701

Richard Sabo
2336 Trailcrest Drive, Bozeman, MT 59718

Received February 2, 2016; revised April 25, 2016; accepted April 28, 2016

Abstract We present the results of a photometry campaign of TU Com performed over a five-year time span. The analysis showed that the possible Blazhko period of 75 days published by the *General Catalogue of Variable Stars* is not correct. We identified two Blazhko periods of 43.6 and 45.5 days. This finding is based on measurement of 124 light maxima. A spectral analysis of the complete light curve confirmed these two periods. Besides the Blazhko amplitude and phase modulations, another long term periodic phase variation has been identified. This long term periodic variation affects the times of maximum light only and can be attributed to a light-travel time effect due to orbital motion of a binary system. The orbital parameters have been estimated by a nonlinear least-square fit applied to the set of (O-C) values. The Levenberg-Marquart algorithm has been used to perform the nonlinear least-square fit. The tentative orbital parameters include an orbital period of 1676 days, a minimal semi-major axis of 1.55 AU, and a small eccentricity of 0.22. The orbital parameter estimation also used 33 (O-C) values obtained from the SWASP survey database. Spectroscopic radial velocity measurements are needed to confirm this binarity. If confirmed, TU Com would be the first Blazhko RR Lyrae star detected in a binary system.

1. Introduction

The star TU Comae Berenices (TU Com) is classified in the *General Catalogue of Variable Stars* (Samus *et al.* 2011) as an RR Lyrae (RRab) variable star with a period of 0.4618091 day and a possible Blazhko period of 75 days. This period of 75 days was derived by Ureche (1965) from photographic observations. Using Fourier analysis of previous observations including ROTSE data (Wozniak *et al.* 2004), Sódor and Jurcisk (2005) questioned this Blazhko modulation. McGrath (1975), who observed this star at the Maria Mitchell Observatory (Nantucket, Massachusetts), did not detect a secondary modulation with a period of 75 days but one with a period of approximately 40 days.

Our results are based on 23,577 observations gathered during 150 nights between January 13, 2009, and May 23, 2015. The specifications of telescopes and CCD cameras used in this project and the number of observations for each telescope are provided in Table 1.

The CCD images were dark- and flat-field corrected with MAXIMDL software (Diffraction Limited 2004), and aperture photometry was performed using LESVEPHOTOMETRY (de Ponthière 2010), a custom software which also evaluates the SNR and estimates magnitude errors. The comparison

Table 1. Telescope and camera specifications, numbers of observations, and photometric mean uncertainties.

Location	*Observer*	*Telescope Type*	*Camera Type*	*Number of Observations*	*Mean Uncertainty (mag.)*
Cloudcroft, New Mexico	Hambsch	F/6.3 Meade 0.30m	SBIG ST9XM	17252	0.014
Mol, Belgium	Hambsch	Celestron 0.30m	SBIG ST8XME	700	0.032
Framingham, Massachusetts	Menzies	F/8 Hyperion 0.32m	SBIG STL-6303	2696	0.022
Bozeman, Montana	Sabo	F/6.8 PlaneWave 0.43m	SBIG STL-1001	906	0.019
Cloudcroft, New Mexico	de Ponthière	F/6.3 Meade 0.30m	SBIG ST-7	1301	0.022
Lesve, Belgium	de Ponthière	F/6.2 Meade 0.20m	SBIG ST-7	722	0.024

Table 2. TU Com comparison stars.

GSC Identification	*UCAC4 Identification*	*R.A. (2000) h m s*	*Dec. (2000) ° ′ ″*	*B*	*V*	*B–V*	*Reference/Check*
2527-162	606-048343	12 13 40.55	+31 00 46.22	14.868	14.167	0.701	C1
2527-073	605-049038	12 14 18.96	+30 59 22.82	15.126	14.473	0.653	C2

stars are given in Table 2. The comparison star coordinates and magnitudes in B and V bands were obtained from the UCAC4 catalog (Zacharias *et al.* 2012). All the observations have been reduced with C1 as the magnitude reference and C2 as the check star. The observations were performed with a V filter and are not transformed to the standard system. The photometric observations were uploaded by the authors to the AAVSO International Database (Kafka 2015) where they can be retrieved.

All the data with an uncertainty larger than 0.050 magnitude have been eliminated from the dataset. The observations were not limited to the time of maxima, as can be seen in the folded light curve presented in Figure 1. This light curve is folded on the pulsation period determined in the next section. The photometric uncertainties for each telescope and location are provided in Table 1.

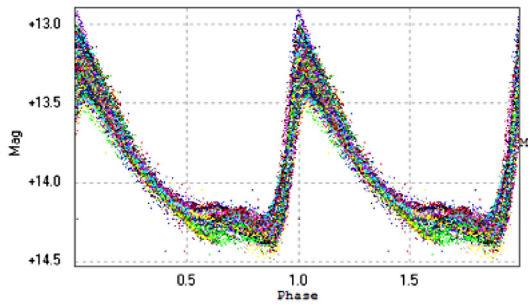

Figure 1. Folded light curve on the pulsation period.

2. Light curve maxima analysis

A custom software (de Ponthiere 2010) fitting the light curve with a smoothing spline function (Reinsch 1967) was used to measure the times and magnitudes of light curve maxima. The observed times of light maxima are compared to a linear ephemeris to get the observed minus calculated (O–C) values. The (O–C) values and M_{max} (Magnitude at Maximum brightness) of the 124 observed maxima are listed in Table 8 given in the Appendix.

A linear regression of (O–C) values has provided a pulsation period of 0.4618665 day, which has been used to establish the pulsation ephemeris.

$$HJD_{Pulsation} = (2456416.6221 \pm 0.0008) + (0.4618665 \pm 0.0000006)\, E_{Pulsation} \quad (1)$$

The origin of the ephemeris has been arbitrarily set to the highest recorded brightness maximum. The derived pulsation period is slightly different from the value of 0.4618091 published in the *General Catalogue of Variable Stars* (Samus *et al.* 2011). Figure 2 shows the (O–C) and M_{max} values in the top and bottom panels, respectively.

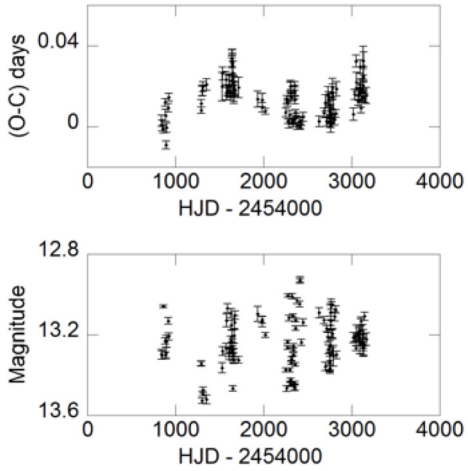

Figure 2. Top panel: O–C values, besides the Blazhko modulation of the times of maxima, a long term periodic variation is evident. Bottom panel: Magnitude at Maximum Brightness, the long term periodic variation seen in (O–C) is not apparent in the Magnitude at Maximum Brightness.

Besides the variations due to the Blazhko effect, a long term periodic variation of the times of maxima (O–C) is apparent from an inspection of Figure 2 (Top). This long term variation is not present in the magnitudes at maximum M_{max} shown in Figure 2 (Bottom). The presence of this long term variation in the (O–C) and not in the M_{max} can be explained by a light-travel time effect caused by an orbital motion around the common center of mass in a binary system.

RR Lyrae stars detected in binary systems are relatively rare; this is probably due to the technical challenges raised by the detection of the light-travel time effect in the observation datasets. At the end of the last century, TU UMa was the only one identified in a binary system (Saha and White 1990; Wade *et al.* 1999; Liska *et al.* 2015). Meanwhile, 12 RR Lyrae stars were recently discovered in the galactic bulge (Hajdu *et al.* 2015), and with data provided by the high precision photometry of the Kepler mission, other RR Lyrae stars in the galactic field have been identified as potential binary systems (Li and Qian 2014; Guggenberger and Steixner 2015). All those RR Lyrae stars are not affected by the Blazhko effect and do not show eclipses. The only RR Lyrae star detected in an eclipsing binary system is the non-classical RR Lyrae OGLE-BLG-RRLYR-02792, which has a mass of 0.26 $M_{\odot}$ (Pietrzynski *et al.* 2012).

To derive the (O–C) values, Hajdu *et al.* (2015) utilized the Hertzsprung (1919) method which compares the light curve to

Table 3. TU Com frequency spectrum components obtained from light curve maxima.

From	*Frequency* (d^{-1})	$\sigma(d^{-1})$	*Period* (d)	σ(d)	*Amplitude*	Φ (cycle)	*SNR*
(O–C) values	0.00061	1.3×10^{-4}	1634.8	356	0.00585 d	0.198	19.1
(O–C) values	0.02209	0.78×10^{-4}	45.28	0.095	0.0229 d	0.044	7.92
M_{max} values	0.02306	2.2×10^{-4}	43.37	0.42	0.108 mag.	0.056	14.8
M_{max} values	0.02204	1.1×10^{-4}	45.36	0.22	0.082 mag.	0.504	11.1

a template. This method is not appropriate for stars influenced by the Blazhko effect since their light curves do not repeat from one pulsation cycle to another. It is for this reason that Hajdu *et al.* (2015) eliminated stars impacted by the Blazhko effect from their investigations.

The periods and amplitudes of the (O–C) and M_{max} values have been determined with PERIOD04 (Lenz and Breger 2005), a Fourier analysis and sine-wave fitting program. The results are presented in Table 3. Two Blazhko periods (43.37 and 45.36 d) are detected in the M_{max} analysis but only one of those (45.28 d) is found in the (O–C) analysis. A long period (1634.8 d) is detected in the (O–C) analysis. As this long period is not detected in the M_{max} analysis, it can be attributed to an orbital motion around a center of mass.

The two close Blazhko periods found in the magnitude at maximum spectrum are also detected in the spectral analysis of the light curve as shown in the next section. The presence of a main Blazhko period and another periodic modulation close to it has been reported for XZ Cyg by LaCluyzé, A., *et al.* (2004). They also detected long term variations of the main Blazhko period over a time span of several decades. Their analyses of XZ Cyg are based on observations covering a time span of several decades, which is not the case for our observations.

In order to detect a potential Blazhko period variation, we have created seasonal subsets of the magnitude at maximum values and applied a Fourier analysis followed by a sine-wave fitting. The results are presented in Table 4. The number of observations for the 2010 and 2012 seasons is too limited to perform a Fourier analysis and the corresponding subsets do not appear in Table 4.

It is unclear if the period variations are due to real Blazhko period deviation or to a non-repetitive Blazhko effect from one cycle to another.

TU Com was also observed by the robotic SuperWasp-North telescope (Butters *et al.* 2010) located on the island of La Palma (Spain) between 2004 and 2008. The star is identified as J121346.95+305907.6 in the SuperWASP database. From the light curves available on the SuperWASP website, 37 brightness maxima have been identified. Their measured (O–C) values are reported in the Appendix (Table 9). The magnitudes at maximum brightness are not reported in this table since it was not possible to reliably determine the offset between the SWASP magnitudes and the reference magnitudes used in our image reduction. The four maxima recorded in 2004 (JD 2453130 to 2453174) have large (O–C) values greater than 2 hours. These (O-C) values should be questioned and are not used in this paper; it is possible that an error occurred in the WASP automatic image reduction or in the data distribution process.

Table 4. TU Com period variation obtained from magnitude at maximum values.

Subset (year)	*Period (d)*	σ(d)	N_{obs}
2009	45.61	1.39	9
2011	43.90	0.82	25
2013	44.09	0.13	29
2014	44.49	0.27	26
2015	41.33	0.83	24

3. Frequency spectrum analysis of the light curve

The light curve of a Blazhko star may be considered as a signal modulated in amplitude and phase. The signal spectrum is characterized by a pattern of multiplets ($kf_o \pm nf_B$) based on a pulsation frequency f_o and Blazhko modulation frequency f_B. Generally, from ground-based observations, only the central triplets are detected, as the other components are hidden in the noise. The amplitudes, phases, and uncertainties of the spectral components have been obtained with PERIOD04 by performing successive Fourier analyses, pre-whitenings, and sine-wave fittings. Only the components having a signal to noise ratio (SNR) greater than 3 have been retained as significant signals.

Table 5 provides the complete list of spectral components. Besides the pulsation frequency f_o and its harmonics nf_o, two groups of triplets corresponding to Blazhko periods and a component based on the suspected orbital period have been found. The frequencies and periods corresponding to Blazhko frequencies f_{B1} and f_{B2} and to an orbital period are given in Table 6. The two Blazhko periods corresponding to f_{B1} and f_{B2} are close to the periods found in the analysis of magnitude at maximum brightness. The orbital period of 1,601 days is in relatively good agreement with the value of 1,634.8 days found in the (O–C) analysis.

During the sine-wave fitting, the pulsation frequency f_o, ($f_0 - f_{B1}$), ($2f_o + f_{B2}$), and ($2f_o - f_{Orb}$) have been left unconstrained and the other frequencies have been forced as combinations of the four unconstrained frequencies. The uncertainties of frequencies, amplitudes, and phases estimated from Monte Carlo simulations have been multiplied by a factor of two as it is known that the Monte Carlo simulations underestimate these uncertainties.

Figure 3 presents the (O–C) values pre-whitened with the assumed orbital period of 1,601 days versus time. By comparison with the top panel of the Figure 2, it can be seen that the long term variation is effectively removed and only variations due to the short term Blazhko effect remain.

The same (O–C) pre-whitened data folded with the 43.66-

Table 5. TU Com multi-frequency fit results.

Component	*f(d⁻¹)*	*σ(f)*	A_i	*σ(A_i) (mag.)*	Φ_i	*σ(Φ_i) (cycle)*	*SNR*
f_o	2.165128	8.69×10^{-7}	0.3998	0.0017	0.3296	0.0006	117.1
$2f_o$	4.330256		0.2050	0.0017	0.9899	0.0015	60.7
$3f_o$	6.495383		0.1178	0.0017	0.7559	0.0021	32.3
$4f_o$	8.660511		0.0636	0.0018	0.4953	0.0042	16.8
$5f_o$	10.82564		0.0400	0.0016	0.2296	0.0075	11.3
$6f_o$	12.99077		0.0302	0.0018	0.9825	0.0080	9.7
$2f_o - f_{Orb}$	4.329631	8.75×10^{-6}	0.0530	0.0016	0.7854	0.0059	15.7
$f_o - f_{B1}$	2.142221	11.1×10^{-6}	0.0300	0.0016	0.7745	0.0086	9.1
$f_o + f_{B1}$	2.188034		0.0395	0.0019	0.0218	0.0084	10.3
$3f_o - f_{B1}$	6.472477		0.0171	0.0015	0.1028	0.0086	4.6
$3f_o + f_{B1}$	6.51829		0.0294	0.0015	0.4460	0.0143	8.1
$2f_o + f_{B2}$	4.352244	12.9×10^{-6}	0.0367	0.0018	0.8150	0.0075	10.0
$f_o - f_{B2}$	2.143139		0.0344	0.0019	0.4456	0.0326	10.1
$f_o + f_{B2}$	2.187117		0.0100	0.0017	0.1479	0.0083	3.0

Table 6. TU Com triplet component frequencies and periods.

Component	*Derived from (d⁻¹)*	*Frequency (d⁻¹) (d)*	*σ (d)*	*Period*	*σ*
f_o		2.165128	8.69 × 10–7	0.461867	1.85×10^{-7}
f_{B1}	$f_o - f_{B1}$	0.022906	1.11 × 10–5	43.66	0.02
f_{B2}	$2f_o - f_{B2}$	0.021989	1.30 × 10–5	45.48	0.02
f_{Orb}	$2f_o - f_{Orb}$	0.000625	8.9 × 10–6	1601.0	22.9

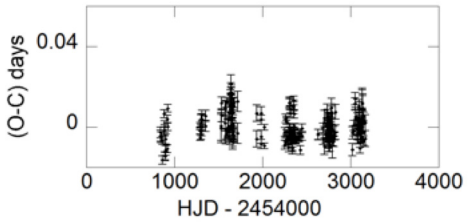

Figure 3. (O–C) values pre-whitened with the 1601-day assumed orbit period.

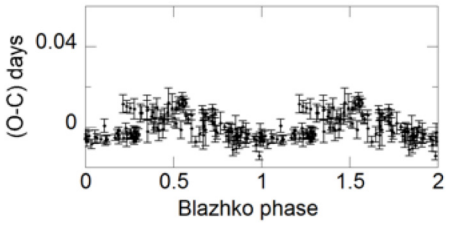

Figure 4. (O–C) values pre-whitened with the 1,601-day assumed orbit period and folded with the 43.66-day Blazhko period.

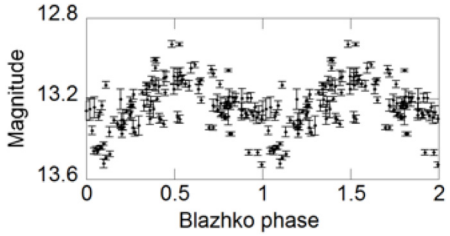

Figure 5. Magnitude at maximum brightness folded with the 43.66-day Blazhko period.

day Blazhko period are shown in the phase diagram of Figure 4, and the phase diagram of the magnitude at maximum using the same Blazhko period is given in Figure 5. In the phase diagrams of (O–C) values and magnitudes at maximum, the remaining scatter of the data is likely due to the presence of the second Blazhko period or to the non-repetitive Blazhko effect from one cycle to another.

4. Orbital parameter estimation

A pulsating star residing in a binary system can be seen as a regular "clock" in orbit around a center of mass. This orbital motion will affect the times of light maxima. For a pulsating star not affected by the Blazhko effect, besides a possible secular pulsation rate acceleration/deceleration, the orbital motion will be the only source of variations of the (O–C) values. Those (O–C) variations allow the evaluation of the orbital parameters by a non-linear least square fit with respect to the light-travel time equation. When applied to Blazhko pulsating stars, the Blazhko effect will be considered as noise affecting the (O–C) measurements. The Blazhko effect will increase the uncertainties of the orbital parameter estimation.

The light-travel time equation due to orbital motion is given by Hilditch (2001):

$$\tau = \frac{(a_{RRL} \sin i)}{c} \quad \frac{(1 - e^2)}{(1+e \cos \nu)} \sin (\nu+\omega) + \tau_0 \qquad (2)$$

where a_{RRL} is the semi-major axis, e is the eccentricity, ν is the true anomaly, i is the orbit inclination, ω the periastron longitude, and c the speed of light. Without the additional term τ_0, the zero-point of τ is reached when the star is at the same distance as the mass center of the binary system, that is, when $\nu + \omega = \pm k \pi$. The zero-point of the (O–C) values obtained in section 2 has been arbitrarily set to the time of the highest recorded light maximum. The additional offset τ_0 is introduced to compensate for the difference between these two zero-points.

The true anomaly can be calculated from:

$$\tan\frac{\nu}{2} = \sqrt{\frac{1+e}{1-e}}\tan\frac{E}{2} \quad (3)$$

where E is the eccentric anomaly which is evaluated by solving the Kepler equation:

$$E - e\sin E = 2\pi\,(t - T_{peri})/P_{orb} \quad (4)$$

and where T_{peri} is the epoch of periastron passage and P_{orb} is the orbital period. The semi-major axis a and the orbital inclination i are linked without additional information on the secondary star.

To obtain the estimation of orbital parameters (a_{RRL} sin i / c, e, ω, P_{orb}, T_{peri}, τ_0) the Levenberg-Marquart algorithm was used to minimize the sum of squares of the residuals $r_i = (O–C)_i - \tau\,(t_i, \boldsymbol{\beta})$ where t_i are the observed times of maxima and **β** the vector of parameters (a_{RRL} sin i / c, e, ω, P_{orb}, T_{peri}, τ_0). For each observed time of maxima, the light-travel time $\tau\,(t_i, \boldsymbol{\beta})$ is obtained by solving the Kepler equation (4) and calculating Equations (3) and (2).

The orbital parameter estimation was performed with the 124 (O–C) values derived from our observations (Table 8) and with 33 (O–C) values obtained from the SuperWASP survey (Table 9). The four (O–C) values corresponding to maxima recorded in 2004 were eliminated as they are abnormally large and are in question.

The results of the least-square fit are:

a_{RRL} sin i / c = 0.00893 d (1.55 AU)
P_{orb} = 1,676 d = 4.59 years
e = 0.22
ω = –0.978 rad
T_{peri} = 2455006 HJD
τ_0 = 0.0117 d

Using these orbital parameters, the theoretical light-travel times have been calculated and are compared to the (O–C) values in Figure 6.

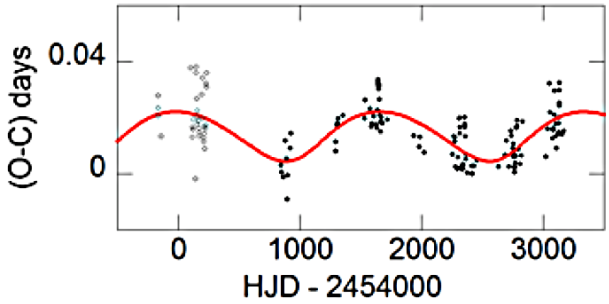

Figure 6. The (O–C) values (black diamonds) already presented in Figure 2 are compared to the light-travel time (red line) calculated from the orbital parameter solution. The (O–C) values derived from the SWASP database for the years 2005 and 2006 are represented with open diamonds.

The estimated orbital parameters are relatively uncertain as the scatter of the (O–C) values used for the orbital parameter estimation is as large as the orbit light-travel time variations.

An estimation of the semi-amplitude of the star's radial velocity may be derived from Equation (5):

$$K = (2\pi a_{RRL}\sin i)/(1-e^2)^{1/2} = 10.3 \text{ km/s}. \quad (5)$$

From Kepler's third law, the mass function for a barycentric orbit $M = (4\pi^2\, a_{RRL}{}^3)/P_{orb}{}^2$ is related to star masses through $M = (G\, m_s{}^3)/(m_{RRL} + m_s)^2$, where m_{RRL} and m_s are the masses of TU Com and the secondary star, respectively, and G is the gravitational constant. If m_{RRL} and m_s are expressed in solar masses $M_\odot$ and P_{orb} in years, G is equal to $4\pi^2$ and Kepler's third law can be rewritten as

$$\frac{m_s{}^3\sin^3 i}{(m_{RRL}+m_s)^2} = \frac{a_{RRL}{}^3\sin^3 i)}{P_{orb}{}^2} \quad (6)$$

Assuming a classical RR Lyrae mass of 0.7 $M_\odot$ for TU Com, the minimum mass of the secondary star ($m_s \sin i$) may be evaluated by solving Equation (6) rewritten as a third order polynomial. With the numerical values of 1.55 AU for (a sin i) and 4.59 year for P_{orb} the real solution of the polynomial provides a minimal mass ($m_s \sin i$) for the secondary star fortuitously equal to 0.70 $M_\odot$. The third order polynomial has been solved for other orbital inclinations and the results are provided in Table 7.

Table 7. Secondary mass and semi-major axes of the two stars for different orbital inclinations.

Orbital Inclination (degrees)	*Secondary Mass ($M_\odot$)*	*a_{RRL} (AU)*	*a_s (AU)*
90	0.70	1.55	1.54
80	0.72	1.57	1.53
70	0.77	1.65	1.50
60	0.87	1.78	1.44
50	1.07	2.02	1.32
40	1.45	2.40	1.16
30	2.36	3.09	0.92
20	5.56	4.52	0.57
10	34.84	8.90	0.18

RR Lyrae stars are old stars and the secondary star probably formed at the same epoch and would have the same metallicity. With these assumptions, it may be assumed that the secondary star is in a more evolved state than the RR Lyrae star and eventually it ended as a white dwarf, because massive stars evolve more rapidly than lower mass ones. It is possible that the secondary star brightness is not large enough to allow spectroscopic measurement of its radial velocity.

If the radial velocities of the two stars may be measured, the mass ratio may be derived from the relationship:

$$\frac{m_s}{m_{RRL}} = \frac{V_{RRL}}{V_s} = \frac{a_{RRL}}{a_s} \quad (7)$$

This relationship also shows that the chances to measure the secondary radial velocity are reduced when the mass is larger.

5. Conclusions

This observational campaign and data analysis has shown that the Blazhko period of 75 days mentioned in the *General Catalog of Variable Stars* is not correct. Alternatively, two Blazhko periods of 43.6 and 45.5 days have been identified from a light curve maxima analysis and confirmed from the spectral analysis of the light curve. The origin of the two Blazhko periods remains unclear; it could be due to a real second period or to a variation of a main Blazhko period or to the non-repetitive Blazhko effect from one cycle to another. A long term periodic variation of the (O–C) values suggests that TU Com is in a binary system with an orbital period of about 1,676 days. A tentative set of orbital parameters have been derived from a non-linear least square fit of the (O–C) values with respect to the light-travel time equation. The authors intend to continue their photometric observations in future years to extend the amount of data and to refine these results. They also invite other amateur astronomers to join their campaign. In order to confirm the binarity of TU Com, it is suggested that this star be integrated into a spectroscopic radial velocity measurement campaign like the study started by Guggenberger *et al.* (2015). Applying the radial velocity method to determine the orbital parameters will be a challenge as the radial velocities are also impacted by the pulsation/motion of the atmospheric layers which will be additionally affected by the Blazhko effect.

6. Acknowledgements

The AAVSO is acknowledged for the use of AAVSOnet telescopes at Cloudcroft (New Mexico). The authors thank Dr. K. Kolenberg and Prof. Dr. G. Rauw for their help with the secondary star evolution analysis and the referee for the comments which helped to clarify and improve the paper. This work has made use of data from DR1 of the WASP data (Butters *et al.* 2010) as provided by the WASP consortium, and the computing and storage facilities at the CERIT Scientific Cloud, reg. no. CZ.1.05/3.2.00/08.0144, which is operated by Masaryk University, Czech Republic.

References

Butters, O. *et al.* 2010, *Astron. Astrophys.*, **520**, L10.

de Ponthière, P. 2010, LESVEPHOTOMETRY, automatic photometry software (http://www.dppobservatory.net).

Diffraction Limited. 2004, MAXIMDL image processing software (http://www.cyanogen.com).

Guggenberger, E., and Steixner, J. 2015, in *The Space Photometry Revolution*, CoRoT Symposium 3, Kepler KASC-7 Joint Meeting, Toulouse, France, R. A. García, J. Ballot, eds., EPJ Web of Conferences, Vol. 101, id.06030.

Guggenberger, E., *et al.* 2015, to be published in CoKon, 105 (http://arxiv.org/abs/1512.00873v1)

Hajdu, G., Catelan, M., Jurcsik, J., Dékány, I., Drake, A. J., and Marquette, J.-B. 2015, *Mon. Not. Roy. Astron. Soc.*, **449**, L113.

Hertzsprung, E. 1919, *Astron. Nachr.*, **210**, 17.

Hilditch, R. W. 2001, *An Introduction to Close Binary Stars*, Cambridge Univ. Press, Cambridge.

Kafka, S. 2015, observations from the AAVSO International Database (https://www.aavso.org/aavso-international-database).

LaCluyzé, A., *et al.* 2004, *Astron. J.*, **127**, 1653.

Lenz, P., and Breger, M. 2005, *Commun. Asteroseismology*, **146**, 53.

Li, L.-J., and Qian, S.-B. 2014, *Mon. Not. Roy. Astron. Soc.*, **444**, 600.

Liska, J., *et al.* 2015, accepted for publication in *Astron. Astrophys.* (http://arxiv.org/abs/1502.03331).

McGrath, M. 1975, *J. Amer. Assoc. Var. Star Obs.*, **4**, 103.

Pietrzynski, G., *et al.* 2012, *Nature*, **484**, 75.

Reinsch, C. H. 1967, *Numer. Math.*, **10**, 177.

Saha, A., and White, R. E. 1990, *Publ. Astron. Soc. Pacific*, **102**, 148.

Samus, N. N., *et al.* 2011, *General Catalogue of Variable Stars*, GCVS database, Version 2011 January (http://www.sai.msu.su/gcvs/gcvs/index.htm).

Sódor, Á., and Jurcsik, J. 2005, *Inf. Bull. Var. Stars*, No. 5641, 1.

Ureche, V. 1965, *Babes-Bolyai Stud. Fasc.*, **1**, 73.

Wade, R., Donley, J., Fried, R., White, R. E., and Saha, A. 1999, *Astron. J.*, **118**, 2442.

Wozniak, P., *et al.* 2004, *Astron. J.*, **127**, 2436.

Zacharias, N., Finch, C. T., Girard, T. M., Henden, A., Bartlett, J. L., Monet, D. G., and Zacharias, M. I. 2012, *The Fourth U.S. Naval Observatory CCD Astrograph Catalog* (UCAC4), VizieR On-line Data Catalog (http://cdsarc.u-strasbg.fr/viz-bin/Cat?I/322).

Appendix

Table 8. TU Com measured brightness maxima.

Maximum HJD	*Error*	*O–C (day)*	*E*	*Magnitude*	*Error*
2454844.8935	0.0028	0.0030	–3403	13.297	0.025
2454849.9716	0.0026	0.0006	–3392	13.301	0.020
2454861.9785	0.0020	–0.0011	–3366	13.059	0.007
2454881.8518	0.0020	0.0120	–3323	13.231	0.016
2454888.7734	0.0029	0.0056	–3308	13.302	0.016
2454892.9157	0.0020	–0.0089	–3299	13.291	0.026
2454901.6995	0.0024	–0.0005	–3280	13.232	0.030
2454918.7984	0.0020	0.0093	–3243	13.131	0.016
2454924.8080	0.0019	0.0146	–3230	13.209	0.018
2455292.4472	0.0015	0.0081	–2434	13.343	0.012
2455293.3744	0.0018	0.0116	–2432	13.344	0.012
2455305.3889	0.0024	0.0175	–2406	13.527	0.013
2455310.4699	0.0025	0.0180	–2395	13.491	0.012
2455311.3954	0.0024	0.0198	–2393	13.474	0.014
2455353.4264	0.0028	0.0209	–2302	13.522	0.022
2455528.9345	0.0070	0.0198	–1922	13.364	0.026
2455534.0216	0.0032	0.0263	–1911	13.281	0.022
2455577.8959	0.0040	0.0233	–1816	13.268	0.027
2455583.8938	0.0038	0.0170	–1803	13.129	0.032
2455589.8991	0.0025	0.0180	–1790	13.068	0.022
2455607.9143	0.0054	0.0204	–1751	13.286	0.025
2455608.8384	0.0045	0.0208	–1749	13.293	0.030
2455624.5386	0.0030	0.0175	–1715	13.234	0.027
2455632.8512	0.0031	0.0165	–1697	13.093	0.022
2455637.9380	0.0034	0.0228	–1686	13.152	0.024
2455642.5675	0.0045	0.0336	–1676	13.207	0.028
2455643.4901	0.0028	0.0325	–1674	13.279	0.011
2455644.4129	0.0026	0.0316	–1672	13.284	0.010
2455645.3363	0.0050	0.0312	–1670	13.288	0.043
2455648.5686	0.0050	0.0305	–1663	13.281	0.025
2455648.5703	0.0060	0.0322	–1663	13.257	0.037
2455650.4122	0.0058	0.0266	–1659	13.467	0.013
2455656.8727	0.0043	0.0210	–1645	13.288	0.020
2455660.5618	0.0026	0.0151	–1637	13.306	0.015
2455661.4891	0.0038	0.0187	–1635	13.324	0.014
2455662.4125	0.0070	0.0184	–1633	13.306	0.036
2455668.8806	0.0043	0.0203	–1619	13.205	0.036
2455671.6500	0.0034	0.0185	–1613	13.139	0.034
2455677.6537	0.0026	0.0180	–1600	13.103	0.021
2455716.4519	0.0050	0.0194	–1516	13.325	0.016
2455933.9852	0.0040	0.0136	–1045	13.097	0.037
2455982.9391	0.0023	0.0096	–939	13.126	0.018
2455983.8664	0.0033	0.0132	–937	13.136	0.025
2456019.4246	0.0014	0.0077	–860	13.201	0.012
2456254.9758	0.0022	0.0070	–350	13.375	0.009
2456261.9102	0.0021	0.0134	–335	13.467	0.015
2456272.9948	0.0010	0.0132	–311	13.264	0.008
2456273.9171	0.0015	0.0117	–309	13.236	0.009
2456279.9123	0.0011	0.0027	–296	13.006	0.008
2456290.9961	0.0023	0.0017	–272	13.117	0.014
2456298.8521	0.0022	0.0060	–255	13.375	0.010
2456309.0270	0.0031	0.0198	–233	13.447	0.010
2456309.9508	0.0024	0.0199	–231	13.443	0.010
2456310.8747	0.0020	0.0200	–229	13.423	0.008
2456315.0281	0.0017	0.0166	–220	13.34	0.007
2456315.9498	0.0018	0.0146	–218	13.319	0.009
2456323.7893	0.0013	0.0024	–201	13.009	0.012
2456334.8733	0.0015	0.0016	–177	13.105	0.007
2456339.0304	0.0019	0.0019	–168	13.256	0.011
2456339.9558	0.0019	0.0035	–166	13.274	0.009
2456340.8788	0.0017	0.0028	–164	13.298	0.008
2456351.9774	0.0029	0.0166	–140	13.46	0.015
2456352.9023	0.0027	0.0178	–138	13.463	0.014
2456353.8284	0.0021	0.0201	–136	13.441	0.010
2456358.9022	0.0021	0.0134	–125	13.347	0.009
2456363.9763	0.0015	0.0070	–114	13.168	0.011
2456364.8983	0.0013	0.0052	–112	13.128	0.008
2456376.9021	0.0018	0.0005	–86	13.032	0.015
2456410.6207	0.0017	0.0029	–13	13.047	0.014
2456414.7748	0.0015	0.0002	–4	12.929	0.017
2456416.6221	0.0009	0.0000	0	12.93	0.008
2456427.7097	0.0022	0.0028	24	13.238	0.015
2456452.6526	0.0022	0.0049	78	13.139	0.017
2456630.9308	0.0026	0.0027	464	13.091	0.026
2456687.7446	0.0024	0.0069	587	13.127	0.018
2456699.7581	0.0041	0.0118	613	13.358	0.021
2456717.7616	0.0023	0.0026	652	13.17	0.015
2456734.8635	0.0045	0.0154	689	13.213	0.024
2456737.6330	0.0036	0.0137	695	13.273	0.022
2456750.5609	0.0031	0.0093	723	13.373	0.018
2456753.3302	0.0060	0.0074	729	13.342	0.033
2456753.7909	0.0033	0.0063	730	13.365	0.019
2456754.7192	0.0055	0.0108	732	13.333	0.048
2456757.4857	0.0041	0.0061	738	13.258	0.030
2456757.4866	0.0033	0.0070	738	13.3	0.028
2456758.4116	0.0065	0.0083	740	13.251	0.043
2456763.4845	0.0036	0.0007	751	13.088	0.041
2456763.4866	0.0031	0.0028	751	13.152	0.027
2456764.4098	0.0024	0.0022	753	13.131	0.023
2456764.4142	0.0043	0.0066	753	13.091	0.038
2456767.6445	0.0022	0.0039	760	13.048	0.025
2456772.7275	0.0021	0.0063	771	13.054	0.019
2456778.7420	0.0033	0.0166	784	13.195	0.021
2456781.5139	0.0039	0.0173	790	13.281	0.018
2456782.4395	0.0048	0.0191	792	13.195	0.026
2456794.4377	0.0079	0.0088	818	13.305	0.052
2456808.7503	0.0026	0.0036	849	13.109	0.024
2456816.6050	0.0019	0.0065	866	13.075	0.018
2456828.6257	0.0036	0.0187	892	13.3	0.018
2457018.9021	0.0031	0.0061	1304	13.214	0.025
2457037.8485	0.0025	0.0160	1345	13.211	0.022
2457049.8734	0.0030	0.0324	1371	13.267	0.012
2457054.9436	0.0047	0.0220	1382	13.202	0.050
2457074.7947	0.0023	0.0129	1425	13.207	0.015
2457080.8020	0.0024	0.0159	1438	13.217	0.018
2457081.7261	0.0031	0.0163	1440	13.19	0.038
2457082.6492	0.0027	0.0156	1442	13.193	0.028
2457091.8921	0.0024	0.0212	1462	13.243	0.051
2457093.7481	0.0033	0.0297	1466	13.234	0.022
2457101.5879	0.0028	0.0178	1483	13.178	0.025
2457104.8167	0.0039	0.0135	1490	13.152	0.030
2457106.6599	0.0025	0.0093	1494	13.133	0.021
2457124.6781	0.0021	0.0147	1533	13.233	0.015
2457125.6022	0.0020	0.0151	1535	13.238	0.015
2457128.3765	0.0056	0.0182	1541	13.199	0.049
2457129.7641	0.0028	0.0202	1544	13.195	0.022
2457130.6878	0.0020	0.0201	1546	13.267	0.012
2457131.6168	0.0034	0.0254	1548	13.243	0.023
2457132.5395	0.0056	0.0244	1550	13.268	0.032
2457133.4715	0.0071	0.0326	1552	13.259	0.048
2457134.3925	0.0070	0.0299	1554	13.251	0.054
2457149.6183	0.0023	0.0141	1587	13.108	0.021
2457166.7087	0.0039	0.0154	1624	13.222	0.030

Table 9. TU Com brightness maxima derived from SuperWASP database.

Maximum HJD	*Error*	*O–C (day)*	*E*	*Maximum HJD*	*Error*	*O–C (day)*	*E*
2453130.5345	0.0079	0.09241	–7115	2454150.7320	0.0033	0.026854	–4906
2453137.4585	0.0022	0.088413	–7100	2454156.7298	0.0046	0.02039	–4893
2453144.4709	0.0167	0.172816	–7085	2454157.6558	0.005	0.022657	–4891
2453174.4205	0.0052	0.101095	–7020	2454158.5747	0.0035	0.017824	–4889
2453831.5834	0.0069	0.027993	–5597	2454165.5038	0.0079	0.018927	–4874
2453832.4998	0.0032	0.02066	–5595	2454169.6550	0.0055	0.013329	–4865
2453833.4265	0.0035	0.023627	–5593	2454170.5818	0.0067	0.016396	–4863
2453856.5096	0.0069	0.013403	–5543	2454171.5038	0.005	0.014663	–4861
2454101.7852	0.0084	0.037901	–5012	2454194.6109	0.0103	0.028439	–4811
2454114.6964	0.0029	0.01684	–4984	2454195.5406	0.0092	0.034406	–4809
2454115.6165	0.0027	0.013207	–4982	2454202.4539	0.0032	0.019709	–4794
2454120.7032	0.0063	0.019376	–4971	2454206.6025	0.0026	0.01151	–4785
2454121.6234	0.0049	0.015843	–4969	2454208.4512	0.0035	0.012744	–4781
2454143.7753	0.0038	–0.00185	–4921	2454213.5362	0.0047	0.017213	–4770
2454145.6606	0.0077	0.035986	–4917	2454214.4571	0.0049	0.01438	–4768
2454146.5865	0.0049	0.038153	–4915	2454215.3754	0.0057	0.008947	–4766

Times of Minima and New Ephemerides for Southern Hemisphere Eclipsing Binary Stars Observed in 2015

Hristo Pavlov
9 Chad Place, St. Clair, NSW 2759, Australia; hristo_dpavlov@yahoo.com

Anthony Mallama
14012 Lancaster Lane, Bowie, MD 20715; anthony.mallama@gmail.com

Brian Loader
14 Craigieburn Street, Darfield 7510, New Zealand; brian.loader@clear.net.nz

Stephen Kerr
22 Green Avenue, Glenlee, QLD 4711, Australia; steve.kerr@outlook.com.au

Received February 2, 2016; revised March 15, 2016; accepted March 18, 2016

Abstract Observers from Australia and New Zealand used video equipment to time eclipses of short-period binary stars. The objects were typically south of –20º declination and had periods of less than a day. Many of those systems had very few observations since their discovery and some of them had not been observed for fifty or more years. We present 44 times of minima of 42 stars, provide revised ephemerides for 7 of these systems, and characterize an orbital period change for RW PsA.

1. Introduction

The development of a new technique for observing eclipsing binary stars (Pavlov and Mallama 2015) enabled observers with video equipment, typically involved in observing occultations, to participate in the observation of short-period variable stars, too. The method allows for determination of times of minima (TOMs) from observations made on a single night, based on a video record which is typically between 3 and 6 hours long. The large number of southern systems that are seldom studied makes the video technique a very useful and important addition to the work done by occultation observers in the southern hemisphere. Those taking part in this program already had the necessary video and timing equipment as well as significant experience using it.

2. Observations and analysis

The data reported here are based on observations done from February through December 2015. Video photometry was performed with the instruments listed in Table 1. The GPS-based video time inserters IOTA-VTI (Video Timers 2011) and KIWI-OSD were used to provide time information accurate to milliseconds of UTC. Eclipses were observed over a period of at least 1.5 hours on each side of the minima. Author HP used a Sloan r' photometric filter, while authors BL and SK observed without a photometric filter only targets that were above 30 degrees altitude.

The observations were recorded on computers running Windows using the OCCUREC software package (Pavlov 2014a). The photometric processing was done with the TANGRA software package (Pavlov 2014b) using aperture photometry and subtraction of the average background. The number of video measurements obtained per timing was on the order of 10,000. TOMs were derived using the Eclipsing Binary add-in for TANGRA (Mallama and Pavlov 2015b) which implements the algorithm of Kwee and van Woerden (1956).

The vast majority of the stars were contact or semi-detached systems. Most of them had a period of less than 1 day with 46% of the stars having a period of less than 0.5 day.

For many of the observed targets the predictions for the TOMs were not very accurate because of the lack of historical observations. Author HP built a software application (MINCALC) that aggregates data from a number of online resources, including the *General Catalogue of Variable Stars* (GCVS; Kholopov *et al.* 1985), the All-Sky Automated Survey Catalogues (ASAS; Pojmański 1997), the Krakow ephemeris (Kreiner 2004), and the O–C Gateway (Paschke 2015), in order to compute more accurate predictions and also provide an error estimate. Still, in several cases the minima turned out to be a few hours away

Table 1. Equipment used by the observers.

Observer	*Initials*	*AAVSO Observer Initials*	*Telescope*	*Camera*	*Timing*
Kerr	SK	KSH	50-mm Olympus Zuiko	WAT-120N+	IOTA-VTI
Loader	BL	—	250-mm Meade Schmidt-Cassegrain	WAT-910BD	KIWI-OSD
Pavlov	HP	PHRA	350-mm Meade Schmidt-Cassegrain	WAT-910BD	IOTA-VTI

The WAT-910BD video cameras were used in a TACOS-BD system (Gault et al. 2014) and the WAT-120N+ camera was used out of the box.

from the MINCALC prediction and additional observations had to be done on subsequent nights in order to obtain sufficient data for deriving a TOM.

The observed TOMs for 42 stars and their O–C values from the Krakow and GCVS ephemerides are presented in Table 2.

3. Revised ephemerides and an orbital period change

O–C diagrams for stars listed in Table 2 were evaluated in order to assess which ephemerides require an update. For each candidate star that was identified, an epoch and a period were fit to all the available TOMs by the method of least squares. Corresponding uncertainties for the new epoch and period were also computed. In cases where the earlier TOMs resulted in

Table 2. Times of minima of southern stars determined using the video technique in 2015.

Star	*Type*	*Obs.*	*Time of Minima (HJD)*	*Uncertainty*	*O–C (GCVS)*	*O–C (Krakow)*
SY Aps	II	HP	2457299.9593	0.0003	+0.0007	+0.0047
V653 Ara	I	HP	2457231.9567	0.0002	–0.0721	+0.0257
EZ Car	II	HP	2457101.0132	0.0004	+0.0343	–0.0017
PX Car	I	HP	2457108.9472	0.0001	–0.1365	+0.0006
BD Cen	II	HP	2457148.0673	0.0003	–0.2499	+0.0066
OV Cen	I	HP	2457149.9871	0.0004	+0.0176	–0.0017
V606 Cen	I	HP	2457156.0428	0.0002	+0.0303	+0.0200
V676 Cen	I	HP	2457151.0120	0.0001	+0.0698	0.0000
V689 Cen	II	HP	2457174.9407	0.0001	+0.0030	+0.0014
TW Cet	I	HP	2457230.2168	0.0002	–0.0299	–0.0014
RW CrA	I	HP	2457230.9457	0.0003	+0.0045	–0.0060
V405 CrA	I	HP	2457254.9972	0.0007	–0.0173	–0.0057
V634 CrA	II	HP	2457151.1775	0.0003	–0.0434	+0.0056
TW Cru	I	HP	2457081.1541	0.0005	+0.0659	+0.0045
AC Cru	II	HP	2457147.9210	0.0002	–0.2049	+0.0018
BF Cru	II	HP	2457099.9710	0.0004	–0.0103	+0.0117
RW Dor	II	HP	2457299.0086	0.0001	–0.0352	+0.0013
RW Dor	I	BL	2457370.9473	0.0003	–0.0333	+0.0034
CI Eri	I	HP	2457298.1954	0.0001	–0.2666	+0.0038
RV Gru	II	HP	2457157.1673	0.0001	–0.0519	–0.0004
SZ Hor	I	HP	2457267.2071	0.0007	–0.1065	–0.0078
RY Ind	I	HP	2457231.196	0.0010	+0.0008	–0.0044
FT Lup	I	BL	2457198.859	0.0002	–0.0721	–0.0046
TW Mus	II	HP	2457114.0737	0.0004	+0.0598	–0.0092
LT Pav	II	HP	2457109.2152	0.0005	+0.0671	+0.0120
MU Pav	I	HP	2457249.1956	0.0001	+0.1165	+0.0120
NP Pav	I	HP	2457255.1803	0.0002	+0.0964	+0.0097
RW PsA	I	HP	2457175.2077	0.0001	–0.0725	–0.0404
AY Pup	I	HP	2457146.9264	0.0005	–0.0766	+0.0111
DS Pup	II	HP	2457113.9639	0.0003	+0.0747	–0.0181
DS Pup	I	HP	2457158.8561	0.0001	+0.0747	–0.0181
V743 Sgr	I	HP	2457150.1689	0.0002	–0.0599	–0.0381
V902 Sgr	II	HP	2457149.1605	0.0005	–0.0612	–0.0492
V1071 Sgr	I	BL	2457224.8786	0.0004	–0.0918	+0.0083
V1647 Sgr	I	SK	2457248.9224	0.0002	–0.0491	–0.0095
V833 Sco	I	HP	2457156.2538	0.0002	–0.1214	+0.0021
RT Scl	I	HP	2457297.9961	0.0002	–0.0580	–0.0255
RS Sct	I	BL	2457272.8844	0.0005	–0.0242	+0.0064
GN TrA	I	HP	2457137.2000	0.0002	+0.0442	–0.0194
BF Vel	I	HP	2457175.9211	0.0002	–0.0505	–0.0139
EQ Vel	I	HP	2457080.9902	0.0004	–0.0179	+0.0221
EU Vel	II	HP	2457148.9619	0.0003	+0.0812	–0.0211
FM Vel	II	HP	2457081.9843	0.0003	+0.0688	+0.0203
FQ Vir	I	BL	2457184.8609	0.0001	+0.0033	–0.0001

The eclipse type indicates "I" for primary or "II" for secondary. The O–C values are given for both the General Catalogue of Variable Stars *(Kholopov et al. 1985) and the Krakow ephemerides (Kreiner 2004).*

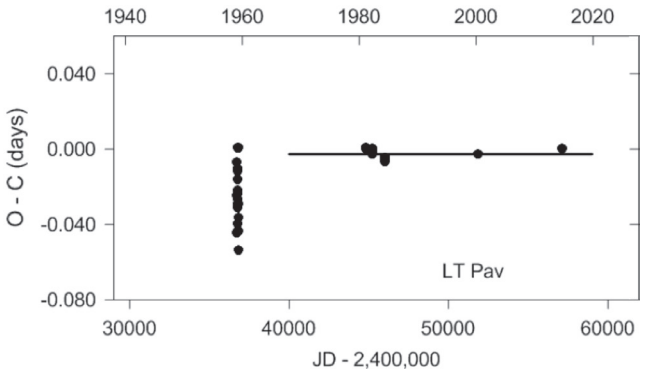

Figure 1. LT Pav. O–C residuals for the ephemeris in Table 3. The span of the best fit line indicates the range of data used in the least squares computation.

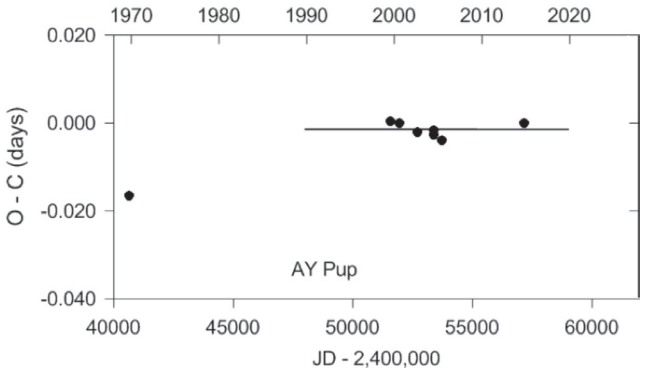

Figure 2. AY Pup. O–C residuals for the ephemeris in Table 3. The span of the best fit line indicates the range of data used in the least squares computation.

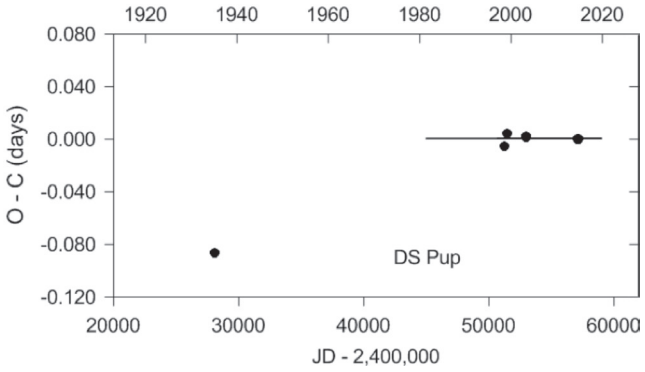

Figure 3. DS Pup. O–C residuals for the ephemeris in Table 3. The span of the best fit line indicates the range of data used in the least squares computation.

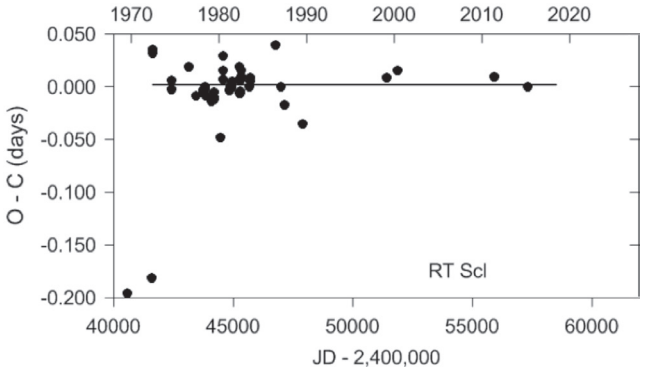

Figure 4. RT Scl. O–C residuals for the ephemeris in Table 3. The span of the best fit line indicates the range of data used in the least squares computation.

Table 3. Revised ephemeris for stars with new periods differing by more than 3.0 standard deviations from the Krakow periods.

Star	*HJD Epoch*	*Uncertainty*	*Period (d)*	*Uncertainty*	*Krakow (d)*	*Sigma*
LT Pav	2457109.4093	0.0022	0.393673633	0.000000078	0.393673300	4.2
RW PsA	2457175.2093	0.0026	0.360447226	0.000000280	0.360450200	10.6
AY Pup	2457146.9249	0.0020	0.468958832	0.000000223	0.468957900	4.2
DS Pup	2457158.8566	0.0025	0.388676139	0.000000239	0.388677700	6.5
V743 Sgr	2457150.1694	0.0025	0.276635676	0.000000081	0.276636800	13.9
V902 Sgr	2457149.1605	0.0016	0.293943837	0.000000066	0.293945670	27.8
RT Scl	2457297.9981	0.0095	0.511557652	0.000000396	0.511558840	3.0

Table 4. RW PsA.

Type: W UMa contact binary
V magnitude range: 11.05–11.76

Period after 2000:	0.360447226 ± 0.000000280 (days)
Period before 2000:	0.360450732 ± 0.000000247 (days)
Difference:	–0.000003506 ± 0.000000373 (Δ days)
Difference:	–0.303 ± 0.032 (Δ seconds)

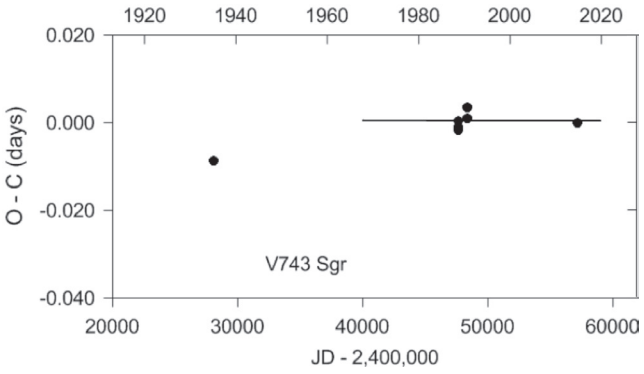

Figure 5. V743 Sgr. O–C residuals for the ephemeris in Table 3. The span of the best fit line indicates the range of data used in the least squares computation.

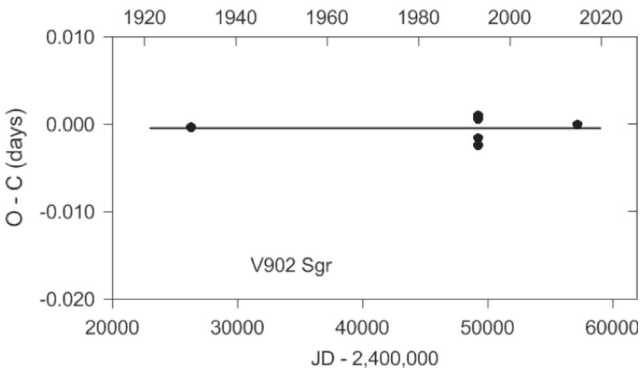

Figure 6. V902 Sgr. O–C residuals for the ephemeris in Table 3. The span of the best fit line indicates the range of data used in the least squares computation.

large O–Cs to the best fit line, those were omitted from a second least squares solution in order to improve the fit to more recent TOMs.

The new periods which were determined for the stars LT Pav, RW PsA, DS Pup, AY Pup, RT Scl, V743 Sgr, and V902 Sgr differed by at least 3.0 standard deviations from those given on the Krakow (Kreiner 2004) web site. The new ephemerides are listed in Table 3 along with differences in standard deviations (sigma) from Krakow periods. The O–C diagrams for all of the stars listed above except RW PsA are shown in Figures 1-6. RW PsA is discussed next.

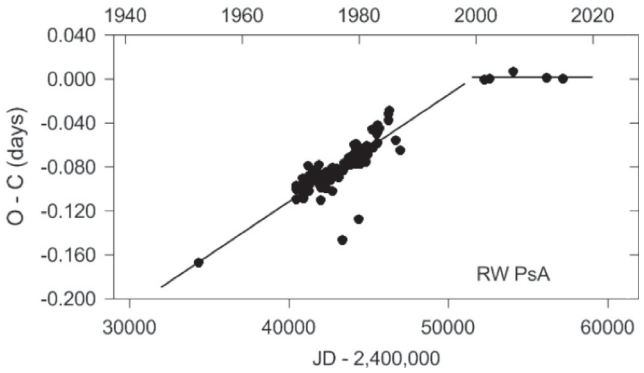

Figure 7. RW PsA O–C diagram showing the period change that occurred around year 2000. The two lines are best fits to the TOMs before and after year 2000.

A distinct orbital period change is evident in the O–C diagram for RW PsA shown in Figure 7. The large size of this change (~0.3 second) is rather surprising considering that the period appears to have remained approximately constant for 50 years before 2000 and for the 15 years following. Information about RW PsA itself and the period change are given in Table 4.

4. Summary and conclusions

The method for timing eclipses of binary stars developed by Pavlov and Mallama (2015) has been expanded into an observing program. The first goal of this program is to obtain TOMs for short-period southern hemisphere stars which have not been regularly observed in the past. In this paper we added TOMs for 42 stars to those of the 8 stars reported on in the original paper.

The second goal of our program is to revise the ephemerides of systems when needed. We have updated the ephemerides of seven stars in this paper.

The third goal is to investigate orbital period changes for stars of particular interest. An example is V752 Cen, for which we found an abrupt period change accompanied by an anomalous and temporary dimming (Mallama and Pavlov 2015a). In the present study we characterize the large period change for RW PsA which occurred around the year 2000.

5. Acknowledgements

This research used information from the International Variable Star Index (VSX) database (Watson *et al.* 2014), operated at AAVSO, Cambridge, Massachusetts, USA.

Bob Nelson's O–C files (Nelson 2014) were used extensively in this study, especially as a source of historical TOM data.

The planning of the observations relied heavily on the meteorological forecast data provided by 7Timer (Ye 2011).

References

Gault, D., *et al.* 2014, The Watec WAT-910BD TACOS System (http://www.kuriwaobservatory.com/TACOS_BD-System.html).

Kholopov, P. N., *et al.* 1985, *General Catalogue of Variable Stars*, 4th Ed., Moscow.

Kreiner, J. M. 2004, *Acta Astron.*, **54**, 207 (http://www.as.up.krakow.pl/ephem).

Kwee, K. K., and van Woerden, H. 1956, *Bull. Astron. Inst. Netherlands*, **12**, 327.

Mallama, A., and Pavlov, H. 2015a, *J. Amer. Assoc. Var. Star Obs.*, **43**, 38.

Mallama, A., and Pavlov, H. 2015b, Eclipsing Binaries Add-in for TANGRA (http://www.hristopavlov.net/tangra3/eb.html).

Nelson, R. 2014, Eclipsing Binary O–C Files (http://www.aavso.org/bob-nelsons-o-c-files).

Paschke, A. 2015, O–C Gateway (http://var.astro.cz/ocgate).

Pavlov, H. 2014a, OCCUREC Software Package for Astronomical Video Recording (http://www.hristopavlov.net/occurec).

Pavlov, H. 2014b, TANGRA3 Software Package for Video Photometry (http://www.hristopavlov.net/tangra3).

Pavlov, H., and Mallama, A. 2015, *J. Amer. Assoc. Var. Star Obs.*, **43**, 80.

Pojmański, G. 1997, *Acta Astron.*, **47**, 467.

Video Timers. 2011, IOTA-VTI video time inserter (http://videotimers.com/home.html).

Watson, C., Henden, A. A., and Price, C. A. 2014, AAVSO International Variable Star Index VSX (Watson+, 2006–2014; http://www.aavso.org/vsx).

Ye, Q.-Z. 2011, *Publ. Astron. Soc. Pacific*, **123**, 113.

A Photometric Study of the Eclipsing Binary Star V2790 Orionis

Edward J. Michaels
Stephen F. Austin State University, Department of Physics and Astronomy, P.O. Box 13044, Nacogdoches, TX 75962; emichaels@sfasu.edu

Received February 2, 2016; revised May 26, 2016, Accepted May 31, 2016

Abstract Presented in this paper is the first precision set of multi-band light curves for the eclipsing binary star V2790 Ori. A new linear ephemeris gives an orbital period of 0.28784176 d. The light curves were analyzed with the Wilson-Devinney program to determine the best-fit stellar model. Star spots were required in the model to account for asymmetries in the light curves. The synthetic light curve solutions presented are consistent with a W-type contact binary.

1. Introduction

V2790 Ori (TYC 1322-294-1, GSC 01322-00294) was identified as an eclipsing binary by Otero *et al.* (2004) from the public data release of the Northern Sky Variability Survey (NSVS; Wozniak *et al.* 2004). The star was classified as an EW type with a period of P = 0.287842 d. Also using observations from the NSVS database, Gettel *et al.* (2006) found that the V-band magnitude ranged from V_{max} = 11.181 to V_{min} = 11.743, and using a newly derived period-color relation estimated a distance of 199 pc. Only a few times of minima have been reported for this system. In this paper a photometric study of V2790 Ori is presented. It is organized into sections with observations and data reduction techniques presented in section 2, period analysis and Wilson-Devinney (WD) models in section 3, and discussion and conclusions in section 4.

2. Observations

Photometric observations of V2790 Ori were acquired using the 0.31-m Ritchey-Chrétien robotic telescope at the Waffelow Creek Observatory (http://obs.ejmj.net/index.php). An SBIG-STXL camera with a KAF-6303E CCD (9μm pixels) was used for imaging on several nights in 2015. Observations using Sloan g', r', and i' passbands were made on January 7, 17, 18, 19, 23, 26, 27. These observations comprise Data Set 1 (DS1). Additional observations were made in the Johnson B and V passbands on November 18 and 19 which comprise Data Set 2 (DS2). A total of 4,651 images were acquired: 449 in Johnson B, 447 in Johnson V, 1,102 in Sloan g', 1,443 in Sloan r', and 1,210 in Sloan i'. Only one passband was observed on each of the January dates to improve cadence while on the November dates both Johnson B and V observations were acquired. All images were calibrated with bias, dark, and flat field frames. MIRA software (Mirametrics 2015) was used for calibration and ensemble differential aperture photometry.

Listed in Table 1 are the coordinates and standard magnitudes of the five comparison stars and the check star (K) used in this study. The standard magnitudes for each passband were taken from the AAVSO Photometric All-Sky Survey (APASS; Henden *et al.* 2014). The instrumental magnitudes for V2790 Ori were converted to standard magnitudes using these comparison stars. A finder chart for these stars is shown in Figure 1. The folded light curves for each passband in standard magnitudes are shown in Figure 2. The time of each observation (T) was converted to orbital phase Φ using

$$\Phi = \frac{T - T_0}{P} - \text{Int}\left(\frac{T - T_0}{P}\right) \quad (1)$$

where T_0 is a time of minimum for a primary eclipse (epoch) and P is the orbital period. Throughout this paper the values used for epoch and period are T_0 = 2357346.7442 and P = 0.28784176 day (see section 3.1). All light curve figures are plotted from phase –0.6 to 0.6 with negative orbital phase defined as Φ – 1. Also shown in the bottom panel of Figure 2 are all the standard Johnson V-magnitudes for the K star. The K star magnitudes listed in Table 1 are averages from all observations for each passband. These average values compare well with the APASS all-sky photometry. For each night a plot of the K star magnitudes was inspected and no significant variability was detected. All the observations in this study are available from the AAVSO International Database (Kafka 2015).

3. Analysis

3.1. Period determination

Using the Kwee and van Woerden (1956) method 14 new times of minima were determined from both DS1 and DS2 observations. These new minima times and all others found in the literature are reported in Table 2. The initial ephemeris used in this study was taken from Otero (2004) and is given by:

$$\text{HJD Min I} = 2451521.695 + 0.287842\ E. \quad (2)$$

Using all the available times of minima an improved ephemeris was determined by least-squares solution and is given by:

$$\text{HJD Min I} = 2457346.7442\ (3) + 0.28784176\ (9)\ E. \quad (3)$$

Figure 3 shows the O–C diagram from Equation 3. There appears to be no secular period change but the O–C diagram hints at a possible small cyclic change. This type of period change could possibly be caused by a third body in the system. A third body in a contact binary is not uncommon but the minima times presently available cannot yet support this supposition since the observations only span about 5 years. Several years of additional times of minima will be necessary to verify if a period change is actually occurring and its cause.

Table 1. Variable (V), comparison (C), and check (K) stars in this study.

Star	*R.A. (2000)* *h m s*	*Dec. (2000)* *° ′ ″*	*B*	*V*	*g′*	*r′*	*i′*	*(B–V)*
V2790 Ori (V)	06 15 31.4	+19 35 22.0						
GSC1322-0961 (C1)	06 15 06.6	+19 32 05.5	11.425	11.002	11.180	10.938	10.913	0.423
			± 0.029	± 0.022	± 0.055	± 0.017	± 0.026	± 0.036
GSC1322-1399 (C2)	06 15 19.7	+19 37 06.6	11.379	11.052	11.181	11.022	11.050	0.327
			± 0.032	± 0.030	± 0.067	± 0.023	± 0.036	± 0.044
GSC1322-1132 (C3)	06 15 35.9	+19 37 58.9	12.420	11.781	12.082	11.607	11.456	0.639
			± 0.034	± 0.024	± 0.070	± 0.023	± 0.037	± 0.042
GSC1322-0698 (C4)	06 15 03.6	+19 33 05.1	12.327	11.825	12.048	11.714	11.642	0.502
			± 0.026	± 0.027	± 0.059	± 0.011	± 0.012	± 0.037
GSC1322-0494 (C5)	06 15 39.4	+19 35 36.6	13.284	12.128	12.686	11.714	11.299	1.156
			± 0.037	± 0.032	± 0.106	± 0.038	± 0.067	± 0.049
GSC1322-1333 (K)	06 15 42.0	+19 38 27.5	11.671	10.769	11.180	10.451	10.219	0.902
			± 0.030	± 0.067	± 0.082	± 0.025	± 0.038	± 0.073
Observed check star magnitudes (K)			11.688	10.733	11.148	10.427	10.231	0.935
			± 0.007	± 0.005	± 0.008	± 0.009	± 0.008	± 0.009

APASS comparison and check star magnitudes and errors. The observed check star magnitudes are the averages over all nights for each passband.

Table 2. Available times of minima and O–C residuals from Equation 2.

Epoch HJD 2400000+	*Error*	*Cycle*	*O-C Linear*	*References*
55520.82050	0.00020	–387.5	0.0005	Nelson 2011
55532.91030	0.00040	–345.5	0.0009	Diethelm 2011
55604.29500	0.00040	–97.5	0.0009	Nagai 2012
55632.35970	0.00040	0.0	0.0010	Nagai 2012
55644.30500	0.00040	41.5	0.0008	Nagai 2012
55896.88270	0.00030	919.0	–0.0026	Diethelm 2012
55902.78500	0.00010	939.5	–0.0010	Nelson 2012
55959.34660	0.00020	1136.0	–0.0004	Hübscher 2013
56288.06100	0.00040	2278.0	–0.0012	Nagai 2013a
56288.20450	0.00040	2278.5	–0.0017	Nagai 2013a
56623.10920	0.00040	3442.0	–0.0008	Nagai 2013b
56623.25470	0.00040	3442.5	0.0007	Nagai 2013b
57041.63261	0.00007	4896.0	0.0007	Present observations
57041.77672	0.00005	4896.5	0.0008	Present observations
57042.64031	0.00005	4899.5	0.0009	Present observations
57042.78361	0.00006	4900.0	0.0003	Present observations
57048.68477	0.00013	4920.5	0.0007	Present observations
57048.82855	0.00007	4921.0	0.0005	Present observations
57049.69193	0.00007	4924.0	0.0004	Present observations
57049.83623	0.00007	4924.5	0.0008	Present observations
57050.69948	0.00006	4927.5	0.0005	Present observations
57050.84323	0.00008	4928.0	0.0003	Present observations
57345.73605	0.00019	5952.5	–0.0007	Present observations
57345.87983	0.00017	5953.0	–0.0009	Present observations
57346.74338	0.00016	5956.0	–0.0008	Present observations
57346.88755	0.00013	5956.5	–0.0006	Present observations

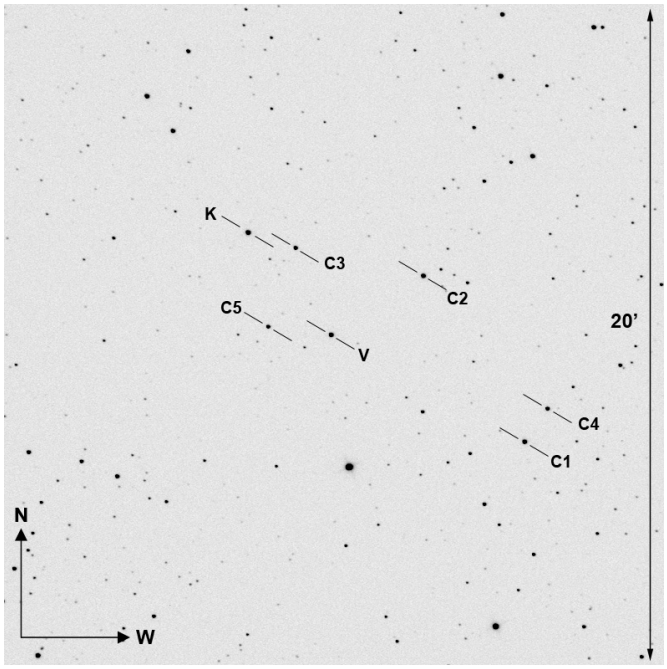

Figure 1. Finder chart for V2790 Ori (V), comparison (C1, C2, C3, C4, and C5) and check (K) stars.

3.2. Temperature, spectral type

V2790 Ori has not been observed spectroscopically, therefore it was necessary to estimate the effective temperature and spectral type from the observed color index. The B and V observations of DS2 were binned with a phase width of 0.01. Both phase and magnitude were averaged in each binned interval. The binned V-magnitudes were then subtracted from the linearly interpolated binned B-magnitudes to form the color index values. These values were averaged at quadrature from phase 0.0 to 0.5. ($\Phi = \pm 0.25$). The resulting observed color index is (B–V) = 0.723 ± 0.010. Figure 4 shows the binned V-magnitude light curve, with the color index shown in the bottom panel. The observed color index of the larger cooler primary star can be determined at phase 0.0, which is a total eclipse. The color index at primary eclipse ($\Phi = \pm 0.05$) has a value of (B–V) = 0.742 ± 0.012. The map of interstellar medium (ISM) dust by Schlafly *et al.* (2014) was not used to determine the color excess for this star. The ISM dust tends to be rather clumpy in this region of the sky due to the star's proximity to the galactic equator (galactic latitude of +1.26°). To determine the effect of dust on this star requires an independent estimate of the color. One method for estimating the star's color index is to use Wang's (1994) period-color relationship for contact binaries given by:

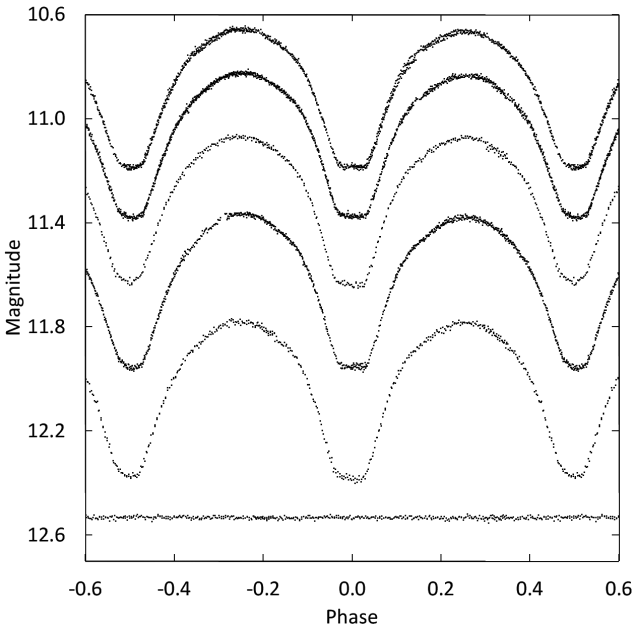

Figure 2. Folded light curves for each observed passband. The differential magnitudes of the variable were converted to standard magnitudes using the calibrated magnitudes of the comparison stars. From top to bottom the light curve passbands are Sloan i', Sloan r', Johnson V, Sloan g', and Johnson B. The bottom curve shows the standard Johnson V magnitudes of the check star (offset +1.8 magnitudes). The standard deviations of check star magnitudes (all nights) are shown in Table 1. Error bars are not shown for clarity.

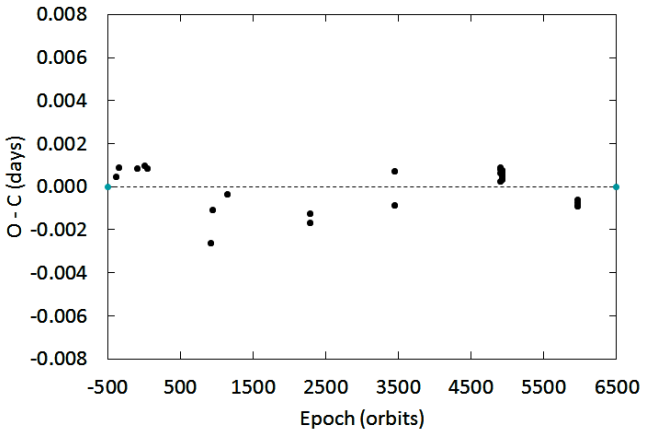

Figure 3. O–C residuals from linear ephemeris fit of Equation 2.

$$(B–V)_0 = 0.62 – 1.31 \log_{10} P. \quad (4)$$

Using the orbital period determined in section 3.1 gives a value of $(B–V)_0 = 0.771$. A second method for estimating the color index is to use Qian's (2003) mass-period relation given by:

$$M = 0.391 (\pm 0.059) + 1.96 (\pm 0.17) P. \quad (5)$$

The calculated value for the more massive star is $M_2 = 0.96 \pm 0.07 M_\odot$. Using Table 5 of Pecaut and Mamajek (2013) gives a color index of $(B – V)_0 = 0.719$ for a main-sequence star of this mass. Both of these estimates indicate dust reddening is not significant for this star. The observed color index at primary eclipse should therefore give a reasonable estimate for the effective temperature. Table 5 of Pecan and Mamajek (2013) gives an effective temperature of 5471K and a spectral type of G8 for the larger cooler star.

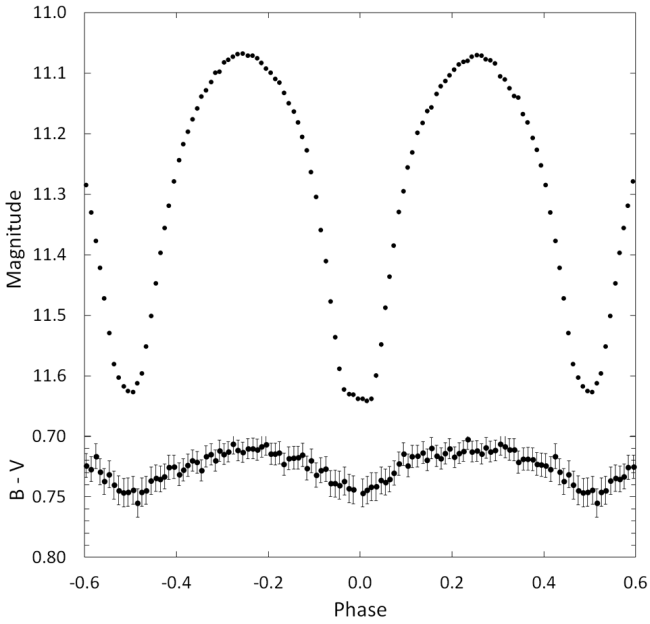

Figure 4. Light curve of all V-band observations in standard magnitudes (top panel). The observations were binned with a phase width of 0.01. The errors for each binned point are about the size of the plotted points. The B–V colors (bottom panel) were calculated by subtracting the binned V magnitudes from the linearly interpolated binned B magnitudes.

3.3. Synthetic light curve modeling

For light curve analysis BINARY MAKER 3.0 (BM3; Bradstreet and Steelman 2002) and the Wilson-Devinney program (WD; Wilson and Devinney 1971; Wilson 1990; Van Hamme and Wilson 1998) were used. There were 8 months separating the observations of DS1 and DS2. It was therefore decided to perform independent solutions for each data set. The solutions could then be compared for consistency and for changes in spot configurations, if any. The observations of DS1, passbands g', r', and i', were used for Solution 1 (S1) and DS2 observations, passbands B and V, were used for Solution 2 (S2). The observations in each passband were binned with a phase interval of 0.01. The average number of observations in each bin was 12 for the Sloan g', r', and i' passbands and 5 for Johnson B and V. The binned magnitudes were converted to relative flux for modeling. BM3 was used first to fit a synthetic light curve to the Sloan g' observations. Standard convective parameters and limb darkening coefficients from Van Hamme's (1993) tabular values were used. The total eclipses provided the necessary constraints for finding the mass ratio. The values from this initial fit were used as the input parameters for computation of a simultaneous 3-color light curve solution for S1 and a 2-color solution for S2 using the WD program. The weight attached to each binned data point for the WD solution was equal to the number of observations forming that point. The light curves indicate a likely contact configuration; therefore, Mode 3 was set in the program. The Method of Multiple Subsets (MMS) (Wilson and Biermann 1976) was employed to minimize

Table 3. V2790 Ori synthetic light curve solutions.

Parameter (no spots)	*Symbol (with spots)*	*Solution 1 (S1) (no spots)*	*Solution 1 (S1) (with spots)*	*Solution 2 (S2) (no spots)*	*Solution 2 (S2) (with spots)*
Gravity Darkening	$g_1 = g_2$	0.32	0.32	0.32	0.32
Bolometric Albedo	$A_1 = A_2$	0.50	0.50	0.50	0.50
Inclination	(°)	83.98 ± 0.26	84.15 ± 0.20	83.79 ± 0.25	83.43 ± 0.21
Effective Temp.	T_1, T_2 (K)	5620 ± 4, 5471	5620 ± 3, 5471	5624 ± 4, 5471	5625 ± 4, 5471
Surface Potential	$\Omega_1 = \Omega_2$	6.730 ± 0.014	6.732 ± 0.010	6.731 ± 0.018	6.731 ± 0.018
Mass Ratio	$q(M_2 / M_1)$	3.168 ± 0.012	3.157 ± 0.008	3.140 ± 0.017	3.141 ± 0.017
Fill-Outs	$f_1 = f_2$	0.17	0.15	0.12	0.12
Luminosity	$L_1 / (L_1 + L2)_{g'}$	0.2966 ± 0.0007	0.2966 ± 0.0007	—	—
	$L_1 / (L_1 + L2)_{r'}$	0.2867 ± 0.0005	0.2867 ± 0.0005	—	—
	$L_1 / (L_1 + L2)_{i'}$	0.2830 ± 0.0005	0.2830 ± 0.0005	—	—
	$L_1 / (L_1 + L2)_B$	—	—	0.3021 ± 0.0007	0.3024 ± 0.0007
	$L_1 / (L_1 + L2)_V$	—	—	0.2919 ± 0.0006	0.2921 ± 0.0006
Limb Darkening	$x_{1g'}$, $x_{2g'}$	0.838, 0.840	0.838, 0.840	—	—
	$y_{1g'}$, $y_{2g'}$	0.091, 0.064	0.091, 0.064	—	—
	$x_{1r'}$, $x_{2r'}$	0.760, 0.767	0.760, 0.767	—	—
	$y_{1r'}$, $y_{2r'}$	0.214, 0.194	0.214, 0.194	—	—
	$x_{1i'}$, $x_{2i'}$	0.680, 0.686	0.680, 0.686	—	—
	$y_{1i'}$, $y_{2i'}$	0.238, 0.221	0.238, 0.221	—	—
	x_{1B}, x_{2B}	—	—	0.853, 0.853	0.853, 0.853
	y_{1B}, y_{2B}	—	—	0.039, 0.009	0.039, 0.009
	x_{1V}, x_{2V}	—	—	0.797, 0.802	0.797, 0.802
	y_{1V}, y_{2V}	—	—	0.165, 0.142	0.165, 0.142
Residuals	$\sum res^2$	0.0196	0.0056	0.0082	0.0053
Spot 1 on Star 1			Hot Spot		Hot Spot
Colatitude	(°)	—	105 ± 5	—	100 ± 8
Longitude	(°)	—	10 ± 3	—	7 ± 5
Spot Radius	(°)	—	14 ± 4	—	12 ± 5
Spot T-factor	(T_{spot} / T_{eff})	—	1.16 ± 0.05	—	1.17 ± 0.09
Spot 2 on Star 2			Cool Spot		Cool Spot
Colatitude	(°)	—	78 ± 4	—	—
Longitude	(°)	—	2 ± 1	—	—
Spot Radius	(°)	—	12 ± 4	—	—
Spot T-factor	(T_{spot} / T_{eff})	—	0.90 ± 0.05	—	—

strong correlations of the parameters and the Kurucz stellar atmosphere model was applied. The fixed inputs included standard convective parameters: gravity darkening, $g_1 = g_2 = 0.32$ (Lucy 1968), albedo value $A_1 = A_2 = 0.5$ (Ruciński 1969), and the effective temperature of the cooler star, T_2, was set to the value determined in section 3.2, 5471K. Logarithmic limb darkening coefficients were calculated by the WD program from tabulated values using the method of Van Hamme (1993). The solution's adjustable parameters include the inclination (i), mass ratio ($q = M_2 / M_1$), potential (Ω, $\Omega_1 = \Omega_2$), temperature of the primary star (T_1), and the normalized flux for each wavelength (L). The best-fit solutions for each data set are shown in Table 3 (columns 3 and 5). The fill-out parameter calculated was defined by Lucy and Wilson (1979) and is given by:

$$f = \frac{\Omega_{inner} - \Omega}{\Omega_{inner} - \Omega_{outer}} \quad (6)$$

where Ω_{inner} and Ω_{outer} are the inner and outer critical equipotential surfaces and Ω is the equipotential surface which describes the stellar surface. BM3 was used to calculate the fill-out values, which are reported in Table 3 for each solution. No third light was noted when included in the adjustable parameters. Only negligible small values resulted, indicating no appreciable contribution to the system's light. The normalized light curves for each passband overlaid by the synthetic solution curves (solid lines) are shown in Figure 5, with the residuals shown in Figure 6.

3.4. Spot model

The asymmetries in eclipsing binary light curves are usually attributed to large cool spots, hot regions such as faculae or gas streams that impact one of the stars. To fit the asymmetries in the light curves a second model was attempted for both DS1 and DS2. Excess light was noted in all five residual curves center at about phase 0.8 (see Figure 6). An over-luminous spot was added to both models to account for this excess light. A deficit of light was also noted between phase 0.2 and 0.5 in the three residual curves from S1. This required a second under-luminous spot in that model. BM3 was used again to obtain a good fit between the synthetic and observed light curves by adjusting each spot's parameters (latitude, longitude, spot size, and temperature). The best-fit spot parameter values from BM3

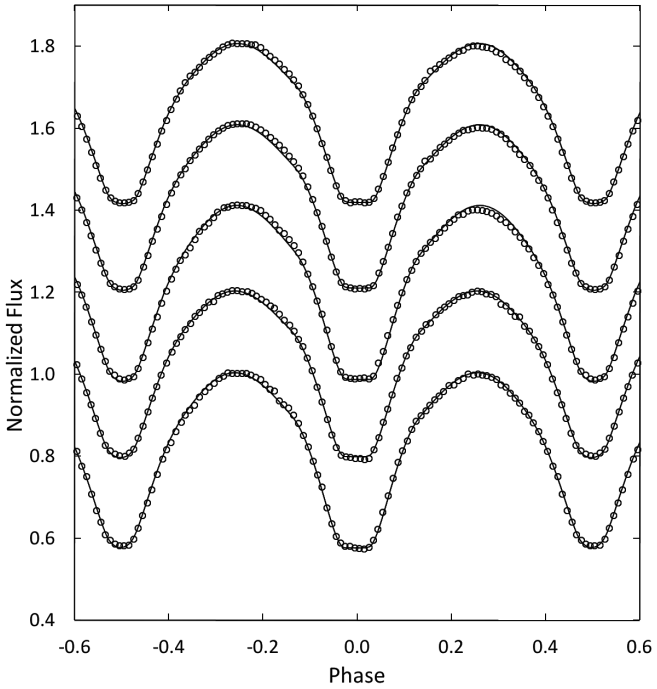

Figure 5. The WD model fit without spots (solid curve) to the observed normalized flux curves for each passband. From top to bottom the passbands are Sloan i', Sloan r', Sloan g', Johnson V, and Johnson B. The Sloan passbands are for solution S1 and the Johnson passbands are for solution S2. Each curve is offset by 0.2 for this combined plot. The best-fit parameters are given in columns 3 and 5 of Table 3. Error bars are omitted from the points for clarity.

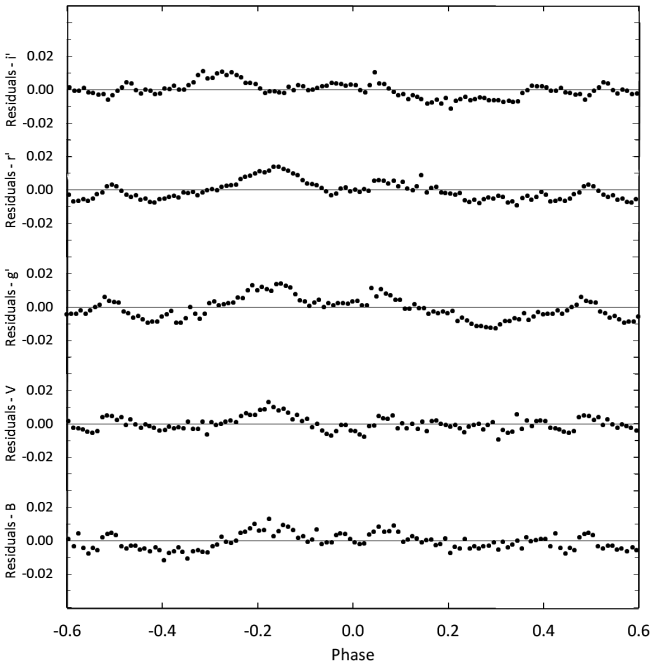

Figure 6. The residuals for the best-fit WD model without spots. The g', r', and i' residuals are from S1 and B and V from S2. Error bars are omitted from the points for clarity.

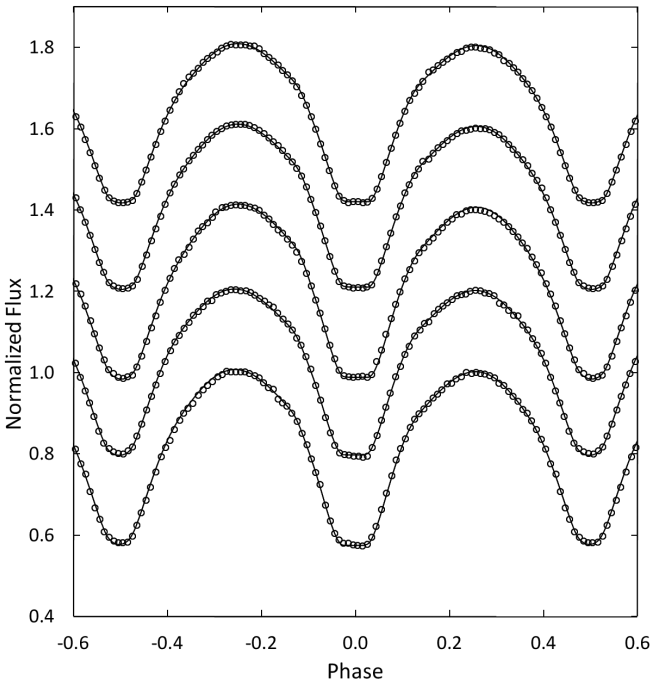

Figure 7. The WD model fit with spots (solid curve) to the observed normalized flux curves for each passband. From top to bottom the passbands are Sloan i', Sloan r', Sloan g', Johnson V, and Johnson B. The Sloan passbands are for solution S1 and the Johnson passbands are for solution S2. Each curve is offset by 0.2 for this combined plot. The best-fit parameters are given in columns 4 and 6 of Table 3. Error bars are omitted from the points for clarity.

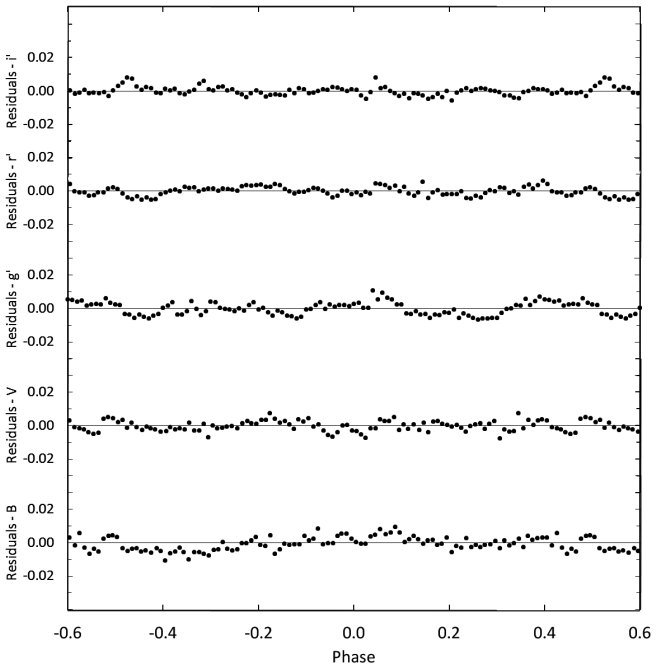

Figure 8. The bottom panel shows the residuals for the spotted WD model in each passband. The g', r', and i' residuals are from S1 and B and V from S2. Error bars are omitted from the points for clarity.

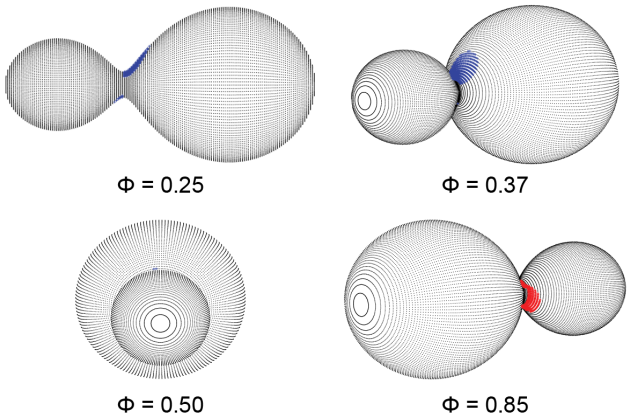

Figure 9. Roche Lobe surfaces of the best-fit WD spot model from S1 with orbital phase shown below each diagram.

Table 4. Provisional stellar parameters for V2790 Ori.

Parameter	*Symbol*	*Value*
Stellar masses	M_1 ($M_\odot$)	0.30
	M_2 ($M_\odot$)	0.96
Semi-major axis	a ($R_\odot$)	1.98
Stellar radii	R_1 ($R_\odot$)	0.58
	R_2 ($R_\odot$)	0.97
Surface gravity	log g_1 (cgs)	4.39
	log g_2 (cgs)	4.44
Mean density	$\overline{\rho}_1$ (g cm^{-3})	2.17
	$\overline{\rho}_2$ (g cm^{-3})	1.46
Stellar luminosity	L_1 V ($L_\odot$)	0.28
	L_2 V ($L_\odot$)	0.68
Bolometric magnitude	$M_{bol,1}$	6.05
	$M_{bol,2}$	5.05

Values in this table are provisional (calculated). Radial Velocity observations are necessary for direct determination of M_1, M_2, and a.

were then included in new WD solution attempts. The stellar parameters from the first solution were held fixed while the spot parameters were adjusted until the solution converged. The spot parameters were then held fixed and the stellar parameters adjusted until the solution converged again. This process was repeated until the model converged to a final solution. The final values for the spotted solution parameters are shown in columns 4 and 6 in Table 3. Figure 7 shows the spotted model fit (solid lines) to the observed light curve for each passband and solution. Figure 8 shows the residuals for the spotted models. For S1 the sum of the residuals squared was 0.0056 for the spotted model and 0.0196 for the unspotted model (3.5 times larger). For S2 the sum of the residuals squared was 0.0053 for the spotted model and 0.0082 for the unspotted model (1.5 times larger). A graphical representation of the spotted S1 solution is shown in Figure 9.

It is interesting to note that the resulting stellar parameters for the spotted S1 and S2 models agreed well except for the spot configuration. S2 did not require the under-luminous spot found in S1. The over-luminous (hot spot) modeled in S1 was found in S2 at almost the same location, size, and temperature. Since the two data sets were separated by 8 months this particular spot may be a long-lived feature in the primary star's photosphere while the under-luminous spot seems to have disappeared.

4. Discussion and conclusions

Several stellar parameters can now be determined. An estimate for the mass of the larger cooler star was found to have a value of $M_2 = 0.96 \pm 0.07\ M_\odot$ (see section 3.2). This value combined with the S1 mass ratio (q) gives a mass for the smaller hotter star of $M_1 = 0.30 \pm 0.07\ M_\odot$. Applying Kepler's Third Law gives the distance between the star's mass centers as $1.98 \pm 0.01\ R_\odot$. Mochnacki (1981) showed the mean stellar densities for contact binaries are given by:

$$\overline{\rho}_1 = \frac{0.0189}{r_1^3\,(1+q)\,P^2} \text{ and } \overline{\rho}_2 = \frac{0.0189q}{r_2^3\,(1+q)\,P^2}\ , \qquad (7)$$

where the stellar radius is normalized to the semimajor axis and P is in days. The computed values are $\overline{\rho}_1 = 2.18$ g cm^{-3} and $\overline{\rho}_2 = 1.47$ g cm^{-3}. Additional stellar parameters were computed with the Wilson and Devinney (1971) light curve program (LC). All the computed stellar parameters are collected in Table 4.

The distance to V2790 Ori can be estimated using an empirical formula derived by Ruciński and Duerbeck (1997) which is given by:

$$M_v = -4.44 \log_{10} P + 3.02\,(B-V)_0 + 0.12. \qquad (8)$$

Equation 8 gives a distance modulus of $(m - M)_v = 4.76$ and distance of 183 ± 19 pc. An additional determination of distance can be made using the bolometric magnitudes in Table 4 combined with the bolometric corrections from Pecaut and Mamajek (2013). The correction for the primary star is $BC_{v1} = -0.14$ and $BC_{v2} = -0.18$ for the secondary star. The calculated magnitude for the system is $M_v = 4.87$, which gives a distance of 174 pc. The two distance determinations differ by about 5% but are a little closer than the 199 pc distance found by Gettel (2006).

W UMa-type binaries most often consist of two cool stars in contact whose spectral types are F, G, or K and their components have nearly equal surfaces temperatures in spite of their often greatly differing masses. This study confirms that V2790 Ori is a member of this class of eclipsing binaries with a high mass ratio of 3.15 and stars differing in temperature by only 150 K. It is a member of the W-type subclass where the larger more massive star is cooler and has less surface brightness than its companion and primary eclipse is an occultation. The best-fit WD solutions with fill-out values between 0.12 and 0.17 are consistent with a contact binary. No secular period change was found but this system needs to be monitored regularly for a possible third body in the system. A spectroscopic radial velocity study of this system, when combined with the photometric solution presented here, would be invaluable in determining the absolute properties of the stars.

5. Acknowledgements

The author wishes to thank Dr. Norman Markworth for reviewing this manuscript and his guidance in the use of the WD program. This research has made use of the SIMBAD database, operated at CDS, Strasbourg, France. This research was made possible through the use of the AAVSO Photometric All-Sky Survey (APASS), funded by the Robert Martin Ayers Sciences Fund.

References

Bradstreet, D. H., and Steelman, D. P. 2002, *Bull. Amer. Astron. Soc.*, **34**, 1224.
Diethelm, R. 2011, *Inf. Bull. Var. Stars*, No. 5960, 1.
Diethelm, R. 2012, *Inf. Bull. Var. Stars*, No. 6011, 1.
Gettel, S. J., Geske, M. T., and McKay, T. A. 2006, *Astron. J.*, **131**, 621.
Henden, A. A., *et al.* 2014, AAVSO Photometric All-Sky Survey, data release 9 (http:www.aavso.org/apass).
Hübscher, J. 2013, *Inf. Bull. Var. Stars*, No. 6084, 1.
Kafka, S. 2015, observations from the AAVSO International Database (https:/www.aavso.org/aavso-international-database).
Kwee, K. K., and van Woerden, H. 1956, *Bull. Astron. Inst. Netherlands*, **12**, 327.
Lucy, L. B. 1968, *Astrophys. J.*, **151**, 1123.
Lucy, L. B., and Wilson, R. E. 1979, *Astrophys. J.*, **231**, 502.
Mirametrics. 2015, Image Processing, Visualization, Data Analysis (http://www.mirametrics.com).
Mochnacki, S. W. 1981, *Astrophys. J.*, **245**, 650.
Nagai, K. 2012, *Var. Star Obs. League Japan*, No. 53, 1**.**
Nagai, K. 2013a, *Var. Star Obs. League Japan*, No. 55, 1.
Nagai, K. 2013b, *Var. Star Obs. League Japan*, No. 56, 1.
Nelson, R. H. 2011, *Inf. Bull. Var. Stars*, No. 5966, 1.
Nelson, R. H. 2012, *Inf. Bull. Var. Stars*, No. 6018, 1.
Otero, S. A., Wils, P., and Dubovsky, P. A. 2004, *Inf. Bull. Var. Stars*, No. 5570, 1.
Pecaut, M. J., and Mamajek, E. E. 2013, *Astrophys. J., Suppl. Ser.*, **208**, 9 (http://www.pas.rochester.edu/~emamajek/EEM_dwarf_UBVIJHK_colors_Teff.txt).
Qian, S. 2003, *Mon. Not. Roy. Astron. Soc.*, **342**, 1260.
Ruciński, S. M. 1969, *Acta Astron.*, **19**, 245.
Ruciński, S. M., and Duerbeck, H. W. 1997, *Publ. Astron. Soc. Pacific*, **109**, 1340.
Schlafly, E. F., *et al.* 2014, *Astrophys. J.*, **789**, 15 (http://faun.rc.fas.harvard.edu/eschlafly/2dmap/querymap.php).
Van Hamme, W. 1993, *Astron. J.*, **106**, 2096.
Van Hamme, W., and Wilson, R. E. 1998, *Bull. Amer. Astron. Soc.*, **30**, 1402.
Wang, J. M. 1994, *Astrophys. J.*, **434**, 277.
Wilson, R. E. 1990, *Astrophys. J.*, **356**, 613.
Wilson, R. E., and Biermann, P. 1976, *Astron. Astrophys.*, **48**, 349.
Wilson, R. E., and Devinney, E. J., 1971, *Astrophys. J.*, **166**, 605.
Wozniak, P. R., *et al.* 2004, *Astron. J.*, **127**, 2436.

Long-Term Radial Velocity Monitoring of the HeI 6678 Line of ζ Tauri

Ernst Pollmann
Emil-Nolde-Str.12, Leverkusen, 51375, Germany; ernestospec@hotmail.de

Received March 1, 2016; revised March 24, 2016 and March 30, 2016; accepted April 15, 2016

Abstract The binary star ζ Tau, one of the brightest Be stars in the northern sky, shows cyclic behavior in the radial velocity (RV) variations on several distinct time scales. The star shows cyclic behavior in the radial velocity of, among others, the HeI 6678 absorption line. With an investigation period of approximately 15 years (December 2000 to February 2016) we have been able to compare three time intervals: quasi-quasi-period = 1503 d in Stefl *et al.* (2007) for 1993-2005, quasi-period = 1325 d in Ruzdjak *et al.* (2009) for 2001–2008, and quasi-period = 1190 d this paper for 2008–2016. The last quasi-period (1190 d (± 35)) points out that the quasi-period found for RV data since 2003 has constantly decreased.

1. Introduction

The binary star ζ Tauri, one of the brightest Be stars in the northern sky, shows cyclic behaviour in the radial velocity (RV) variations on several distinct time scales. It is also a spectroscopic binary with a 133-day orbital quasi-period established by Harmanec (1984). Its orbital RV variations are superimposed on the cyclic long-term and short-term ones. ζ Tau also shows cyclic behavior in the radial velocity of, among others, the HeI 6678 absorption line. As far we know the first long-term investigation (time quasi-period 1993–2005) of the RV of the HeI 6678 absorption line was performed by Stefl *et al.* (2007). The result of that monitoring until circa 2007 led to a long-term quasi-quasi-period of 1503 days.

2. Observations

The spectra presented here for the RV measurements of the HeI 6678 line were taken at different locations with a 20-cm Newtonian and a 40-cm Schmid-Cassegrain telescope. Spectrographs with spectral resolving power of 10,000 to 20,000 were used. The signal to noise ratio of these spectra was of the order of magnitude S/N = 200–300. The spectra have been reduced with standard procedures (instrument response, normalization, wavelength calibration) by using the program VSPEC (Desnoux 2016).The evaluation of the heliocentric RV was performed by the profile mirror method. This method measures the Doppler shift of spectra by correlation of the spectral line with their mirroring around the laboratory wavelength, and is particularly suitable for the evaluation of asymmetrical lines within exactly specified profile ranges.

3. Long-term changes

With our much longer investigation quasi-period of approximately 15 years (December 2000 to February 2016) we have been able to compare the 1503-day quasi-period of Stefl *et al.* (2007) with our results. Such a long investigation quasi-period was possible because we were able to combine radial velocity data from Ruzdjak *et al.* (2009) with our data of the Astronomical Ring for Access to Spectroscopy (ARAS) group (2016). This long-term monitoring is shown in Figure 1. In order to recognize the separate cyclic behavior of the Ruzdjak *et al.* data and the ARAS data, the corresponding separate phase plots are shown in Figures 2 and 3. The overlay of both quasi-periods is shown in Figure 4. For this analysis the program AVE (AVE Software 1999) was used.

Altogether three time intervals are now for a comparative investigation available: 1) the 1503-day quasi-period in Stefl *et al.* (2007) 1993–2005; 2) the 1325-day quasi-period in Ruzdjak *et al.* (2009) 2001–2008; and 3) the 1190-day quasi-period this paper 2008–2016.

The comparison of Figures 2, 3, and 4 points out that the quasi-period found for RV data since 2003 has constantly decreased, as well as the amplitude of the RV variations. Even more

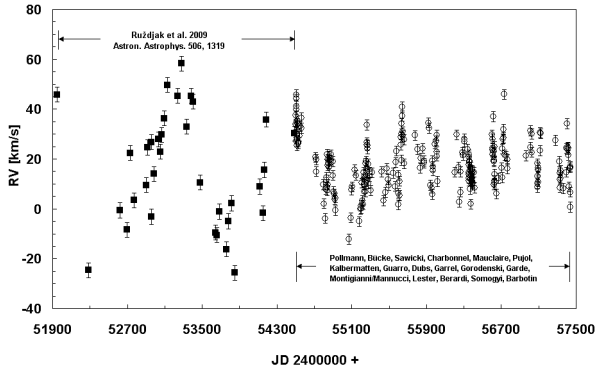

Figure 1. RV Long-term monitoring of the HeI6678 line from December 2000 to February 2016.

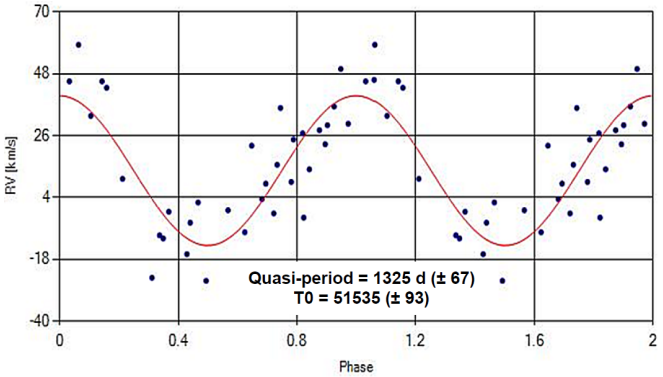

Figure 2. RV variation (quasi-quasi-period = 1325 d (± 67)) of Ruzdjak *et al.* (2009) data in Figure 1.

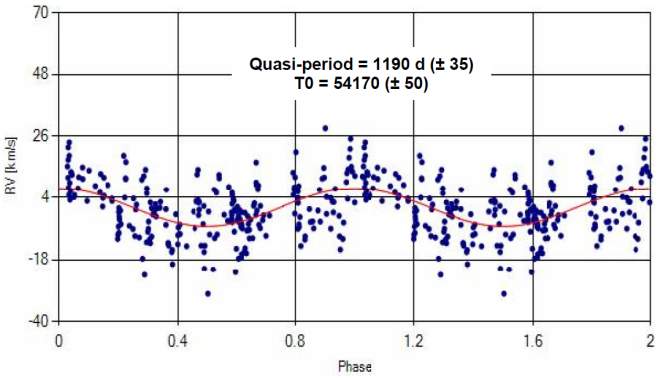

Figure 3. RV variation (quasi-quasi-period = 1190 d (± 35)) of ARAS (2016) data in Figure 1.

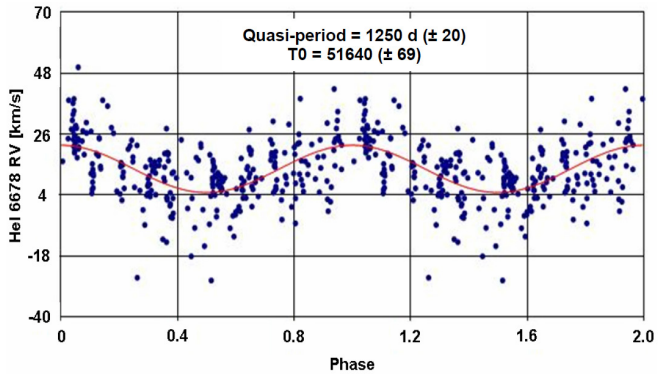

Figure 4. RV variation (quasi-quasi-period = 1250 d (± 20)) of the ARAS (2016) and Ruzdjak *et al.* (2009) data in Figure 1.

complicated behavior of the RV variation of H-alpha and or HeI profiles is documented in Ruzdjak *et al.* (2009; their Figure 2).

4. Orbital variations

One of the most interesting studies of the RV variations in the spectrum of ζ Tau is the paper by Ruzdjak *et al.* (2009). We were fortunate to start a long-term observing campaign of the HeI 6678 line at the time, when the investigations of the researchers of the mentioned paper ended, approximately at JD 2454500. Our findings on the HeI 6678 RV orbital variability of 132.2 d (± 0.8) and 131.3 d (± 0.9) obtained with different analysis programs (Pollmann *et al.* 2012) are very close to those of Ruzdjak *et al.* (2009) for the most important parameters.

5. Discussion

The attempts to detect long-term cyclic RV variations of the HeI 6678 absorption line in the spectrum of ζ Tau—Stefl *et al.* (2007) quasi-period = 1503 d; Ruzdjak *et al.* (2009) quasi-period = 1325 d (± 67); this paper, quasi-period = 1190 d (± 35)—point out that the quasi-period found for RV data since 2003 has constantly decreased, as documented in Ruzdjak *et al.* 2009 (their Figure 2). In addition, it is necessary to take into account the overlaid medium-term orbital RV period of 133 days (Harmanec 1984; Ruzdjak *et al.* 2009; Pollmann *et al.* 2012).

6. Acknowledgements

I am grateful to Sara and Carl Sawicki (Alpine, Texas) for their helpful improvements and suggestions in language. I am grateful, too, to Prof. Dr. Anatoly Miroshnichenko (University of North Carolina at Greensboro) for his comprehensive support improving this work in several aspects.

References

ARAS group. 2016, Astronomical Ring for Access to Spectroscopy (ARAS; http://www.astrosurf.com/aras/).

AVE software. 1999, AVE (Analisis de Variabilidad Estelar, Version 2.51; http://www.astrogea.org/soft/ave/introave.htm).

Desnoux, V. 2016, VSPEC Visual Spec software (http://www.astrosurf.com/vdesnoux).

Harmanec, P. 1984, *Bull. Astron. Inst. Czechoslovakia*, **35**, 164.

Pollmann, E., Mauclaire, B., and Bücke, R. 2012, *Inf. Bull. Var. Stars*, No. 6099, 5.

Ruzdjak, D., *et al.* 2009, *Astron. Astrophys.*, **506**, 1319.

Stefl, S., Okazaki, A. T., Rivinius, T., and Baade, D. 2007, in *Active OB-Stars: Laboratories for Stellar and Circumstellar Physics*, ASP Conf. Ser. 361, Astronomical Society of the Pacific, San Francisco, 274.

Analysis of Pulsating Components in the Eclipsing Binary Systems LT Herculis, RZ Microscopii, LY Puppis, V632 Scorpii, and V638 Scorpii

Margaret Streamer
Variable Stars South; 3 Lupin Place, Murrumbateman, NSW 2582, Australia; m.stream@bigpond.com

Terry Bohlsen
Variable Stars South; Mirranook, Armidale, NSW 2350, Australia

Yenal Ogmen
Variable Stars South; P.O. Box 756, Nicosia, North Cyprus via Mersin 10, Turkey

Received March 7, 2016; revised April 12, 2016; accepted April 20, 2016

Abstract Eclipsing binary stars are especially valuable for studies of stellar evolution. If pulsating components are also present then the stellar interior can be studied using asteroseismology techniques. We present photometric data and the analysis of the δ Scuti pulsations that we have discovered in five eclipsing binary systems. The systems are: LT Herculis, RZ Microscopii, LY Puppis, V632 Scorpii, and V638 Scorpii. The dominant pulsation frequencies range from 13 to 29 cycles per day with semi-amplitudes of 4 to 20 millimagnitudes.

1. Introduction

Members of Variable Stars South have discovered seven systems with pulsating components found while obtaining accurate eclipse timings to update light elements of poorly studied southern eclipsing binaries (Moriarty *et al.* 2013; Streamer *et al.* 2015). We have previously reported the pulsation properties of three of these binary systems (Moriarty *et al.* 2013). Here we report the pulsation properties of four more of these binaries and include an eighth, newly discovered system, LY Puppis.

The evolutionary history of pulsating stars, in this case δ Scuti type, in a binary system is considerably different from those of isolated δ Scuti stars, making the former valuable for investigations of the stellar interior and other astrophysical properties of this type of star.

Ground-based astronomers, at best, can only obtain uninterrupted portions of light curves of eclipsing binary systems spanning entire nights. A team of observers in different longitudes can provide better coverage but all are constrained by cloud, full moon, changes in air mass, poor seeing and/or transparency and the unavoidable day/night and seasonal cycles. Nevertheless, high frequency pulsations, such as the δ Scuti type, are readily detected in high-cadence data sets.

Fourier analysis of the individual light curves reveals the frequency and amplitude of the pulsations which in turn gives information about the stellar interior. However, analysis of such short duration observations, in which only a few pulsation cycles are observed, must be considered cautiously. Also, cycle count ambiguities are present if data sets from consecutive nights are combined and sampled (see Murphy (2015) for a review of aliasing in the context of Fourier analysis of δ Scuti stars). At best, only one or two frequencies are reliably identified from short-duration data. In contrast, space-based instrumentation, such as the Kepler Mission, provides data of high precision, long duration, and continuity. Fourier analysis of Kepler data typically reveals multiple frequencies. For example, Hambleton *et al.* (2013) identified 32 frequencies in the binary KIC 4544587.

Fourier analysis of the pulsations we observed gives frequencies and amplitudes of the dominant pulsations confirming the δ Scuti component of the systems studied. LT Her has previously been reported to have a δ Scuti component by Liakos and Niarchos (2015) but none of the other of our targets are listed in their catalogue.

2. Observations and analysis

Time series photometry was performed with the instruments given in Table 1. Each observer used NTP software such as DIMENSION 4 (Thinking Man Software 1992–2014) to synchronize their computer's clock to UTC. A fast cadence was used to acquire the photometric data to ensure good coverage of the pulsations and for accurate determination of the eclipse times of minima. Typical exposure times were of 60 to 120 seconds with delays between each exposure (for image download) of about 30 seconds. Targets were also observed during secondary eclipses and out of eclipse for the longest duration possible in

Table 1. Photometric equipment used by the authors.

Observer	*Initials*	*Telescope*	*Camera*
Streamer	MS	350-mm Meade Schmidt-Cassegrain	SBIG ST8XME CCD
Ogmen	YO	356-mm Meade LX200R (ACF)	SBIG ST8XME CCD
Bohlsen	TB	200-mm Vixen VC200L Cassegrain	SBIG ST10XME CCD

any one night to maximize the time span available for Fourier analysis of the pulsations.

Most CCD imaging was done with Johnson V filters; some data for LT Her were also obtained with a clear filter. The images were reduced using aperture photometry; details of the comparison stars are given in Table 2. The resulting magnitude data are untransformed. Details of the observation logs are also given in Table 2 along with the spectral classification of each system as reported in the literature.

Times of minima were determined using the Polynomial fit in PERANSO (Vanmunster 2013). Pulsation frequencies were analysed using Fourier methods in PERIOD04 (Lenz and Breger 2005), using as many data sets as possible for each target. For analysis of pulsations in secondary eclipses, a polynomial fit to the eclipse curve was first subtracted.

Additionally, Bohlsen determined the spectral type of V632 Sco from a spectrum obtained with a LISA spectrograph on a Celestron C11 SCT using an Atik 314L+ CCD with a resolution of R = 1000 and a S/N of approximately 100. The spectrum was calibrated using a neon calibration light.

The spectrum was compared to known standards in the MK Spectral classification system, with a resolution of 3.6 Angstrom, from the Dark Sky Observatory at the Appalachian State University (Gray 2013). The accuracy of the spectral classification was limited by the resolution and the S/N of equipment.

3. Results and Discussion

Updated light elements for RZ Mic, V632 Sco, and V638 Sco were previously reported by Streamer *et al.* (2015). Regression analysis of three primary minima for LT Her give a current epoch (HJD) of 2455752.3219 ± 0.0028 and a period of 1.0840 ± 0.0001 days. Only one complete primary eclipse has been observed for LY Pup, giving an improved epoch of 2456695.1274 ± 0.0027 HJD using the period of 2.8879 ± 0.0001 days from the *General Catalogue of Variable Stars* (GCVS; Kholopov *et al.* 1985) as reference.

Results of the Fourier analysis of the pulsations for each target are given in Table 3 with examples of power spectra given in Figure 1. Examples of primary and secondary eclipses, as well as uneclipsed portions of the orbital cycle, for each target are shown in Figures 2 through 15.

3.1. RZ Microscopii

RZ Mic (V mag. = 11.35, P = 3.9830 days) has a 0.95-magnitude primary eclipse and a 0.25-magnitude secondary eclipse. The primary eclipse is about 0.5 magnitude deeper than reported in the International Variable Star Index (VSX; Watson *et al.* 2014) but our results agree with ASAS observations (Pojmański 1997). Of all the targets reported here, RZ Mic has the highest-amplitude δ Scuti pulsations. The pulsations are evident during all orbital phases (Figures 2, 3, and 4) although during the primary eclipse (Figure 2) they only appear as distortions on the otherwise smooth curve. Two pulsation frequencies were identified, with the dominant frequency being 13.52 ± 0.04 cycles/day with a semi-amplitude of 19 ± 0.6 millimagnitudes (Table 3). A much lower amplitude (4 ± 0.7 mmag.) second frequency (25.67 ± 0.20 c/d) was also consistently extracted from the individual data sets. The same frequencies were confirmed when observations from four consecutive nights were combined and analyzed.

3.2. LY Puppis

LY Pup (V mag. = 12.35, P = 2.8879 days) has eclipses of over 9 hours duration. Thus, observing complete eclipses during the short summer nights when the target is visible in Australia is difficult. However, one complete primary eclipse of 0.85 magnitude was obtained and is shown in Figure 5. Pulsations are hardly evident in this eclipse although they are seen in other incomplete primary eclipses. One of these is also shown in Figure 5. In contrast, pulsations are easily detected during the small secondary eclipse of 0.03 magnitude (Figure 6) and in uneclipsed portions of the light curve (Figure 7). Two pulsation frequencies were extracted: a primary frequency of 27.15 ± 0.13 c/d with a semi-amplitude of 20 ± 1 mmag. and a slightly lower one of 25.45 ± 0.48 c/d with an amplitude approximately half that of F1 (9 ± 1 mmag.). The two light curves (Figures 6 and 7) clearly show these amplitude differences. The high amplitude, primary frequency, F1, has only been observed twice out of the six data sets analyzed. The short time-span of each data set, coupled with the similarity of the two extracted frequencies, suggests the addition/interference of each frequency component creates a beat pattern which obscures the high-amplitude frequency. Examples of the power spectra for the data sets exhibiting the two different frequencies are shown in Figure 1.

Table 2. Comparison stars and their magnitudes, observation logs and spectral type of each binary system.

Binary System	*Comparison Star*	*V Mag. Comp.*	*Number of Nights Observed*	*Number of Hours Observed*	*Phase Observed*	*Spectral Type*
LT Her	GSC 0966 1191	9.774	7	27	0.0–0.25,	A2V+[F3][1]
	GSC 0966 1345	11.07			0.35–0.6,	A2V[2]
					0.8–1.0	
RZ Mic	GSC 7972 0135	11.310	19	174	0.0–1.0	A5+[F4.5][1]
LY Pup	GSC 6555 0556	10.568	12	71.5	0.0–1.0	(A5)+[K0IV][1]
V632 Sco	GSC 7891 0318	11.551	10	48.5	0.0–0.24,	F2 + [K4–K5][3]
	GSC 7891 0006	10.929			0.37–1.0	F0V or F1V[4]
V638 Sco	GSC 7891 0378	11.110	13	81.4	0.4–1.0	A(8)+[G8IV][1]

Notes: 1—Spectral types from Svechnikov and Kuznetsova (1990); 2—Spectral type from Ebbighausen and Penegor (1974) ; 3—Spectral type from Giuricin et al. (1984); 4—Bohlsen, this work.

Table 3. Dominant frequencies with their semi-amplitudes for each target.

Binary System	*Pulsation F1 (cycles/day)*	*Pulsation F2 (cycles/day)*	*Pulsation Amp 1 (millimag.)*	*Pulsation Amp 2 (millimag.)*
LT Her	28.87±0.09		6±1	
RZ Mic	13.52±0.04	25.67±0.20	19±0.6	4±0.7
LY Pup	27.15±0.13	25.45±0.48	20±1	9±1
V632 Sco	25.58±0.10		6±1	
V638 Sco	15.23±0.23		5±1	

3.3. LT Herculis, V632 Scorpii, and V638 Scorpii

LT Her, V632 Sco, and V638 Sco are all characterized by low amplitude pulsations from 4 to 6 mmag. Only one pulsation frequency was reliably extracted from the data for each target. Even though the three targets are not particularly dim, the pulsation amplitudes are small and approaching the limits of detection for our equipment. Good photometric conditions were needed to reliably record the pulsations. However, we are confident of the existence of pulsations in these target systems as they have been recorded numerous times and independently by members of our group.

The data for LT Her (V mag. = 10.5, P = 1.0840 days) were collected using different comparison stars with either no filter or a V filter. For easier comparison, Figures 8 and 9 are given as Δ magnitudes rather than as untransformed magnitudes. A primary eclipse (Figure 8) shows the distortions imposed upon the light curve by the pulsations of the primary component and Figure 9 shows the pulsations clearly at the end of an eclipse. The single frequency extracted (28.87 ± 0.09 c/d) has a semi-amplitude of 6 ± 1 mmag. Liakos and Niarchos (2015) have also reported a primary frequency of 30.800c/d which differs slightly from what we determined. The latter did not report errors or the amplitude of this frequency, so it is difficult to establish if the differences are real.

Earlier studies of LT Her by Ebbighausen and Penegor (1974) clearly show pulsations, although they interpreted the effect to be due to gas transfer between the component stars.

Data reduction of observations of V632 Sco (V mag. = 11.2, P = 1.6102 days) is hampered by the close proximity of other stars which are not completely resolved during poor seeing conditions. However, after numerous observations by three different observers, we are confident that a pulsating component is present in the binary system (Figures 10, 11, and 12). A dominant frequency of 25.63 ± 0.14 c/d with semi-amplitude 6 ± 1 mmag. was extracted from the data sets.

Our spectral classification for V632 Sco is F0V or F1V, suggesting that the primary component is hotter than that given by Giuricin *et al.* (1984) who determined the spectral classification for the system as F2 + [K4-K5].

The pulsations in V638 Sco (V mag. = 10.8, P = 2.3583 days) have the lowest amplitude of all the targets reported in this paper. Excellent photometric conditions are needed to see the pulsations which have a semi-amplitude of only 4 ± 1 mmag. Figure 13 shows a primary eclipse which is distorted by the effects of the pulsations. Figures 14 and 15 illustrate the effects of poor seeing on the results. The first secondary eclipse (Figure 14) was observed under excellent conditions whereas Figure 15 shows an eclipse observed close to the date of full moon with poor transparency. The frequency of the dominant pulsation is 15.23 ± 0.23 c/d.

4. Conclusions

Our photometric data for the five systems described here indicate that the primary components are the pulsators. The primary eclipses of all the targets show distortions caused by the pulsations of the primary star, indicating that all the systems are inclined to our line-of-sight. The pulsations also show greater amplitude during the primary eclipses caused by the spatial filtering effect (Gamarova *et al.* 2003) when the secondary star blocks some of the primary star's light allowing discrete pulsation zones to be observed independently of others.

The frequencies and amplitudes of the pulsations are typical of those of δ Scuti stars. The spectral classifications (Table 2) also indicate that the primaries are in the instability strip of the H-R diagram.

Two types of binaries with pulsating components are recognized. The first type consists of detached systems with no mass exchange, with the pulsator being a typical δ Sct star. The second type, oscillating EA systems (oEAs), has been defined by Mkrtichian *et al.* (2004) as eclipsing Algol (EA) binaries with a pulsating, δ Sct star. These types of binaries are semi-detached with the primary component undergoing mass accretion from a larger secondary that has filled its Roche lobe. The evolution of the δ Sct component in these systems is different from those in the first category.

We are conducting additional photometric studies combined with radial velocity measurements for a better understanding of each of these targets and to determine in which of these categories our targets fit.

5. Acknowledgements

Margaret Streamer thanks Dr. Simon Murphy, Sydney Institute for Astronomy, University of Sydney, for his help and advice on the correct use of PERIOD04. Margaret Streamer acknowledges grants from Variable Stars South to purchase software. This research has made use of the International Variable Star Index (VSX) database, operated at AAVSO, Cambridge, Massachusetts, USA.

References

Ebbighausen, E. G., and Penegor, G. 1974, *Publ. Astron. Soc. Pacific*, **86**, 203.

Gamarova, A. Yu., Mkrtichian, D. E., Rodriguez, E., Costa, V.,

and Lopez-Gonzalez, M. J. 2003, in *Interplay of Periodic, Cyclic and Stochastic Variability in Selected Areas of the H-R Diagram*, ed. C. Sterken, ASP Conf. Ser. 292, Astronomical Society of the Pacific, San Francisco, 369.

Giuricin, G., Mardirossian, F., and Mezzetti, M. 1984, *Astrophys. J., Suppl. Ser.*, **54**, 421.

Gray, R. O. 2013, A Digital Spectral Classification Atlas, (http://stellar.phys.appstate.edu/Standards/stdindex.html; http://ned.ipac.caltech.edu/level5/Gray/frames.html).

Hambleton, K. M., *et. al.* 2013, *Mon. Not. Roy. Astron. Soc.*, **434**, 925.

Kholopov, P. N., *et al.* 1985, *General Catalogue of Variable Stars*, 4th ed., Moscow.

Lenz, P., and Breger, M. 2005, *Commun. Asteroseismology*, **146**, 53.

Liakos, A., and Niarchos, P. 2015, in *Living Together: Planets, Host Stars and Binaries*, ed. S. M. Rucinski, G. Torres, and M. Zejda, ASP Conf. Ser. 496, Astronomical Society of the Pacific, San Francisco, 195.

Mkrtichian, D. E., *et. al.* 2004, *Astron. Astrophys.*, **419**, 1015.

Moriarty, D. J. W., Bohlsen, T., Heathcote, B., Richards, T., and Streamer, M. 2013, *J. Amer. Assoc. Var. Star Obs.*, **41**, 182.

Murphy, S. J. 2015, *Investigating the A-Type Stars Using Kepler Data*, in Springer Theses (http://link.springer.com/book/10.1007/978-3-319-09417-5).

Pojmański, G. 1997, *Acta Astron.*, **47**, 467.

Streamer, M., *et al.* 2015, *J. Amer. Assoc. Var. Star Obs.*, **43**, 67.

Svechnikov, M. A., and Kuznetsova, E. F. 1990, A*pproximate Photometric and Absolute Elements of Eclipsing Variable Stars*, A. M. Gorky Univ. of the Urals, Sverdlovsk (http://cdsarc.u-strasbg.fr/viz-bin/Cat?V/124).

Thinking Man Software. 1992–2014, DIMENSION 4 software (http://www.thinkman.com/dimension4/).

Vanmunster, T. 2013, Light Curve and Period Analysis Software: PERANSO v.2.50 (http://www.peranso.com/).

Watson, C., Henden, A. A., and Price, C. A., 2014, AAVSO International Variable Star Index VSX (Watson+, 2006–2014; http://www.aavso.org/vsx).

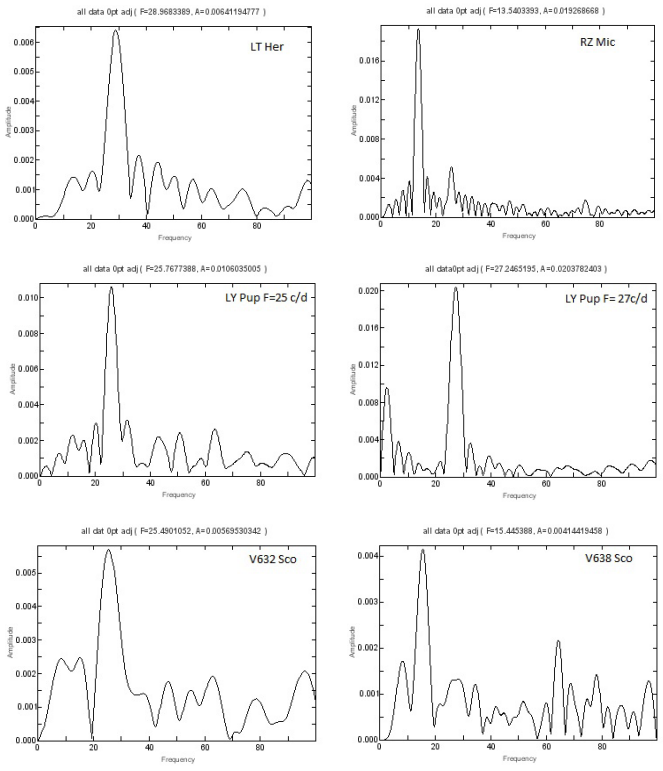

Figure 1. Power spectra for each target.

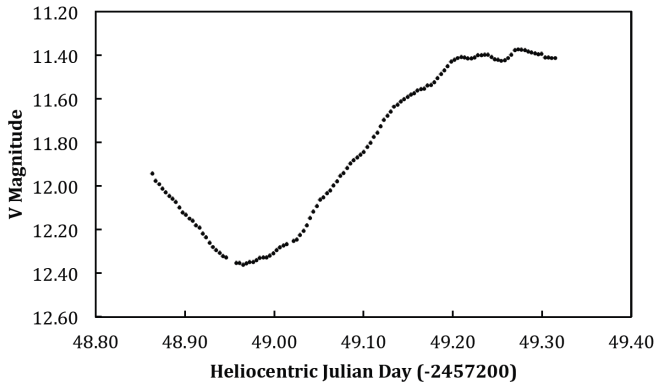

Figure 2. A primary eclipse of RZ Mic.

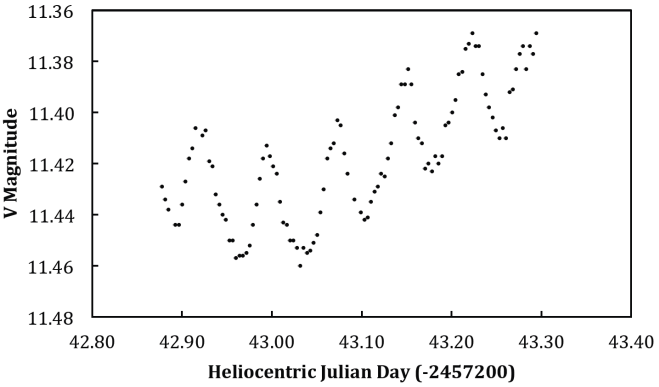

Figure 3. A partial secondary eclipse of RZ Mic.

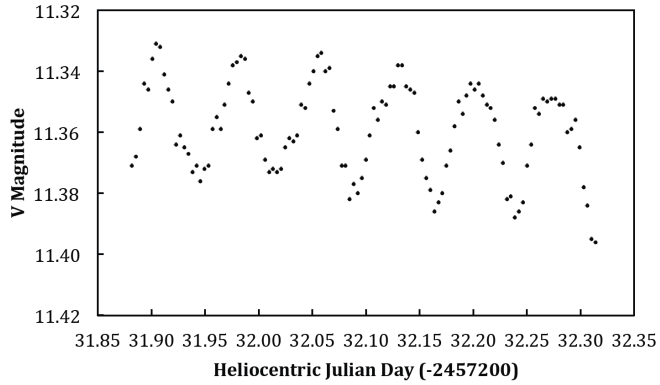

Figure 4. RZ Mic just after quadrature.

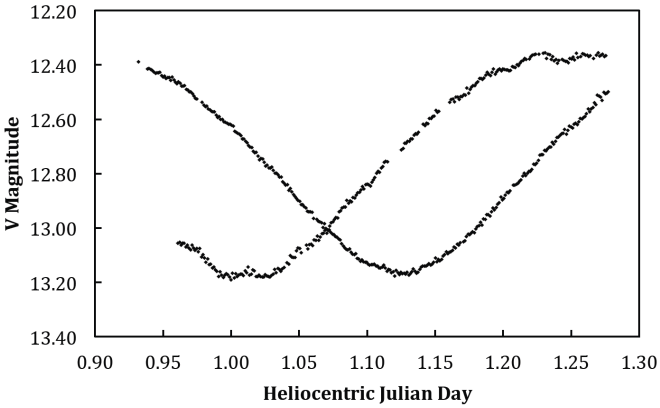

Figure 5. Primary eclipses of LY Pup. The complete eclipse began HJD 2456694.93. The partial eclipse was observed three nights later beginning 2456697.96 .

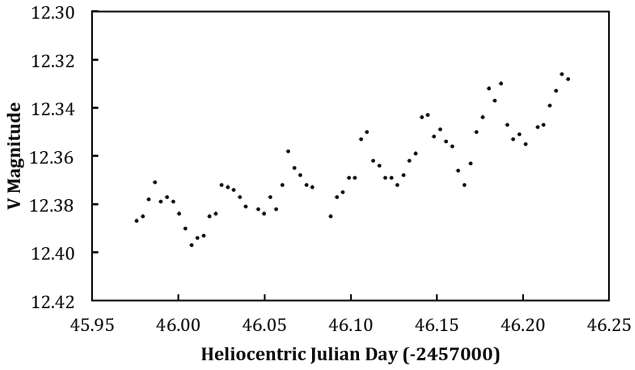

Figure 6. Ascent from a secondary eclipse of LY Pup.

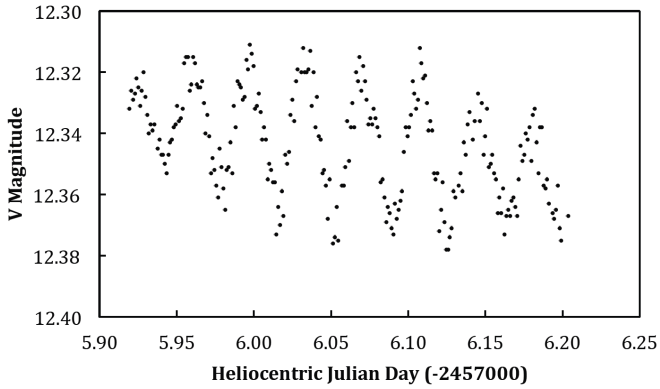

Figure 7. LY Pup out of eclipse.

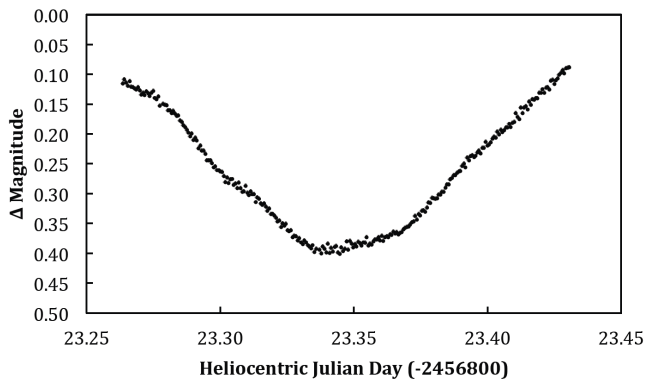

Figure 8. A primary eclipse of LT Her.

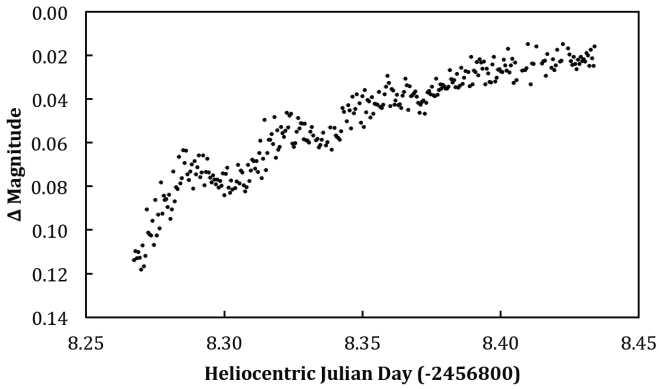

Figure 9. LT Her coming out of primary eclipse.

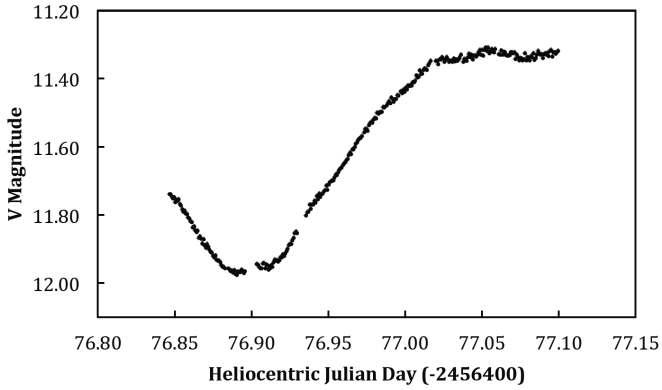

Figure 10. A primary eclipse of V632 Sco.

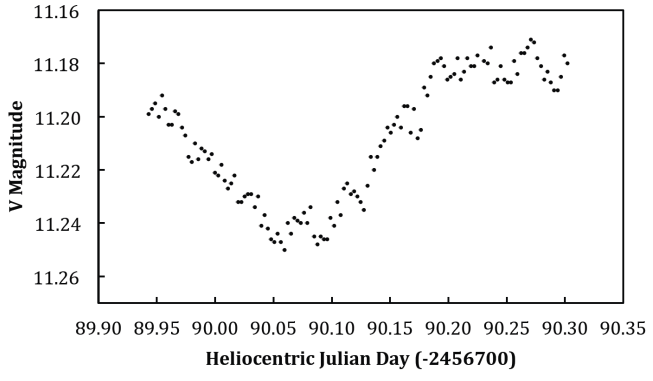

Figure 11. A secondary eclipse of V632 Sco.

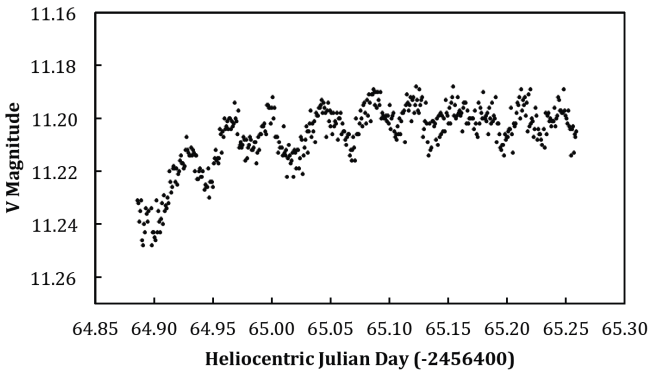

Figure 12. V632 Sco out of eclipse.

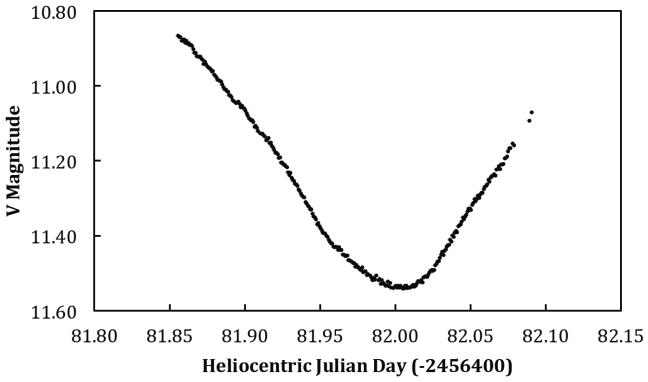

Figure 13. A primary eclipse of V638 Sco.

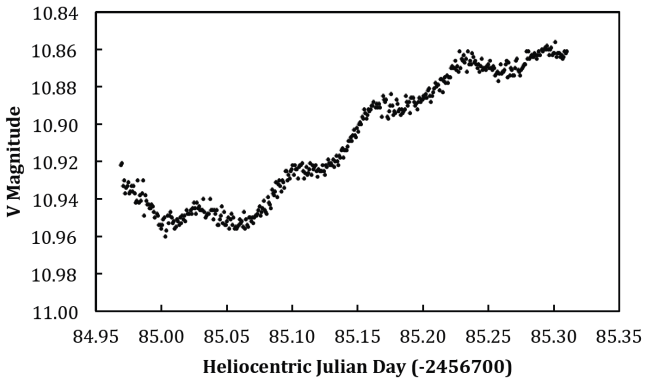

Figure 14. A partial secondary eclipse of V638 Sco.

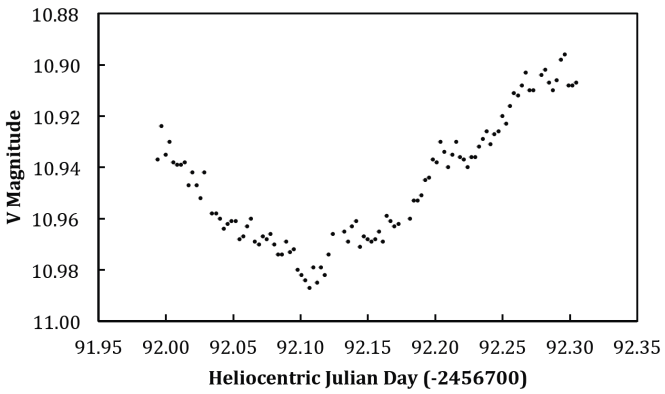

Figure 15. A secondary eclipse of V638 Sco.

Intermittent Multi-Color Photometry for V1017 Sagittarii

Arlo U. Landolt
Department of Physics and Astronomy, Louisiana State University, Baton Rouge, LA 70803; landolt@phys.lsu.edu

and

Visiting astronomer, Cerro Tololo Inter-American Observatory, National Optical Astronomical Observatory, which is operated by the Association of Universities for Research in Astronomy, Inc., under contract with the National Science Foundation

Received March 26, 2016; revised May 31, 2015; accepted June 7, 2016

Abstract *UBVRI* photoelectric photometry is presented for the dwarf nova V1017 Sgr.

1. Introduction

The star V1017 Sgr, coordinates R. A. = $18^h\ 32^m\ 04.476^s$, Dec. = –29º 23' 12.59" (J2000), originally was discovered to be variable by Ida E. Woods, as reported by Bailey (1919). They also noted a previous brightening which occurred in 1901. Additional names for V1017 Sgr include Nova Sgr 1919, HV 3519, AAVSO 1825–29, 2MASS J18320447-2923125, and UCAC4 304-232890. Kraft (1964), from 200-inch telescope spectra, reported the spectrum, which showed faint wide emission at the Balmer lines, to be that of a late-type star, with a suggested spectral type of G5 IIIp. He deduced the star to be a binary, based upon its composite spectrum. Sekiguchi (1992) described a spectroscopic orbit with a period of 5.714 days, thereby giving V1017 Sgr a long period for a star that was thought to be a dwarf or classical nova.

A broad discussion of available data was given by Webbink *et al.* (1987). Vidal and Rodgers (1974) supplied supporting detail. Schaefer (2010) deduced that V1017 Sgr was not a recurrent nova. He noted eruptions in 1901, 1919, 1973, and 1991, with only the 1919 eruption of size to be designated a nova event. The other increases in brightness were identified as representing a dwarf nova. Pagnotta and Schaefer (2014) reiterated that the brightest eruption was typical of a classical nova, whereas all other brightenings resembled dwarf nova eruptions.

Downes et al. (2001) provide a chart for V1017 Sgr. The partially blended bright star immediately to the east of V1017 Sgr is CD −29◦15053. The living repository provided by Downes et al. (2001) is located at https://archive.stsci.edu/prepds/cvcat/, via Google, say. One then clicks on the Search field in A Catalog and Atlas of Cataclysmic Variables Archival Edition, types in the variable's GCVS Name, submits, clicks on GCVS Name, and the chart appears.

There is no AAVSO APASS photometry for V1017 Sgr in the UCAC4 catalog (Zacharias *et al.* 2013), most likely due to the blending of its image with that of CD –29º 15053.

The red star just to the east of V1017 Sgr, CD –29º 15053, lies at R. A. = $18^h\ 32^m\ 05.596^s$, and Dec. = –29º 23' 09.91", J2000. This star also has been catalogued as UCAC2 122-203212 and UCAC4 304-232904. The AAVSO APASS magnitude and color indices in UCAC4 for CD –29º 15053 are: $V = 10.147 \pm 0.010$; $B = 11.762 \pm 0.010$; hence, $(B–V) = +1.615 \pm 0.014$; $r = 9.524 \pm 0.010$, $i = 9.089 \pm 0.010$; hence, $(r–i) = +0.435 \pm 0.014$. There appears to be no spectral type in the literature for CD –29º 15053.

2. Observations

The dwarf nova V1017 Sgr has been observed on 41 nights at the Cerro Tololo Inter-American Observatory (CTIO) telescopes in the time interval between 1973 March 16 and 2001 October 7 ($2441757.8746 \leq JD \leq 2452189.56316$, for a span of 10,431 days or 28 years). Data were taken at the 0.4-m, (Lowell) 0.6-m, the 0.9-m, (Yale) 1.0-m, and 1.5-m CTIO telescopes. The 1973 and 1974 data have been published in Landolt (1975). The new data presented in this paper were obtained during 33 nights between 28 June 1975 and 7 October 2001. The data were taken through the filters described in Landolt (1975, 1983, 1992) in the order *VBUUBV* or *VBURIIRUBV*. An average 20 standard stars were observed each night. Extinction measurements were made and applied on a nightly basis.

Two problems may occur within some of these photoelectric data for V1017 Sgr and CD –29º 15053. The star field in which they are located is very crowded, and hence finding a spot for the sky readings was a challenge. The separation of V1017 Sgr and CD –29º 15053 is 1.14 seconds in right ascension and 2.46 arcseconds in declination, which leads to an angular separation of 15.2 arcseconds. This separation was on the order of the diaphragm sizes used (14 to 17 arcsec) at the different CTIO telescopes; hence each star's image had to be placed slightly off-center during its integration. Therefore, under some observing conditions, the closeness of the two stars together with the seeing, etc., had a possible effect on the measurements; see Figures 1 and 2. Since V1017 Sgr itself always is more than three magnitudes, some 20 times, fainter than its close neighbor, CD –29º 15053, the brighter star was little affected by its position in the photometer diaphragm. On the other hand, one had to be very careful in positioning V1017 Sgr in the diaphragm in such a way to minimize any possible effect of the nearby much brighter CD –29º 15053.

3. Discussion

The data acquisition information for 1973 and 1975 was discussed in Landolt (1975). The resulting *UBV* magnitudes and color indices for the 1975 and 1977 data were tied into the *UBV* photometric system as defined in Johnson *et al.* (1966). Data

Table 1. Photometric Errors per Night

UT (mmddyy)	*JD* (2400000.0+	*Telescope*	*Filter*	*RMS Errors Recovered Standards*					
				V	*(B–V)*	*(U–B)*	*(V–R)*	*(R–I)*	*(V–I)*
062875	42591.5	CTIO 1.0-m	UBV	0.027	0.022	0.017	—	—	—
062975	42592.5	CTIO 1.0-m	UBV	0.018	0.016	0.011	—	—	—
060977	43303.5	CTIO 0.6-m	UBV	0.015	0.006	0.016	—	—	—
061177	43305.5	CTIO 0.6-m	UBV	0.015	0.007	0.012	—	—	—
040978	43607.5	CTIO 0.4-m	UBVRI	0.013	0.009	0.022	0.008	0.010	0.009
041078	43608.5	CTIO 0.4-m	UBVRI	0.014	0.006	0.023	0.004	0.007	0.006
061278	43671.5	CTIO 0.6-m	UBVRI	0.010	0.007	0.010	0.004	0.004	0.005
110278	43814.5	CTIO 0.9-m	UBVRI	0.005	0.006	0.014	0.004	0.004	0.005
062479	44048.5	CTIO 0.9-m	UBVRI	0.009	0.010	0.018	0.005	0.006	0.006
062579	44049.5	CTIO 0.9-m	UBVRI	0.009	0.008	0.016	0.005	0.005	0.007
070880	44428.5	CTIO 0.9-m	UBV	0.008	0.012	0.010	—	—	—
091280	44494.5	CTIO 0.9-m	UBV	0.014	0.007	0.011	—	—	—
091680	44498.5	CTIO 0.9-m	UBVRI	0.010	0.011	0.023	0.007	0.006	0.008
061081	44765.5	CTIO 1.5-m	UBVRI	0.011	0.013	0.044	0.011	0.017	0.022
081081	44826.5	CTIO 0.4-m	UBV	0.010	0.009	0.011	—	—	—
102681	44903.5	CTIO 0.9-m	UBV	0.013	0.016	0.025	—	—	—
102881	44905.5	CTIO 0.9-m	UBVRI	0.014	0.009	0.023	0.007	0.004	0.007
091482	45226.5	CTIO 1.5-m	UBVRI	0.016	0.014	0.050	0.008	0.008	0.008
070583	45520.5	CTIO 1.5-m	UBVRI	0.006	0.007	0.006	0.003	0.004	0.004
092083	45597.5	CTIO 1.5-m	UBVRI	0.003	0.010	0.037	0.005	0.010	0.010
102183	45628.5	CTIO 0.9-m	UBVRI	0.005	0.007	0.012	0.002	0.004	0.005
051584	45835.5	CTIO 1.5-m	UBVRI	0.012	0.016	0.034	0.006	0.011	0.011
100584	45978.5	CTIO 0.9-m	UBVRI	0.010	0.006	0.015	0.008	0.005	0.007
101184	45984.5	CTIO 0.9-m	UBVRI	0.016	0.005	0.027	0.005	0.003	0.004
052486	46574.5	CTIO 1.5-m	UBVRI	0.008	0.008	0.066	0.006	0.017	0.017
102388	47457.5	CTIO 1.5-m	UBVRI	0.009	0.010	0.042	0.008	0.006	0.009
061390	48055.5	CTIO 1.5-m	UBVRI	0.006	0.009	0.023	0.005	0.006	0.010
061693	49154.5	CTIO 1.5-m	UBVRI	0.007	0.004	0.016	0.005	0.009	0.011
073195	49929.5	CTIO 1.5-m	UBVRI	0.004	0.008	0.020	—	—	—
082196	50316.5	CTIO 0.9-m	UBVRI	0.006	0.009	0.029	0.004	0.004	0.007
092598	51081.5	CTIO 1.5-m	UBVRI	0.008	0.009	0.032	0.007	0.011	0.014
100701	52189.5	CTIO 1.5-m	UBVRI	0.010	0.010	0.034	0.005	0.014	0.015
			ave.	0.011	0.010	0.023	0.006	0.008	0.009
			±	0.005	0.004	0.013	0.002	0.004	0.004

taken between and including 1975 through 1996 were tied into *UBVRI* standard stars as defined in Landolt (1983). The 1998 and 2001 data were tied into standard stars defined in Landolt (1992). The 1978 through 2001 data were reduced following precepts outlined in Landolt (2007).

The rms photometric errors calculated for each night were based on the recovered magnitudes and color indices of the standard stars. The relevant values are listed in Table 1. Columns one and two give the UT date of observation and the corresponding Julian Date, respectively. The telescope at which the data were obtained is given in the third column, and the filters through which the data were taken are in the fourth column. The last six columns provide the rms errors of the recovered standard stars' magnitude and colors for that night. The last two lines in Table 1 show that the average rms error of the recovered standard star photometry was one percent or less, except for (*U–B*).

The fifty-one final magnitudes and color indices for V1017 Sgr are listed in Table 2. Column one indicates the central Heliocentric Julian Day (HJD)for the time of observation. The remaining columns list the magnitude and color indices. This photometry is plotted in Figures 1 and 2. V1017 Sgr ranged in brightness between $12.822 \leq V \leq 13.996$ magnitudes, based on these 51 measures taken in the 1978–2001 time window. Its long term brightness in the *V* magnitude averaged 13.563 ± 0.217, based on all these data. This magnitude is close to the $V = 13.59 \pm 0.07$ reported by Webbink *et al.* (1987) from a reported 14 measures. This data set shows an overall fading by V1017 Sgr of 0.15 magnitude over the time interval covered by these data. Furthermore, the data show trends in the color indices: (*B–V*) is 0.015 magnitude more blue, (U–B) 0.029, (V–R) 0.038, (R–I) 0.030, and (V–I) 0.030 magnitude all more red. The significance in these correlations between the colors and Heliocentric Julian Days, however, is low; hence, one should be cognizant of probable over-interpretation.

As pointed out in Section 2, the scatter in the data points for V1017 Sgr may be due in part to the smaller telescopes used to collect the early data (see Table 1), together with the possible incursion of light from the nearby bright star CD –29º 15053. On the other hand, the latter star is known to be constant at the two percent level (see Table 3), and scatter in its *V* magnitude measures are a small fraction of the scatter seen in the V1017 Sgr *V* measures. Hence, the V1017 Sgr variations in brightness are in great part real.

No attempt has been made to identify or refine the orbital period of 5.714 days published by Sekiguchi (1992), as that problem is being addressed in a paper in preparation (Vargas-Salazar *et al.* 2016).

Table 2. UBVRI Photometry for V1017~Sgr.

HJD	*V*	*(B–V)*	*(U–B)*	*(V–R)*	*(R–I)*	*(V–I)*
2442591.82359	13.497	+1.070	+0.278	—	—	—
2442591.82571	13.459	+1.075	+0.289	—	—	—
2442592.82191	13.707	+0.966	–0.007	—	—	—
2442592.82380	13.724	+1.029	–0.080	—	—	—
2443303.90123	13.463	+1.112	+0.363	—	—	—
2443303.90295	13.381	+1.190	+0.250	—	—	—
2443303.90630	13.383	+1.104	+0.544	—	—	—
2443303.90800	13.536	+1.072	+0.169	—	—	—
2443305.89185	13.634	+1.203	+0.057	—	—	—
2443305.89369	13.608	+1.147	+0.295	—	—	—
2443305.89775	13.703	+1.059	+0.162	—	—	—
2443305.90038	13.722	+0.977	+0.190	—	—	—
2443607.87998	13.188	+1.195	+0.424	+0.638	+0.673	+1.311
2443607.90544	13.204	+1.244	+0.560	+0.660	+0.669	+1.330
2443608.90411	12.822	+1.530	+0.389	+0.475	+0.664	+1.137
2443671.90114	13.461	+1.240	+0.312	+0.695	+0.714	+1.409
2443814.51006	13.686	+0.864	+0.196	+0.724	+0.712	+1.434
2444048.71406	13.436	+1.026	+0.093	+0.695	+0.672	+1.368
2444048.72020	13.421	+1.091	+0.080	+0.663	+0.648	+1.312
2444049.69430	13.509	+1.083	–0.030	+0.702	+0.665	+1.367
2444049.70061	13.402	+1.061	+0.255	+0.702	+0.673	+1.374
2444428.72820	13.754	+1.107	+0.414	—	—	—
2444494.63202	13.597	+1.147	+0.382	—	—	—
2444494.63930	13.601	+1.138	+0.326	—	—	—
2444498.52823	13.467	+1.129	+0.189	+0.728	+0.660	+1.389
2444498.53068	13.421	+1.120	+0.374	+0.700	+0.662	+1.363
2444765.86779	13.674	+1.102	+0.346	+0.681	+0.642	+1.324
2444826.65622	13.052	+1.062	+0.611	—	—	—
2444826.65841	13.388	+1.186	+0.305	—	—	—
2444903.53862	13.530	+1.077	+0.256	—	—	—
2444905.55055	13.649	+1.118	+0.250	+0.708	+0.690	+1.400
2445226.51913	13.996	+1.068	+0.230	+0.721	+0.665	+1.387
2445520.77007	13.674	+1.101	+0.212	+0.676	+0.662	+1.338
2445597.58313	13.766	+1.129	+0.183	+0.709	+0.659	+1.368
2445628.55302	13.602	+1.161	+0.442	+0.653	+0.653	+1.306
2445835.81847	13.625	+1.075	+0.013	+0.683	+0.650	+1.334
2445835.82925	13.647	+0.985	+0.276	+0.689	+0.644	+1.334
2445835.83477	13.625	+1.042	+0.196	+0.685	+0.645	+1.331
2445835.84351	13.608	+1.086	+0.314	+0.659	+0.651	+1.311
2445978.58027	13.692	+1.287	+0.380	+0.645	+0.664	+1.310
2445984.54172	13.909	+1.145	+0.812	+0.747	+0.712	+1.460
2446574.84662	13.964	+1.230	+0.099	+0.800	+0.554	+1.350
2447457.56591	13.821	+1.195	+0.260	+0.722	+0.683	+1.398
2448055.81705	13.962	+1.156	+0.280	+0.692	+0.693	+1.383
2449154.87026	13.646	+0.963	+0.064	+0.675	+0.649	+1.329
2449929.49768	13.451	+1.046	+0.292	—	—	—
2449929.50437	13.402	+1.101	+0.275	—	—	—
2450316.51702	13.450	+1.111	+0.302	+0.699	+0.678	+1.378
2450316.52880	13.458	+1.090	+0.254	+0.715	+0.682	+1.398
2451081.53255	13.681	+1.106	+0.272	+0.688	+0.672	+1.360
2452189.56316	13.639	+1.113	+0.248	+0.691	+0.668	+1.354

The photometry which describes the nearby star, CD –29º 15053, is given in Table 3. This photometry is plotted in Figures 3 and 4. The average brightness and color indices for CD –29º 15053 are given in the last line of Table 3. As is evident in Table 3, on individual nights where multiple observations were obtained, the photometry repeated to well under one percent. However, even though the star appears to be constant in brightness and colors, the author thought it useful to publish the 29 individual measurements taken on 23 different nights, just in case the star does turn out to be variable. For instance, in their survey of G and K giants, Henry *et al.* (2000) have shown that "roughly one-fourth of their G giants, half of their K giants, and all of their M0 giants" are variable in light. The variability of some giant stars also is described in Percy (2007). One cannot tell with assurance from the colors alone whether CD –29º 15053 is a dwarf or giant star, but from its location within UBVRI color-color plots, it most likely is a giant. The star is quite red in (U–B), in part due to the considerable reddening in the area. Given the small number statistics, is it sensible to look at the measures obtained and centered on UT 2443303.9, UT 2443305.89, UT 2445835.8, and UT 2450316.5 ($V = 10.193 \pm 0.007$, 10.194 ± 0.013, 10.191 ± 0.003, and 10.183 ± 0.004, respectively) and deduce a meaningful trend? The data do cover a time period of 21 years. Careful and properly standardized photometry would be useful.

Table 3. UBVRI Photometry for CD –29º 15053.

HJD	*V*	*(B–V)*	*(U–B)*	*(V–R)*	*(R–I)*	*(V–I)*
2442591.82771	10.162	+1.629	+1.707	—	—	—
2443303.89892	10.187	+1.620	+1.690	—	—	—
2443303.90483	10.201	+1.603	+1.702	—	—	—
2443303.90969	10.191	+1.616	+1.782	—	—	—
2443305.89020	10.185	+1.633	+1.767	—	—	—
2443305.89569	10.203	+1.603	+1.722	—	—	—
2443607.88530	10.232	+1.645	+1.774	+0.912	+0.817	+1.731
2443671.90418	10.161	+1.649	+1.636	+0.900	+0.806	+1.707
2443814.51336	10.151	+1.609	+1.704	+0.916	+0.812	+1.730
2444048.71723	10.198	+1.627	+1.768	+0.899	+0.815	+1.715
2444049.69744	10.190	+1.631	+1.793	+0.888	+0.820	+1.707
2444498.53315	10.185	+1.623	+1.809	+0.900	+0.817	+1.719
2444765.87296	10.165	+1.655	+1.850	+0.905	+0.811	+1.717
2444903.54074	10.174	+1.611	+1.777	—	—	—
2444905.55367	10.147	+1.645	+1.786	+0.909	+0.803	+1.714
2445226.52239	10.191	+1.640	+1.853	+0.903	+0.799	+1.704
2445520.77361	10.178	+1.650	+1.925	+0.900	+0.825	+1.727
2445597.58681	10.183	+1.663	+1.689	+0.906	+0.810	+1.717
2445628.55589	10.155	+1.636	+1.739	+0.899	+0.813	+1.713
2445835.82161	10.194	+1.636	+1.758	+0.888	+0.838	+1.727
2445835.83191	10.188	+1.654	+1.758	+0.906	+0.838	+1.746
2445835.83773	10.191	+1.648	+1.789	+0.896	+0.838	+1.736
2445978.58380	10.160	+1.642	+1.767	+0.905	+0.811	+1.718
2447457.57190	10.187	+1.630	+1.781	+0.918	+0.808	+1.713
2448055.81358	10.224	+1.666	+1.910	+0.906	+0.831	+1.737
2449154.87540	10.163	+1.612	+1.795	+0.909	+0.804	+1.718
2449929.50111	10.183	+1.622	+1.739	—	—	—
2450316.52187	10.186	+1.639	+1.732	+0.904	+0.819	+1.724
2450316.53359	10.180	+1.641	+1.729	+0.898	+0.823	+1.722
ave.	10.183	+1.634	+1.767	+0.903	+0.817	+1.721
±	0.020	0.017	0.063	0.008	0.012	0.011

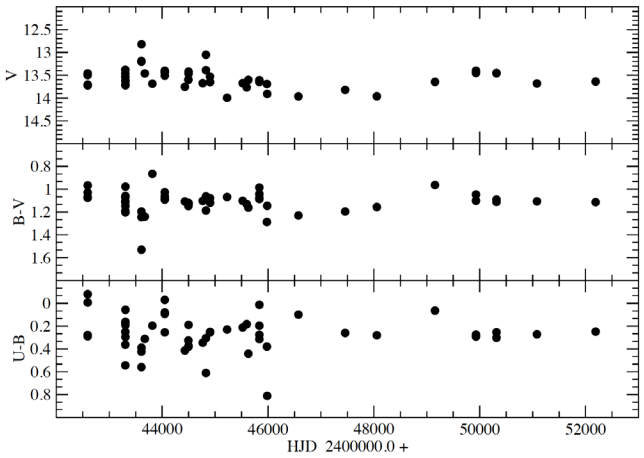

Figure 1. *V* magnitude and (*B–V*) and (*U–B*) color index light curves for V1017 Sgr.

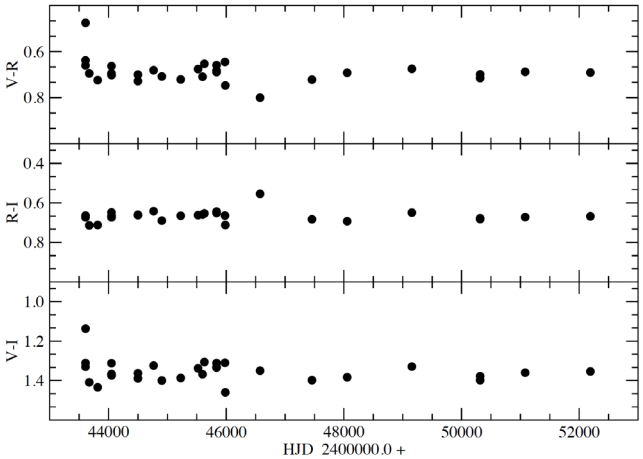

Figure 2. (*V–R*), (*R–I*), and (*V–I*) color index light curves for V1017 Sgr.

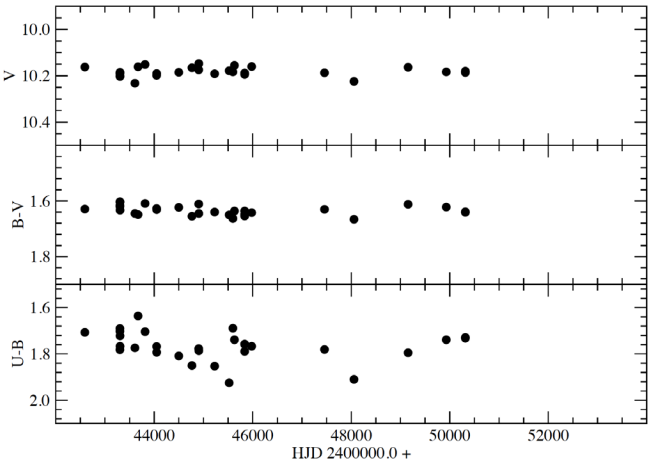

Figure 3. *V* magnitude and (*B–V*) and (*U–B*) color index light curves for the nearby star CD –29º 15053.

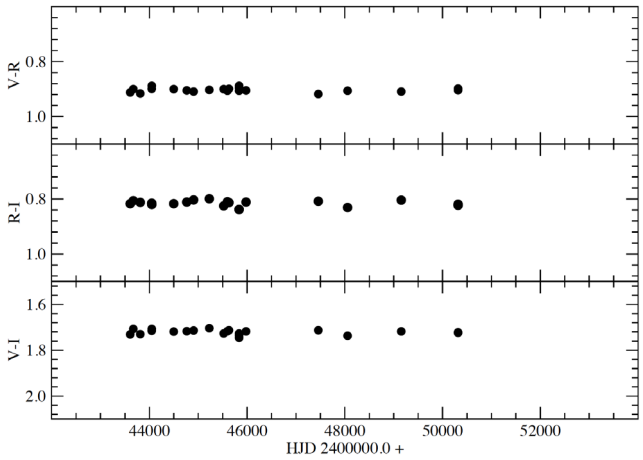

Figure 4. (*V–R*), (*R–I*), and (*V–I*) color index light curves for the nearby star CD –29º 15053.

4. Summary

In summary, very detailed information and summaries regarding the known characteristics of V1017 Sgr may be found in Webbink *et al.* (1987), Sekiguchi (1992), many locations in Warner (1995), Schaefer (2010), and in Pagnotta and Schaefer (2014). The new data herein should be useful in a more indepth study of V1017 Sgr as in Vargas-Salazar *et al.* (in preparation 2016).

5. Acknowledgements

It is a pleasure to thank the staff of CTIO for their help in making the observing runs a success. John Percy refreshed the author's memory about various aspects of stellar variability. The author thanks the referee, A. Henden, for helpful comments on the manuscript.

The data reported in this paper came from observing runs supported by AFOSR grants 77-3218 and 82-0192, STScI CW-0004-85, and NSF grants MPS 75-01890 and AST 9114457, 9313868, 9528177, 0097895, and 0803158.

References

Bailey, S. I. 1919, *Harvard Bull.*, No. 693, 1.

Downes, R. A., Webbink, R. F., Shara, M. M., Ritter, H., Kolb, U., and Duerbeck, H. W. 2001, *Publ. Astron. Soc. Pacific*, **113**, 764.

Henry, G.W., Fekel, F. C., Henry, S. M., and Hall, D. S. 2000, *Astrophys. J., Suppl. Ser.*, **130**, 201.

Johnson, H. L., Mitchell, R. I., Iriarte, B., and Wisniewski, W. Z. 1966, *Comm. Lunar Planet. Lab.*, **4**, 99.

Kraft, R. P. 1964, *Astrophys. J.*, **139**, 457.

Landolt, A. U. 1975, *Publ. Astron. Soc. Pacific*, **87**, 265.

Landolt, A. U. 1983, *Astron. J.*, **88**, 439.

Landolt, A. U. 1992, *Astron. J.*, **104**, 340.

Landolt, A. U. 2007, in *The Future of Photometric, Spectrophotometric, and Polarimetric Standardization*, ed. C. Sterken, ASP Conf. Ser. 364, Astronomical Society of the Pacific, San Francisco, 27.

Pagnotta, A., and Schaefer, B. E. 2014, *Astrophys. J.*, **788**, 164.

Percy, J. R. 2007, *Understanding Variable Stars*, Cambridge University Press, Cambridge, p. 203.

Schaefer, B. E. 2010, *Astrophys. J., Suppl. Ser.*, **187**, 275.

Sekiguchi, K. 1992, *Nature*, **358**, 563.

Vargas-Salazer, I. *et al.* 2016, in preparation.

Vidal, N. V., and Rodgers, A. W. 1974, *Publ. Astron. Soc. Pacific*, **86**, 26.

Warner, B. 1995, *Cataclysmic Variable Stars*, Cambridge University Press, Cambridge, 566.

Webbink, R. F., Livio, M., Truran, J. W., and Orio, M. 1987, *Astrophys. J.*, 314, 653.

Zacharias, N., Finch, C. T., Girard, T. M., Henden, A., Bartlett, J. L., Monet, D. G., and Zacharias, M. I. 2013, *Astron. J.*, **145**, 44.

The Variable Star V Sculptoris

Arlo U. Landolt
Department of Physics and Astronomy, Louisiana State University, Baton Rouge, LA 70803; landolt@phys.lsu.edu
and
Visiting astronomer, Cerro Tololo Inter-American Observatory, National Optical Astronomical Observatory, which is operated by the Association of Universities for Research in Astronomy, Inc., under contract with the National Science Foundation.

Received April 13, 2016; accepted April 21, 2016

Abstract Multicolor photometry is presented for V Scl and six nearby sequence stars.

1. Introduction

The star V Sculptoris (V Scl) is a variable star of the Mira type. It is star 254-000149 in the UCAC4 catalogue (Zacharias *et al.* 2012), with coordinates R.A. = $00^h\ 08^m\ 37.362^s$, and Dec. = –39º 13' 04.91" (2000). V Scl also has been known as HD 409, HV 67, and AAVSO AUID 000-BBB-200. This long period variable star varies something like $8.7 \leq V \leq 15$th magnitude with a period on the order of 296.1 days (Watson *et al.* 2014).

Introductory comments concerning Mira variables are given in Percy (2007). Sample light curves are illustrated in Sterken (1996).

2. Observations

Data for V Scl were obtained by the author intermittantly over a period of fifteen years during his standard star program work. The CTIO 1.5-m telescope together with a photoelectric photometer and *UBVRI* filters were used to acquire the data on 1983 September 21, 1986 December 14, 1988 October 23, and 1998 September 26, all Universal Time (UT) dates. The data were reduced following procedures discussed in Landolt (2007), and were tied into *UBVRI* photometric standard stars current at the time of the data acquisition (Landolt 1983, 1992).

3. Discussion

The finding chart for V Scl and the stars which were observed near it are identified in Figure 1. The chart is based on a digitized version of the Palomar Observatory Sky Survey I (POSS I) blue survey (Palomar Observatory 1950–1957). The size of the field as presented in the chart is just under twenty arc minutes on a side. The sequence stars' identifications are listed in Table 1. The first column gives identification as used in Figure 1 and Table 1. The AAVSO AUID identifications are given in the second column. The third column lists the UCAC4 identification numbers (Zacharias *et al.* 2013), whose coordinates are in columns four and five.

The reduction process included the recovery of the magnitudes and color indices of the standard stars used in the observational program. These errors, as a function of UT observed date and for the magnitude and color indices, are given in Table 2. All nights were photometric. However, the observing window for the night 1998 September 26 UT ended with incoming fog.

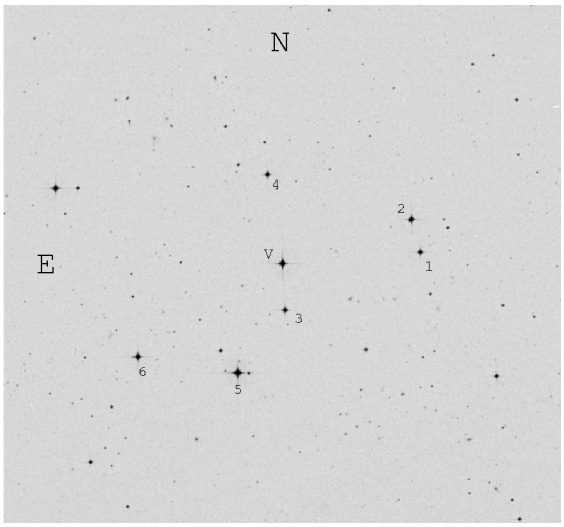

Figure 1. Chart for V Scl and neighboring stars.

Table 1. Sequence star name inter-comparison.

This Paper Star Name	*AUID*	*UCAC4*	*R.A. (J2000.0) h m s*	*Dec. (J2000.0) º ′ ″*
1	000–BJZ–991	254–000146	00 08 12.412	–39 12 47.83
2	000–BJZ–990	255–000151	00 08 13.883	–39 11 38.06
3	000–BJJ–803	254–000148	00 08 37.153	–39 14 42.52
4	000–BJJ–805	255–000156	00 08 39.793	–39 09 57.58
5	—	254–000152	00 08 45.891	–39 16 52.22
6	000–BBB–208	254–000154	00 09 03.866	–39 16 13.55

Table 2. RMS photometric errors for each night.

UT (mmddyy)	*V m*	*(B–V) m*	*(U–B) m*	*(V–R) m*	*(R–I) m*	*(V–I) m*
092183	0.012	0.014	0.029	0.006	0.012	0.012
121486	0.009	0.008	0.022	0.004	0.011	0.011
102388	0.009	0.010	0.042	0.008	0.006	0.009
092698	0.005	0.014	0.043	0.010	0.003	0.008

The observed magnitudes and color indices for V Scl and for the stars in its vicinity are located in Table 3 and Table 4, respectively. The number of decimals carried for the photometry in Table 3 was dictated by the accuracy of the original data. At its faintest, V Scl was too faint at the shorter wavelengths to obtain the highest accuracy given the equipment then available. In fact, although a very small signal was measured through the

Table 3. UBVRI photometry of V Scl.

UT (mmddyy)	*HJD*	*V m*	*(B–V) m*	*(U–B) m*	*(V–R) m*	*(R–I) m*	*(V–I) m*
092183	2445598.71595	15.07	+2.4	—	+3.085	+2.569	+5.667
092183	2445598.73077	15.08	+1.6	—	+3.065	+2.566	+5.643
121486	2446778.58947	13.864	+1.440	+0.203	—	—	—
121486	2446778.59206	13.856	+1.534	+0.440	+2.754	+2.525	+5.284
102388	2447457.65698	13.098	+1.544	+0.510	+2.536	+2.433	+5.005
092698	2451082.79679	10.020	+1.311	+0.508	—	—	—
092698	2451082.79890	10.014	+1.313	+0.474	—	—	—
092698	2451082.80034	10.022	+1.314	+0.509	—	—	—

Table 4. UBVRI photometry of stars near V Scl.

								Mean Error of Single Observation					
This Paper Star Name	*V m*	*(B–V) m*	*(U–B) m*	*(V–R) m*	*(R–I) m*	*(V–I) m*	*n*	*V m*	*(B–V) m*	*(U–B) m*	*(V–R) m*	*(R–I) m*	*(V–I) m*
1	12.991	+0.458	-0.023	+0.304	+0.292	+0.596	3	0.005	0.018	0.024	0.013	0.015	0.002
2	12.317	+0.598	+0.070	+0.345	+0.357	+0.703	3	0.001	0.018	0.009	0.005	0.006	0.005
3	12.790	+0.544	+0.043	+0.322	+0.311	+0.633	5	0.007	0.002	0.018	0.002	0.013	0.012
4	13.158	+0.379	-0.220	+0.264	+0.305	+0.568	4	0.007	0.017	0.015	0.005	0.009	0.014
5	11.561	-0.041	-0.090	-0.019	-0.026	-0.045	6	0.004	0.007	0.018	0.007	0.006	0.008
6	12.194	+0.638	+0.161	+0.360	+0.344	+0.705	3	0.003	0.005	0.036	0.003	0.003	0.001

U filter on 1983 September 21 UT, the reduced (*U–B*) value was deemed not credible, and hence was not retained.

Well determined photoelectric photometry should be useful in setting the zero point for visual and photographic photometry. Hence the data points for V Scl in Table 3 were compared to the photometry of V Scl in the AAVSO International Database (Kafka 2015), when such photometry existed. The comparison indicated that AAVSO database data near 1983 September 21 UT were on the order of 0.5 magnitude brighter than in Table 3. AAVSO database data reported near the dates 1986 December 14 UT, 1988 October 23 UT, and 1998 September 26 UT appear something like 0.4 magnitude fainter than photometry in Table 3. An AAVSO chart of 1950 equinox vintage of V Scl included a star labelled 13.3, near V Scl, as the faintest sequence star then available in the field. On the most recent AAVSO chart for V Scl, that same star is labelled 12.8. Similarly, a star labelled 12.6 on the 1950s chart currently is listed as 12.2. The older archived data need a zero point adjustment when the need arises for a more robust comparison to modern data.

Current photometry of stars in the vicinity of V Scl is given in Table 4. Star identifications which correspond to those identified in Figure 1 appear in the first column. Columns two through seven provide new photometry for these stars. The eighth column gives the total number of measures obtained. The last six columns present the mean error of a single magnitude and color index observation for these stars near V Scl.

Comparison of current sequence star photometry was made with APASS photometry, Data Release 6 (DR 6) in the UCAC4 catalogue, in the sense APASS photometry minus photometry in Table 4. The *V* magnitude comparsion was found to be –0.019 ± 0.014, and the (*B–V*) color index comparison was +0.020 ± 0.024.

4. Acknowledgements

It is a pleasure to thank the staff of CTIO for their help in making the observing runs a success, and to James L. Clem and Krista Romita for reminders in turning the manuscript into the appropriate format.

This work has been funded by AFOSR grants 77-3218 and 82-0192, STScI CW-0004-85 and NSF grants AST-9528177 and AST-0803158.

This research has made use of the VizieR catalogue access service and of the SIMBAD database, both at CDS, Strasbourg, France.

References

Kafka, S. 2015, variable star observations from the AAVSO International Database (https://www.aavso.org/aavso-international-database).

Landolt, A. U. 1983, Astron. J., 88, 439.

Landolt, A. U. 1992, Astron. J., 104, 340.

Landolt, A. U. 2007, in *The Future of Photometric, Spectrophotometric, and Polarimetric Standardization*, ed. C. Sterken, ASP Conf. Ser. 364, Astronomical Society of the Pacific, San Francisco, 27.

Palomar Observatory Sky Survey I (POSS I). 1950–1957 (http://stdatu.stsci.edu/cgi-bin/dss_form).

Percy, J. R. 2007, *Understanding Variable Stars*, Cambridge University Press, Cambridge, 209.

Sterken, C. 1996, in *Light Curves of Variable Stars*, eds., C. Sterken, C. Jaschek, Cambridge University Press, Cambridge, 106.

Watson, C., Henden, A. A., and Price, C. A. 2014, AAVSO International Variable Star Index VSX (Watson+, 2006–2014; http://www.aavso.org/vsx).

Zacharias, N., Finch, C. T., Girard, T. M., Henden, A., Bartlett, J. L., Monet, D. G., and Zacharias, M. I. 2012, The Fourth U.S. Naval Observatory CCD Astrograph Catalog (UCAC4), VizieR On-line Data Catalog (http://cdsarc.u-strasbg.fr/viz-bin/Cat?I/322).

Zacharias, N., Finch, C. T., Girard, T. M., Henden, A., Bartlett, J. L., Monet, D. G., and Zacharias, M. I. 2013, *Astron. J.*, **145**, 44.

A Photometric Study of the Eclipsing Binary Star V958 Monocerotis

Edward J. Michaels
Stephen F. Austin State University, Department of Physics and Astronomy, P.O. Box 13044, Nacogdoches, TX 75962; emichaels@sfasu.edu

Received April 30, 2016; revised May 24, 2016; accepted June 7, 2016

Abstract Presented are new precision multi-band observations for the eclipsing binary V958 Mon. The orbital period is less than 0.3 day and the light curves exhibit total eclipses. A new ephemeris was determined and a simultaneous four-color light curve solution was obtained with the Wilson-Devinney program. The geometric and photometric elements derived are consistent with a W-type contact binary.

1. Introduction

The Northern Sky Variability Survey (NSVS) has provided a wealth of new variable star discoveries, many of which are W Ursae Majoris contact binaries (Wozniak *et al.* 2004). From this survey V958 Mon was first identified as an EW/KW-type eclipsing binary by Otero *et al.* (2004). It was also found in NSVS data by an automated variable star classification technique (Hoffman *et al.* 2009). A photometric orbital period of P = 0.29829 day was reported. The Large Sky Area Multi-Object Fiber Spectroscopic Telescope (LAMOST) survey gives an effective temperature for V958 Mon of T_{eff} = 4990 K, a metallicity of [Fe/H] = –0.02, a heliocentric radial velocity of V_r = –34.31 km/sec, and surface gravity of log g = 4.115 (cgs) (Luo *et al.* 2015). One time of minimum light was observed by Diethelm (2011) and second one by Nelson (2011). In Zejda *et al.*'s (2012) *Catalogue of Variable Stars in Open Cluster Fields*, V958 Mon is listed as a member of the nearby galactic cluster Platais 6 (HIP 29713). The distance to this cluster is 348 pc (Kharchenko *et al.* 2005).

In this paper a photometric study of V958 Mon is presented. It is organized into three sections. The observations and data reduction techniques are presented in section 2. New times of minima and a period analysis are presented in section 3. Light curve analysis using BINARY MAKER 3.0 (BM) and the Wilson-Devinney (WD) model is presented in section 4. Discussion and conclusions are presented in section 5.

2. Observations

Photometric observations were made using an SBIG-STXL camera with a cooled KAF-6303E CCD (–30°C) and the 0.31-m Ritchey-Chrétien robotic telescope of the Waffelow Creek Observatory (http://obs.ejmj.net/index.php). Images were acquired in each of four passbands on the following nights in 2015: December 2, 3, 4, 5, and 6. A total of 1,855 images were obtained: 531 in Johnson V, 443 in Sloan g', 442 in Sloan r', and 439 in Sloan i'. This set of data was used in the light curve analysis of section 4 of this paper. Additional Johnson B and V images had also been acquired earlier in 2015 (February 8, 9, 10, 11, 12, 13, 17, and 18) for determining new times of minima. All images were calibrated with bias, dark, and flat field frames. MIRA software (Mirametrics 2015) was used for calibration and ensemble differential aperture photometry.

The seven comparison stars (C1–C7) and the check (K) star used in this study are listed in Table 1 with a finder chart shown in Figure 1. The standard magnitudes for each of these stars was taken from the AAVSO Photometric All-Sky Survey (APASS; Henden *et al.* 2014). The instrumental magnitudes of V958 Mon were converted to standard magnitudes using these comparison stars. The time for each observation was converted to orbital phase using:

$$\Phi = \frac{T - T_0}{P} - \mathrm{Int}\left(\frac{T - T_0}{P}\right) \quad (1)$$

where T is the Heliocentric Julian Date of the observation, T_0 is a time of minimum for a primary eclipse (epoch), and P is the orbital period. Throughout this paper the values used for epoch and period are T_0 = 2457363.715748 and P = 0.29830597 day (see section 3.1). All light curves are plotted from phase –0.6 to 0.6 with negative orbital phase defined as Φ – 1. Figure 2 shows the folded light curves for each passband in standard magnitudes. In the bottom panel of Figure 2 are the Johnson V standard magnitudes for the K star. For each night a plot of the K star magnitudes for each passband was inspected and no significant variability was detected. All the observations in this study are available from the AAVSO International Database (Kafka 2015).

On one night of excellent seeing, December 6, it was discovered that V958 Mon has a close companion star. The star is located approximately 4.0 ± 0.1 arcsec from V958 Mon at a position angle of 338 ± 2 degrees. All photometry was performed with an aperture size that included both stars since on most nights the stars were not resolved. To measure the approximate light contribution from the companion star, a separate data reduction was performed for the December 6 observations using a smaller aperture that excluded the companion's light. Using the smaller aperture the peak magnitude at phase 0.25 was differenced with the peak magnitude using the larger aperture which included both stars. The magnitude differences for each passband provided the initial starting values for third light in the WD model of section 4.

3. Analysis

3.1. Period determination

The initial ephemeris used in this study was taken from Otero *et al.* (2004) and is given by:

Table 1. Stars used in this study.

Star	R.A. (2000) h m s	Dec. (2000) ° ′ ″	V	g′	r′	i′
V958 Mon	06 22 58	+04 28 18				
[1]GSC 0140-0872 (C1)	06 22 30	+04 19 11	11.708 ± 0.036	12.322 ± 0.021	11.243 ± 0.050	10.787 ± 0.057
[1]GSC0140-1016 (C2)	06 21 17	+04 34 54	11.826 ± 0.043	11.973 ± 0.037	11.695 ± 0.059	11.615 ± 0.064
[1]GSC 0140-0737 (C3)	06 21 41	+04 36 44	12.147 ± 0.025	12.224 ± 0.022	12.093 ± 0.041	12.127 ± 0.040
[1]GSC 0140-0615 (C4)	06 22 14	+04 21 29	12.295 ± 0.057	12.965 ± 0.025	11.814 ± 0.030	11.291 ± 0.049
[1]GSC 0141-1058 (C5)	06 22 42	+04 25 54	12.416 ± 0.040	12.572 ± 0.014	12.300 ± 0.053	12.263 ± 0.031
[1]GSC 0140-1059 (C6)	06 22 06	+04 29 51	12.549 ± 0.032	13.180 ± 0.027	12.063 ± 0.034	11.562 ± 0.049
[1]GSC 0140-1171 (C7)	06 22 10	+04 23 24	12.567 ± 0.036	13.448 ± 0.023	11.856 ± 0.041	11.116 ± 0.043
[2]GSC 0140-1153 (K)	06 22 10	+04 35 10	12.743 ± 0.040	12.909 ± 0.014	12.626 ± 0.039	12.588 ± 0.042
[3]Observed check star magnitudes (K)			12.744 ±0.010	12.934 ± 0.010	12.631 ± 0.012	12.566 ± 0.013

APASS [1]comparison stars (C1–C7) and [2]check (K) star magnitudes and errors. The observed [3]check star magnitudes are the averages over all nights for each passband.

HJD Min I = 2451525.891 + 0.298305 E. (2)

Using the Kwee and van Woerden (1956) method, eight new times of minima were determined from the observations. These minima and two others found in the literature are reported in Table 2. A new linear ephemeris was determined by least-squares solution and is given by:

HJD Min I = 2457363.7158 (15) + 0.29830597 (8) E. (3)

This ephemeris should be useful for predicting future minima times. Figure 3 shows the O-C diagram from Equation 3.

3.2. Temperature, spectral type

The temperature of the cooler secondary star was determined from the (g'–r') color index at primary minimum (Φ = ±0.025). Since the minimum is a total eclipse, only light from the secondary star is measured at this orbital phase. All g' and r' observations were binned with a phase width of 0.01. Both phase and magnitude were averaged in each bin interval. The binned r' magnitudes were subtracted from the linearly interpolated binned g' magnitudes which gives a (g'–r') color of 0.724 ± 0.022 at primary minimum. Figure 4 shows the binned r' magnitude light curve and the bottom panel the color index. The (g'–r') color was transformed to (B–V) using Bilir's (2005) transformation equation,

$$(B-V) = \frac{(g' - r') + 0.252}{1.124} . \quad (4)$$

This gives an observed color index of (B–V) = 0.868 ± 0.020. The color excess for this star is likely very small. V958 Mon lies approximately along the same line of sight as the Platais 6 cluster and is also somewhat closer than the cluster. The measured color excess for the cluster is E(B–V) = 0.000 (Kharchenko *et al.* 2005) which means the reddening for V958 Mon is probably quite small. Using Table 5 of Pecaut and Mamajek (2013) gives an effective temperature of T_{eff} = 5111 ± 57K for the secondary star. This temperature compares well with the LAMOST value of 4990 K.

3.3. Synthetic light curve modeling

The light curves were analyzed using BINARY MAKER 3.0 (BM3) (Bradstreet and Steelman 2002) and the WD program (Wilson and Devinney 1971; Van Hamme and Wilson 1998). The observations were binned in both phase and magnitude with a phase interval of 0.01. On average each binned data point was formed by four observations. The binned magnitudes were then converted to relative flux for light curve modeling. BM3 was used to make the initial synthetic light curve fit to each observed light curve using standard convective parameters and limb darkening coefficients from Van Hamm's (1993) tabular values. The parameters resulting from the initial fits to each light curve were averaged. These averages were used as the input values for the computation of a simultaneous 4-color light curve solution with the WD program. The weight given to each input data point was set to the number of observations that formed the point. Mode 3 was set in the program since the light curves are typical of a short-period contact binary with the flat bottoms of both minima indicating total eclipses. The Kurucz stellar atmosphere model was used and logarithmic limb darkening coefficients were calculated by the program. The Method of Multiple Subsets (MMS) was employed to minimize strong correlations of the parameters (Wilson and Biermann 1976). The fixed inputs included standard convective parameters: gravity darkening, $g_1 = g_2 = 0.32$ (Lucy 1968), albedo value $A_1 = A_2 = 0.5$ (Ruciński 1969), and the effective temperature of the cooler star, T_2, was set to the value of 5111K determined in section 3.2. The solution's adjustable parameters include the

Table 2. Available times of minima and O–C residuals from Equation 3.

Epoch HJD 2400000+	*Error*	*Cycle*	*O-C Linear*	*References*
55588.6470	0.0003	13619.5	0.00094	Nelson 2011
55907.8323	0.0003	14689.5	–0.00115	Diethelm 2011
57065.7080	0.0001	18571.0	–0.00011	this paper
57066.6032	0.0001	18574.0	0.00015	this paper
57071.6742	0.0001	18591.0	0.00000	this paper
57359.8379	0.0001	19557.0	0.00013	this paper
57360.7327	0.0002	19560.0	0.00001	this paper
57361.7766	0.0002	19563.5	–0.00012	this paper
57362.8209	0.0002	19567.0	0.00008	this paper
57363.7158	0.0002	19570.0	0.00007	this paper

inclination (i), mass ratio ($q = M_2 / M_1$), potential ($\Omega, \Omega_1 = \Omega_2$), temperature of the primary star (T_1), the normalized flux for each wavelength (L), and third light (l). The best-fit solution is shown in column 2 of Table 3. The parameters with formal errors are the adjusted ones with the subscripts 1 and 2 referring to the primary and secondary stars being eclipsed at Min I and Min II, respectively. The fill-out parameter was calculated by BM3. It is defined by:

$$f = \frac{\Omega_{inner} - \Omega}{\Omega_{inner} - \Omega_{outer}}, \quad (5)$$

where Ω_{inner} and Ω_{outer} are the inner and outer critical equipotential surfaces and Ω is the equipotential surface that describes the stellar surface (Lucy and Wilson 1979). The third light in the solution is the percent of light contributed at an orbital phase of 0.25 by a nearby field star (see section 2). The normalized light curves for each passband overlaid by the synthetic solution curves (solid lines) are shown in Figure 5, with the residuals shown in Figure 6.

3.4. Spot model

The asymmetries often seen in eclipsing binary light curves are usually attributed to large cool spots, hot regions such as faculae, or gas streams that impact one of the stars. The light curves of V958 Mon show no obvious O'Connell effect but excess light was noted in the residual curves on either side of secondary eclipse (Figure 6). To fit the asymmetries in the light curves, a second solution was attempted by adding an over-luminous spot to the larger star. Since the excess light was reasonably symmetric about secondary minimum, the spot should be located along or close to the line of centers between the two stars either above or below the contact region. Both of these spot locations were modeled with BM3 by adjusting each spots parameters (latitude, longitude, spot size, and temperature) until a good fit was obtained between the synthetic and observed light curves. Both spot positions produced almost equally good fits. The spot modeled below the contact region had a marginally better fit, therefore its parameters were included in a new WD solution attempt. The stellar parameters from the first solution were held fixed while the spot parameters were adjusted until the solution converged. The spot parameters were then held fixed and the stellar parameters adjusted until the solution converged again. This process was repeated until the model converged to a final solution. The final values for the spotted solution parameters are shown in column 3 of Table 3. Figure 7 shows the spotted model fits (solid lines) to the observed light curves and Figure 8 shows the residuals. The differences between the stellar parameters for each model (spotted and unspotted) are very small. The sum of the residuals squared for the spotted solution was 0.013 and 0.023 for the unspotted model (1.8 times larger). A graphical representation of the spotted solution is shown in Figure 9.

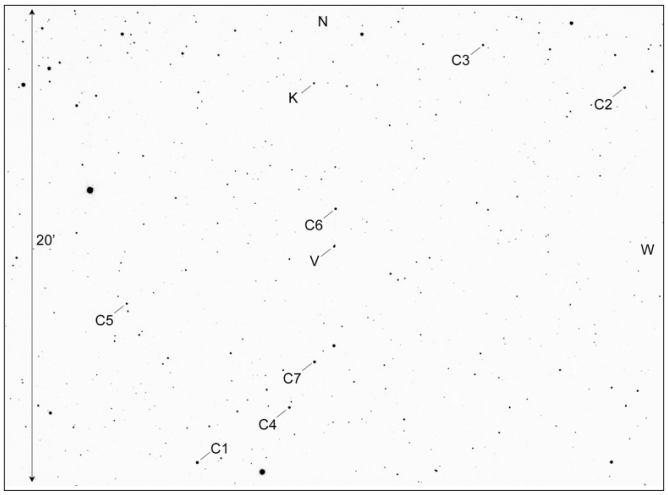

Figure 1. Finder chart for V958 Mon (V), comparison (C1–C7), and check (K) stars.

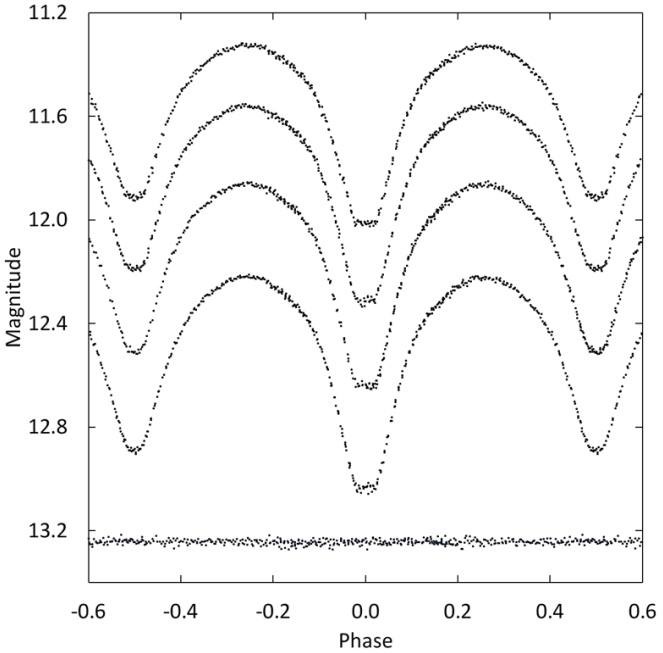

Figure 2. Folded light curves for each observed passband. The differential magnitudes of the variable were converted to standard magnitudes using the calibrated magnitudes of the comparison stars. From top to bottom the light curve passbands are Sloan i', Sloan r', Johnson V, Sloan g'. The bottom curve shows the Johnson V magnitudes of the check star (offset +0.5 magnitude). The standard deviations of check star magnitudes (all nights) are shown in Table 1. Error bars are not shown for clarity.

Table 3. V958 Mon synthetic light curve solutions.

parameter	*Solution (no spots)*	*Solution (with spot)*
phase shift	0.0002 ± 0.0001	0.0003 ± 0.0001
i (°)	86.4 ± 0.4	86.4 ± 0.4
T_1 (K)	5465 ± 3	5465 ± 2
T_2 (K)	5111*	5111*
$\Omega_1 = \Omega_2$	5.489 ± 0.026	5.489 ± 0.026
$q(M_2 / M_1)$	2.253 ± 0.018	2.250 ± 0.019
filling factor	19%	19%
$L_1 / (L_1 + L_2)$ (B)	—	—
$L_1 / (L_1 + L_2)$ (V)	0.4100 ± 0.0007	0.4101 ± 0.0004
$L_1 / (L_1 + L_2)$ (g')	0.4242 ± 0.0007	0.4243 ± 0.0006
$L_1 / (L_1 + L_2)$ (r')	0.3973 ± 0.0007	0.3974 ± 0.0005
$L_1 / (L_1 + L_2)$ (i')	0.3864 ± 0.0006	0.3864 ± 0.0004
l_3 (V)**	0.0112 ± 0.0042	0.0121 ± 0.0042
l_3 (g')	0.0244 ± 0.0042	0.0262 ± 0.0042
l_3 (r')	0.0183 ± 0.0044	0.0198 ± 0.0043
l_3 (i')	0.0362 ± 0.0043	0.0375 ± 0.0043
r_1 side	0.3120 ± 0.0009	0.3103 ± 0.0007
r_2 side	0.4703 ± 0.0036	0.4884 ± 0.0039
spot parameters		
colatitude (°)	—	113 ± 2
longitude (°)	—	356 ± 1
spot radius (°)	—	12 ± 2
temp.- factor	—	1.17 ± 0.04

** Assumed. ** Third lights are the percent of light contributed at orbital phase 0.25.*

Table 4. Stellar parameters for V958 Mon.

Parameter	*Symbol*	*Value*
Stellar masses	M_1 ($M_\odot$)	0.43 ± 0.06
	M_2 ($M_\odot$)	0.98 ± 0.06
Semi-major axis	a ($R_\odot$)	2.11 ± 0.01
Mean stellar radii	R_1 ($R_\odot$)	0.68 ± 0.01
	R_2 ($R_\odot$)	0.98 ± 0.02
Stellar luminosity	L_1 ($L_\odot$)	0.38 ± 0.05
	L_2 ($L_\odot$)	0.59 ± 0.07
Bolometric magnitude	$M_{bol,1}$	5.82 ± 0.06
	$M_{bol,2}$	5.33 ± 0.09
Surface gravity	log g_1 (cgs)	4.41 ± 0.06
	log g_2 (cgs)	4.45 ± 0.03
Mean density	$\overline{\rho}_1$ (g cm^{-3})	1.91 ± 0.10
	$\overline{\rho}_2$ (g cm^{-3})	1.46 ± 0.08

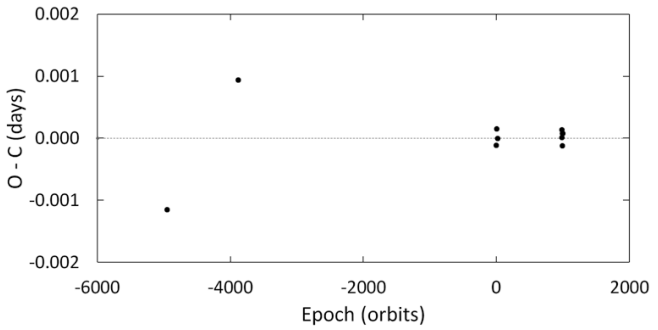

Figure 3. O–C residuals from linear ephemeris fit of Equation (3).

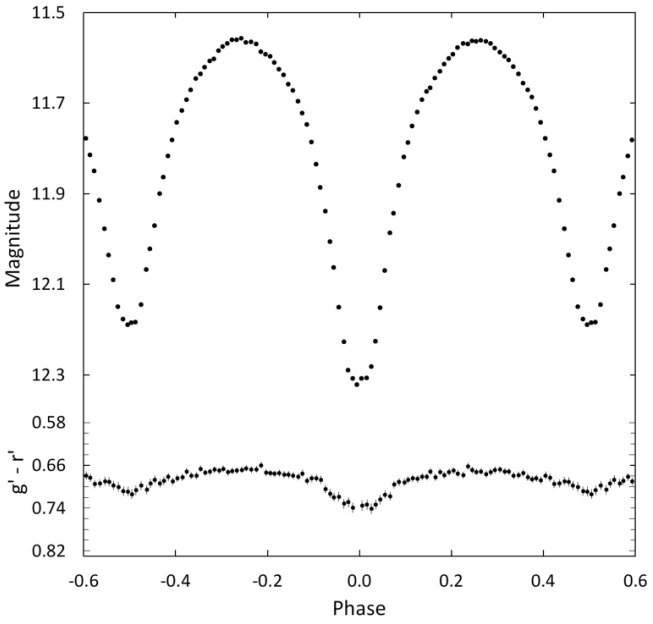

Figure 4. Light curve of all r'-band observations in standard magnitudes (top panel). The observations were binned with a phase width of 0.01. The errors for each binned point are about the size of the plotted points. The g'–r' colors (botttom panel) were calculated by subtracting the binned Sloan g' magnitudes from the linearly interpolated binned Sloan r' magnitudes.

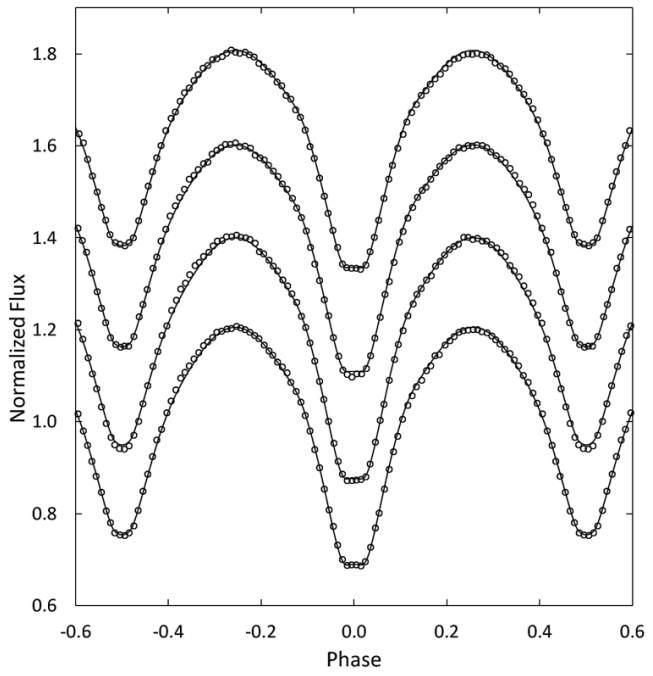

Figure 5. The WD model fit without spots (solid curve) to the observed normalized flux curves for each passband. From top to bottom the passbands are Sloan i', Sloan r', Johnson V, and Sloan g'. Each curve is offset by 0.2 for this combined plot. The best-fit parameters are given in column 2 of Table 3. Error bars are omitted from the points for clarity.

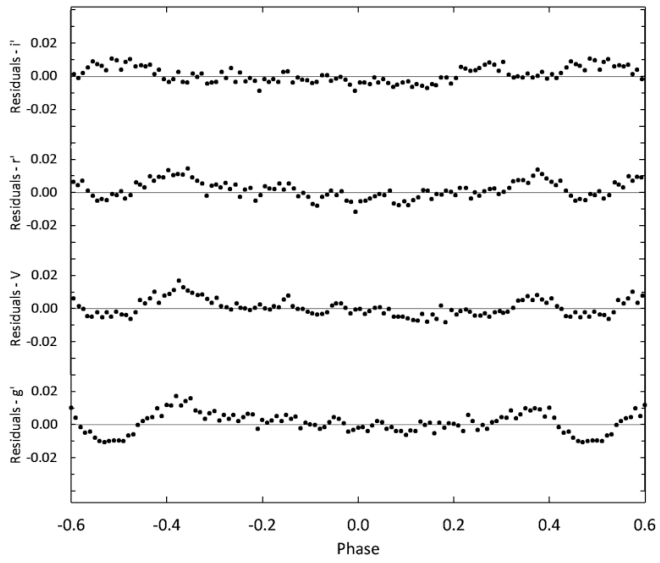

Figure 6. The residuals for the best-fit WD model without spots. Error bars are omitted from the points for clarity.

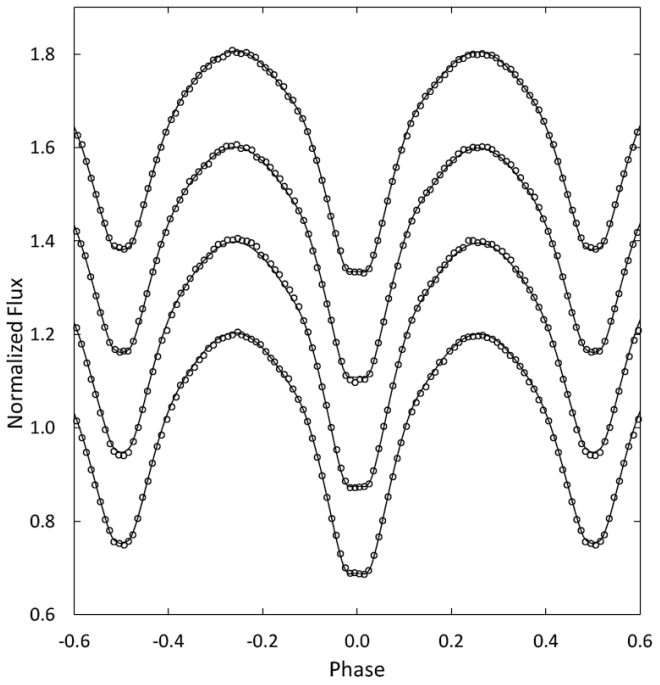

Figure 7. The WD model fit with spots (solid curve) to the observed normalized flux curves for each passband. From top to bottom the passbands are Sloan i', Sloan r', Johnson V, and Sloan g'. Each curve is offset by 0.2 for this combined plot. The best-fit parameters are given in column 3 of Table 3. Error bars are omitted from the points for clarity.

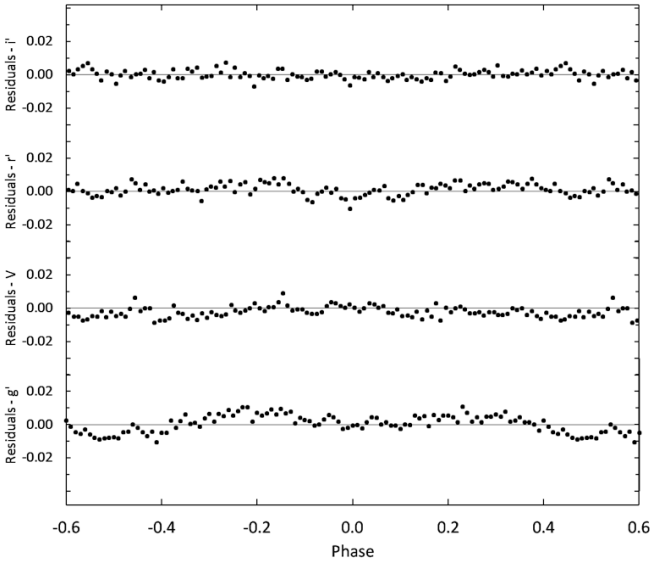

Figure 8. The residuals for the spotted WD model in each passband. Error bars are omitted from the points for clarity.

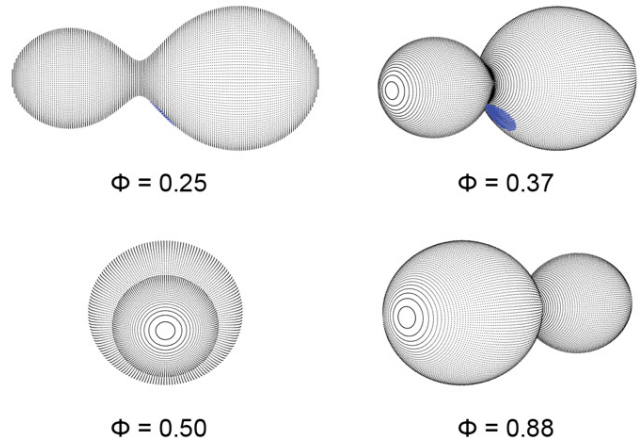

Figure 9. Roche Lobe surfaces of the best-fit WD spot model with orbital phase shown below each diagram.

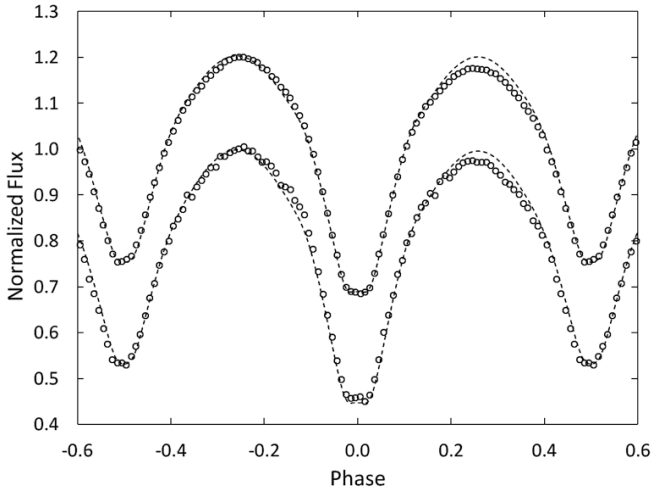

Figure 10. The WD model without spots overlaid (dashed curve) onto the February 2015 Johnson BV normalized flux curves. Johnson V is the top curve (offset by 0.2) and Johnson B the bottom. Error bars are omitted from the points for clarity.

4. Discussion and conclusions

W-type eclipsing binaries of W UMa type most often consist of two cool stars in contact whose spectral types are F, G, or K and whose components have nearly equal surface temperatures in spite of their often greatly differing masses. This study confirms that V958 Mon is a member of the W-type subclass where the larger more massive star is cooler and has less surface brightness than its companion and primary minimum is an occultation. The best-fit WD solution with a fill-out value of 19% is consistent with a contact binary. Given the total eclipses observed, the derived parameters should have good accuracy, as shown by Wilson (1978) and Terrell and Wilson (2005). The stellar parameters can now be determined for each star. From Qian's (2003) statistical study of contact systems the mass of the larger cooler star is given by:

$$M_2 = 0.391\ (\pm 0.059) + 1.96\ (\pm 0.17)\ P\ , \qquad (6)$$

where P is the orbital period. This equation gives the secondary star's mass, $M_2 = 0.98 \pm 0.06\ M_\odot$, and combined with the mass ratio gives the primary star's mass, $M_1 = 0.43 \pm 0.06\ M_\odot$. Applying Kepler's Third Law gives the distance between the stars' mass centers, $2.11 \pm 0.01\ R_\odot$. Mochnacki (1981) showed the mean stellar densities for contact binaries are given by:

$$\bar{\rho}_1 = \frac{0.0189}{r_1^3\ (1 + q)\ P^2} \text{ and } \bar{\rho}_2 = \frac{0.0189q}{r_2^3\ (1 + q)\ P^2}\ , \qquad (7)$$

where the stellar radius is normalized to the semi-major axis and P is in days. The computed values are $\bar{\rho}_1 = 1.91\ g\,cm^{-3}$ and $\bar{\rho}_2 = 1.46\ g\,cm^{-3}$. The stellar radii, surface gravities, luminosities, and bolometric magnitudes were calculated by the Wilson and Devinney (1971) light curve program (LC). All the absolute stellar parameters are presented in Table 4.

The light curves shown in Figure 2 have equal maxima but Johnson V-band and B-band observations taken 11 months earlier displayed a noticeable O'Connell effect. This can be seen in Figure 10, which shows the B and V light curves overlaid with the WD solution without spots (dashed line). For the V-band light curve, the maximum at orbital phase 0.25 was 0.15 magnitude fainter than the maximum at phase 0.75. These changes in the light curves are most likely the result of changing spot configurations. This is an indication of magnetically active stars which are often found in short period low-mass contact binaries such as V958 Mon.

A distance estimate to V958 Mon can be made using Ruciński and Duerbeck's (1997) luminosity calibration for contact binaries that is based on HIPPARCOS parallaxes. This empirical relationship is given by:

$$M_v = -4.44\ \log_{10}(P) + 3.02\ (B-V)_o + 0.12\ . \qquad (8)$$

Substituting into Equation 8 the orbital period and the observed (B–V) color index gives an absolute magnitude of $M_V = 5.07 \pm 0.22$. Using the apparent V-magnitude at quadrature, $m_V = 11.861 \pm 0.005$, gives a distance modulus of $(m - M)_V = 6.79 \pm 0.22$ and an estimated distance of 228 ± 23 pc. A correction for interstellar extinction was not applied due to the very small color excess for this star (see section 3.2).

A spectroscopic study of V958 Mon would be invaluable in confirming the absolute parameters of the component stars presented here. This star should be patrolled frequently. Several years of new minima times will be necessary to determine if any orbital period change is occurring. Period changes can result from magnetic braking, conservative mass exchange between the stars, or orbital motion about a third body. Lastly, V958 Mon does not appear to be a member of the Platais 6 cluster. Platais 6 is a very young cluster with an age of 60.3 Myr (Wu *et al.* 2009). When W UMa stars evolve to the beginning of their contact phase, they can range in age from 4.8 to 12.5 Gyr (Gazeas and Stepień 2008). With V958 Mon currently in its contact phase, it is far older than the Platais 6 stars.

5. Acknowledgements

The author wishes to thank Professor P. G. Niarchos for his careful readings, corrections, and valuable comments and suggestions on the draft version of this manuscript. This research was made possible through the use of the AAVSO Photometric All-Sky Survey (APASS), funded by the Robert Martin Ayers Sciences Fund. This research has made use of the SIMBAD database, operated at CDS, Strasbourg, France. Data from the Guo Shou Jing Telescope (the Large Sky Area Multi-Object Fiber Spectroscopic Telescope, LAMOST) were also used in this study. This telescope is a National Major Scientific Project built by the Chinese Academy of Sciences. Funding for the project has been provided by the National Development and Reform Commission. LAMOST is operated and managed by National Astronomical Observatories, Chinese Academy of Sciences.

References

Bilir, S., Karaali, S., and Tunçel, S. 2005, *Astron. Nachr.*, **326**, 321.

Bradstreet, D. H., and Stelman, D. P. 2002, *Bull. Amer. Astron. Soc.*, **34**, 1224.

Diethelm, R. 2011, *Inf. Bull. Var. Stars*, No. 5992, 1.

Gazeas, K., and Stepień, K. 2008, *Mon. Not. Roy. Astron. Soc*., **390**, 1577.

Henden, A. A., *et al.* 2014, AAVSO Photometric All-Sky Survey, data release 9 (http:www.aavso.org/apass).

Hoffman, D. I., Harrison, T. E., and McNamara, B. J. 2009, *Astron. J.*, **138**, 466.

Kafka, S. 2015, observations from the AAVSO International Database (https:/www.aavso.org/aavso-international-database).

Kharchenko, N. V., Piskunov, A. E., Roeser, S., Schilbach, E., and Scholz, R.-D. 2005, *Astron. Astrophys.*, **438**, 1163.

Kwee, K. K., and van Woerden, H. 1956, *Bull. Astron. Inst. Netherlands*, **12**, 327.

Lucy, L. B. 1968, *Astrophys. J.*, **151**, 1123.

Lucy, L. B., and Wilson, R. E. 1979, *Astrophys. J.*, **231**, 502.

Luo, A-Li, *et al.* 2015, *Res. Astron. Astrophys.*, **15**, 1095.

Mirametrics. 2015, Image Processing, Visualization, Data Analysis (http://www.mirametrics.com).

Mochnacki, S. W. 1981, *Astrophys. J.*, **245**, 650.
Nelson, R. H. 2011, *Inf. Bull. Var. Stars*, No. 6018, 1.
Otero, S. A., Wils, P., and Dubovsky, P. A. 2004, *Inf. Bull. Var. Stars*, No. 5570, 1.
Pecaut, M. J., and Mamajek, E. E. 2013, *Astrophys. J., Suppl. Ser.*, **208**, 9, (http://www.pas.rochester.edu/~emamajek/EEM_dwarf_UBVIJHK_colors_Teff.txt).
Qian, S., 2003, *Mon. Not. Roy. Astron. Soc.*, **342**, 1260.
Ruciński, S. M. 1969, *Acta Astron.*, **19**, 245.
Ruciński, S. M., and Duerbeck, H. W. 1997, *Publ. Astron. Soc. Pacific*, **109**, 1340.
Terrell, D., and Wilson, R. E. 2005, *Astrophys. Space Sci.*, **296**, 221.
Van Hamme, W. 1993, *Astron. J.*, **106**, 2096.
Van Hamme, W., and Wilson, R. E. 1998, *Bull. Amer. Astron. Soc.*, **30**, 1402.
Wilson, R. E. 1978, *Astrophys. J.*, **224**, 885.
Wilson, R. E., and Biermann, P. 1976, *Astron. Astrophys.*, **48**, 349.
Wilson, R. E., and Devinney, E. J. 1971, *Astrophys. J.*, **166**, 605.
Wozniak, P. R., *et al.* 2004, *Astron. J.*, **127**, 2436.
Wu, Z.-Y., Zhou, X., Ma, J., and Du, C.-H. 2009, *Mon. Not. Roy. Astron. Soc.*, **399**, 2146.
Zejda, M., Paunzen, E., Baumann, B., Mikulášek, Z., and Liška, J. 2012, *Astron. Astrophys.*, **548**, A97.

Monitoring the Continuing Spectral Evolution of Nova Delphini 2013 (V339 Del) with Low Resolution Spectroscopy

Howard D. Mooers
William S. Wiethoff
Department of Earth and Environmental Sciences, University of Minnesota Duluth, Duluth, MN 55812; send email correspondence to hmooers@d.umn.edu

Alexander Evich
Department of Physics and Astronomy, University of Minnesota Duluth, Duluth, MN 55812

Received December 7, 2015; accepted December 31, 2015

Abstract The continuing spectral evolution of Nova Delphini 2013 (V339 Del) is presented with low-resolution spectroscopy collected with a 100 line per millimeter diffraction grating. Spectra were collected on 3 July 2014, and 14 September 2015, 321 and 759 days after peak visible brightness on 16 August 2013. An imaging system was mounted on an equatorially–mounted, 14-inch Schmidt-Cassegrain telescope. The continuum is no longer visible in the spectra, however, OIII (5007 Å) and Hα (6563 Å) are prominent and NII (5755), Hγ (4340 Å) and CIII/NIII (4640 Å) can still be discerned at +759 days.

1. Introduction

Nova Delphini 2013 (V339 Del) erupted on 14 August 2013 UT (Itagaki 2013) and reached a peak magnitude of 4.3 (Munari *et al*. 2013) on 16 August 2015 UT. Mooers and Wiethoff (2014) presented a 125-day, low-resolution spectral record of the nova acquired with relatively modest equipment available to nearly any amateur astronomer. Here we update the spectral evolution of this bright nova with additional low resolution spectra collected on 3 July 2014 UT and 14 September 2015 UT, 321 and 759 days after maximum visible brightness, respectively. In particular, we emphasize the capabilities for this type of observation that have become available to the amateur astronomer. Although this low resolution spectral analysis will not lend significantly to the understanding of nova evolution, it does provide a mechanism for the amateur to study variable stars in a rigorous way and learn the techniques of professional observational astronomy. There are, however, many ways that the amateur community plays a critical role in variable star research, and their contributions have been recognized for many years (Lankford 1981; Percy 1998). The professional community is limited in the number and availability of equipment, particularly large telescopes, as time on them is typically reserved for "deep" objects. For many projects the professional astronomers rely on the amateur community and smaller telescopes that are relatively abundant. In fact, the AAVSO was founded in the idea of forging strong collaborations between amateur and professional astronomers (for example, the Citizen Sky Program (https://www.aavso.org/citizensky); see also the AAVSO Vision/Mission Statement (https://www.aavso.org/visionmission)).

In the study of variable stars, the contribution of photometric observations of the amateur community is critical given the large number of variable star candidates. With the proliferation of very capable backyard telescopes and the rapidly decreasing cost of high-quality astronomical cameras, filters, and software, the professional astronomers have come to rely on amateurs to produce reliable, high-quality data. Variable stars are an important tool in astrophysics for the understanding of stellar origin and evolution including stellar properties, such as mass, radius, luminosity, temperature, internal and external structure, and composition. Much of this information would be difficult or impossible to obtain in other ways.

2. Methods

The imaging system is mounted on a 14-inch Schmidt Cassegrain telescope on an equatorial mount. As with the spectra described by Mooers and Wiethoff (2014) the spectrum reported here was acquired with a STAR ANALYZER® 100 (Paton Hawksley Education, Ltd. 2014), a 100-line-per-mm diffraction grating. The grating was mounted 70 mm from the sensor of a Meade DSI Pro II CCD camera, which has a Sony ICX429ALL CCD with dimensions of 752 (H) × 582 (V) pixels of size of 8.6 (H) × 8.3 (V) μm, yielding a chip size of 7.4 × 5.95 mm and a plate scale of 0.429 arcsec per pixel. Spectral dispersion was 13.75 Å/pixel. The camera was mounted at prime focus with no focal reducer. Images were shot at f/11 with a focal length of 4,086 mm. Spectral resolution is 46.3.

Images were acquired on 3 July and 14 September 2015 UT. Photometry was measured using AIP4WIN software (Berry and Burnell 2000) and the spectrum was analyzed with RSPEC® software (Field Tested Systems 2014).

3. Results

Figure 1a shows N Del 2013 at its maximum magnitude of 4.3 (Munari *et al.* 2013) on 16 August 2013. Figure 1b was taken on 14 September 2015 with a calculated apparent visual magnitude of 13.61 and 13.25 using AIP4WIN software and the GSC and USNO A 2.0 catalogues, respectively, for calibration magnitudes. Figure 1c shows the spectrum of N Del 2013 acquired on 14 September 2015. The continuum is no longer visible, however, the OIII (5007 Å) and Hα (6563 Å) emission

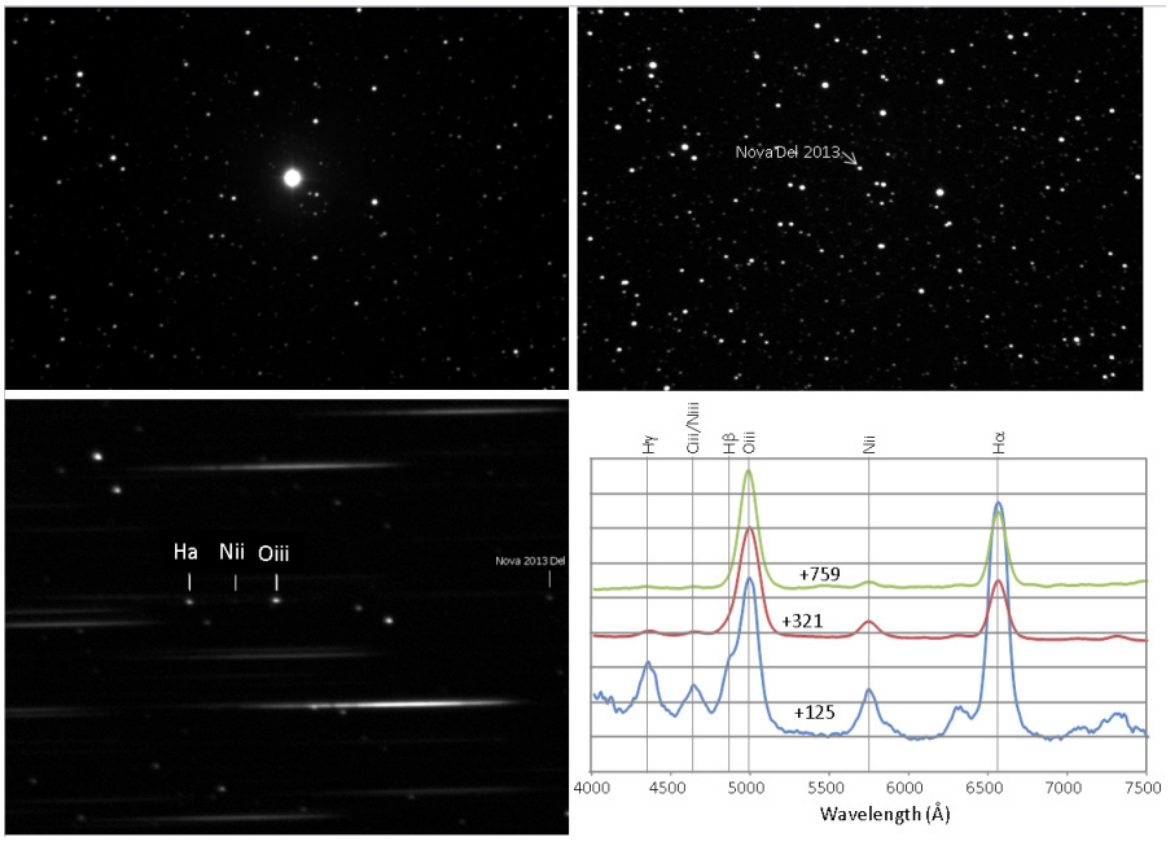

Figure 1. N Del 2013 (V339 Del): a) at maximum magnitude of 4.3 on 16 August 2013; b) calculated apparent visual magnitude of 13.61 and 13.25 on 14 September 2015; c) spectrum acquired on 14 September 2015, continuum no longer visible but the OIII (5007 Å) and Hα (6563 Å) emission lines are prominent and the NII (5755) emission line is also faintly visible; d) the calibrated, normalized spectra acquired on 3 July 2014 and 14 September 2015, along with the spectrum from day +125 (Mooers and Wiethoff 2014). Hγ (4340 Å) and CIII/NIII (4640 Å) that were clearly visible at +125 days can still be discerned at +759 days.

lines are prominent and the NII (5755) emission line is also faintly visible (Figure 1c). Figure 1d shows the calibrated, normalized spectra acquired on 3 July 2014 and 14 September 2015, along with the spectrum from day +125 (Mooers and Wiethoff 2014). Hγ (4340 Å) and CIII/NIII (4640 Å) that were clearly visible at 125 days can still be discerned at 759 days.

4. Discussion and conclusions

The amateur astronomical community has played a significant role in data collection for the professional community. Often amateurs are captivated by the prospect of producing fabulous astrophotography and along the way learn the techniques of professional image processing. However, the knowledge and tools of the amateur community are easily applied to problems of variable star research. The study of Mooers and Wiethoff (2014), and this continuation and update of the evolving spectrum of N Del 2013, illustrate potential for furthering the development of the amateur astronomical community (Percy 1998). Although the nebular phase of classical novae continues to evolve over many years (Krautter and Williams 1989; Slavin *et al.* 1995), most of the spectral evolution is beyond the capabilities of low-resolution spectroscopy. However, this kind of study piques the interest, develops the analytical skills, and demonstrates the capabilities of the amateur astronomer.

References

Berry, R., and Burnell, J. 2000, Astronomical Image Processing, Willman-Bell, Richmond, VA.

Field Tested Systems, LLC. 2014, RSPEC® software (http://www.rspec-astro.com).

Itagaki, K. 2013, *IAU Cent. Bur. Astron. Telegrams Transient Object Followup Rep.* 2013, 08 14.584 (http://www.cbat.eps.harvard.edu/unconf/followups/J20233073+2046041.html).

Krautter, J., and Williams, R. E. 1989, *Astrophys. J.*, **341**, 968.

Lankford, J. 1981, *Social Stud. Sci.*, **11**, 275.

Mooers, H. D., and Wiethoff, W. S. 2014, *J. Amer. Assoc. Var. Star Obs.*, **42**, 161.

Munari, U., Dallaporta, S., Cherini, G., Valisa, P., Cetrulo, G., Milani, A., and Ghirotto, L. 2013, *Astron. Telegram*, No. 5304, 1 (http://www.astronomerstelegram.org/?read=5304).

Paton Hawksley Education, Ltd. 2014, STAR ANALYZER® 100, 100 line per mm diffraction grating (http://www.patonhawksley.co.uk/staranalyser.html).

Percy, J. R. 1998, in *New Trends in Astronomy Teaching*, eds. L. Gouguenheim, D. McNally, J. R. Percy, IAU Colloquium 162, Cambridge Univ. Press, Cambridge, 205.

Slavin, A. J., O'Brien, T. J., and Dunlop, J. S. 1995, *Mon. Not. Roy. Astron. Soc.*, **276**, 353.

Observing Globular Cluster RR Lyrae Variables with the BYU West Mountain Observatory

Elizabeth J. Jeffery
Michael D. Joner
Department of Physics and Astronomy, Brigham Young University, Provo, UT 84604; joner@byu.edu

Received March 29, 2016; revised April 15, 2016; accepted April 19, 2016

Abstract We have utilized the 0.9-meter telescope of the Brigham Young University West Mountain Observatory to secure data on six northern hemisphere globular clusters. Here we present representative observations of RR Lyrae stars located in these clusters, including light curves. We compare light curves produced using both DAOPHOT and ISIS software packages. Light curve fitting is done with FITLC. We find that for well-separated stars, DAOPHOT and ISIS provide comparable results. However, for stars within the cluster core, ISIS provides superior results. These improved techniques will allow us to better measure the properties of cluster variable stars.

1. Introduction

Globular clusters (GCs) provide an important environment for studying RR Lyrae (RRL) variable stars. Our ability to maximize information in these data rests upon our ability to adequately measure photometry for the RRL cluster members. The stars in a typical GC field are crowded, at times making photometry difficult. This is especially true for stars in the cluster core. Good photometry of stars in a GC often requires the use of point-spread function (PSF) fitting techniques, though at times even this may be inadequate if the field is especially crowded, like in the overly-crowded GC core. When the stars are especially crowded, image subtraction methods may provide superior results.

This report includes a summary of results that have been presented at several venues in the past six months. These include the 2015 October conference in Hungary on High-precision Studies of RR Lyrae Stars (Jeffery *et al.* 2016), the 2015 November AAVSO Annual Meeting in Massachusetts (Joner and Jeffery 2016), and the 2016 January Winter Meeting of the American Astronomical Society in Florida (Jeffery and Joner 2016).

In this report, we present representative results of new time-series observations of six northern hemisphere GCs, and compare light curves obtained using PSF fitting photometry and image subtraction methods. We fit light curves to the resulting data points using the template-fitting program FITLC (Sarajedini *et al.* 2009). The use of photometric techniques appropriate to different levels of crowding will allow us to obtain better light curves for GC RRLs, resulting in a better determination of the properties of the cluster variable stars.

2. Observations

We have observed six northern GCs with the 0.9-meter telescope at the West Mountain Observatory (WMO) that is owned and operated by Brigham Young University (BYU). WMO is located approximately 23 km southwest of the main BYU campus in Provo, Utah. The observations were done using a Fairchild 3041-UV 2048 × 2048 CCD. Using this CCD on the 0.9-meter results in a plate scale of 0.61 arcseconds per pixel, and a field of view of 20.8 arcminutes in each dimension.

The GCs we observed are: NGC 5272 (M3), NGC 5466, NGC 5904 (M5), NGC 6205 (M13), NGC 6341 (M92), and NGC 7078 (M15). Observations for five GCs (all but NGC 5466) were secured in a standard UBVRI filter set during the 2012 observing season; NGC 5466 was observed in 2014 in BVR filters. For each cluster we have between 69 and 229 individual observations, resulting in well-sampled light curves. We reduced the raw data frames using standard procedures in the IRAF CCDRED package for flat, dark, zero, and overscan corrections.

We have summarized our observations in Table 1. Target stars in these clusters are previously identified RRLs from the catalog of Clement *et al.* (2001). Comparison stars across the field of view were used for differential photometry. These stars were chosen based on similar brightness to the variables and were verified to be non-variable over the entire baseline of observations.

Table 1. Log of Cluster Observations.

Cluster	*Number of V[1] Observations*	*Dates Observed*
NGC 5272 (M3)	219	Apr–Aug 2012
NGC 5466	69	Mar–Jul 2014
NGC 5904 (M5)	170	Apr–Jul 2012
NGC 6205 (M13)	229	Apr–Sep 2012
NGC 6341 (M92)	217	Mar–Aug 2012
NGC 7078 (M15)	91	Jun–Sep 2012

Note: 1 Observation sequences were completed in UBVRI filters, except in the case of NGC 5466 which was observed in BVR filters. Only the number of V images is listed here; the number of images in the other filters is comparable.

3. Photometry and light curves

We measured photometry to construct light curves using two different methods: PSF-fitting methods using DAOPHOT/ALLSTAR (Stetson 1987) and image subtraction methods employed by the ISIS software suite (Alard 2000). Here we describe each method and compare the resulting light curves.

3.1. DAOPHOT

We utilized DAOPHOT to obtain instrumental magnitudes for all stars in the globular cluster frames. Briefly, tasks within DAOPHOT were used to do the following: find coordinates for all stars on the frame (using DAOFIND); perform aperture photometry to determine instrumental magnitude zeropoints and calculate sky values; construct a spatially varying PSF for each image using well separated stars; and simultaneously fit (using ALLSTAR) the PSF to each star on the frame. The result was instrumental magnitudes for all targets and comparison stars.

The first results shown here are for the RRLs in the moderately crowded fields in the cluster NGC 5466. The well-known anomalous Cepheid, BL Boo, is one of the brighter target objects in this field. In Figure 1, we show results for BVR photometry obtained for BL Boo using DAOPHOT. Even though the results for some of the data points were affected by deteriorating observing conditions (shown by larger error bars), it is clear that DAOPHOT produces well-defined light curves for stars with this level of crowding.

In order to demonstrate that DAOPHOT analysis is generally acceptable for moderately crowded fields like those found in NGC 5466, we show results for nine of the 20 RRL stars listed for the cluster in the catalog of Clement *et al.* (2001). The BVR plots for these representative variables are displayed in Figure 2. Once again, it is clear that analysis with DAOPHOT is adequate for stars in fields outside the GC core.

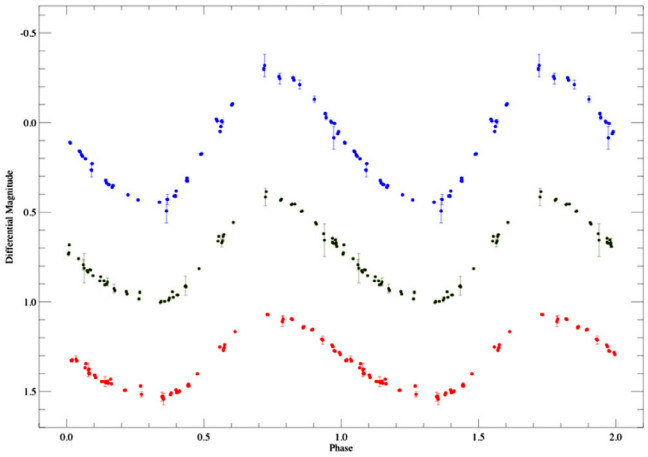

Figure 1. DAOPHOT B (top (blue) plot), V (middle (green) plot) and R (lower (red) plot) photometry for the anomalous Cepheid, BL Boo, located in NGC 5466. The points with larger error bars were secured on nights with rapidly changing observing conditions. All of the points are shown with error bars, but in most cases these are comparable to the size of the points that are used in the plot. Clearly, DAOPHOT PSF-fitting provides photometry for a well-defined light curve for this level of crowding.

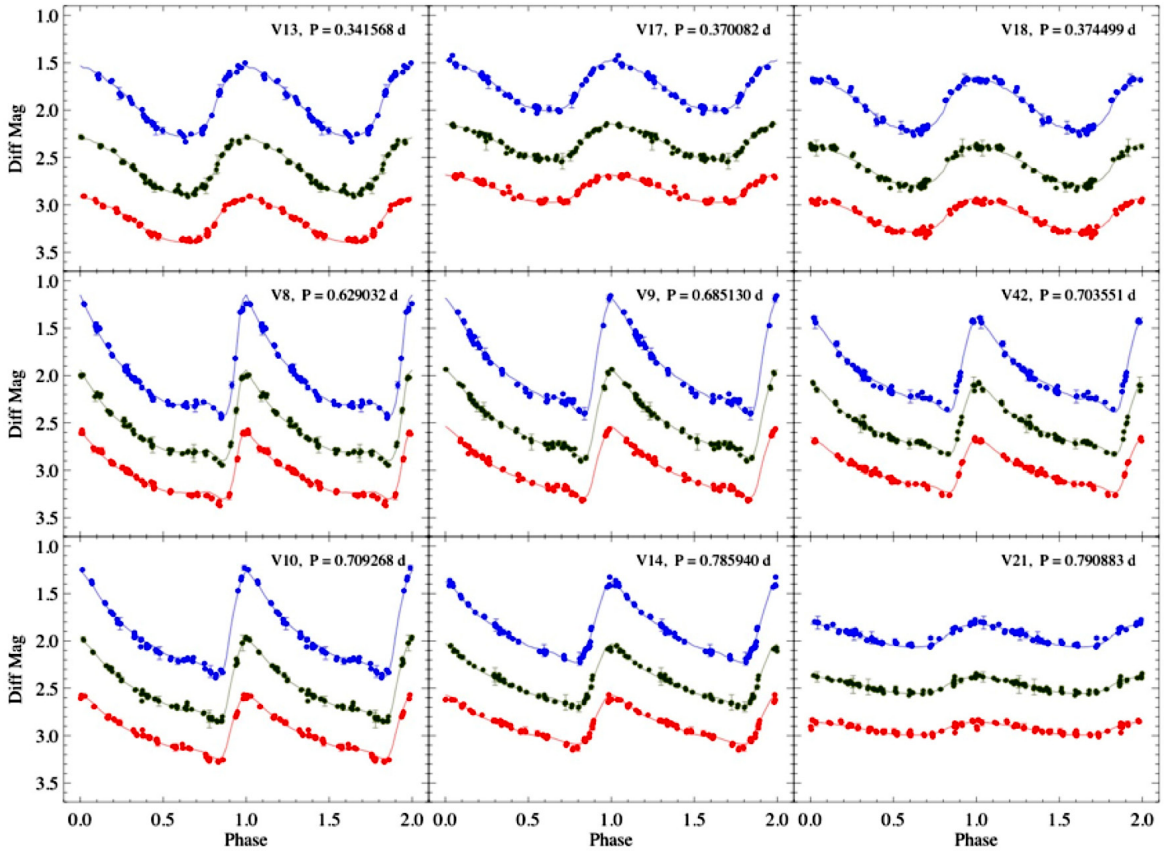

Figure 2. DAOPHOT B (upper (blue) plots), V (middle (green) plots), and R (lower (red) plots) photometry for nine RRL stars in the cluster NGC 5466. All of the points are plotted with error bars but in most cases these are smaller than the size of the individual points. In each case, the curve was fit and the period found using FITLC. The photometry determined using DAOPHOT is consistent from night to night and the resulting light curves are adequately sampled in all filters.

3.2. ISIS

We also obtained light curves of cluster variable stars by measuring the differential flux of the target stars using the image subtraction routines in the ISIS software (Alard 2000). The ISIS software package is freely available for download from Alard's website.

The first step in using ISIS is to align all of the images for each field. Next, we selected the best GC images, and used ISIS to create a reference image for each target cluster. Each individual image is subsequently subtracted from this reference image. This results in non-variable stars subtracting out, leaving only flux from the variable stars. The result of this process is a less contaminated measurement of the flux from the variable stars in a field.

Because ISIS determines differential flux (not magnitude) values, we converted these to differential magnitude values using the method outlined in Szekely *et al.* (2007). To determine this relationship, we used the high-amplitude, well-separated star V11 in the cluster M3. We show this relationship in Figure 3. The red line is the calculated fit (found via a standard linear, least squares regression). For comparison, in Figure 3 we also show data for another well-separated star in M3, V37. Note the fit to the data for both stars is in excellent agreement, increasing our confidence in this transformation.

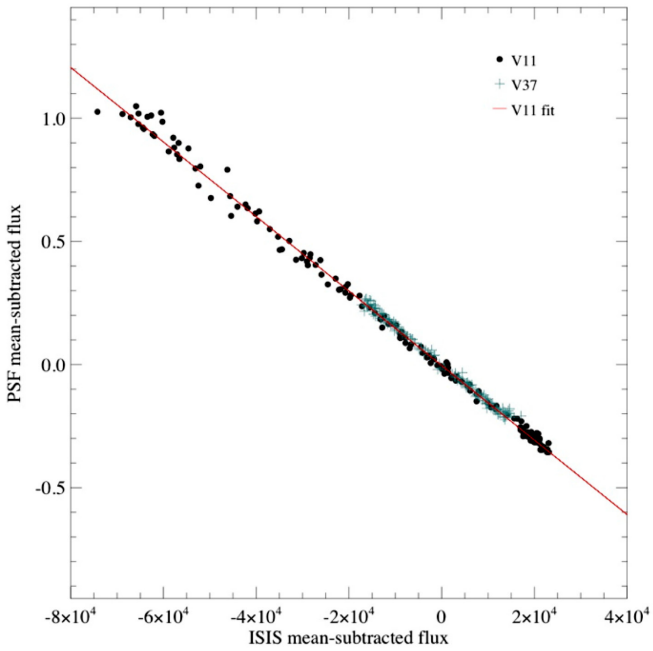

Figure 3. The relationship between mean-subtracted flux values from ISIS and DAOPHOT. We determined the fit (line) using a well-separated, high amplitude star (V11 in the cluster M3). For comparison, we also show data for another well-separated star in M3, V37 (plus symbols). We note the excellent agreement of the data for the star to the fit from V11.

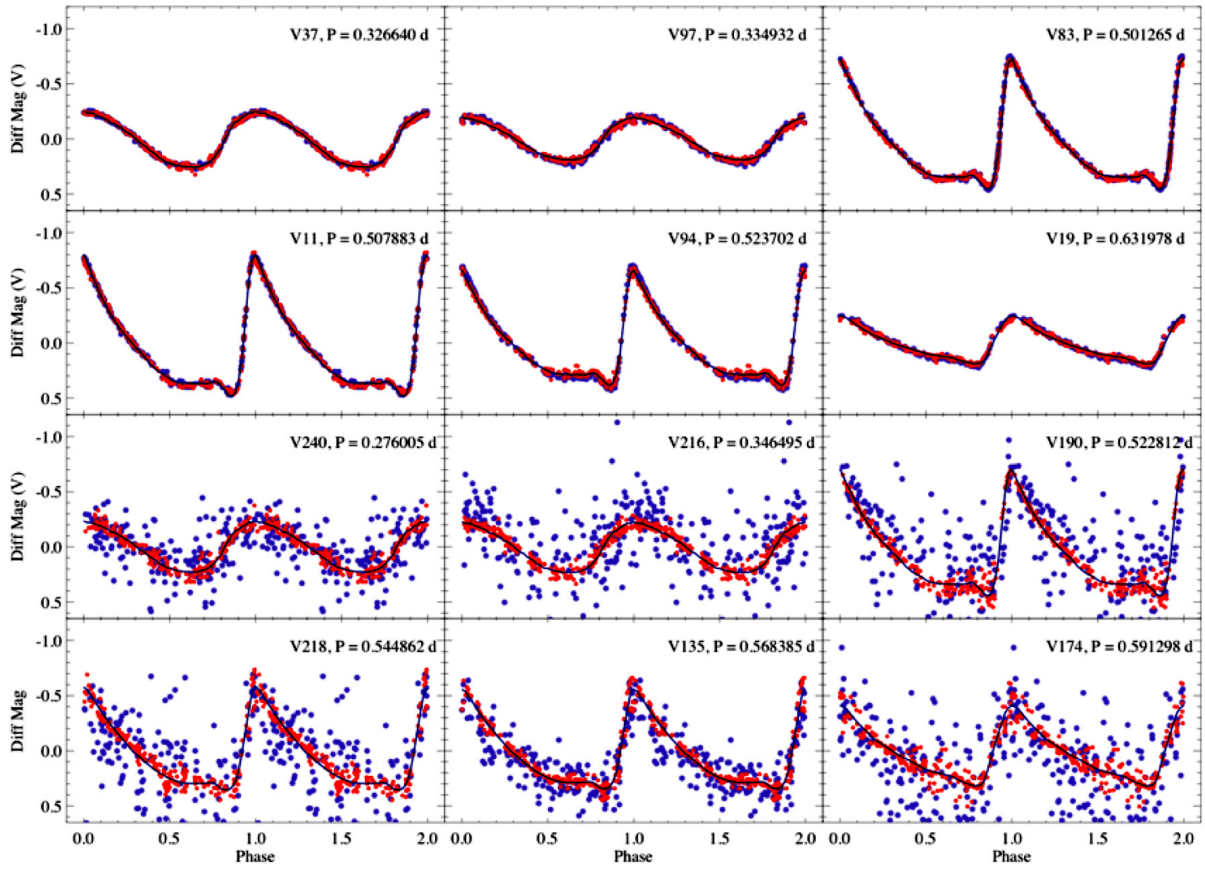

Figure 4. Light curves for 12 RRL stars in M3. Six RRLs (V11, V19, V37, V83, V94, and V97) shown in the top two rows are well separated from nearby neighbors due to locations in the outer portion of the GC. The other six RRLs (V135, V174, V190, V216, V218, and V240) are located in the crowded cluster core. DAOPHOT (dark (blue) dots) and ISIS (light (red) dots) photometry are plotted for comparison, along with the best fit template and period, found by FITLC. The results obtained from ISIS photometry are clearly superior in the crowded cluster core.

Once we determined the relationship between output values from ISIS and DAOPHOT, we converted all ISIS differential flux values to differential magnitudes. This allowed for direct comparison between the two, as well as light curves that can be analyzed. We used FITLC (Sarajedini *et al.* 2009) to fit an RRL template to determine periods. Template fitting was done on transformed ISIS light curves.

In Figure 4, we compare light curves determined from DAOPHOT and ISIS methods for 12 stars in M3: six RRLs (V11, V19, V37, V83, V94, and V97) are well-separated from nearby neighbors in the cluster halo and the other six RRLs (V135, V174, V190, V216, V218, and V240) are in the crowded cluster core. As can be seen in this figure, for stars without nearby companions, DAOPHOT and ISIS provide comparable results. However, the light curves found using ISIS are superior in the crowded cluster core. The periods listed in Figure 4 are those found by FITLC.

4. Summary

We have presented representative observations of GC RRLs secured with the WMO 0.9-m telescope. We have constructed light curves using both DAOPHOT PSF-fitting photometry routines and image subtraction methods employed by the ISIS software package. For stars that are well separated from other stars, we show that DAOPHOT and ISIS provide comparable results. For stars in the crowded cluster core, we demonstrate that superior light curves are obtained from ISIS analysis. Using these methods, we are able to determine improved periods for RRL stars in the crowded cluster core using the template-fitting program FITLC. Such methods hold great promise for studying all RRL stars in various GCs, including those found in the crowded cluster core.

5. Acknowledgements

We appreciate the comments from the anonymous referee. They have helped to clarify sections of this paper to make the information more useful to readers. We acknowledge continued support from the BYU College of Physical and Mathematical Sciences for operation of the West Mountain Observatory. Some of the observations included in this presentation were secured within the term of NSF/PREST grant AST-0618209.

References

Alard, C. 2000, *Astron. Astrophys, Suppl. Ser.*, **144**, 363.

Clement, C., *et al.* 2001, *Astron. J.*, **122**, 2587.

Jeffery, E., and Joner, M. 2016, American Astronomical Society Meeting Abstracts, 227, 144.10.

Jeffery, E., Joner, M., and Walton, R. 2016, *Commun. Konkoly Obs,*, in press.

Joner, M., and Jeffery, E. 2016, *J. Amer. Assoc. Var. Star Obs.*, **44**, in press.

Sarajedini, A., Mancone, C. L., Lauer, T. R., Dressler, A., Freedman, W., Trager, S. C., Grillmair, C., and Mighell, K. J. 2009, *Astron. J.*, **138**, 184.

Szekely, P. Kiss, L. L., Jackson, R., Derekas, A., Csák, B., and Szatmáry, K. 2007, *Astron. Astrophys.*, **463**, 589.

Stetson, P. B. 1987, *Publ. Astron. Soc. Pacific*, **99**, 191.

Recent Maxima of 74 Short Period Pulsating Stars

Gerard Samolyk
P.O. Box 20677, Greenfield, WI 53220; gsamolyk@wi.rr.com

Received January 12, 2016; accepted January 15, 2016

Abstract This paper contains times of maxima for 74 short period pulsating stars (primarily RR Lyrae and δ Scuti stars). These maxima represent the CCD observations received by the AAVSO Short Period Pulsator (SPP) section in 2015.

1. Recent observations

The accompanying list contains times of maxima calculated from CCD observations made by participants in the AAVSO's Short Period Pulsator (SPP) Section. This list will be web-archived and made available through the AAVSO ftp site at ftp:ftp.aavso.org/public/datasets/gsamoj441.txt. The error estimate is included. RR Lyr stars in this list, along with data from earlier AAVSO publications, are included in the GEOS database at: http://rr-lyr.ast.obs-mip.fr/dbrr/dbrr-V1.0_0.php. This database does not include δ Scuti stars. These observations were reduced by the writer using the PERANSO program (Vanmunster 2007). Column F indicates the filter used.

The linear elements in the *General Catalogue of Variable Stars* (GCVS; Kholopov *et al.* 1985) were used to compute the O–C values for most stars. For a few exceptions where the GCVS elements are missing or are in significant error, light elements from another source are used: RZ Cap and DG Hya (Samolyk 2010), and VY LMi (Henden and Vidal-Sainz 1997).

References

Henden, A. A., and Vidal-Sainz, J. 1997, *Inf. Bull. Var. Stars.*, No. 4535, 1.

Kholopov, P. N., *et al.* 1985, *General Catalogue of Variable Stars*, 4th ed., Moscow.

Samolyk, G., 2010, *J. Amer. Assoc. Var. Stars*, **38**, 12 .

Vanmunster, T. 2007, PERANSO period analysis software (http://www.peranso.com).

Table 1. Recent times of maxima of stars in the AAVSO Short Period Pulsator program.

Star	*JD (max) Hel. 2400000 +*	*Cycle*	*O–C*	*F*	*Observer*	*Error*	*Star*	*JD (max) Hel. 2400000 +*	*Cycle*	*O–C*	*F*	*Observer*	*Error*
SW And	57026.4074	87940	–0.4393	V	T. Arranz	0.0008	AC And	57288.5955	47267	0.0555	V	T. Arranz	0.0027
SW And	57244.8804	88434	–0.4523	V	R. Sabo	0.0012	AC And	57293.6090	47277	–0.1823	V	T. Arranz	0.0008
SW And	57249.7483	88445	–0.4495	V	K. Menzies	0.0009	AC And	57298.4451	47286	–0.0723	V	T. Arranz	0.0025
SW And	57274.5161	88501	–0.4493	V	T. Arranz	0.0007	AC And	57306.3076	47301	–0.0867	V	T. Arranz	0.0007
SW And	57285.5713	88526	–0.4511	V	T. Arranz	0.0006	AC And	57310.5470	47309	–0.0484	V	T. Arranz	0.0016
SW And	57289.5515	88535	–0.4514	V	T. Arranz	0.0006	AC And	57353.4432	47391	–0.2126	V	T. Arranz	0.0008
SW And	57292.6472	88542	–0.4517	V	T. Arranz	0.0007	AT And	57233.8809	24137	–0.0109	V	R. Sabo	0.0021
SW And	57296.6273	88551	–0.4521	V	T. Arranz	0.0007	AT And	57284.4737	24219	–0.0051	V	T. Arranz	0.0013
SW And	57297.5130	88553	–0.4510	V	T. Arranz	0.0006	AT And	57287.5537	24224	–0.0097	V	T. Arranz	0.0010
SW And	57309.4535	88580	–0.4520	V	T. Arranz	0.0006	AT And	57305.4448	24253	–0.0091	V	T. Arranz	0.0014
SW And	57311.6642	88585	–0.4527	V	T. Arranz	0.0007	AT And	57334.4434	24300	–0.0055	V	T. Arranz	0.0011
SW And	57314.7610	88592	–0.4519	V	N. Simmons	0.0007	AT And	57355.4153	24334	–0.0087	V	T. Arranz	0.0011
SW And	57334.6620	88637	–0.4534	V	G. Samolyk	0.0009	DY And	57331.7137	35251	–0.1721	V	K. Menzies	0.0016
SW And	57340.4117	88650	–0.4534	V	T. Arranz	0.0006	SW Aqr	57321.6261	70159	–0.0028	V	G. Samolyk	0.0008
SW And	57347.3755	88666	–0.5660	V	T. Arranz	0.0005	SW Aqr	57321.6264	70159	–0.0025	V	N. Simmons	0.0008
SW And	57351.3525	88675	–0.5696	V	T. Arranz	0.0005	TZ Aqr	57256.8294	34503	0.0125	V	G. Samolyk	0.0015
SW And	57356.3330	88686	–0.4541	V	T. Arranz	0.0007	YZ Aqr	57307.6553	39757	0.0698	V	G. Samolyk	0.0012
SW And	57360.3139	88695	–0.4537	V	T. Arranz	0.0006	AA Aqr	57336.6354	60090	–0.1557	V	G. Samolyk	0.0013
XX And	57283.5870	25176	0.2678	V	T. Arranz	0.0011	BO Aqr	57314.6034	22612	0.2028	V	G. Samolyk	0.0015
XX And	57291.5388	25187	0.2694	V	T. Arranz	0.0011	BR Aqr	57279.7933	40765	–0.2028	V	G. Samolyk	0.001
XX And	57304.5466	25205	0.2677	V	T. Arranz	0.0008	CY Aqr	57285.3473	376434	0.0139	V	T. Arranz	0.0002
XX And	57309.6072	25212	0.2691	V	T. Arranz	0.0009	CY Aqr	57285.4083	376435	0.0139	V	T. Arranz	0.0002
XX And	57335.6281	25248	0.2711	V	N. Simmons	0.0011	CY Aqr	57287.3616	376467	0.0139	V	T. Arranz	0.0002
XX And	57335.6282	25248	0.2712	B	N. Simmons	0.0012	CY Aqr	57297.6160	376635	0.0140	V	G. Samolyk	0.0005
XX And	57359.4753	25281	0.2676	V	T. Arranz	0.0011	CY Aqr	57297.6773	376636	0.0142	V	G. Samolyk	0.0005
ZZ And	57335.6639	58621	0.0294	V	R. Sabo	0.0019	CY Aqr	57312.5702	376880	0.0138	V	G. Samolyk	0.0006
AC And	57229.5789	47155	–0.1469	V	T. Arranz	0.0007	CY Aqr	57312.6315	376881	0.0140	V	G. Samolyk	0.0004
AC And	57239.5589	47174	–0.1443	V	T. Arranz	0.0014	CY Aqr	57312.6929	376882	0.0144	V	G. Samolyk	0.0004
AC And	57251.5989	47197	–0.1823	V	T. Arranz	0.0008	CY Aqr	57312.7536	376883	0.0140	V	G. Samolyk	0.0005
AC And	57261.5954	47216	–0.1632	V	T. Arranz	0.0009	CY Aqr	57334.5440	377240	0.0137	V	G. Samolyk	0.0005

Table continued on following pages

Table 1. Recent times of maxima of stars in the AAVSO Short Period Pulsator program, cont.

Star	*JD (max) Hel. 2400000 +*	*Cycle*	*O–C*	*F*	*Observer*	*Error*
CY Aqr	57334.6052	377241	0.0139	V	G. Samolyk	0.0005
CY Aqr	57334.6665	377242	0.0141	V	G. Samolyk	0.0005
DN Aqr	57280.7810	45531	0.0476	V	G. Samolyk	0.0025
SY Ari	55963.5040	35043	–0.0618	V	K. Menzies	0.0013
SY Ari	57341.6633	37475	–0.0719	V	K. Menzies	0.0015
TZ Aur	57072.3690	94900	0.0156	V	T. Arranz	0.0009
TZ Aur	57079.4174	94918	0.0139	V	T. Arranz	0.0006
TZ Aur	57081.3750	94923	0.0131	V	T. Arranz	0.0004
TZ Aur	57082.5508	94926	0.0139	V	K. Menzies	0.0006
TZ Aur	57090.3848	94946	0.0144	V	T. Arranz	0.0006
TZ Aur	57092.3445	94951	0.0157	V	T. Arranz	0.0006
TZ Aur	57330.8739	95560	0.0153	V	G. Samolyk	0.0007
BH Aur	56563.8698	30284	0.0043	V	N. Simmons	0.0011
BH Aur	57021.3313	31287	0.0077	V	T. Arranz	0.0014
BH Aur	57063.2880	31379	0.0042	V	T. Arranz	0.0009
BH Aur	57073.3237	31401	0.0059	V	T. Arranz	0.0008
BH Aur	57081.5323	31419	0.0049	V	K. Menzies	0.0011
BH Aur	57088.3743	31434	0.0055	V	T. Arranz	0.0008
BH Aur	57098.4077	31456	0.0050	V	T. Arranz	0.0008
BH Aur	57109.3525	31480	0.0036	V	T. Arranz	0.0005
BH Aur	57303.6476	31906	0.0044	V	T. Arranz	0.0007
BH Aur	57311.8584	31924	0.0056	V	R. Sabo	0.0012
BH Aur	57333.7509	31972	0.0058	V	N. Simmons	0.0011
BH Aur	57334.6571	31974	–0.0002	V	T. Arranz	0.0008
BH Aur	57335.5732	31976	0.0038	V	T. Arranz	0.0007
RS Boo	57090.8236	40601	–0.0055	V	G. Samolyk	0.0014
RS Boo	57093.8382	40609	–0.0096	V	K. Menzies	0.0007
RS Boo	57143.6490	40741	–0.0076	V	N. Simmons	0.0009
RS Boo	57204.4047	40902	–0.0034	V	T. Arranz	0.0007
RS Boo	57207.4251	40910	–0.0018	V	T. Arranz	0.0007
RS Boo	57210.4400	40918	–0.0056	V	T. Arranz	0.0008
RS Boo	57227.4185	40963	–0.0073	V	T. Arranz	0.0006
ST Boo	57090.9171	60919	0.1047	V	G. Samolyk	0.0015
ST Boo	57194.8291	61086	0.0942	V	R. Sabo	0.0014
ST Boo	57208.5146	61108	0.0893	V	T. Arranz	0.001
ST Boo	57213.4900	61116	0.0864	V	T. Arranz	0.0007
ST Boo	57223.4445	61132	0.0842	V	T. Arranz	0.0008
ST Boo	57244.6013	61166	0.0831	V	K. Menzies	0.0014
ST Boo	57246.4672	61169	0.0822	V	T. Arranz	0.0012
SW Boo	57096.8545	28286	0.4387	V	G. Samolyk	0.0015
SZ Boo	57039.9653	56233	0.0085	V	K. Menzies	0.0008
SZ Boo	57125.7074	56397	0.0081	V	K. Menzies	0.0008
TV Boo	57140.8047	104080	0.1115	V	G. Samolyk	0.0014
TV Boo	57211.4308	104306	0.0992	V	T. Arranz	0.0014
TW Boo	57116.8461	56786	–0.0850	V	G. Samolyk	0.0010
UU Boo	57050.0340	45884	0.2838	V	R. Sabo	0.0007
UU Boo	57208.5924	46231	0.2908	V	K. Menzies	0.0009
UY Boo	57139.7294	23513	0.9168	V	G. Samolyk	0.0011
UY Cam	57329.9001	81503	–0.0907	V	G. Samolyk	0.0022
RW Cnc	57043.9135	31958	0.2139	V	K. Menzies	0.0008
RW Cnc	57053.7670	31976	0.2178	V	G. Samolyk	0.0011
RW Cnc	57159.3749	32169	0.2163	V	T. Arranz	0.0006
RW Cnc	57350.8953	32519	0.2170	V	K. Menzies	0.0007
TT Cnc	57094.7530	30438	0.1132	V	R. Sabo	0.0015
VZ Cnc	57053.7121	96187	0.0179	V	G. Samolyk	0.0007
VZ Cnc	57348.8965	97842	0.0104	V	R. Sabo	0.0018
KV Cnc	57149.3802	8741	–0.0950	V	T. Arranz	0.0007
KV Cnc	57150.3919	8743	–0.0873	V	T. Arranz	0.0008
KV Cnc	57154.4195	8751	–0.0757	V	T. Arranz	0.0008
SS CVn	57087.8880	36499	–0.3550	V	G. Samolyk	0.0011
SS CVn	57114.6769	36555	–0.3633	V	K. Menzies	0.0010
RV Cap	57313.6517	52330	–0.0543	V	G. Samolyk	0.0009
RZ Cap	57256.7768	14643	0.0006	V	G. Samolyk	0.0011
VW Cap	57278.6022	101409	0.2099	V	G. Samolyk	0.0025
YZ Cap	57255.7569	49463	0.0469	V	G. Samolyk	0.0015
RR Cet	57276.8555	43570	0.0154	V	R. Sabo	0.0018
RR Cet	57335.4765	43676	0.0155	V	T. Arranz	0.0006
RV Cet	57320.7192	29206	0.2482	V	G. Samolyk	0.0014
RZ Cet	56619.6737	44482	–0.2052	V	N. Simmons	0.0012
RZ Cet	57278.8652	45773	–0.2122	V	R. Sabo	0.0023
UU Cet	57335.6180	26609	–0.1673	V	G. Samolyk	0.0018
XX Cyg	57205.6816	94541	0.0045	V	G. Samolyk	0.0006
XX Cyg	57205.8164	94542	0.0044	V	G. Samolyk	0.0006
XX Cyg	57223.6182	94674	0.0040	V	G. Samolyk	0.0006
XX Cyg	57223.7545	94675	0.0054	V	G. Samolyk	0.0007
XX Cyg	57223.8871	94676	0.0032	V	G. Samolyk	0.0009
XX Cyg	57233.7324	94749	0.0033	V	R. Sabo	0.0005
XX Cyg	57257.6044	94926	0.0042	V	N. Simmons	0.0008
XX Cyg	57271.7641	95031	0.0030	V	K. Menzies	0.0004
XX Cyg	57348.6377	95601	0.0035	V	R. Sabo	0.0006
XZ Cyg	53798.8304	20733	–1.7007	V	H. Smith	0.0014
XZ Cyg	53890.7413	20930	–1.7297	V	H. Smith	0.0011
XZ Cyg	54226.7001	21650	–1.7949	V	H. Smith	0.0009
XZ Cyg	54232.7615	21663	–1.8006	V	H. Smith	0.0013
XZ Cyg	54248.6236	21697	–1.8063	V	H. Smith	0.002
XZ Cyg	54260.7615	21723	–1.8026	V	H. Smith	0.0012
XZ Cyg	54266.8329	21736	–1.7983	V	H. Smith	0.0015
XZ Cyg	54300.4115	21808	–1.8221	V	H. Smith	0.0019
XZ Cyg	57201.7276	28026	–2.4466	V	G. Samolyk	0.0015
XZ Cyg	57210.5945	28045	–2.4470	V	T. Arranz	0.0006
XZ Cyg	57212.4630	28049	–2.4453	V	T. Arranz	0.0007
XZ Cyg	57218.5247	28062	–2.4507	V	T. Arranz	0.0005
XZ Cyg	57223.6572	28073	–2.4519	V	G. Samolyk	0.0006
XZ Cyg	57226.4542	28079	–2.4551	V	T. Arranz	0.0008
XZ Cyg	57227.8534	28082	–2.4560	V	G. Samolyk	0.0009
XZ Cyg	57231.5857	28090	–2.4573	V	T. Arranz	0.0005
XZ Cyg	57232.5192	28092	–2.4572	V	T. Arranz	0.0006
XZ Cyg	57235.7835	28099	–2.4598	V	G. Samolyk	0.0009
XZ Cyg	57236.7179	28101	–2.4588	V	K. Menzies	0.0013
XZ Cyg	57245.5791	28120	–2.4649	V	T. Arranz	0.0005
XZ Cyg	57250.7162	28131	–2.4615	V	G. Samolyk	0.0011
XZ Cyg	57256.7827	28144	–2.4621	V	G. Samolyk	0.0012
XZ Cyg	57258.6521	28148	–2.4595	V	G. Samolyk	0.0008
XZ Cyg	57261.4535	28154	–2.4583	V	T. Arranz	0.0005
XZ Cyg	57276.3848	28186	–2.4614	V	T. Arranz	0.0005
XZ Cyg	57279.6457	28193	–2.4674	V	H. Smith	0.0006
XZ Cyg	57280.5783	28195	–2.4682	V	H. Smith	0.0006
XZ Cyg	57289.4390	28214	–2.4748	V	T. Arranz	0.0006
XZ Cyg	57290.3716	28216	–2.4756	V	T. Arranz	0.0006
XZ Cyg	57304.3747	28246	–2.4735	V	T. Arranz	0.0006
XZ Cyg	57311.3809	28261	–2.4678	V	T. Arranz	0.0005
XZ Cyg	57321.6419	28283	–2.4742	V	H. Smith	0.0007
DM Cyg	57209.5699	34838	0.0812	V	T. Arranz	0.0007
DM Cyg	57214.6090	34850	0.0820	V	T. Arranz	0.0006
DM Cyg	57225.5278	34876	0.0844	V	T. Arranz	0.0007
DM Cyg	57227.6242	34881	0.0815	V	T. Arranz	0.0006
DM Cyg	57228.4655	34883	0.0831	V	T. Arranz	0.0007
DM Cyg	57230.5628	34888	0.0811	V	T. Arranz	0.0006
DM Cyg	57237.7006	34905	0.0813	V	R. Sabo	0.0012
DM Cyg	57240.6384	34912	0.0801	V	T. Arranz	0.0007
DM Cyg	57241.4780	34914	0.0800	V	T. Arranz	0.0008
DM Cyg	57243.5797	34919	0.0824	V	T. Arranz	0.0008
DM Cyg	57253.6521	34943	0.0781	V	T. Arranz	0.0006
DM Cyg	57262.4737	34964	0.0827	V	T. Arranz	0.0009
DM Cyg	57267.5116	34976	0.0822	V	T. Arranz	0.0007
RW Dra	57093.8790	39999	0.2509	V	K. Menzies	0.0015
RW Dra	57211.6904	40265	0.2464	V	G. Samolyk	0.0015
RW Dra	57217.4575	40278	0.2556	V	T. Arranz	0.0007
RW Dra	57225.4238	40296	0.2494	V	T. Arranz	0.0005
RW Dra	57240.4432	40330	0.2096	V	T. Arranz	0.001
RW Dra	57260.4147	40375	0.2498	V	T. Arranz	0.0006
XZ Dra	57195.6846	32041	–0.1298	V	G. Samolyk	0.0012

Table continued on next page

Table 1. Recent times of maxima of stars in the AAVSO Short Period Pulsator program, cont.

Star	JD (max) Hel. 2400000 +	Cycle	O–C	F	Observer	Error
SV Eri	57333.8932	30514	1.0009	V	G. Samolyk	0.0012
BB Eri	57327.8652	31178	0.2944	V	G. Samolyk	0.0012
RR Gem	57050.4368	39500	–0.5369	V	T. Arranz	0.0008
RR Gem	57064.3378	39535	–0.5418	V	T. Arranz	0.0006
RR Gem	57087.3830	39593	–0.5406	V	T. Arranz	0.0007
RR Gem	57089.3723	39598	–0.5378	V	T. Arranz	0.0006
RR Gem	57091.3561	39603	–0.5406	V	T. Arranz	0.0006
RR Gem	57095.3305	39613	–0.5393	V	T. Arranz	0.0005
RR Gem	57112.4120	39656	–0.5422	V	T. Arranz	0.0006
RR Gem	57114.3959	39661	–0.5448	V	T. Arranz	0.0004
RR Gem	57116.3838	39666	–0.5435	V	T. Arranz	0.0004
RR Gem	57118.3738	39671	–0.5400	V	T. Arranz	0.0006
RR Gem	57120.3579	39676	–0.5425	V	T. Arranz	0.0006
GQ Gem	57045.6439	46829	–0.2056	V	K. Menzies	0.0019
TW Her	57130.8053	89053	–0.0168	V	K. Menzies	0.0006
TW Her	57202.7356	89233	–0.0145	V	R. Sabo	0.0009
TW Her	57312.6225	89508	–0.0176	V	R. Sabo	0.0008
VX Her	57195.7508	77838	–0.0415	V	G. Samolyk	0.001
VX Her	57211.6878	77873	–0.0425	V	G. Samolyk	0.0008
VX Her	57239.4646	77934	–0.0435	V	T. Arranz	0.0007
VZ Her	57201.6964	46358	0.0781	V	G. Samolyk	0.0007
VZ Her	57272.5885	46519	0.0774	V	K. Menzies	0.0007
AR Her	57096.8378	33282	–0.9811	V	G. Samolyk	0.0015
AR Her	57184.7471	33469	–0.9670	V	G. Samolyk	0.0011
AR Her	57193.6641	33488	–0.9806	V	G. Samolyk	0.0015
AR Her	57201.6891	33505	–0.9460	V	G. Samolyk	0.0011
AR Her	57203.5673	33509	–0.9480	V	T. Arranz	0.0009
AR Her	57204.5093	33511	–0.9460	V	T. Arranz	0.0009
AR Her	57206.3878	33515	–0.9476	V	T. Arranz	0.0007
AR Her	57229.4190	33564	–0.9478	V	T. Arranz	0.0011
AR Her	57237.4091	33581	–0.9482	V	T. Arranz	0.0009
DL Her	57129.9107	31982	0.0403	V	R. Sabo	0.0015
DL Her	57214.5242	32125	0.0510	V	T. Arranz	0.0009
DL Her	57220.4483	32135	0.0588	V	T. Arranz	0.0009
DL Her	57225.7685	32144	0.0544	V	R. Sabo	0.0012
DL Her	57236.4040	32162	0.0406	V	T. Arranz	0.0008
DL Her	57252.3911	32189	0.0537	V	T. Arranz	0.0012
DY Her	56451.7530	154828	–0.0286	V	N. Simmons	0.0007
DY Her	57094.8793	159155	–0.0302	V	K. Menzies	0.0011
DY Her	57170.6811	159665	–0.0304	V	N. Simmons	0.0007
DY Her	57202.4865	159879	–0.0321	V	T. Arranz	0.0004
DY Her	57229.6869	160062	–0.0312	V	G. Samolyk	0.0005
LS Her	57050.0299	125841	0.0099	V	R. Sabo	0.0019
SZ Hya	57089.7044	30546	–0.2474	V	G. Samolyk	0.0009
UU Hya	57096.6364	33630	–0.0009	V	G. Samolyk	0.0016
DG Hya	57081.8064	6241	0.0127	V	G. Samolyk	0.0017
DH Hya	57095.6902	53005	0.0966	V	G. Samolyk	0.0011
RR Leo	57095.8028	30505	0.1432	V	R. Sabo	0.0009
TV Leo	57116.7444	29836	0.1242	V	G. Samolyk	0.0013
TV Leo	57383.8704	30233	0.1277	V	R. Sabo	0.0021
WW Leo	57044.8399	36763	0.0452	V	R. Sabo	0.0017
WW Leo	57096.6866	36849	0.0472	V	N. Simmons	0.0020
AA Leo	57044.9719	29146	–0.1021	V	R. Sabo	0.0017
VY LMi	57045.9326	12465	0.0157	V	K. Menzies	0.0017
U Lep	57355.7773	27522	0.0433	V	G. Samolyk	0.0010
SZ Lyn	57036.5928	156902	0.0245	V	K. Menzies	0.0008
SZ Lyn	57084.4463	157299	0.0257	V	T. Arranz	0.0005
SZ Lyn	57093.6076	157375	0.0263	V	N. Simmons	0.0008
SZ Lyn	57314.9153	159211	0.0319	V	G. Samolyk	0.0005
SZ Lyn	57327.8136	159318	0.0330	V	G. Samolyk	0.0006
SZ Lyn	57327.9344	159319	0.0332	V	G. Samolyk	0.0008
SZ Lyn	57355.6584	159549	0.0342	V	G. Samolyk	0.0008
SZ Lyn	57355.7787	159550	0.0340	V	G. Samolyk	0.0005
SZ Lyn	57355.8989	159551	0.0336	V	G. Samolyk	0.0006
RR Lyr	57213.8016	25210	–0.3539	V	G. Samolyk	0.0010
RZ Lyr	57206.7296	31342	–0.0526	V	G. Samolyk	0.0012
RZ Lyr	57316.6549	31557	–0.0444	V	R. Sabo	0.0015
ST Oph	57197.8713	63886	–0.0246	V	G. Samolyk	0.0009
AV Peg	57224.8378	34414	0.1669	V	R. Sabo	0.0009
AV Peg	57263.4847	34513	0.1667	V	T. Arranz	0.0006
AV Peg	57278.7097	34552	0.1671	V	R. Sabo	0.0009
AV Peg	57283.3942	34564	0.1671	V	T. Arranz	0.0005
AV Peg	57294.7165	34593	0.1685	V	R. Sabo	0.0010
AV Peg	57310.3308	34633	0.1678	V	T. Arranz	0.0005
AV Peg	57350.5415	34736	0.1699	V	K. Menzies	0.0010
BH Peg	57286.6817	27959	–0.1216	V	R. Sabo	0.0015
BH Peg	57309.7505	27995	–0.1285	V	R. Sabo	0.0014
BH Peg	57311.6848	27998	–0.1172	V	R. Sabo	0.0012
DY Peg	57305.5786	175568	–0.0160	V	N. Simmons	0.0004
DY Peg	57305.6516	175569	–0.0159	V	N. Simmons	0.0005
DY Peg	57312.5796	175664	–0.0159	V	N. Simmons	0.0004
DY Peg	57312.6522	175665	–0.0162	V	N. Simmons	0.0004
DY Peg	57312.7259	175666	–0.0154	V	N. Simmons	0.0007
DF Ser	57206.6925	62816	0.1002	V	G. Samolyk	0.0010
RV UMa	57053.7658	25591	0.1313	V	G. Samolyk	0.0017
RV UMa	57080.9148	25649	0.1329	V	G. Samolyk	0.0012
RV UMa	57169.3803	25838	0.1350	V	T. Arranz	0.0007
RV UMa	57176.3991	25853	0.1329	V	T. Arranz	0.0007
RV UMa	57190.4408	25883	0.1328	V	T. Arranz	0.0007
RV UMa	57191.3797	25885	0.1356	V	T. Arranz	0.0006
RV UMa	57198.3963	25900	0.1313	V	T. Arranz	0.0008

Recent Minima of 193 Eclipsing Binary Stars

Gerard Samolyk
P.O. Box 20677, Greenfield, WI 53220; gsamolyk@wi.rr.com

Received February 18, 2016; accepted February 18, 2016

Abstract This paper continues the publication of times of minima for eclipsing binary stars from observations reported to the AAVSO Eclipsing Binary section. Times of minima from CCD observations received by the author from November 2015 through January 2016 are presented.

1. Recent observations

The accompanying list contains times of minima calculated from recent CCD observations made by participants in the AAVSO's eclipsing binary program. This list will be web-archived and made available through the AAVSO ftp site at ftp://ftp.aavso.org/public/datasets/gsam2j441.txt. This list, along with the eclipsing binary data from earlier AAVSO publications, is also included in the Lichtenknecker database (Kreiner 2011) administrated by the Bundesdeutsche Arbeitsgemeinschaft für Veranderliche Sterne e. V. (BAV) at: http://www.bav-astro.de/LkDB/index.php?lang=en. These observations were reduced by the observers or the writer using the method of Kwee and Van Woerden (1956). The standard error is included when available. Column F indicates the filter used. A "C" indicates a clear filter.

The linear elements in the *General Catalogue of Variable Stars* (GCVS; Kholopov *et al.* 1985) were used to compute the O–C values for most stars. For a few exceptions where the GCVS elements are missing or are in significant error, light elements from another source are used: CD Cam (Baldwin and Samolyk 2007), AC CMi (Samolyk 2008), CW Cas (Samolyk 1992), EF Ori (Baldwin and Samolyk 2005), GU Ori (Samolyk 1985).

The light elements used for QX And, EK Aqr, TY CMi, BB CMi, BH CMi, CZ CMi, VY Cet, XY Cet, YY CrB, LS Del, BC Her, EF Her, V338 Her, V899 Her, V1033 Her, V1034 Her, V1054 Her, WZ Leo, V423 Oph, V913 Oph, ZZ Peg, V351 Peg, V404 Peg, CP Psc, DZ Psc, V1121 Tau, V1123 Tau, V1223 Tau, V1234 Tau, and MS Vir are from Kreiner (2004).

The light elements used for DD Aqr, GK Aqr, MU Aqr, OS Aqr, V1542 Aql, BM Ari, BN Ari, V410 Aur, V641 Aur, XY Boo, DN Boo, GH Boo, GM Boo, GP Boo, IK Boo, CX CMi, GZ Gem, V1057 Her, V1065 Her, V1092 Her, V474 Hya, XX Leo, CE Leo, GU Leo, GV Leo, HI Leo, DZ Ori, FF Ori, KV Peg, VZ Psc, V1332 Tau, V1370 Tau, BU Tri, BV Tri, HN UMa, QT UMa, GR Vir, IR Vir, and NN Vir are from Paschke (2014).

The light elements used for V562 Aur, V388 Gem, EU Hya, V409 Hya, V723 Per, V725 Per, V737 Per, V1047 Per, and V391 Vir are from the AAVSO VSX site (Watson *et al.* 2014). O–C values listed in this paper can be directly compared with values published in the AAVSO EB monographs.

References

Baldwin, M. E., and Samolyk, G. 2005, *Observed Minima Timings of Eclipsing Binaries No. 10*, AAVSO, Cambridge, MA.

Baldwin, M. E., and Samolyk, G. 2007, *Observed Minima Timings of Eclipsing Binaries No. 12*, AAVSO, Cambridge, MA.

Kholopov, P. N., *et al.* 1985, *General Catalogue of Variable Stars*, 4th ed., Moscow.

Kreiner, J. M. 2004, "Up-to-date linear elements of eclipsing binaries," *Acta Astron.*, **54**, 207 (http://www.as.up.krakow.pl/ephem/).

Kreiner, J. M. 2011, Lichtenknecker-Database of the BAV (http://www.bavdata-astro.de/~tl/cgi-bin/varstars_cgi).

Kwee, K. K., and van Woerden, H. 1956, *Bull. Astron. Inst. Netherlands*, **12**, 327.

Paschke, A. 2014, "O–C Gateway" (http://var.astro.cz/ocgate/).

Samolyk, G. 1985, *J. Amer. Assoc. Var. Star Obs.*, **14**, 12.

Samolyk, G. 1992, *J. Amer. Assoc. Var. Star Obs.*, **21**, 34.

Samolyk, G. 2008, *J. Amer. Assoc. Var. Star Obs.*, **36**, 171.

Watson, C., Henden, A. A., and Price, C. A. 2014, AAVSO International Variable Star Index VSX (Watson+, 2006–2016; http://www.aavso.org/vsx).

Table 1. Recent times of minima of stars in the AAVSO eclipsing binary program.

Star	*JD (min) Hel. 2400000 +*	*Cycle*	*O–C (day)*	*F*	*Observer*	*Error (day)*	*Star*	*JD (min) Hel. 2400000 +*	*Cycle*	*O–C (day)*	*F*	*Observer*	*Error (day)*
RT And	57335.5555	25748	–0.0106	V	G. Samolyk	0.0001	AB And	57358.2724	64023	–0.0380	V	L. Corp	0.0001
TW And	57333.7179	4442	–0.0546	V	G. Samolyk	0.0001	AD And	57388.5585	18643.5	–0.0345	V	G. Samolyk	0.0002
WZ And	54117.6513	19040	0.0406	V	V. Petriew	0.0002	BX And	57344.6137	34118	–0.0792	V	K. Menzies	0.0001
XZ And	57336.5492	24578	0.1790	V	G. Samolyk	0.0001	BX And	57388.5403	34190	–0.0809	V	G. Samolyk	0.0001
XZ And	57355.5510	24592	0.1789	V	G. Samolyk	0.0001	DS And	57347.6409	20984.5	0.0039	V	K. Menzies	0.0001
AB And	57328.5677	63933.5	–0.0384	V	G. Samolyk	0.0002	DS And	57390.5873	21027	0.0033	V	N. Simmons	0.0001
AB And	57334.5425	63951.5	–0.0376	V	N. Simmons	0.0001	QX And	57390.6496	11865.5	–0.0013	V	N. Simmons	0.0002

Table continued on following pages

Table 1. Recent times of minima of stars in the AAVSO eclipsing binary program, cont.

Star	JD (min) Hel. 2400000 +	Cycle	O–C (day)	F	Observer	Error (day)	Star	JD (min) Hel. 2400000 +	Cycle	O–C (day)	F	Observer	Error (day)
RY Aqr	57347.6074	8402	–0.1294	V	S. Cook	0.0004	V380 Cas	57333.6873	23347	–0.0704	V	G. Samolyk	0.0002
CX Aqr	57319.7305	37530	0.0134	C	G. Frey	0.0002	SS Cet	57392.6456	5024	0.0612	V	G. Samolyk	0.0001
DD Aqr	56953.6766	12659	0.0046	C	G. Frey	0.0001	TT Cet	57342.6575	51027	–0.0748	V	E. Primucci	0.0001
DD Aqr	57299.7597	13139	0.0028	C	G. Frey	0.0001	TT Cet	57358.6946	51060	–0.0743	C	G. Frey	0.0001
EK Aqr	52581.5925	266	–0.0120	V	G. Samolyk	0.0006	TW Cet	57333.6688	47215.5	–0.0301	V	G. Samolyk	0.0002
EK Aqr	55115.7963	8533.5	0.0005	V	G. Samolyk	0.0009	TW Cet	57357.5901	47291	–0.0311	V	E. Primucci	0.0001
EK Aqr	57335.6484	15775.5	0.0021	C	G. Frey	0.0002	TX Cet	57355.6740	19266	0.0114	V	G. Samolyk	0.0001
EX Aqr	56912.7158	4961	0.0107	C	G. Frey	0.0001	VY Cet	57327.7764	14165	0.0009	C	G. Frey	0.0001
EX Aqr	57282.7036	5377	0.0147	C	G. Frey	0.0002	XY Cet	56978.7001	1610	0.0014	C	G. Frey	0.0001
GK Aqr	56958.7347	31502	0.0124	C	G. Frey	0.0001	XY Cet	57042.6625	1633	0.0074	C	G. Frey	0.0002
GK Aqr	57289.7561	32513	0.0172	C	G. Frey	0.0006	YY CrB	54198.8140	4511	0.0016	V	V. Petriew	0.0002
MU Aqr	56898.7169	19966	0.0094	C	G. Frey	0.0001	YY Del	57263.7332	18036	0.0103	C	G. Frey	0.0001
MU Aqr	57238.7218	21215	0.0122	C	G. Frey	0.0001	DM Del	57256.7316	15101	–0.1090	C	G. Frey	0.0002
OS Aqr	56944.7084	8371	–0.0098	C	G. Frey	0.0001	LS Del	57329.6247	13273	0.0002	C	G. Frey	0.0003
KP Aql	57336.5799	5030.5	–0.0174	V	S. Cook	0.0004	YY Eri	57329.8483	48984	0.1549	V	G. Samolyk	0.0001
V417 Aql	57297.7116	38584.5	0.0729	C	G. Frey	0.0001	WW Gem	54124.6865	22734	0.0342	V	V. Petriew	0.0014
V1542 Aql	57230.7352	12259	0.0081	C	G. Frey	0.0001	AL Gem	57331.9031	22286	0.0866	V	K. Menzies	0.0002
V1542 Aql	57283.7647	12386	0.0104	C	G. Frey	0.0002	GZ Gem	54106.6961	15205	0.0003	V	V. Petriew	0.0002
RX Ari	57336.5468	18393	0.0661	V	G. Samolyk	0.0003	HR Gem	54143.6805	22287	0.0141	V	V. Petriew	0.0003
RX Ari	57340.6640	18397	0.0648	C	G. Frey	0.0002	V388 Gem	57044.6467	9070	0.0069	C	G. Frey	0.0007
SS Ari	57335.7195	45093.5	–0.3479	V	G. Samolyk	0.0001	AK Her	57170.7405	35548	0.0161	C	G. Frey	0.0002
SS Ari	57336.7311	45096	–0.3513	V	S. Cook	0.0003	BC Her	56868.7447	1415	–0.0054	C	G. Frey	0.0001
BM Ari	57334.6827	12106	–0.0007	C	G. Frey	0.0001	BC Her	56902.7065	1426	–0.0034	C	G. Frey	0.0001
BN Ari	57395.6270	19607.5	–0.0197	V	K. Menzies	0.0001	BC Her	57291.7084	1552	0.0039	C	G. Frey	0.0002
SX Aur	57335.8103	14192	0.0166	V	K. Menzies	0.0001	CC Her	57164.7295	10090	0.2690	C	G. Frey	0.0001
WW Aur	57392.7771	9682	0.0017	V	G. Samolyk	0.0001	EF Her	56834.7656	916	0.0159	C	G. Frey	0.0004
AP Aur	57331.8376	26148.5	1.5607	V	K. Menzies	0.0001	V338 Her	57171.6912	3577	0.0025	C	G. Frey	0.0002
AR Aur	57388.5789	4592	–0.1237	V	G. Samolyk	0.0001	V899 Her	57226.7714	11222	–0.0004	C	G. Frey	0.0005
CL Aur	57330.8473	19579	0.1728	V	G. Samolyk	0.0001	V1033 Her	57161.7305	15640	–0.0042	C	G. Frey	0.0001
EP Aur	54106.8641	47034	0.0118	V	V. Petriew	0.0001	V1034 Her	56869.7549	5359	–0.0016	C	G. Frey	0.0002
EP Aur	57327.8611	52484	0.0152	V	G. Samolyk	0.0001	V1034 Her	57231.7448	5803	–0.0011	C	G. Frey	0.0001
IM Aur	54159.6236	10939	–0.0939	V	V. Petriew	0.0004	V1054 Her	56809.7603	6648	0.0045	C	G. Frey	0.0002
V410 Aur	54389.8633	16076.5	–0.0430	V	V. Petriew	0.0002	V1054 Her	56833.7438	6685	0.0044	C	G. Frey	0.0002
V562 Aur	57407.6608	11155	0.0219	V	K. Menzies	0.0002	V1054 Her	57218.7753	7279	0.0011	C	G. Frey	0.0005
V641 Aur	57391.7913	12116	–0.0015	V	K. Menzies	0.0001	V1057 Her	56860.7730	5898	–0.0028	C	G. Frey	0.0001
XY Boo	57153.7457	46415	0.0056	C	G. Frey	0.0001	V1057 Her	57195.7204	6253	–0.0056	C	G. Frey	0.0002
AC Boo	54196.8134	80641	0.1207	V	V. Petriew	0.0001	V1065 Her	57189.7492	14813	–0.0050	C	G. Frey	0.0001
DN Boo	57154.6796	5038	–0.0016	C	G. Frey	0.0002	V1092 Her	57224.7169	12497	–0.0044	C	G. Frey	0.0002
GH Boo	57173.6866	8967	–0.0029	C	G. Frey	0.0008	EU Hya	57089.6768	29508	–0.0347	C	G. Frey	0.0001
GM Boo	57186.7187	14359	0.0110	C	G. Frey	0.0002	V409 Hya	57145.6957	8451	0.0514	C	G. Frey	0.0004
GP Boo	57168.7335	7218	–0.0088	C	G. Frey	0.0002	V474 Hya	57062.7020	9233	–0.0081	C	G. Frey	0.0001
IK Boo	57190.6827	12563	–0.0148	C	G. Frey	0.0001	SW Lac	57328.5928	37582	–0.0878	V	G. Samolyk	0.0001
Y Cam	57361.6819	4356	0.4544	V	N. Simmons	0.0002	DG Lac	57335.7433	5813	–0.2258	V	G. Samolyk	0.0002
CD Cam	57329.8383	5976.5	–0.0075	V	G. Samolyk	0.0003	UU Leo	57333.8940	7106	0.1992	V	N. Simmons	0.0001
CD Cam	57398.6157	6066.5	–0.0067	V	G. Samolyk	0.0003	UV Leo	57411.8484	31614	0.0418	V	G. Samolyk	0.0001
VZ CVn	54211.6954	18198	–0.0018	V	V. Petriew	0.0002	VZ Leo	57087.6706	23785	–0.0596	C	G. Frey	0.0001
TU CMa	57406.7178	26981	–0.0096	V	G. Samolyk	0.0002	VZ Leo	57392.8478	24065	–0.0561	V	G. Samolyk	0.0001
TY CMi	57133.6681	3566	–0.0096	C	G. Frey	0.0002	WZ Leo	57106.7141	3271	0.0004	C	G. Frey	0.0001
YY CMi	57107.6789	26585	0.0182	C	G. Frey	0.0001	WZ Leo	57355.9607	3448	–0.0010	V	G. Samolyk	0.0002
AC CMi	57105.7403	5912	0.0048	C	G. Frey	0.0001	XX Leo	57097.7259	8657	–0.0122	C	G. Frey	0.0001
AK CMi	57375.8475	25224	–0.0230	V	G. Samolyk	0.0002	AM Leo	54170.7483	31923	0.0089	V	V. Petriew	0.0001
BB CMi	57092.6674	5792	–0.0118	C	G. Frey	0.0002	AM Leo	57390.8634	40726	0.0095	V	R. Sabo	0.0003
BH CMi	57071.6610	8174	–0.0013	C	G. Frey	0.0002	BL Leo	54121.0377	33598	–0.0226	V	V. Petriew	0.0001
CX CMi	57096.7303	4586	0.0154	C	G. Frey	0.0002	CE Leo	57152.7215	31220	–0.0047	C	G. Frey	0.0001
CZ CMi	57103.7242	10796.5	–0.0062	C	G. Frey	0.0001	GU Leo	57073.7071	13241	0.0055	C	G. Frey	0.0002
TV Cas	57348.5968	7032	–0.0289	V	S. Cook	0.0004	GV Leo	57102.6941	16302	–0.0207	C	G. Frey	0.0001
TW Cas	57328.5956	10726	0.0051	V	G. Samolyk	0.0001	GV Leo	57121.7674	16373.5	–0.0186	C	G. Frey	0.0001
ZZ Cas	57330.6394	19214	0.0166	V	G. Samolyk	0.0002	HI Leo	57110.7238	14025	0.0081	C	G. Frey	0.0001
AB Cas	57330.5747	10693	0.1305	V	G. Samolyk	0.0001	T LMi	54130.7820	2892	–0.0934	V	V. Petriew	0.0001
AB Cas	57334.6747	10696	0.1298	V	N. Simmons	0.0001	T LMi	57334.8514	3953	–0.1220	V	G. Samolyk	0.0001
CW Cas	54347.8062	39878	–0.0414	V	V. Petriew	0.0001	Z Lep	57335.9367	30101	–0.1895	V	G. Samolyk	0.0002
CW Cas	54347.9650	39878.5	–0.0420	V	V. Petriew	0.0001	RR Lep	57356.6156	29472	–0.0404	V	E. Primucci	0.0002
CW Cas	57335.6701	49248.5	–0.0935	V	K. Menzies	0.0001	RY Lyn	54124.7867	7831	–0.0473	V	V. Petriew	0.0001
OX Cas	57334.6350	6453.5	0.0264	V	G. Samolyk	0.0003	UU Lyn	54115.8573	20155	–0.0054	V	V. Petriew	0.0001
V364 Cas	57329.6155	14903	–0.0249	V	G. Samolyk	0.0002	UU Lyn	54117.7309	20159	–0.0056	V	V. Petriew	0.0002
V375 Cas	57329.6562	15398	0.2296	V	G. Samolyk	0.0001	β Lyr	57233.90	637	1.96	B	G. Samolyk	0.02

Table continued on next page

Table 1. Recent times of minima of stars in the AAVSO eclipsing binary program, cont.

Star	*JD (min) Hel. 2400000 +*	*Cycle*	*O–C (day)*	*F*	*Observer*	*Error (day)*
β Lyr	57233.90	637	1.96	V	G. Samolyk	0.03
β Lyr	57233.98	637	2.03	R	G. Samolyk	0.02
β Lyr	57240.40	637.5	1.99	B	G. Samolyk	0.03
β Lyr	57240.44	637.5	2.02	V	G. Samolyk	0.02
β Lyr	57240.44	637.5	2.03	R	G. Samolyk	0.02
EP Mon	57333.9332	1292	0.0269	V	G. Samolyk	0.0001
V423 Oph	56838.7850	3604	–0.0235	C	G. Frey	0.0001
V456 Oph	56829.7003	14697	0.0221	C	G. Frey	0.0004
V456 Oph	56893.7090	14760	0.0229	C	G. Frey	0.0001
V456 Oph	57214.7675	15076	0.0255	C	G. Frey	0.0001
V456 Oph	57277.7603	15138	0.0264	C	G. Frey	0.0001
V501 Oph	57268.6719	27230	–0.0125	C	G. Frey	0.0007
V506 Oph	57237.7109	13466	0.0327	C	G. Frey	0.0001
V913 Oph	56830.7831	2258	0.0428	C	G. Frey	0.0004
V913 Oph	57225.7731	2464	0.0468	C	G. Frey	0.0001
DZ Ori	57065.7959	17330	0.0014	C	G. Frey	0.0002
EF Ori	57375.7451	3103	0.0078	V	G. Samolyk	0.0003
ET Ori	57334.8369	32232	–0.0024	V	N. Simmons	0.0001
FF Ori	57067.6643	13726	0.0037	C	G. Frey	0.0001
FH Ori	57061.6589	14486	–0.4319	C	G. Frey	0.0001
FH Ori	57334.8501	14613	–0.4380	V	G. Samolyk	0.0002
FL Ori	57362.8770	7747	0.0407	V	R. Sabo	0.0002
FR Ori	57088.6805	33093	0.0358	C	G. Frey	0.0001
FR Ori	57390.7222	33435	0.0360	V	G. Samolyk	0.0002
FZ Ori	57344.7740	33302	–0.0381	V	K. Menzies	0.0001
GU Ori	57375.7239	30394	–0.0574	V	G. Samolyk	0.0003
V648 Ori	57059.6628	19098	0.0670	C	G. Frey	0.0001
U Peg	57328.5566	55544.5	–0.1593	V	N. Simmons	0.0001
U Peg	57335.3025	55562.5	–0.1594	V	L. Corp	0.0002
TY Peg	57294.6991	5447	–0.4073	C	G. Frey	0.0001
TY Peg	57390.5530	5478	–0.4122	V	G. Samolyk	0.0001
ZZ Peg	56913.7217	6613	–0.0017	C	G. Frey	0.0002
ZZ Peg	57272.7652	7151	0.0020	C	G. Frey	0.0001
AT Peg	57332.7567	10569	0.0190	C	G. Frey	0.0001
BB Peg	57330.5856	37527.5	–0.0179	V	N. Simmons	0.0001
BG Peg	57330.5784	6043	–2.2266	V	G. Samolyk	0.0003
BN Peg	57239.7563	32726	–0.0001	C	G. Frey	0.0001
BO Peg	56923.7015	19488	–0.0433	C	G. Frey	0.0001
BO Peg	57255.7059	20060	–0.0449	C	G. Frey	0.0001
BO Peg	57309.6846	20153	–0.0463	C	G. Frey	0.0001
BX Peg	57351.4801	46916	–0.1193	V	K. Menzies	0.0001
DI Peg	56955.7049	16520	0.0034	C	G. Frey	0.0001
DI Peg	57308.7680	17016	0.0053	C	G. Frey	0.0001
DI Peg	57390.6267	17131	0.0051	V	R. Sabo	0.0001
EE Peg	56967.7273	4339	0.0142	C	G. Frey	0.0003
EE Peg	57306.7620	4468	0.0093	C	G. Frey	0.0002
GP Peg	57351.5802	16516	–0.0530	V	K. Menzies	0.0001
KV Peg	57326.6913	20892	–0.0154	C	G. Frey	0.0002
KV Peg	57337.6779	20916	–0.0156	C	G. Frey	0.0002
V351 Peg	56924.7168	14200	0.0156	C	G. Frey	0.0002
V351 Peg	57290.7793	14817	0.0207	C	G. Frey	0.0002
V404 Peg	57284.6954	11414	–0.0318	C	G. Frey	0.0001
V404 Peg	57336.6771	11538	–0.0288	C	G. Frey	0.0001
RT Per	57326.6982	28197	0.0991	V	S. Cook	0.0004
RT Per	57355.5790	28231	0.1003	V	G. Samolyk	0.0001
XZ Per	57355.8055	12025	–0.0722	V	G. Samolyk	0.0001
DZ Per	54341.8010	34442	0.0162	V	V. Petriew	0.0004
IT Per	54103.5381	16118	0.0004	V	V. Petriew	0.0004
V432 Per	57335.8584	66750.5	0.0619	V	G. Samolyk	0.0002
V723 Per	57399.5528	7467.5	0.1317	V	K. Menzies	0.0002
V725 Per	57394.6364	667	0.0919	V	K. Menzies	0.0002
V737 Per	57393.5073	15978.5	0.0559	V	K. Menzies	0.0001
V737 Per	57393.6912	15979	0.0565	V	K. Menzies	0.0001
V1047 Per	57328.9085	1472.5	–0.0199	V	S. Cook	0.0009
V1047 Per	57329.8595	1473	–0.0240	V	S. Cook	0.0007
VZ Psc	57304.6685	51567.5	0.0037	C	G. Frey	0.0002
VZ Psc	57328.3122	51658	0.0035	R	L. Corp	0.0004
CP Psc	57305.7071	7025	0.0016	C	G. Frey	0.0002
DZ Psc	57295.7185	13098	0.0097	C	G. Frey	0.0001
RW Tau	57390.5741	4228	–0.2668	V	G. Samolyk	0.0001
RZ Tau	57328.9136	47278	0.0781	V	K. Menzies	0.0002
RZ Tau	57359.6749	47352	0.0795	C	G. Frey	0.0001
TY Tau	57041.6624	33275	0.2631	C	G. Frey	0.0003
TY Tau	57375.6471	33585	0.2676	V	G. Samolyk	0.0001
WY Tau	57330.9012	28767	0.0623	V	K. Menzies	0.0001
AC Tau	57330.8456	5723	0.1292	V	G. Samolyk	0.0001
AH Tau	57343.7202	78999.5	0.0218	C	G. Frey	0.0001
CD Tau	54133.6167	3643	0.0051	V	V. Petriew	0.0001
EQ Tau	54388.8184	41528	–0.0263	V	V. Petriew	0.0001
EQ Tau	54388.9893	41528.5	–0.0261	V	V. Petriew	0.0001
EQ Tau	57338.7461	50170	–0.0322	C	G. Frey	0.0001
EQ Tau	57344.7189	50187.5	–0.0329	V	K. Menzies	0.0001
EQ Tau	57375.6100	50278	–0.0339	V	G. Samolyk	0.0001
V1121 Tau	57365.7217	10756	–0.0094	C	G. Frey	0.0001
V1123 Tau	54420.8149	4802.5	0.0003	V	V. Petriew	0.0003
V1123 Tau	57344.6378	12113	0.0063	C	G. Frey	0.0002
V1223 Tau	57369.6776	11422	–0.0018	C	G. Frey	0.0001
V1234 Tau	57037.6486	12191	–0.0189	C	G. Frey	0.0004
V1332 Tau	57375.6294	13571	0.0139	C	G. Frey	0.0003
V1370 Tau	57391.6485	20045	–0.0007	V	K. Menzies	0.0001
V1370 Tau	57415.5849	20126	–0.0012	V	K. Menzies	0.0001
RV Tri	54365.8193	11056	–0.0253	V	V. Petriew	0.0001
BU Tri	54365.7706	1239.5	0.0015	V	V. Petriew	0.0003
BU Tri	54365.9219	1240	0.0050	V	V. Petriew	0.0003
BV Tri	54365.9189	739.5	0.0054	V	V. Petriew	0.0005
W UMa	57335.8589	34679	–0.0941	V	G. Samolyk	0.0001
TY UMa	54191.6681	41346.5	0.2414	V	V. Petriew	0.0001
UX UMa	54116.0531	84828	0.0014	V	V. Petriew	0.0001
UX UMa	54175.6448	85131	0.0016	V	V. Petriew	0.0001
UX UMa	54197.6719	85243	0.0016	V	V. Petriew	0.0001
VV UMa	54105.7766	12061	–0.0501	V	V. Petriew	0.0001
XY UMa	54134.8980	39496	0.0266	V	V. Petriew	0.0001
XY UMa	54196.6906	39625	0.0290	V	V. Petriew	0.0001
XZ UMa	54104.8624	6493	–0.0874	V	V. Petriew	0.0001
AF UMa	57390.7187	5819	0.6062	V	G. Samolyk	0.0005
BM UMa	54145.8066	61932	0.0082	V	V. Petriew	0.0001
HN UMa	54186.6435	14862	–0.0163	V	V. Petriew	0.0015
HN UMa	54199.6483	14896	–0.0202	V	V. Petriew	0.0015
QT UMa	57415.7038	12357	0.0036	V	K. Menzies	0.0001
AG Vir	57108.7276	18169	–0.0085	C	G. Frey	0.0002
AW Vir	57174.6802	34328	0.0279	C	G. Frey	0.0001
AZ Vir	57162.7371	37711	–0.0239	C	G. Frey	0.0001
BF Vir	57159.7063	17311	0.1150	C	G. Frey	0.0001
BH Vir	57160.7084	17053	–0.0122	C	G. Frey	0.0001
GR Vir	57187.7353	34790.5	0.0051	C	G. Frey	0.0001
IR Vir	56780.7548	18829	0.0048	C	G. Frey	0.0001
IR Vir	57140.7084	19803.5	–0.0024	C	G. Frey	0.0001
MS Vir	57184.7150	14994	0.0006	C	G. Frey	0.0002
NN Vir	57180.7612	18058	0.0070	C	G. Frey	0.0001
V391 Vir	56771.7148	15557	0.0128	C	G. Frey	0.0005
V391 Vir	56777.7382	15574	0.0128	C	G. Frey	0.0002
V391 Vir	57126.7247	16559	–0.0020	C	G. Frey	0.0001
BO Vul	57335.5901	10970	–0.0238	V	G. Samolyk	0.0001

An Undergraduate Research Experience on Studying Variable Stars

Ariel Amaral
John Percy (corresponding author)
Department of Astronomy and Astrophysics, and Dunlap Institute for Astronomy and Astrophysics, University of Toronto, Toronto ON M5S 3H4, Canada; john.percy@utoronto.ca

Received December 11, 2015; revised April 26, 2016; accepted April 26, 2016

Abstract We describe and evaluate a summer undergraduate research project and experience by one of us (AA), under the supervision of the other (JP). The aim of the project was to sample current approaches to analyzing variable star data, and topics related to the study of Mira variable stars and their astrophysical importance. This project was done through the Summer Undergraduate Research Program (SURP) in astronomy at the University of Toronto. SURP allowed undergraduate students to explore and learn about many topics within astronomy and astrophysics, from instrumentation to cosmology. SURP introduced students to key skills which are essential for students hoping to pursue graduate studies in any scientific field. Variable stars proved to be an excellent topic for a research project. For beginners to independent research, it introduces key concepts in research such as critical thinking and problem solving, while illuminating previously learned topics in stellar physics. The focus of this summer project was to compare observations with structural and evolutionary models, including modelling the random walk behavior exhibited in the (O–C) diagrams of most Mira stars. We found that the random walk could be modelled by using random fluctuations of the period. This explanation agreed well with observations.

1. Introduction

Variable star analysis is an excellent way for students to develop and integrate their science, math, and computing skills, motivated by the knowledge that they are doing real science, with real data (Percy 2008). This paper describes a summer undergraduate research experience by co-author Amaral, supervised by co-author Percy, within the context of a formal program in which students' research is supplemented by a "professional development" program.

In the past, Percy has assigned students a small, self-contained research project which will lead to a publishable paper with the student as co-author (e.g. Percy and Huang 2015). In the present case, there were two significant differences. First: Amaral had been exposed, in a broad way, to the nature and evolution of Mira stars in a third-year course in astrophysics, and was specifically interested in becoming familiar with a variety of ways of using observations to understand Mira stars. Second: this project was carried out within a formal educational framework. We are aware that this *Journal* wishes to feature more papers in the area of science education. Such papers are most useful if they include a description and evaluation of the educational project or activity, for the benefit of readers who organize or participate in such projects and activities, or who may wish to become involved with them.

We therefore begin with a summary of the Mira star project, which includes three parts: the reliable identification of double-mode pulsators, and the interpretation of (O–C) diagrams in terms of evolution, and of random fluctuations. We then describe and evaluate the overall summer experience.

2. Summer project

Author Amaral, having learned about Mira stars and their evolution in a third-year astrophysics course, decided that she wanted to sample various ways of comparing Mira star observations with models of their structure and evolution. That led to the following sub-projects.

2.1. Identifying bimodal pulsators

Variable star data usually come in the form of light curves, which often extend as far back as a century. Much of this data, especially for Mira stars, is collected by skilled amateur astronomers. This is necessary because there are many variable stars, and observing their changes in magnitude regularly over many years is extremely time-consuming—too much so for professional astronomers. To analyze the massive amount of data on these stars, time series analysis is necessary. Specifically for this section of the project, we used Fourier analysis. Fourier analysis attempts to fit a sum of sinusoids to the light curve. It scans a pre-chosen range of periods, at fine resolution. If a sinusoid with a particular period fits the data, then we can say that period is present. Fourier analysis thus generates a power spectrum, which picks up any periodic variations in the light curve. The peaks in the power spectrum represent possible periods of pulsation of the variable star.

Many pulsating red giant stars pulsate in two or more modes. This effect can be found by looking at the power spectrum and selecting and evaluating the prominent peaks. Fourier analysis makes it very easy to detect the modes of pulsation, though this process comes with many challenges. The power spectrum can contain false periods, namely, alias, spurious, and harmonic periods. One-year alias periods can be detected as peaks in the power spectrum which differ in frequency from the real periods by 1/365.25 cycle per day. They are caused by the fact that some stars are only visible at certain times of the year, thus creating a periodicity in the obtaining of data. Spurious periods are periods of exactly one year found in the power spectrum. Finally, harmonic periods are a result of the Fourier transform fitting sinusoids to a non-sinusoidal light curve. It is common to find incorrect multi-modal stars identified in the literature in cases where the power spectrum was not carefully analyzed.

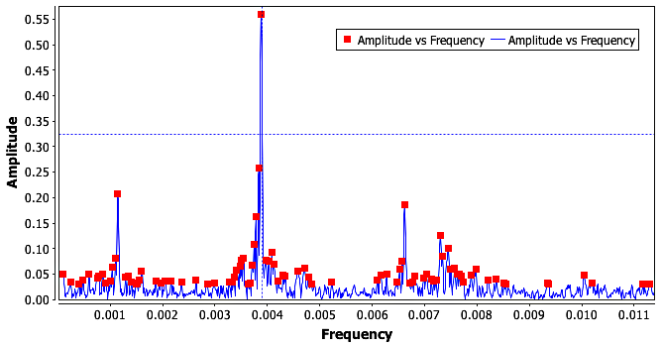

Figure 1. The amplitude spectrum of V Boo. The strongest peak is at 257.7 days, or 0.00388 cycle/day. The peaks at 0.00114 and 0.00662 cycle/day are yearly aliases of this. The peak at 0.00730 cycle/day or 137.0 days is a true secondary period.

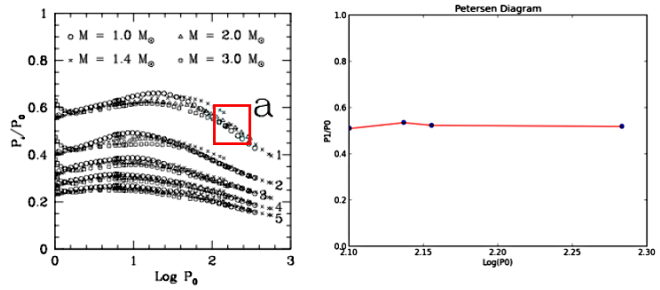

Figure 2. The figure on the left is a theoretically derived Petersen Diagram from Xiong and Deng (2007) for various assumed masses and overtones. We compare this to the figure on the right which is a Petersen diagram created using the bimodal stars detected. This figure represents the area on the Xiong and Deng (2007) diagram that is within the red square.

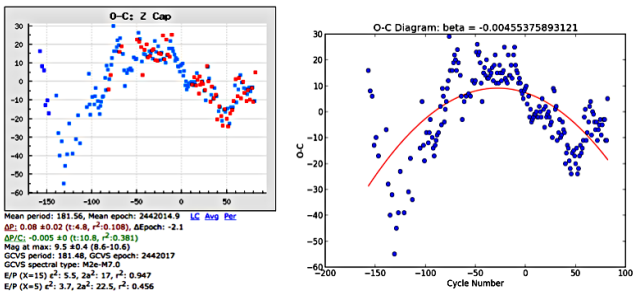

Figure 3. The figure on the left shows the O–C diagram for Z Cap (from http://var.astronet.se/mirainfooc.php). The figure on the right is an example of fitting a parabola to the exact same data and obtain β which is the rate of period change. Notice the parabolic shape.

Being able to locate multi-modal pulsators accurately is extremely useful when comparing with theoretical structural models, which can provide theoretical periods and period ratios. Petersen diagrams are graphs of period ratios plotted against the log of the longer periods. Xiong and Deng (2007) have developed structural and pulsational models for red giants which use an improved treatment of convection, and assuming non-adiabatic oscillations, and have used these to make theoretical Petersen diagrams. By properly detecting bimodal stars, observed period ratios can be compared with the theoretical ones produced by Xiong and Deng.

For this part of the project, we used visual observations of pulsating red giants from the AAVSO International Database (Kafka 2015), and analyzed them with the AAVSO VSTAR time series analysis software (Benn 2013). We examined the following stars which showed possible evidence of bimodal behavior: ST And, V Aqr, V Boo, WZ Cas, W Cyg, U LMi, BQ Ori, and Y Tau, looking carefully for periods which were not spurious. We consider the following four stars to be bimodal; P0, P1 (both in days) and P1/P0 are given: V Boo: 256, 137, 0.535; WZ Cas: 370, 192, 0.519; U LMi: 273, 143, 0.524; BQ Ori: 247, 126, 0.510. These period ratios are consistent with the theoretical period ratios found in Xiong and Deng (2007) for fundamental and first-overtone pulsation.

Using the four stars considered for period analysis above we produced a Petersen diagram to compare to the theoretically derived Petersen diagrams found in Xiong and Deng (2007). Comparing observed Petersen diagrams to theoretical ones allows for a direct test of the structural theory used to derive the modelled Petersen diagrams. Such a comparison is also useful to determine the secondary period of a suspected bimodal pulsator if the main period of pulsation is known as well as the stellar mass. As can be seen from Figure (2), using only four sample stars to generate a Petersen diagram results in only a fraction of the theoretical curve to be covered; however, the reader can observe how important an accurate detection of the periods of bimodal stars can be in such a comparison.

2.2. Rates of period changes

Due to the fact that Mira stars have been observed and analyzed continually for up to a century—or longer in some cases—it is a well documented phenomenon that the periods of pulsations of many Mira stars tend to change. These changes in period can be classified by specific features, such as sudden changes, continuous changes (over a long period of time), and meandering changes. The best way to analyze any changes in the period is to use an (O–C) diagram; see Figure (3) on the left for an example. From a light curve one can measure times of maximum brightness, and generate an (O-C) diagram. (O–C) stands for "Observed" minus "Calculated," and can be generated by taking the observed times of maxima from the data and subtracting from them the calculated times of maxima, assuming the period to be constant. Due to the method used to calculate (O–C) diagrams, any linear changes in period will show up as parabolic on the diagram. A parabola opening upward will signify a positive period change, and a downward opening parabola will signify a negative period change. An (O–C) diagram allows for smaller changes in the period to be more detectable, because small changes in period have a cumulative effect on the times of maxima. (O–C) diagrams can also be used to calculate the rate of period change for the set of data. The average rate of period change can be determined by fitting a quadratic equation to the (O–C) diagram. The coefficient of the quadratic term is given by Equation (1), where K_0 is the quadratic coefficient and $\overline{P}$ is the average period over the time interval. A quadratic fit is used because, as mentioned above, linear changes in period show up as parabolic changes in the (O–C) diagrams, see Figure (3) on the right.

$$K_0 = \frac{\overline{P}}{2}\frac{dP}{dt} \qquad (1)$$

By using Equation (1) it is possible, in principle, to determine the evolutionary behavior of each star. Mira stars are slowly moving up the asymptotic giant branch (AGB) in the H-R diagram, and as such a slow period change due to this movement is expected, as well as very rapid period changes due to occasional thermal pulses (and possibly other factors such as extreme mass loss, super winds, and shock waves). By determining the amount of period change, it is possible to determine what physical processes are happening within the star.

Stars on the AGB have a degenerate core of carbon contained within a shell of helium burning which is surrounded by a shell of hydrogen burning. Once the helium-burning shell is burnt up, the fusion source will be provided solely by the hydrogen-burning layer. The helium will be fusing unstably for a long period of time, causing periods of intense burning when the helium-fusing layer is reignited. These periods of intense helium-shell burning are called thermal pulses. The majority of the time on the AGB is spent during the inter-pulse quiescent phases. During the thermal pulse the luminosity of the star peaks at a maximum and then decreases to less than it was before the pulse (Wood and Zarro 1981). A thermal pulse is expected to last about 10^3 years, therefore a star only spends about 1–2 percent of its time on the AGB in a thermal pulse phase (Wood and Zarro 1981). The thermal pulse is expected to drastically affect the period of the star. It is hypothesized that perhaps the Mira stars which exhibit the highest rate of period change are those which have had a recent thermal pulse or which are currently undergoing a thermal pulse. As mentioned previously, the value $\beta = \frac{dP}{dt}$ represents the *average* period change occurring, though when attempting to determine evolutionary properties it can be difficult because β includes period changes due to "random walk fluctuations" (see section 2.3). Karlsson (2014) attempted to deal with this issue by averaging the β of 362 stars in an attempt to average out these supposedly random fluctuations. Values of β, and other information about these stars is contained on his website. Templeton *et al.* (2005) have determined values of β for 547 Miras, using wavelet analysis.

2.3. Random walk fluctuations

Stemming from the discussion of period changes in section 2.2, we attempt to discuss the random walk behavior mentioned previously which has been observed in the majority of Mira stars. Random walks show up as meandering or winding changes in the period over time. They are on too short a time-scale to be due to a thermal pulse, or other known evolutionary factors. Since Mira stars can be found on the AGB, and they come from medium to low mass progenitors, they contain *extremely* large convective cells. Theoretical calculations done by Schwarzschild (1975) have estimated that only around a dozen convection cells would exist on the surface at one period of time; compare this to the millions on the surface of the Sun. Convection is a branch of stellar physics which is not as well understood, mostly due to the fact that convective turbulence is extremely difficult to model. These extremely large convection cells would thus have a significant impact on the processes occurring within the star, and add a factor of randomness to the periods of Miras. In attempt to quantify this effect, we used a previously calculated estimate done by Percy and Colivas (1999) who used the Eddington and Plakidis (1929) formalism. By using 391 Miras and determining the amount by which they fluctuate from their main pulsation period, we were able to take the approximately average value of ±0.2 percent change in period, per period, to model this random effect.

Using this information, it is possible to develop a simulation which can show the effect of this 0.2 percent random fluctuation on the pulsation period of Mira variable stars over time. Though Miras can sometimes be bimodal pulsators (usually pulsating in the fundamental and first overtone), the value used for this simulation can be approximated to just the main pulsation period. This simulation can be done quite easily using Python, using the RANDOM library to generate these random fluctuations. The Python RANDOM library uses the Mersenne Twister algorithm to generate random float values within a given range. The random fluctuation can be taken into account by using the recursive formula in Equation (2), where K_{rand} is a random number determined with 0.2 percent fluctuation.

$$P_{n+1} = P_n + K_{rand} \quad (2)$$

See the right side of Figure (4) for an example of period-versus-time graph generated using the method described above, and beneath it, the corresponding (O–C) diagram. By changing the period-versus-time graphs to (O–C) diagrams we were able to compare the generated (O–C) diagrams to (O–C) diagrams from actual Mira stars. We used the (O–C) diagrams provided by Karlsson (http://var.astronet.se/mirainfooc.php) to compare with our simulated diagrams. By doing this we found that we could generate similar (O–C) curves to the ones found in Karlsson's database. See Figure (4) for the (O–C) diagram of T Gru, which is being compared to the (O–C) diagrams generated by our simulation. Sometimes changing the 0.2 percent fluctuation rate was necessary (since 0.2 percent represents the average fluctuation value in the range found by Percy and Colivas). By changing the fluctuation amount and comparing to observed data we could determine which stars were more heavily influenced by these random fluctuations. By being able to approximately recreate (O–C) diagrams of Mira stars with our simulation we can conclude that these random walk fluctuations observed in many Mira stars (which could be caused by the random motions of convective cells) in the period can indeed be modelled and explained by random period fluctuations.

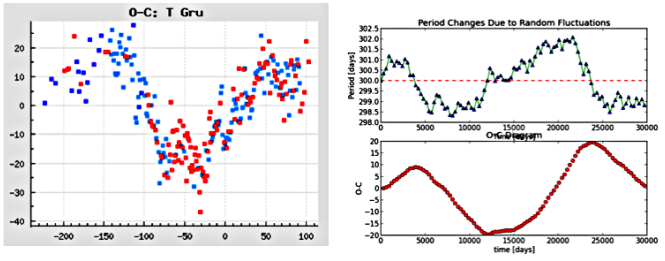

Figure 4. The figure on the left shows the (O–C) diagram for T Gru; notice its meandering features. The upper figure on the right is a simulated period-versus-time graph and the lower figure on the right is its corresponding (O–C) diagram. The simulation can be compared to the (O–C) diagram of T Gru.

2.4. Educational benefits

The project as a whole had many educational benefits, such as working with a research supervisor, planning a project, reading research papers (applying what was learned in the SURP workshops—see section 3), writing this report and giving a presentation, graphical and statistical concepts, and learning a lot about a specific topic—Mira stars. As outlined in section 2, this summer project focused mainly on pulsating red giant stars such as Miras and semiregular variables, in which we compared observations to models to determine key structural and evolutionary information. Coming into this summer with no prior experience in research, the topic of variable stars was able to serve as the perfect introduction to research, by applying the knowledge acquired in previous astronomy courses on stellar structure and evolution to this summer project. However, each section of the project led to many other specific educational benefits that allowed many wide-ranging skills to be developed that could be used in further astrophysical research.

This project served as an introduction to research from which skills were developed in order to deal with imperfect data. By learning how to use previously existing software (VSTAR), in section 2.1, we were able to apply the method of Fourier analysis to determine periods. The *false* periods identified in this section were an example of artefacts, which often arise when dealing with imperfect data. Both the skills learned from dealing with the artefacts which were a result from imperfect data, and the methods to analyze these data (time series analysis and Fourier transforms) are widely applicable in other areas of astrophysical research and in the sciences more generally.

Connecting and comparing observation to theory is an important part of research and this sort of analysis was ongoing within the project. For example, in section 2.1, by using Petersen diagrams created using observational data we were able to compare to theoretically determined Petersen diagrams (and hence the structural models in which they were derived). In addition to this, in section 2.2 we were able to use the rate of period change to determine what evolutionary state the star was in and therefore determine more about how Mira stars evolve and their overall place in stellar evolution.

Dealing with imperfect data is an important skill to master when doing research within any scientific field. In section 2.2 of the project we were able to learn the importance of curve fitting to imperfect data, and how curve fitting can lead to important scientific results. As section 2.2 focuses on understanding ways of measuring period changes, an important property present when studying Mira variable stars, we used curve-fitting techniques to determine the rates of period changes of the stars analyzed. The two methods that were used to determine the period changes were wavelet analysis and (O–C) diagrams. These two methods gave us ways to visualize changes with time and how to measure these effects. Understanding how and why both of these techniques work is important, as they have a much broader application within other fields of stellar astronomy, and build upon using curve fitting to determine the values of period changes.

Section 2.3 of the project allowed for use of custom-written code, whereas the previous parts of the project required only the use of VSTAR (pre-existing software). Much of research in astronomy (and other related scientific fields) relies heavily on the use of computer programming to analyze data. Writing code (using Python) to perform simulations is a great way to improve computer programming skills.

Simulations are important in many areas of astronomy, therefore by being able to incorporate these simple simulations in this project one can learn more about the subject (Mira stars and their period fluctuations), and that the fluctuations observed can be reproduced using these random fluctuation simulations, see section 2.3. This gives us insight and understanding as to the powerful role simulations play in studying astronomy as they can be used to describe astronomical phenomena and lead to deeper understanding about the subjects.

Variable star astronomy introduces some important topics that are essential for most research conducted in physics, such as Fourier transforms, polynomial fitting, and time series analysis. Therefore, the topic of variable stars served as a perfect introductory research topic, due to the fact that much of the required physics for understanding it is taken in courses previous to third year undergraduate level. It serves as an opportunity for astronomy or physics students to apply much of the knowledge learned in their courses from first and second year to a research problem while learning important skills and gaining research experience.

3. Summer Undergraduate Research Program

The annual Summer Undergraduate Research Program (SURP) at the University of Toronto is jointly hosted by the Department of Astronomy and Astrophysics (DAA), the Canadian Institute for Theoretical Astrophysics (CITA), and the Dunlap Institute (DI). Here we provide a description of the SURP 2015 program along with thoughts and comments. SURP was very capably organized by a committee of postdocs; see Acknowledgements for their names. SURP in 2015 ran from May 4 until August 17. It allowed undergraduate students from across Canada to conduct independent research under the direct supervision of a faculty member in DAA, CITA, or DI. Over the four months, students worked on projects from all areas of astrophysics, ranging from instrumentation to cosmology. Since many undergraduates are new to conducting independent research, SURP focused a lot on building necessary skills that would be useful for students hoping to pursue a career in any area of research. In fact, many of these skills could be applied to a wide variety of careers.

The program began with an intensive two-week crash course in computing, which introduced students to the basics of Python using Unix terminals to execute commands. This was extremely useful, especially to some of the younger students who had not yet had the opportunity to use Python. The second week of the crash course was exclusively for those conducting research in CITA, though it would have been beneficial for all SURP students. A useful addition to the research program would have been an "introduction to research" workshop which could cover topics such as how to prepare for a research project, what to expect throughout the summer, what makes good research etc.

The program was structured so that research was conducted every weekday. On Tuesdays and Thursdays, the whole group

of summer students met together for one hour and discussed the progress they had made in their projects. Along with weekly meetings, special workshops were also held to help students learn essential skills that are necessary for foundations of research. The workshops offered were: inquiry-based learning, how to write an abstract, how to prepare figures, and how to give a good presentation. At the end, there was a formal evaluation of SURP, and suggestions were made for modifications in 2016.

On Tuesdays the focus was on paper discussion, led by a graduate student. An academic paper, which would have been read during the week, was discussed for an hour. The purpose of this exercise was to show students how to read academic papers properly, and how to identify important points to look for in order to get as much information out of the papers as possible. Knowing how to read academic papers properly is an important skill to learn, especially for undergraduate students who, prior to this summer, would have been used to reading textbooks instead of academic articles. The styles of writing can be quite different. Another beneficial aspect of the paper discussions was the variety of the papers, which were taken from many different fields within astrophysics every week.

During Thursday meetings, the students' progress on their research was discussed in a scholarly context, allowing students to raise issues about their research and to share any problems that they may have run into. These discussions were extremely useful in giving us practice in presenting our ideas in a scholarly way, but in a friendly environment. These meetings also served as an opportunity for students to discuss any problems they had run into during their research, and for other students to help out. They also allowed students to see what other students were working on during the summer, enabling students to learn more about different fields of research. However, these meetings would have been more beneficial if students were given a longer discussion time. One hour a week seemed far too short to get into much detail with anyone's project, especially when you consider the multiple projects that were discussed in one meeting session. Opening up another one-hour meeting session per week, so that students would meet three times a week, would have been more useful.

Students were also given the opportunity to give two talks on their research in an academic setting, one in the middle of the summer, and one final presentation at the end of the summer. The audience included all of the SURP students as well as many faculty members and graduate students of the department. Students were given an allotted time (12 minutes) in which they had to present their research and answer any questions that the audience might have. Presentations are not always a part of undergraduate classes, which are more often taught in lecture format, so this provided students with a good opportunity to practice their skills giving academic talks. Tips from the "How To Give Good Talks" workshop were extremely useful when having to give the midterm and final presentation. The good thing about having two presentations was that it gave students the opportunity to learn and improve from the first presentation with feedback from their supervisor and to incorporate elements of other students' presentations that worked very well [The presentations were uniformly interesting and professional—JP]. Students were also required to write an abstract of the final presentation for the formal abstract book; a workshop was offered as a guide to how to do this effectively. Having the workshop made writing the abstract a lot easier, and gave students experience with writing abstracts—something that researchers must do very often.

DAA and DI are extremely involved in outreach events. These events provide the general public with an inside look at the University of Toronto and encourage and satisfy interest in astronomy. Outreach is an important part of doing science; it helps raise public understanding about science, whilst also helping to spark interest in the subject that can be particularly helpful to younger generations. SURP students had the opportunity to participate in these outreach events that ranged from astronomy-themed lectures to open-house telescope tours. I was personally able to operate the campus telescopes to engage with an interested audience in order to teach them about different astronomical objects. It was an amazing opportunity to discuss topics that I am extremely passionate about with a different audience, and I will continue to participate in these outreach events after the summer is over. [In 2015–2016, Ariel was hired by DAA as a Teaching Assistant—a rare honor here for an undergraduate—JP].

The Dunlap Institute hosts an annual one-week Instrumentation Summer School at the end of July or beginning of August. The Summer School gives advanced students an introduction to astronomical instrumentation from leading North American experts in the field. SURP students were allowed to attend the Dunlap Summer School lectures. They covered various subtopics within the broader topic of instrumentation, such as Radio and Microwave Astronomy, Fourier Transform Spectrometry, and Adaptive Optics. I found this experience extremely valuable, as the topic of instrumentation is scarcely discussed in an undergraduate classroom, but yet is something that is fundamental to astronomy. I left the lectures with a deeper understanding of the basics of instrumentation that has already helped me in my studies. I found these lectures extremely interesting; they actually sparked a previously unknown interest in radio astronomy, as it is something I knew so little about before attending these lectures.

4. Conclusion

Through this project we were able to apply methods learned to analyze variable star data to determine important information about Mira variable stars and their place in stellar evolution and their structure. We found that, by using light curve and Fourier transforms, bimodal pulsators can be identified, as well as how the Fourier method of analyzing data can result in false and alias periods—something which we found present in literature. By using a select few bimodal stars for further analysis, we were able to plot a Petersen diagram, see Figure 2, in which we found that our method of determining periods accurately matched with theoretical Petersen diagrams. We then used (O–C) diagrams to study the rates of period changes within Mira stars, see Figure 3. We were able to relate the rate of period changes derived for the stars to their current evolutionary state. Finally, combining the knowledge learned about both structural and evolutionary models of Mira variable stars, we attempted to explain the

Random Walk fluctuations observed in the periods of Mira stars. Motivated by the fact that Mira stars contain extremely large convection cells which add a random factor to their properties, we simulated period versus time graphs for a star experiencing random fluctuations. We find that these simulations accurately model the random walk behavior observed from data, see Figure 4.

This project was completed within the Summer Undergraduate Research Program (SURP), which provided a structured format for the research projects done by participating students. The wide range of workshops, lectures, and outreach opportunities offered by SURP perfectly supplemented the work done in this project, and allowed for an enhanced summer experience which provided many critical and necessary skills that are essential for future research. A program such as SURP would be extremely beneficial to any undergraduate student who is interested in pursuing research, and my project could serve as a perfect introductory topic for someone new to research. The topic of variable stars served as an ideal introductory project to research, as important skills were learned and it allowed for the opportunity to build upon the knowledge of stellar astrophysics learned in many introductory courses.

5. Acknowledgements

We thank the AAVSO observers who made the observations on which part of this project is based, the AAVSO staff who archived them and made them publicly available, and the developers of the VSTAR package which was used to analyze them. We also thank Thomas Karlsson for making his excellent Mira-star database publicly available. SURP 2015 was very capably organized by Drs. Nicolas Crouzet, Sebastian Daemgen, Christa van Laerhoven, Laura Newburgh, and Aaron Zimmerman. This project was supported by the University of Toronto Work-Study Program.

References

Benn, D. 2013, VSTAR data analysis software (http://www.aavso.org/vstar-overview).

Eddington, A. S., and Plakidis, S. 1929, *Mon. Not. Roy. Astron. Soc.*, **90**, 65.

Kafka, S. 2015, observations from the AAVSO International Database (https://www.aavso.org).

Karlsson T. 2014, *J. Amer. Assoc. Var. Star Obs.*, **42**, 280.

Percy, J. R. 2008, in *Preparing for the 2009 International Year of Astronomy: A Hands-On Symposium*, Astron. Soc. Pacific Conf. Ser. 400, Astronomical Society of the Pacific, San Francisco, 363.

Percy, J. R., and Colivas, T. 1999, *Publ. Astron. Soc. Pacific*, **111**, 94.

Percy, J. R., and Huang, D. J. 2015, *J. Amer. Assoc. Var. Star Obs.*, **43**, 118.

Schwarzschild, M. 1975, *Astrophys. J.*, **195**, 137.

Templeton, M. R., Mattei, J. A., and Willson, L. A. 2005, *Astron. J.*, **130**, 776.

Wood, P. R., and Zarro, D. M. 1981, *Astrophys. J.*, **247**, 247.

Xiong, D. R., and Deng, L. 2007, *Mon. Not. Roy. Astron. Soc.*, **378**, 1270.

Book Review

Received April 28, 2016

Solar Science: Exploring Sunspots, Seasons, Eclipses, and More

Dennis Schatz and Andrew Fraknoi, 2016, 353 pages, ISBN: 978-1-941316-07-8. Price $39.95 US, softcover. Published by National Science Teachers Association Press.

Just in time for the "All-American" eclipse of the sun on August 21, 2017, we have an excellent new textbook about our "daytime star." The sun is especially useful for teaching, because it's conveniently available during school hours, whereas "the stars come out at night, the students don't." The sun is also central to the physical, biological, environmental, and Earth sciences, and has deep connections to history and culture.

Schools are potentially the most efficient and effective channel for mass astronomy education and outreach, since they reach almost everyone, not just those with a prior interest in astronomy (mostly greying white males like me). Unfortunately, most teachers have little or no background in astronomy, or astronomy teaching, so high-quality textbooks, teacher resources, and teacher workshops are essential.

Authors Schatz and Fraknoi have been leaders in astronomy education almost since their graduate school days at UC Berkeley—Dennis through the Pacific Science Center, and Andy through the Astronomical Society of the Pacific, and Foothill College in California. Between them, they have enough awards to paper a wall. In this book, they have drawn on their long experience and expertise to produce a book which is timely, relevant, attractive (full-color), understandable, and pedagogically strong. It's based on the 5 E model: engage, explore, explain, elaborate, and evaluate. The effective use of these and other "best practices" is one reason why I recommend this book so highly.

Evaluation is a topic which is often left to the end of a formal education project such as a textbook. One of the *first* questions that we should ask is: what do I want my students to know, and be able to do? In this book, evaluation is not by the usual memorization and regurgitation of number facts, but by providing engaging activities and projects which develop students' research and communication skills. Both the "elaborate" and "evaluate" sections have ideas which are suitable for these. For me, they were another great strength of the book. The book is recommended (by the publisher) for grades 5 to 8 but, as mentioned below, it is useful for other levels as well. There are ideas which would even be useful at the college "Astro 101" level. The information, activities, and projects are also useful for informal education—science clubs and fairs, youth groups, (daytime) star parties, etc.

The book is divided into four chapters, with a total of 45 classroom-tested, hands-on, inquiry-based activities. Each chapter begins with recommended teaching times for each activity, links to the national Next Generation Science Standards and the Common Core State Standards, and strategies for applying the 5 E model to that chapter.

Chapter 1 is on understanding and tracking the *daily* motion of the sun. In my province of Ontario, Canada, the grade 1 science curriculum requires students to observe and record daily and seasonal changes in their environment. This encourages them to develop skills of observation, and of recording in various formats. In this and the other chapters, there is a strong emphasis on observation, record-keeping, modeling, and visualizing in three dimensions. Safety considerations, of course, are emphasized throughout.

Chapter 2 deals with understanding and tracking the *annual* motion of the sun, and the seasons. This is a minefield! Research shows that, if students are taught about seasons using traditional methods in elementary and secondary school and in college, they will still believe that seasonal changes in temperature are caused by Earth's changing distance from the sun! This misconception is mentioned by the authors, but I would have recommended even more and stronger advice on how to confront this and other deeply-rooted misconceptions, and how to "teach around" these.

Chapter 3 is about solar activity and space weather, including different kinds of electromagnetic radiation from the sun. In my province, this is in the grade 9 science curriculum. This material would also be useful in other science courses, such as physics. The increasing societal implications of this material (to climate change, and space activity, for instance) make this chapter very broadly relevant and interesting.

Chapter 4 is about sun-moon-Earth relations, including phases, eclipses, and more. These topics are also rife with misconceptions, so inquiry-based, hands-on, 3D activities are essential. It's almost impossible to teach these topics with 2D diagrams, which are not to scale, and which go back and forth randomly between an observer-centered frame of reference, and an external one.

Each chapter also includes video connections, math connections, literacy connections, cross-curricular connections, and resources for teachers. Math connections are important, because one of the recommmended remedies for the current "crisis" in students' math achievement is to teach math across the curriculum. The cross-curricular connections are equally important, both because of the sun's broad relevance to science and technology, and also because of its deep links to geography, history, and culture. Although the book is USA-centered, many of the activities require students to think about how the sun appears in other parts of the world.

There is a website (www.nsta.org/solarscience) where teachers can view or download resources such as worksheets. The book also comes with a 16-page *Observer's Guide to Viewing the Eclipse*, and with eclipse glasses which conform to international

standards. The observer's guide can be downloaded, free of charge, from the NSTA website (www.nsta.org/publications/press/extras/files/solarscience/SolarScienceinsert.pdf). The guide and the book will be useful to those formal and informal educators who are blessed with totality, and to the rest of us who will have to settle for a partial eclipse. That includes the AAVSOers who observe the sun, and who engage in public outreach—which is almost all of us.

John R. Percy
Editor-in-Chief, *Journal of the AAVSO*,
and Department of Astronomy and Astrophysics,
and Ontario Institute for Studies in Education
University of Toronto, Toronto, ON M5S 3H4, Canada

email: john.percy@utoronto.ca

Abstracts of Papers and Posters Presented at the 104th Annual Meeting of the AAVSO, Held in Woburn, Massachusetts, November 13–14, 2015

General Paper Session Part I

AAVSO Research Highlights on CV Research

Stella Kafka
AAVSO Headquarters, 49 Bay State Road, Cambridge, MA 02138; skafka@aavso.org

Abstract I will present recent research highlights of research on Cataclysmic Variables, emphasizing the AAVSO's contributions to the progress of the field.

The Great UXOR Hunt--an Update

Michael Poxon
9 Rosebery Road, Great Plumstead, Norfolk, NR13 5EA, United Kingdom; mike@starman.co.uk

Abstract Details of the UXOR campaign run by the AAVSO's YSO group, with notes on spatial distribution and new avenues for "UXOR Hunting."

The First Results from the DESK Survey

Joey Rodriguez (The KELT Team)
Vanderbilt Astronomy Group, Physics and Astronomy Department, Vanderbilt University, 6301 Stevenson Center, Nashville, TN 37235; rodriguez.jr.joey@gmail.com

Abstract Young stellar objects (YSOs) are typically surrounded by protoplanetary circumstellar disks. One way to probe the size, mass, and composition of these disks is to observe a star being eclipsed by its own disk. So far only a few of these events have been discovered and analyzed in the literature. New wide-field time domain surveys are an ideal tool to search for rare eclipse events, depending on the coverage, cadence, and baseline of the survey. The Kilodegree Extremely Little Telescope (KELT) exoplanet survey covers a large portion of the sky, including a significant fraction of the galactic plane. Using time-series photometry from KELT we are looking for disk-eclipsing events, specifically in young stellar associations. To date, we have discovered three previously unknown large dimming events around the young stars RW Aurigae, V409 Tau, and TYC 2505-672-1. We attribute the dimming of RW Aurigae to its tidally disrupted disk, while for V409 Tau the dimming is interpreted to be caused by a feature, possibly a warp or perturbation, in its nearly edge-on circumstellar disk. TYC 2505-672-1 appears to be similar to epsilon Aurigae, with an M-giant being eclipsed every ~69 years by a white dwarf with an accretion disk surrounding it. I will describe our results and discuss how we are planning to search for these kinds of objects in future surveys such as LSST.

Revisiting Caroline Furness's *An Introduction to the Study of Variable Stars* on its Centenary (Poster)

Kristine Larsen
Department of Physics and Earth Sciences, Central Connecticut State University, 1615 Stanley Street, New Britain, CT 06053; Larsen@ccsu.edu

Abstract A century and one month ago (October 1915) Dr. Caroline Ellen Furness (1869–1936), Director of the Vassar College Observatory, published *An Introduction to the Study of Variable Stars*. Issued in honor of the fiftieth anniversary of the founding of Vassar College, the work was meant to fill a void in the literature, namely as both an introduction to the topic of variable stars and as a manual explaining how they should be observed and the resulting data analyzed. It was judged to be one of the hundred best books written by an American woman in the last hundred years at the 1933 World's Fair in Chicago. The book covers the relevant history of and background on types of variable stars, star charts, catalogs, and the magnitude scale, then describes observing techniques, including visual, photographic, and photoelectric photometry. The work finishes with a discussion of light curves and patterns of variability, with a special emphasis on eclipsing binaries and long period variables. Furness's work is a valuable snapshot of the state of astronomical knowledge, technology, and observing techniques from a century ago. This presentation will analyze both Furness's book and its reception in the scientific community, and draw parallels to current advice given to beginning variable star observers.

Identifying SRD Variables Among "Miscellaneous" ASAS Stars (Poster)

Michael Quinonez
Kristine Larsen
Department of Physics and Earth Sciences, Central Connecticut State University, 1615 Stanley Street, New Britain, CT 06053; Larsen@ccsu.edu

Abstract The International Variable Star Index (VSX) contains a large number of stars observed and analyzed by the All Sky Automated Survey (ASAS). While ASAS is a powerful tool in terms of the sheer volume of data it collects, its automated light curve analysis is not always robust enough to reliably identify stars that are not strictly regular in their magnitude variations. As a consequence, it was suspected that potentially many variable stars of the semiregular type were instead added to the VSX under a miscellaneous (MISC) classification. A subset of these semiregular stars, known as SRD variables, has a well-defined set of parameters regarding their classification—they are of the F, G, or K spectral type, their amplitudes of light

variation are between 0.1 and 4 magnitudes, and their periods of variation can span 30 to 1,100 days. Furthermore, SRD variables are giants or supergiants, and therefore typically distant with small proper motions. A search was made through stars listed as MISC in the VSX using the above parameters, as well detailed light curve analyses via the AAVSO's VStar program, in order to find ASAS SRDs that were misclassified as MISC. This study of 90 stars has yielded five new SRDs to date. In addition, some data pertaining to several stars that were not confirmed to be of the SRD type were found to contain errors, and have since been revised accordingly in VSX.

How Accurately Can We Predict Eclipses for Algol? (Poster)

David Turner
St. Mary's University, Department of Astronomy and Physics, 56 Shalimar Crescent, Dartmouth, NS B2W 4L8, Canada; turner@ap.smu.ca

Abstract β Persei, or Algol, is a very well known eclipsing binary system consisting of a late B-type dwarf that is regularly eclipsed by a GK subgiant every 2.867 days. Eclipses, which last about 8 hours, are regular enough that predictions for times of minima are published in various places, *Sky & Telescope* magazine and *The Observer's Handbook*, for example. But eclipse minimum lasts for less than a half hour, whereas subtle mistakes in the current ephemeris for the star can result in predictions that are off by a few hours or more. The Algol system is fairly complex, with the Algol A and Algol B eclipsing system also orbited by Algol C with an orbital period of nearly 2 years. Added to that are complex long-term O–C variations with a periodicity of almost two centuries that, although suggested by Hoffmeister to be spurious, fit the type of light travel time variations expected for a fourth star also belonging to the system. The AB sub-system also undergoes mass transfer events that add complexities to its O–C behavior. Is it actually possible to predict precise times of eclipse minima for Algol months in advance given such complications, or is it better to encourage ongoing observations of the star so that O–C variations can be tracked in real time?"

Searching for Atmospheric Signatures of Other Worlds

Mercedes Lopez-Morales
Harvard-Smithsonian Center for Astrophysics, 60 Garden Street, Cambridge, MA 02138; mlopez-morales@cfa.harvard.edu

Abstract The field of exoplanets continues to evolve at giant steps. With about 2000 planets already discovered around other stars, the next big challenge is to detect and characterize their atmospheres: What is the chemical composition of the atmospheres of those planets? What is their temperature? Do they have clouds? In this talk I will review what we have learned about exoplanets in the past two decades and the current and future efforts to unveil their atmospheres.

Hubble Exoplanet Pro/Am Collaboration

Dennis M. Conti
141 E. Bay View Drive, Annapolis, MD 21403; dennis_conti@hotmail.com

Abstract A collaborative effort is being organized between a world-wide network of amateur astronomers and a Hubble Space Telescope (HST) science team. The purpose of this collaboration is to supplement an HST near-infrared spectroscopy survey of some 15 exoplanets with ground-based observations in the visible range.

The purpose of the Hubble survey is to characterize the atmosphere of the target planets. The purpose of the ground-based observations is to develop light curves in the visible spectrum of the same planetary transits that HST will be observing in order to: 1) help better refine the ephemeris of the subject planets, and 2) determine any unusual activity such as star spots or flares on the planet's host star.

In addition to the science contributions to the HST exoplanet survey, this collaboration could provide the framework for future such collaborations between professional and amateur astronomers.

The Quest for Identifying BY Draconis Stars within a Data Set of 3,548 Candidate Cepheid Variable Stars

Jessica Johnson
1615 Stanley Street, New Britain, CT 06050; johnsonj@my.ccsu.edu

Abstract A spreadsheet of 3,548 automatically classified candidate Cepheid variable stars from the ASAS (All Sky Automated Survey) photometry data was provided to AAVSO (American Association of Variable Star Observers) members for analysis. It was known that the computer filters had significantly overpopulated the list. Patrick Wils originally investigated a small subset of the data using 2MASS, PPMXL, and ROTSE data, and discovered that the vast majority of the 84 candidates he surveyed appeared to have been misidentified, demonstrating the need to reclassify these variables. The most common misidentification seemed to be of BY Draconis stars (K and M spotted dwarfs), which led to an ongoing project to systematically identify BY Draconis stars from this data set. The stars are sorted using the International Variable Star Index (VSX) information and ASAS light curves to search for prior reclassification by other authors in the time since the initial population of the candidate list (e.g. using ROTSE data), along with infrared photometry (2MASS) and proper motion (PPMXL) data. An analysis of light curves and phase plots using the AAVSO software VSTAR is the final step in identifying potential BY Draconis stars. The goal of this project has been to submit updated identifications for these stars to VSX. This final presentation on this project will identify the last set of reclassified BY Draconis stars and discuss future directions for this research.

General Paper Session Part II

An Update on the Status of RR Lyrae Research—Report of the RRL2015 Meeting (October, Hungary)

Katrien Kolenberg
Harvard-Smithsonian Center for Astrophysics, 60 Garden Street, Cambridge, MA 02138; kkolenberg@cfa.harvard.edu

Abstract In October 2015 we organized the first international meeting focused on RR Lyrae research, with the goal to discuss recent developments and future RR Lyrae plans. The Scientific rationale is the following:

The field of RR Lyrae studies is vigorous and has recently gained new momentum. These pulsating variable stars are part of the space photometric revolution: continuous, high-precision observations shed new light on the still mysterious Blazhko-modulation, unexpected dynamical phenomena have been discovered, novel ideas and hypotheses have emerged. On the theoretical front multidimensional hydrocodes are about to mature, allowing for an improved description of the interaction between convection and pulsation, and the exploration of nonradial motions. Ongoing and future sky surveys, like OGLE, VVV, and LSST, will provide an overwhelming amount of data enabling researchers to address a multitude of astrophysical questions where RR Lyrae stars play a significant role. Long-awaited astrometric data from the GAIA satellite will give a boost to the study and application of these galactic and extragalactic standard candles. The aim of this conference is to bring together theorists and observational astronomers working on distant areas to share their latest results and vision about the future of RR Lyrae research, while putting these fascinating objects into a wide astrophysical context from pulsation theory to near-field cosmology.

I will give an overview of the results shared at this meeting, and highlight the potential role of the AAVSO in this fascinating subfield."

Observing RR Lyrae Variables in the M3 Globular Cluster with the BYU West Mountain Observatory

Michael D. Joner
Brigham Young University, Department of Physics and Astronomy, N488 ESC, Provo, UT 84602; xxcygni@gmail.com

Abstract We have utilized the 0.9-meter telescope of the Brigham Young University West Mountain Observatory to secure data on the northern hemisphere globular cluster NGC 5272 (M3). We made 216 observations in the V filter spaced between March and August 2012. We present light curves of the M3 RR Lyrae stars using different techniques. We compare light curves produced using DAOPHOT and ISIS software packages for stars in both the halo and core regions of this globular cluster. The light curve fitting is done using FITLC.

Time Series Observations of the 2015 Eclipse of b Persei (not beta Persei)

Donald F. Collins
138 College View Drive, Swannanoa, NC 28778; dcollins@warren-wilson.edu

Abstract The bright (V = 4.6) ellipsoidal variable b Persei consists of a close non-eclipsing binary pair that shows a nearly sinusoidal light curve with a ~1.5 day period. This system also contains a third star that orbits the binary pair every 702 days. AAVSO observers recently detected the first ever optical eclipse of A-B binary pair by the third star as a series of snapshots (D. Collins, R. Zavala, J. Sanborn—AAVSO Spring Meeting, 2013); abstract published in Collins, *JAAVSO*, 41, 2, 391 (2013); b Per mis-printed as β Per therein. A follow-up eclipse campaign in mid-January 2015 recorded time-series observations. These new time-series observations clearly show multiple ingress and egress of each component of the binary system by the third star over the eclipse duration of 2 to 3 days. A simulation of the eclipse was created. Orbital and some astrophysical parameters were adjusted within constraints to give a reasonable fit to the observed light curve.

Astronomical League Observing Programs Supported by the AAVSO

Mike Simonsen
AAVSO Headquarters, 49 Bay State Road, Cambridge, MA 02138; msimonsen@aavso.org

Abstract The Astronomical League provides many different observing programs designed to provide direction and goals for League members. The programs have certificates and pins to recognize the observers' accomplishments and for demonstrating their observing skills with a variety of instruments and objects. The AAVSO supports a Variable Star Observing award and the Astronomical League has recently agreed to adopt a new Binocular Variable Star Program.

Mr. Birmingham and His New Star

John O'Neill
16 Pemberton Road, Topsfield, MA 01983; varstarnights@gmail.com

Abstract The year 2016 sees two anniversaries connected with the Irish astronomer John Birmingham (1816–1884): the 200th anniversary of his birth and the 150th anniversary of his discovery of the nova outburst in T Coronae Borealis.

Impacts of Extended Periods of Low Solar Activity on Climate

William F. Denig
Chief Solar-Terrestrial Physics Division, National Centers for Environmental Information, 325 Broadway, Boulder, CO 80305; William.Denig@noaa.gov

(presented by Rodney Howe)

Abstract There has been great interest in determining the length and amplitude of Solar Cycle 24 in recent years, in part due to increasing speculation that the current solar minimum is anomalously quiet and perhaps signaling the beginning of a decreased period of solar activity in the coming decades. We aim to examine the current solar minimum and compare it to previous solar minima in order to: determine if the current minimum shares characteristics with other historically quiet solar minima (sometimes referred to as grand minima); outline the potential consequences of a grand minimum with respect to climate; and predict the future of Solar Cycle 24.

Should We Try to Re-Construct the American Relative Sunspot Index (R_a)?

Rodney Howe
3343 Riva Ridge Drive, Fort Collins, CO 80526; ahowe@frii.com

Abstract The new correction of the international sunspot number (ISN), called the Sunspot Number Version 2.0, led by Frédéric Clette (Director of the World Data Centre [WDC]-SILSO), Ed Cliver (National Solar Observatory), and Leif Svalgaard (Stanford University), nullifies the claim that there has been a Modern Grand Maximum. This comes from the International Astronomical Union (IAU) press release, August 2015 (http://www.iau.org/news/pressreleases/detail/iau1508/).

This ISN re-construction raises some questions for the AAVSO: should we try to re-construct the American Relative Index (R_a) to go along with the ISN reconstruction? Here we present the historical and current reconstructed ISN, with comparisons to the AAVSO American Relative R_a Index. If the AAVSO decides to re-construct the American R_a Index, then it will be important to digitize all available data back to 1947 and up to 2000 (the AAVSO currently has digitized data from 2000 to present). These archives exist at AAVSO HQ in different formats of raw observations from many observers over the past 70 years. However, not all raw data used since 1947 are extant.

Why are the Daily Sunspot Observations Interesting? One Observer's Perspective

Frank Dempsey
RR #1, 3285 Sideline 20, Locust Hill, ON L0H 1J0, Canada; cosmicfrank99@gmail.com

Abstract Daily sunspot counts made for the AAVSO Solar Section may cause the observer to feel in touch with the daily (and longer-term) changes on the sun's surface, and this connection may be more interesting when the solar observer remains aware of the larger solar and geomagnetic environment. The daily sunspot observations may become more interesting when correlated with transient events including solar flares, filaments, coronal holes, and coronal mass ejections that can be followed in near-real time multi-wavelength X-ray and UV solar images as well as particle flux and magnetic field measurements.

General Paper Session Part III

Last Rites for Cataclysmic Variables: Death by Fire, or Ice?

Joseph Patterson
Center for Backyard Astrophysics, 25 Claremont Avenue, Apt. 7C, New York, NY 10027; jop@astro.columbia.edu

Abstract Cataclysmic binaries lose angular momentum as they age, and thus the component stars in the binary spiral ever closer together. As the spiraling-in proceeds, the shrinking Roche lobe "strangles" the donor star, forcing it to transfer mass. Since we can measure the rate of mass transfer pretty well, we know the rate of angular momentum loss pretty well.

But when we calculate this we find that CVs reach the end of the line after about one billion years. That's too soon! It implies that there should be an old-age home somewhere for CVs, where the stars look discernibly different from the working-age population that we know about. Does this class exist? Many students of this problem think that the answer is probably yes, although so far we have not found a single confirmed example.

Of course, CVs also suffer classical-nova and dwarf-nova eruptions. It's assumed that these are of little consequence, because they are just transient blips in the overall evolution. We have discovered some evidence that this assumption may be false—that CVs may actually end their lives in a paroxysm of nova outbursts. In this picture, every star will become a T Pyx; we only know of one because the timescale of this final phase of self-destruction is so short.

APASS as a Tool for Calibrating the Cepheid Period-Luminosity Relation

David Turner
St. Mary's University, Department of Astronomy and Physics, 56 Shalimar Crescent, Dartmouth, NS B2W 4L8, Canada; turner@ap.smu.ca

Abstract In a recent study of field reddenings for Cepheid variables (Turner 2015, *Rev. Mex. Astron. Astrofis.*, submitted), the author noticed that the field of the classical Cepheid S Sge contained five B-type stars of well-defined reddening, $E(B–V) = 0.10 \pm 0.01$, implying a reddening of $E(B–V) = 0.09 \pm 0.01$ for S Sge. The stars also appeared to be constrained in distance in a color-magnitude diagram. Given the well-defined reddening for B-stars in the surrounding field, a search was made using the AAVSO Photometric All Sky Survey (APASS) of other

potential B and A-type companions. A sizeable number of such stars appear to define a well-populated main sequence in the color-magnitude diagram for the field, with an implied distance of 646 ±17 parsecs and age of log t = 7.9. Presumably the stars represent the remains of a dissolved open cluster where S Sge was created. Additional searches for such cluster remains are possible with APASS for the fields of other distance scale calibrators with well-defined field reddenings.

New Release of the BSM Epoch Photometry Database

Arne Henden
106 Hawkins Pond Road, Center Harbor, NH 03226; arne@aavso.org

Abstract The Bright Star Monitor (BSM) Epoch Photometry Database (EPD) is a searchable catalog of all observations made by one of the AAVSO's five BSM systems. The newest release of this database contains some 100 million datasets, from both northern and southern hemispheres, taken over the last six years. These have been calibrated by both nightly visits to Landolt standard fields as well as through the use of the Tycho2 photometric catalog. The paper will describe how the observations were made, how to access the catalog, and the limitations to the photometric accuracy. Some examples of well-studied fields will be shown.

A Chart Display and Reporting App for Windows

Michael Poxon
9 Rosebery Road, Great Plumstead, Norfolk, NR13 5EA, United Kingdom; mike@starman.co.uk

Abstract Details are presented for a windows application which allows simultaneous display of AAVSO charts and report-formatting software in the hope that other members will offer suggestions from their own experiences with charts and reporting.

Finding New Variable Stars

Michael D. Joner
Brigham Young University, Department of Physics and Astronomy, N488 ESC, Provo, UT 84602; xxcygni@gmail.com

Abstract Initial findings are presented for several new variable stars that have been identified using CCD photometry done with the 0.9-meter telescope located at the BYU West Mountain Observatory.

The AAVSO Hall of Fame

Mike Simonsen
AAVSO Headquarters, 49 Bay State Road, Cambridge, MA 02138; msimonsen@aavso.org

Abstract We propose the AAVSO create a Hall of Fame. Much like the baseball or football hall of fame, each year we would induct a number of people, hold a ceremony, present awards, and hear acceptance speeches. In this paper we outline the process, costs, and the justifications for an AAVSO Hall of Fame.